

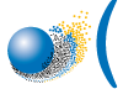
# Bioluminescence a proxy of biological activity in the deep sea ?

Study in the laboratory and *in situ* of bioluminescence linked  
to the environmental variables.

Séverine MARTINI  
PhD thesis 2013  
Mediterranean Institute of Oceanography (MIO)



La photographie de couverture est la propriété de Phil Hart,  
Bioluminescence en Australie, 11 Janvier 2013  
[www.philhart.com](http://www.philhart.com).



Institut Pythéas  
Observatoire des Sciences de l'Univers  
Aix-Marseille Université



Aix-Marseille Université  
Institut Méditerranéen d'Océanologie (MIO)  
Ecole Doctorale des sciences de l'environnement (ED-251)

THÈSE DE DOCTORAT  
Discipline : Océanographie

---

**La bioluminescence un proxy d'activité  
biologique en milieu profond ?**

Etude au laboratoire et *in situ* de la bioluminescence  
en relation avec les variables environnementales.

---

Présentée par : Séverine MARTINI  
Sous la direction de : Christian TAMBURINI et David NERINI

Soutenance prévue le 6 décembre 2013

Jury composé de :

Dr. François SCHMITT	DR CNRS	LOG, France	Rapporteur
Pr. Richard LAMPITT	Professor	NOCS, UK	Rapporteur
Dr. Patricia BONIN	DR CNRS AMU	MIO, France	Examinateur
Dr. Steven HADDOCK	adjunct Associate Professor	MBARI, USA	Examinateur
Dr. David NERINI	MCF AMU	MIO, France	co-Directeur
Dr. Christian TAMBURINI	CR CNRS AMU	MIO, France	Directeur

Institut Méditerranéen  
d'Océanologie (MIO),  
Campus de Luminy ,  
162, Avenue de Luminy,  
13288 Marseille, Cedex 09  
France

Ecole doctorale des sciences  
de l'environnement (ED 251),  
Europôle Méditerranéen de l'Arbois,  
BP 80,  
13545 Aix-en-Provence, Cedex 04  
France

*A la Baleine Blanche,  
à Salam, à Iluna,*

Parce que, finalement, tout a commencé là.  
Des quarts de nuit, passés dans l'humide cockpit, accrochée à la barre,  
négociant les vagues, et regarder des heures durant, alternativement,  
les Pléiades dans le ciel et le sillage lumineux...

*"La mer est sans routes, la mer est sans explications..."*  
A Barrico.



---

## Remerciements

---

Ce travail a été financé par une bourse ministérielle MNRT (2010-2013). Un financement EC2CO (projet BIOLUX 2011-2013) a permis la réalisation des expérimentations. Je remercie **Richard Sempéré** de m'avoir accueillie, tout d'abord au sein du LMGEM, et maintenant au MIO. Merci à **Bruno Hamelin** de m'avoir permis d'enseigner, en tant que monitrice, au sein de l'OSU Pytheas. Merci à **Pierre Rochette** de m'avoir acceptée au sein de l'Ecole doctorale "Sciences de l'environnement" (ED251).

First of all, I would like to sincerely thank Pr. François G. Schmitt, Pr. Richard Lampitt, Dr. Steven Haddock and Pr. Patricia Bonin for accepting to judge my work and to be present during my PhD defense.

Je tiens à remercier mes deux directeurs de thèses, **Christian Tamburini** et **David Ne-rini**, pour ce sujet, passionnant. J'ai tenu, avec conviction, à conserver à la fois une approche mathématique et expérimentale dans mon travail de recherche. Loin d'être évident... Pourtant, j'ai eu le privilège d'être entourée d'une équipe dont les compétences et l'ouverture d'esprit m'ont permis de naviguer et d'apprendre beaucoup, dans chacun de ces domaines. **Christian**, la liste de mes remerciements est longue. Merci de m'avoir ouvert la porte de la HP-team il y a 6 ans et de l'avoir toujours laissée ouverte depuis. Ta confiance m'est précieuse depuis toutes ces années. Tes conseils et nos discussions m'ont permis de construire ma réflexion scientifique, et c'est un plaisir de travailler avec toi autant scientifiquement qu'humainement. Merci aussi d'avoir toujours su conjuguer

avec mon entêtement, et mon impatience ! **David**, merci pour la confiance que tu m'as accordée, parfois plus que je ne m'en accordais moi-même. Merci également de m'avoir transmis un intérêt grandissant pour l'enseignement. Comme disait un grand philosophe, "*Il y a souvent de l'admiration dans les yeux d'un doctorant pour son directeur...*" -Dr Y. Eynaud, 2012.

**Charles-François Boudouresque**, merci d'avoir accepté de co-encadrer les débuts de cette thèse, et de m'avoir enseigné (entre autres) la rigueur scientifique qui me manque encore souvent.

**Marc Garel**. Merci Marc, d'avoir été là à chaque fois que j'avais besoin de données, d'une réponse, de discuter du dernier package sous R, ou d'une commande vraiment extraordinaire sous LATEX!!! Merci pour ta présence quand les manips ne marchent pas et quand il y a une super-idée-à-essayer-absolument. Merci pour ton professionnalisme, tes connaissances et ta disponibilité.

Merci à l'équipe BIOLUX :

**Laurie Casalot**, je te remercie d'avoir été aussi présente au cours de ces 3 années, un plaisir de travailler avec toi, and thank you to improve my english... L'équipe fermenteur : **Sylvain Davidson**, **Yannick Combet-Blanc**, et **Richard Auria**, ce fût riche scientifiquement, même si, malheureusement, tout n'a pas abouti comme je le souhaitais ! **Valérie Michotey**, et **Sophie Guasco** merci pour votre implication dans les manips de biomol et pour avoir pris le temps de me donner des explications, inlassablement...

Merci à :

**Bruno Charrière** (pour ta gentillesse et tes blagues... parfois drôles), **Dominique Le-fèvre** (tout vient à point à qui sait attendre), **Gégé Grégori** (pour ta bonne humeur et tes conseils pour la suite), **Cécile Militon** (pour avoir guidé mes premiers pas de monitrice), **Christos Panagiotopoulos**, **Jean-Christophe Poggiale**, **Philippe Cuny**, **France Van Wambeke**, **Cathy**, **Marc**, **Najib**, **Anne**, **Dominique Estival**, **Dominique Poirot** et **Brigitte Pantat** merci beaucoup d'avoir été là, dans le labyrinthe administratif, aux capitaines et équipages des navires océanographiques...

Je remercie la collaboration ANTARES :

Tout particulièrement, **Stéphanie Escoffier**, **Christian Curti**, et **Sylvain Henry** du CPPM pour votre aide, souvent indispensable, et toujours appréciée.

**Agnès Dominjon** et **Rémi Barbier** de l'In2p3 et le Centre Commun de Quantimétrie à Lyon pour avoir encouragé mes idées... parfois peu lumineuses ! **Vincent Grossi** et **Muriel Pacton** pour votre réactivité.

Je tiens à adresser mes remerciements aux étudiants de licence qui ont suivi mes enseignements ainsi qu'aux stagiaires de passage au laboratoire. L'enseignement fût une part importante de mes 3 années de doctorat, que j'ai accompli avec un véritable intérêt et que je souhaite avoir l'opportunité de poursuivre. Un grand merci aux précédents doctorants de la HP-Team, **Badr Al Ali**, **Mehdi Boutrif** et **Anne Robert**.

Merci à mes amis les plus précieux, qu'ils soient parapentistes (Pascal, Stéph, Serge, Lily, Fredo, Pierrick...), tangueros/as (Philippe, Cédric, Michel, Patrick, Julio, Géraldine, Jordi, Andrea...), plongeurs (l'ELM), doctorants (Maxime, Nico, Marie...), grimpeurs (Micka), slackeurs (Mathieu), marcheurs (Mathieu & Mathieu), navigateurs (Thom), de partout (Erwan) ou de n'importe où (Bobo, Nourmouhamad)... pour ce qui fut essentiel à chaque instant, au cours de ces 3 années. A mon aile aussi, pour ne m'avoir jamais laissée tomber pendant la rédaction ! Un merci particulier à Micka et Saraline, à Morgan, véritable co-équipier de thèse, et à Axel.

Enfin, je remercie, infiniment, mes parents, pour votre soutien, pour votre présence, pour m'apprendre depuis toujours que : "*L'imagination est plus importante que le savoir*" - *A. Einstein* Et que "*Les gens qui ne rient jamais ne sont pas des gens sérieux.*" -*A. Allais*.

A ma grande soeur.

A Fanny, merci pour ces moments partagés ensemble qui ont fait ces 3 années époustouflantes ! Pour les embruns, les strato-cumulus, nos aléas de doctorantes et notre amitié, indispensable ces dernières années. A toi bientôt...

Mes remerciements s'adressent également à tous ceux qui m'ont questionné, écouté, parfois beaucoup appris sur la bioluminescence en pleine mer et dans les abysses. Merci à toutes ces personnes grâce auxquelles je me suis attachée avec curiosité, et passion à ce sujet.



---

## Liste des abréviations

---

<b>Abréviation</b>	<b>...in english</b>	<b>...en français</b>
ANTARES	Astronomy with a Neutrino Telescope and Abyss environmental RESearch	Astronomie à l'aide d'un télescope à neutrinos et recherche environnementale des abysses
PMT	Photomultiplier Tube	Photomultiplicateur
ADCP	Acoustic Doppler Current Profiler	Profileur de courant par mesure acoustique Doppler
CTD	Conductivity Temperature Depth	Conductivité température profondeur
HPB	High Pressure Bottle	Bouteille haute pression
<i>r</i>	Growth rate	Taux de croissance
<i>K</i>	Carrying capacity	Capacité limite
HHG	Hilbert-Huang decomposition	Décomposition d'Hilbert-Huang
IMF	Intrinsic Mode Function	Fonction de mode intrinsèque
DOC	Dissolved Organic Carbon	Carbone organique dissout
POC	Particulate Organic Carbon	Carbone organique particulaire
OD	Optical Density	Densité Optique
BR	Bacterial Respiration	Respiration bactérienne
BP	Biomass Production	Production de biomasse
BGE	Bacterial Growth Efficiency	Efficacité de croissance bactérienne
NW	North-Western	Nord-Ouest
PPi	Inorganic Pyrophosphate	Pyrophosphate inorganique
AMP	Adenosine-5'-MonoPhosphate	Adénosine-5'-Monophosphate
FMN	Flavine MonoNucleotid oxidized	Flavine mononucléotide oxydée
FMNH <sub>2</sub>	Flavine MonoNucleotid reduced	Flavine mononucléotide réduite
ATP	Adenosine-5'-TriPhosphate	Adénosine-5'-triphosphate
CFU	Colony Forming Units	Unité formant des colonies
CCCP	Carbonyl Cyanid m-Chlorophenylhydrazone	Carbonyle cyanide m-chlorophenylhydrazone
AHL	N-Acylated Homoserine Lactone	N-acylated homoserine Lactone
UFA	Unsaturated Fatty Acid	Acides gras insaturés
PUFA	Poly-Unsaturated Fatty Acid	Acides gras poly-insaturés
SFA	Saturated Fatty Acid	Acides gras saturés

---

## Table des matières

---

<b>1</b>	<b>Introduction and objectives</b>	<b>1</b>
1.1	Marine bioluminescence . . . . .	2
1.1.1	Phylogenetic diversity of bioluminescent organisms . . . . .	2
1.1.2	Chemical reaction producing light . . . . .	6
1.1.3	Bioluminescence <i>in situ</i> observation . . . . .	9
1.1.4	Sensitivity of bioluminescence to environmental variables . . . . .	15
1.1.5	Ecological roles in the marine environment . . . . .	20
1.2	Afterthought and objectives of the study . . . . .	24
1.2.1	Multidisciplinary objectives . . . . .	24
1.2.2	A study at several scales . . . . .	26
<b>2</b>	<b><i>In situ</i> bioluminescence in the deep Mediterranean Sea (ANTARES site)</b>	<b>29</b>
2.1	Introduction : interest of recording long time series in environmental science	31
2.2	Instrumentation and mathematical concepts for the observation of oceanographic variables . . . . .	33
2.2.1	ANTARES site and environmental context . . . . .	33
2.2.2	Description of the IL07 instrumented line . . . . .	34
2.2.3	Data description : the regression trees approach . . . . .	37
2.3	Multivariate survey at high frequency and real-time sampling . . . . .	38
2.3.1	Water masses proxies . . . . .	38

2.3.2 Currentology . . . . .	40
2.3.3 Bioluminescence interaction with current . . . . .	42
2.3.4 Univariate and multivariate approaches using regression-tree method	43
2.3.5 Analysis of <i>in situ</i> images from bioluminescent organisms . . . . .	46
2.4 Article 1 . . . . .	51
2.4.1 Foreword . . . . .	51
2.4.2 Deep-sea bioluminescence blooms after dense water formation at the ocean surface . . . . .	52
2.5 Conclusions . . . . .	73
<b>3 In situ dataset analyzes using statistical methods adapted to time series</b>	<b>77</b>
3.1 Article 2 . . . . .	78
3.1.1 Foreword . . . . .	78
3.1.2 Relation between deep bioluminescence and oceanographic variables : a statistical analysis using time-frequency decompositions. . . . .	79
3.2 Complementary data . . . . .	109
<b>4 In the laboratory, effects of forcing variables using a bioluminescent bacterial strain as a model.</b>	<b>113</b>
4.1 Introduction : working with controlled variables and models. . . . .	114
4.2 Description of <i>Photobacterium phosphoreum</i> ANT-2200 strain . . . . .	115
4.3 Article 3 . . . . .	117
4.3.1 Foreword . . . . .	117
4.3.2 Effects of hydrostatic pressure on growth and luminescence of a moderately-piezophilic luminous bacteria <i>Photobacterium phospho-</i> <i>reum</i> ANT-2200 . . . . .	118
4.4 Effects of hydrostatic pressure and growth medium on growth, luminescence and oxygen consumption . . . . .	138
4.4.1 Growth medium . . . . .	138
4.4.2 High-pressure and oxygen consumption system . . . . .	139
4.4.3 Data acquisition into High Pressure Bottles . . . . .	141
4.5 Conclusions . . . . .	145
<b>5 In situ prokaryotic survey, quantification and bacterial bioluminescence : estimation at the ANTARES station</b>	<b>151</b>

5.1	Introduction : from laboratory to <i>in situ</i> measurements . . . . .	152
5.2	Article 4 . . . . .	155
5.2.1	Temporal survey of prokaryotic communities, presence and activity of bioluminescent bacteria at the deep ANTARES station (North- western Mediterranean Sea) . . . . .	155
5.3	Conclusions . . . . .	178
<b>6</b>	<b>Conclusions and Perspectives</b>	<b>181</b>
6.1	Conclusions . . . . .	182
6.1.1	Is bioluminescence a proxy ? . . . . .	182
6.1.2	Is bioluminescence linked to biological activity ? . . . . .	185
6.1.3	Does bioluminescence play a major role in the deep sea ? . . . . .	187
6.2	Perspectives . . . . .	188
6.2.1	Physiological parameters determination using bioreactor culture .	189
6.2.2	Proposal for the detection of bioluminescent organisms . . . . .	193
<b>Bibliographie</b>		<b>197</b>
<b>Table des figures</b>		<b>219</b>
<b>Liste des tableaux</b>		<b>225</b>



# CHAPITRE 1

---

## Introduction and objectives

---

### Sommaire

---

<b>1.1</b>	<b>Marine bioluminescence</b>	<b>2</b>
1.1.1	Phylogenetic diversity of bioluminescent organisms	2
1.1.2	Chemical reaction producing light	6
1.1.3	Bioluminescence <i>in situ</i> observation	9
1.1.4	Sensitivity of bioluminescence to environmental variables	15
1.1.5	Ecological roles in the marine environment	20
<b>1.2</b>	<b>Afterthought and objectives of the study</b>	<b>24</b>
1.2.1	Multidisciplinary objectives	24
1.2.2	A study at several scales	26

---

## 1.1 Marine bioluminescence

The luminescence describes the production of cold light, by opposition to the incandescence. This term includes the phosphorescence, the fluorescence as well as the bioluminescence. The first two phenomena are an emission of light following the absorption of photons while the bioluminescence is the production of photons after a chemical reaction by living organisms.

The bioluminescence phenomenon is known since Antiquity. Aristote (348-322 BC) already reports light emission by dead fish. Thereafter, in the *Naturalis Historia*, Pline (23-79 AD. JC) also describes various bioluminescent organisms such as glowing worms, "mushroom", or cnidarians. Moreover, in the History, marine bioluminescence, sometimes, played an unexpected role. Indeed, during the First World War, the submarine U-34, was the last German submarine sunk by the allies, identified by its luminescent wake. During the Second War, these wakes sometimes allowed the pilots to return to their aircraft carrier at night. Finally, during the Gulf War, american soldiers had to change the path followed by vessels to avoid the shoals of bioluminescent Dinoflagellates that might betray their presence.

### 1.1.1 Phylogenetic diversity of bioluminescent organisms

In terrestrial environments, few organisms have been described as bioluminescent. Conversely, in marine environments, nearly 90% of organisms are estimated able of bioluminescence emission ([Widder, 2010](#)) and are extensively described in the literature (see Figure 1.1). Some non-planktonic groups (moving independently of water-mass movements), such as cephalopods (210 bioluminescent species) or teleosts (273 bioluminescent species), are well represented among bioluminescent organisms ([Poupin et al., 1999](#); [Herring, 1987, 1985](#)).

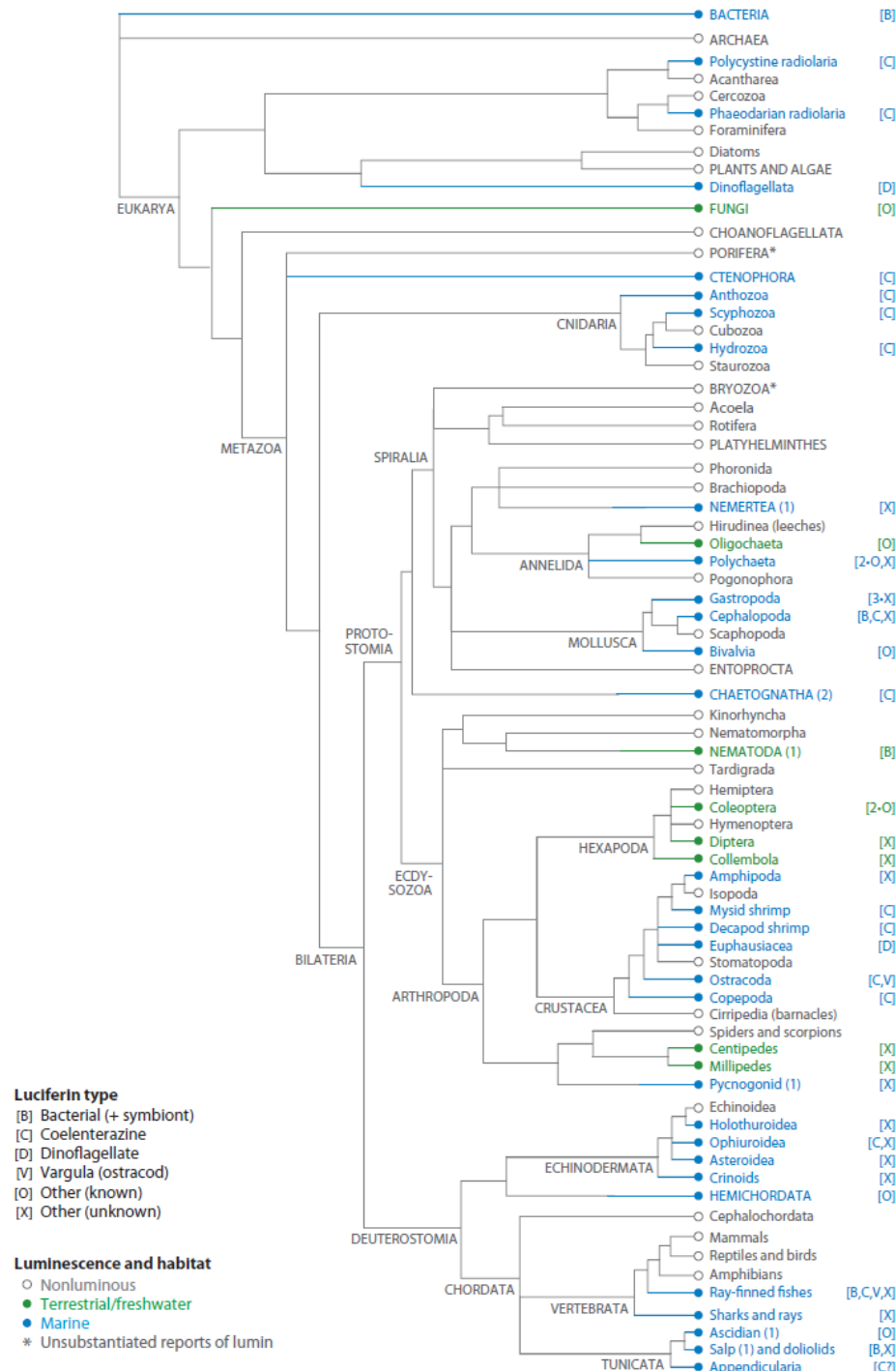


FIGURE (1.1) Phylogenetic representation of the diversity of bioluminescent organisms, from Haddock et al. (2010).

Planktonic phylogenetic groups, for which the largest number of bioluminescent species have been described, are: Bacteria, Dinoflagellates, Radiolarians, Cnidarians and Ctenophora, Crustaceans (Copepods, Amphipods, Euphausiids, Decapods), Chaetognathes and Tunicates. Bioluminescent species are also described within the Molluscs (Gastropods), Annelids (Polychaetes) and Echinodermata (Holothuroidea) (see Figure 1.1). Amongst prokaryotes<sup>1</sup>, only Bacteria have been described as able to emit light. Archaea are, to our knowledge, not described as bioluminescent.

Bioluminescent bacterial strains have been described, from the beginnings of microbiology, with the work of B. Fischer in 1887, Mr. Beijerinck in 1889 and ZoBell in 1946. Luminescent bacteria<sup>2</sup> are Gammaproteobacteria, Gram-negative, non-spore forming, chemоорganotrophe, heterotrophic, and mostly aerobic. The known bioluminescent species belong to the genera *Vibrio*, *Photobacterium*, *Shewanella* and *Photorhabdus*. Amongst these genera, *Photorhabdus* is the only terrestrial one, the others being present in marine environments.

To illustrate this diversity, (Poupin et al., 1999) proposed a non-exhaustive list in the Iroise sea, based on the literature. About 500 bioluminescent planktonic species, including six bacterial species, are described. Phylogenetically, the faculty of bioluminescence is randomly distributed in the living world (Herring, 1987). Phylogenetic analyzes suggested that bioluminescence is a genetic trait that evolved independently between 30 and 50 times (Haddock et al., 2010). However, the authors of these phylogenetic syntheses, bringing together observations of bioluminescent organisms, highlight the difficulties of establishing such inventory. On the one hand, the techniques of *in situ* observations of this phenomenon have changed in a few decades. These observations are constraint by the difficulty of capturing these bioluminescent organisms. On the other hand, the physiological state of the organisms determines the observation of light emission for some species. The photon emission sometimes decreases, due to the capture, to *in situ* stimulation or to changing conditions (pressure, temperature ... ) after sampling (Herring, 1976).

---

1. procaryote est un terme non-phylogénétique regroupant Bacteria et Archaea

2. In the following manuscript, the term "bacteria" will be used for procaryotes

Upon bioluminescence emission, the observation and measurement of emission spectrum in marine organisms revealed a wide range of colors in the visible wavelength (Widder et al., 1983; Haddock and Case, 1999, see Figure 1.2). However, in the marine environment, where the blue wavelength penetrates more deeply, the majority of organisms emits at about 475 nm. For example, all bioluminescent bacteria emit at 490 nm. For coastal and benthic species, a shift was noticed in the emission wavelength to the green one. Other wavelengths of bioluminescence emission, from violet to red, have also been observed but less frequently.

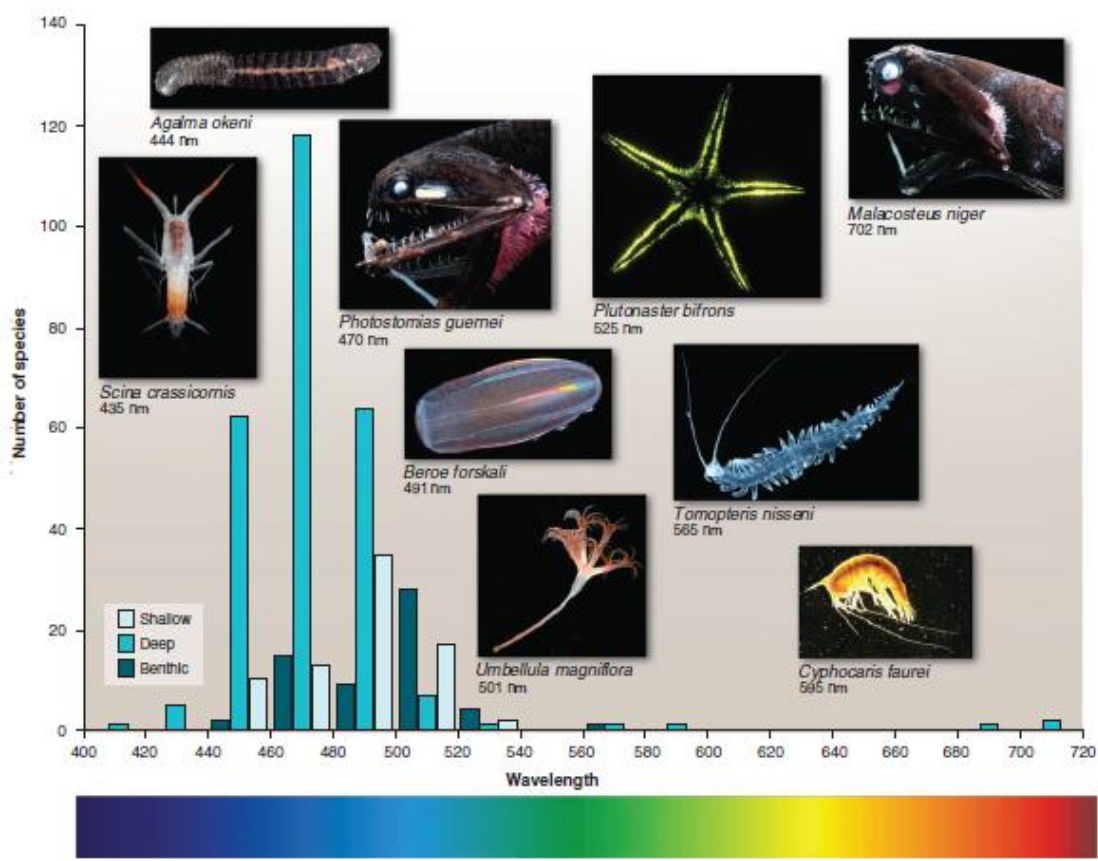


FIGURE (1.2) Classification of the number of bioluminescent species depending on their wavelength emission for marine organisms. Main bioluminescent species are emitting for wavelength between 450 and 520 nm, in blue-green emission, from Widder (2010)

### 1.1.2 Chemical reaction producing light

#### Eukaryotic reaction

The first experiments on bioluminescence are associated to R. Boyle (1627-1691), an English chemist, member of the "invisible college", and R. Hooke (1635-1702). These scientists observed that bioluminescence can not take place in the absence of air (the gaseous composition of the air, and in particular the presence of oxygen, was not known at this time). Subsequently, in 1885, the French biologist Raphael Dubois used, for the study of bioluminescence, beetles of the family *Elateridae* and gender *Pyrophorus* (Illiger, 1809), from Central America. He took two bright thoracic organs of an individual and grounded them. After some time, the light turned off. The second body was immersed in boiling water and the light turned off suddenly. When R. Dubois grounded together the two bodies, the mass became luminous. The phenomenon was then explained by the presence, in the organs, of a substance, that he called luciferin, emitting light until its complete oxidation, when the reaction is activated by a diastase enzyme (luciferase). The luciferin-luciferase reaction is an enzyme-substrate type. In the presence of oxygen, luciferin will react with the enzyme luciferase producing a molecule of oxyluciferin and light (see Figure 1.3; Shimomura, 2012). Luciferin and luciferase are generic terms. The composition of these molecules may differ depending on the species. Within the diversity of living systems, 5 luciferin-luciferase couples have been differentiated (Haddock et al., 2010; Wiles et al., 2005).



FIGURE (1.3) Schematic reaction inducing bioluminescence. The luciferin substrate interacts with ATP and is modified into luciferyl-adenylate. The second step of the reaction is the oxygenation (using molecular O<sub>2</sub>) of luciferyl-adenylate into oxyluciferin by the luciferase enzymatic action. This excited molecule get back to a stable state with photon emission (bioluminescence).

### Bacterial reaction

In Bacteria, the genes involved in the bioluminescence reaction are organized in cluster in which the *lux* ICDABFEG genes are organized in operon (called *lux* operon, see Figure 1.4).

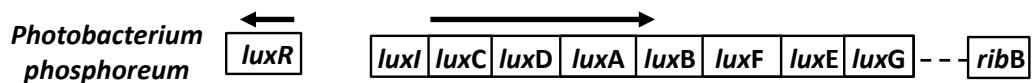


FIGURE (1.4) *Lux* genes organization for the bioluminescent *Photobacterium phosphoreum* bacterial strains. Arrows represent the direction of transcription. Modified from [Dunlap and Kita-Tsukamoto \(2006\)](#).

*luxA* and *luxB* genes encode the two subunits of the bacterial luciferase, an heterodimer of 77 kDa (see [Stabb, 2005](#), Figure 1.5). The *luxC*, *luxD* and *luxE* genes encode the reductase complex allowing the regeneration of the aldehyde, oxidized during the enzyme-substrate reaction ([Ruby and Nealson, 1976](#); [Meighen, 1988, 1991](#)). The *luxF* gene encodes a 23-kDa flavoprotein. The sequence of this protein has about 40% homology to the carboxy terminus of the subunit *luxB*. So it seems that this gene comes from gene duplication of *luxB* ([Meighen, 1993](#); [Soly et al., 1988](#)). The *luxF* gene was only identified in marine bioluminescent bacterial species from meso- to bathypelagic environments. Although its function is not yet established, the *luxF* gene appears not to be essential in the bioluminescence reaction ([Sung and Lee, 2004](#)). Finally, the *lux* operon is regulated by the *luxI* and *luxR* genes. The *luxI* gene synthesizes an autoinducer, the acetyl-homoserine lactone (AHL) which will bind to the product of the *luxR* gene. This *luxI* / *luxR* system will then activate the operon expression ([Miller and Bassler, 2001](#)). These genes are involved in the quorum-sensing response, for a low cell density, LuxI is produced at a basal level. When the population increases and the concentration of LuxI is high enough, it will bind to LuxR to activate the operon transcription and therefore, the production of bioluminescence (see Figure 1.6 and Figure 1.7 B [Meighen, 1993](#)).

Bacterial reaction (see Figure 1.5) induces the oxidation of one molecule of flavin mononucleotide reduced ( $\text{FMNH}_2$ ) and the reduction of a long chain of aldehyde ( $\text{RCHO}$ ). This reaction will produce a molecule of flavin mononucleotide oxidized (FMN) and a long fatty-acid chain ( $\text{RCOOH}$ ) with the production of light (Hastings, 1986; Meighen, 1988). Other proteins such as LuxC and LuxD are responsible for the regeneration of the aldehyde. LuxG protein transfer the electron from  $\text{NAD(P)H}$  to FMN in order to regenerate  $\text{FMNH}_2$ .

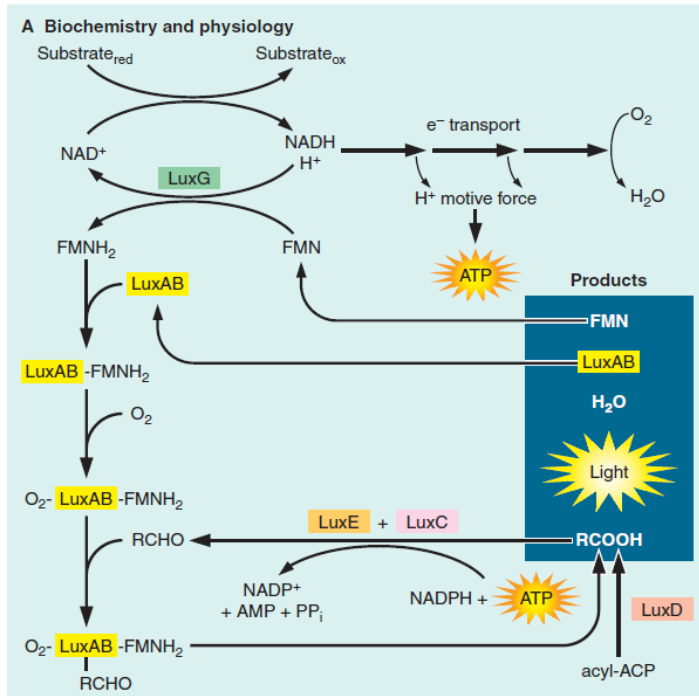


FIGURE (1.5) Chemical reaction inducing *Vibrio fischeri* bioluminescence. Lux AB sequentially binds  $\text{FMNH}_2$ ,  $\text{O}_2$  and an aldehyde ( $\text{RCHO}$ ) that are converted into an acid, FMN and water. Energy stored as ATP is consumed in regenerating the aldehyde substrate. Then, they are released from the enzyme with the concomitant production of light. From Stabb (2005).

A breakthrough in the study of this phenomenon was discovered by Shimomura et al. (1962) with the purification of a protein (aequorin) from a species of Cnidarian (*Aequorea*). This protein, with the addition of  $\text{Ca}^{2+}$ , also causes an intramolecular reaction with bioluminescence emission and without the necessary presence of oxygen. The amount of

emitted photons is proportional to the protein concentration. A similar reaction has been observed in *Cheatopterus* with the addition of  $\text{Fe}^{2+}$ . These new types of proteins do not correspond to the luciferin and luciferase previously described. Therefore, the generic term of photoprotein has been proposed (Shimomura and Johnson, 1969; Prasher et al., 1992, see Table 1.1).

TABLE (1.1) Progress in research on bioluminescence, modified from Shimomura (2012)

Date	Advanced
1885	Discovery of the luciferin-luciferase system
1947	ATP requirement for the firefly bioluminescence
1954	$\text{FMNH}_2$ requirement for bacterial bioluminescence
1962	Aequorine discovery
1966	Photoprotein concept
1974	Identification of a long chain of aldehyde in bioluminescent bacteria
1975	Coelenterazine discovery
1981	Discovery of the autoinducer structure in bacterial luminescence
1984-1985	Cloning firefly luciferase
1985-1986	Cloning bacterial luciferase
1996	Bacterial luciferase structure
2005	Firefly luciferase structure

### 1.1.3 Bioluminescence *in situ* observation

Bradner et al. (1987) classify bioluminescent organisms into two main groups. The first group is composed by bacteria capable of producing a constant light emission without response to external stimulation. Bioluminescent bacteria emit light when the growing conditions are favorable leading to activation of quorum-sensing phenomenon and in presence of oxygen (see paragraph 1.1.5). This bacterial bioluminescence is not detectable using the bioluminescence sensors developed so far.

The second group of bioluminescent organisms defined by Bradner et al., 1987 includes a large phylogenetic diversity of individuals capable of emitting flashes. These organisms

are luminescent "naturally" as a result of biological stimulation or only after mechanical stimulation. Within this group, for most multicellular species, luminescence is controlled by nerve. On the opposite, in unicellular organisms, such as Dinoflagellates or Radiolarians, the bioluminescence is triggered by a pressure differential, resulting in a cell-surface deformation. Mechanical-transducer processes are not fully known. However, it is likely that the mechanical stimulus activates mechano-receptors causing, thereafter, a potential action to the tonoplast, leading to the acidification of the cytoplasm (due to the proton-flux vacuole). This pH reduction directly activates the chemical reaction of bioluminescence ([Fritz et al., 1990](#)). The instrumentation for measuring marine bioluminescence, which has greatly expanded from the 60s to the present day (see Table [1.2](#)), uses this mechanical-stimulation property to detect bioluminescent organisms.

## Quantification of eukaryotic bioluminescence

The term 'non-stimulated' or 'spontaneous' bioluminescence ([Widder et al., 1989](#)) was replaced by 'natural', referring to a bioluminescence reaction generated by stimulus of biological organisms ([Craig et al., 2011](#)). Visual sensors (cameras) are used for the automatic detection of this bioluminescence called 'natural'. The majority of observations and the most common assumptions in the literature estimate very low frequency of these bioluminescence events ([Priede et al., 2006; Widder, 2002](#)). However, the frequency of observations seems controversial and dependent on the instrumentation developed. For example, [Gillibrand et al. \(2007\)](#) measure the frequency of this spontaneous bioluminescence at about 1 event  $\text{h}^{-1}$  between 2,000 and 3,000 m depth. Other studies have estimated the natural bioluminescence to the order of 0.12 event  $\text{h}^{-1}$  at 2,400 m depth. However, recently, [Vacquié-Garcia et al. \(2012\)](#) determined a significantly higher frequency at about 13-25 events  $\text{min}^{-1}$ , between 600 and 1,000 m depth. This frequency was unexpectedly measured by photomultipliers, together with the ARGOS system, that were used in this study during dives of elephant seals (*Mirounga leonina*). From their observations, [Craig et al. \(2011\)](#) provide a linear relationship between the depth and the number of events per minute. This relationship estimated between 1,500 and 2,750 m depth, shows, however, extreme variability maybe due to sampling in spatially

TABLE (1.2) Bathyphotometers developed for *in situ* bioluminescence measurements using mechanical stimulation. Modified from Herren et al. (2005). D: diameter, V: volume. NA: Non Available value.

Source	Deployment	Excitation	flux	D (cm)	V (L)
Clarke and Kelly (1965)	profiler ( $\rightarrow$ 2,000 m)	impeller	0.37 L s $^{-1}$	2.5	NA
Soli (1966)	shallow profiler	impeller, detector	variable	2.54	0.1
Seliger et al. (1970)	towed	impeller	0.2 L s $^{-1}$	1.3	NA
Hall and Staples (1978)	profiler ( $\rightarrow$ 200 m)	turbulence, pump	NA	NA	0.025
Aiken and Kelly (1984)	profiler ( $\rightarrow$ 1,000 m)	turbulence	1-5 dm $^3$ s $^{-1}$	2.8	0.02
			$\hat{a}$ 5 m s $^{-1}$		
Greenblatt et al. (1984)	turbulence		1.1 L s $^{-1}$	1.6	0.025
Nealson (1985)	profiler ( $\rightarrow$ 300 m)	1 L s $^{-1}$	2.5	0.1	
Swift et al. (1985)	profiler	impeller	0.25 L s $^{-1}$	1.4	NA
Buskey (1992)	profiler	inlet grid	6.3 L s $^{-1}$	NA	4.7
Widder et al. (1993)	profiler	inlet grid	16-44 L s $^{-1}$	12	11.3
Neilson et al. (1995)	Sea mooring	inlet propeller/surge	1-12 L s $^{-1}$	12.7	5
Fucile (1996)	profiler (2 m s $^{-1}$ )	inlet grid	15.7 L s $^{-1}$	10	2
Geistdoerfer and Vincendeau (1999)	profiler ( $\rightarrow$ 600 m)	inlet grid	0.5 L s $^{-1}$	1.7	0.19
McDuffey and Bird (2002)	shipboard	turbulence	1 L s $^{-1}$	1.3	0.049
Bivens et al. (2002)	profiler	turbulence	1 L s $^{-1}$	1.5	0.025
Herren et al. (2005)	multiplateform	impeller	0.5 L s $^{-1}$	3.2	0.5

heterogeneous environment. Finally, the literature remains poor in the estimation of the non-stimulated bioluminescence in benthic and pelagic environments. Therefore, its importance is relatively unknown. This lack of information seems to be directly connected to the instrumentation used to estimate such bioluminescence.

Marine bioluminescence is widely observed from the coast to the open sea and from the surface to the deep, where bioluminescence emission was observed up to 7,500 m (Priede et al., 2006). In the bathypelagic environment (deeper than 1,000 m), bioluminescence is the only source of visible light, giving it a major role in the detection of meso- and bathypelagic organisms. On a vertical profile of the water column in the Atlantic, the observed bioluminescence decreases linearly up to 2,500 m then, staying at a stable intensity up to 4,000 m (Geistdoerfer and Cussatlegras, 2001). According to Rudyakov and Tseytlin (1989), beyond 1,000 m depth, most of the bioluminescence would be emitted by mesoplankton (0.2 to 20 mm of diameter).

## Quantification of potentially bioluminescent bacteria

According to Yetinson and Shilo (1979), in the eastern Mediterranean, the amount of cultivable bioluminescent bacteria (Unit Forming Colony UFC) along the coast and at different seasons is estimated constant. In contrast, the bioluminescent bacterial diversity in the water column varies. Potentially bioluminescent marine bacterial species are: *Vibrio*, *Photobacterium*, and *Shewanella*, all belonging to the subclass of Gammaproteobacteria. Amongst these species, *Photobacterium phosphoreum* (Cohn 1878) would be the most represented in the Mediterranean (Gentile et al., 2009). It is ranked among the gram-negative Bacteria, rod-shaped, chemoorganotrophe, non-sporulating, heterotrophic and mobile with 1-3 flagella (Dunlap and Kita-Tsukamoto, 2006). According to Hastings and Nealson (1977); Dunlap (1984) and Makemson (1986), the emission of bioluminescence by this bacterial strain is estimated between  $10^3$  and  $10^4$  photons  $s^{-1}$   $cell^{-1}$ . For all bioluminescent bacterial species, these values may vary from 1 to  $10^5$  photons  $s^{-1}$   $cell^{-1}$  according to the same authors, or  $10^2$  to  $10^4$  photons  $s^{-1}$  according to Bose et al. (2008). It depends on the strain, the environment or the *lux*-gene activation.

Ruby et al. (1980) estimated that, from 100 to 1,000 m in the Atlantic, between 0.4 and 30 UFC, belonging to *P. phosphoreum*, were found in 100 mL. They described little seasonal variation and few other bacterial species associated. From 4,000 to 7,000 m depth, few bacterial cells are observable (<0.1 UFC). In the Mediterranean, in the Strait of Sicily (Ionian Sea), *P. phosphoreum* represents nearly 87% of bioluminescent bacteria while *Vibrio* and *Shewanella* spp. are occasionally encountered. Gentile et al. (2009) estimated that in the Tyrrhenian Sea, the isolated bacteria up to 500 m depth are mainly associated to *P. phosphoreum*, whereas, up to 2,750 m depth, isolated bacteria belong only to *Photobacterium kishitanii* (taxonomically close to *P. Phosphoreum*).

*P. phosphoreum* is described as a bacterial strain found almost only in combination with fish, mainly in the intestines, and not in the organs devoted to luminescence (Herring, 1982). Hastings and Marechal (unpublished, see Nealson and Hastings, 1979) grew on Petri dish bacteria from the gut of Sicily-deep-water fish (Messina). Amongst these, 40 to 100 % of UFC are luminescent and represented by the single species *P. phosphoreum*. An hypothesis to explain the abundance of *P. phosphoreum* in the water column is that this bacterium is the major organism in the fish digestive tract. The constant rejection of feces, in the environment, will lead to an increase, in the water column, in free-living or attached to the particles bacteria.

### **Effective bacterial bioluminescence, communication "cell-to-cell"**

The presence of potentially bioluminescent bacterial strains in the sea does not indicate a bioluminescent activity. Indeed, the bioluminescence reaction is controlled by the autoinduction of genes. Each cell produces a quantity of molecules, called autoinducers (N-Acylated homoserine lactone or AHL for *Vibrio fischeri*) and cross cell membranes. The accumulation of autoinducers will allow transcription of *lux* gene, the synthesis of luciferase and, thereafter, the emission of bioluminescence (Nealson et al., 1970; Eberhard and Hastings, 1972, see Figures 1.7 and 1.6). This phenomenon, called "quorum sensing" has been described historically in *Vibrio fischeri*, in the 1970s. This form

of communication "cell-to-cell" is widely described and assimilated to the one of a multi-cellular organism.

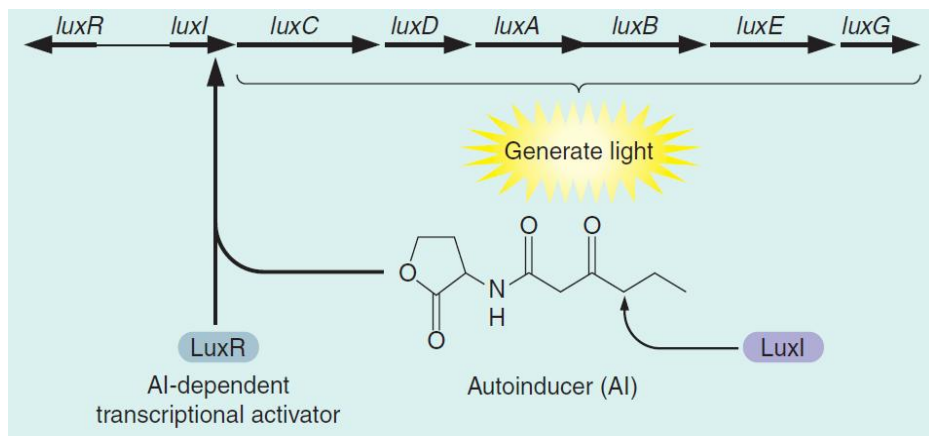


FIGURE (1.6) Genetics and quorum sensing, from [Stabb \(2005\)](#). *luxI* and *luxR* are involved into the quorum sensing regulation. The autoinducer (AI) LuxI interacts with LuxR and leading to the stimulation of *lux* genes.

In the marine environment, these autoinducers are quickly diluted and the cell concentration necessary to the light emission (estimated between  $10^8$  and  $10^9$  cells  $\text{mL}^{-1}$ ) is rarely achieved. However, in the light organs of some species, bioluminescent bacteria can reach a concentration of  $10^{11}$  cells  $\text{mL}^{-1}$ . Such concentration can also be reached by bacterial colonization of organic particles ([Hmelo et al., 2011](#)), or marine snow ([Azam, 1998](#); [Alldredge and Cohen, 1987](#)) leading to a sufficient concentration of autoinducer and consequently the emission of bioluminescence (see Figure 1.7).

Finally, all the informations in these studies, for both Eukaryotes and bioluminescent bacteria, remain dependent on instrumentation or methodology. Indeed, so far, only the stimulated bioluminescence (second group organization described in paragraph [1.1.1](#), [Bradner et al., 1987](#)) was quantifiable automatically using *in situ* instrumentation. On the contrary, the quantification of bioluminescent bacteria has to be carried out through the discrete sampling of sea water, allowing only the quantification of cultivable bacteria (estimated to be about 1% of total bacteria).

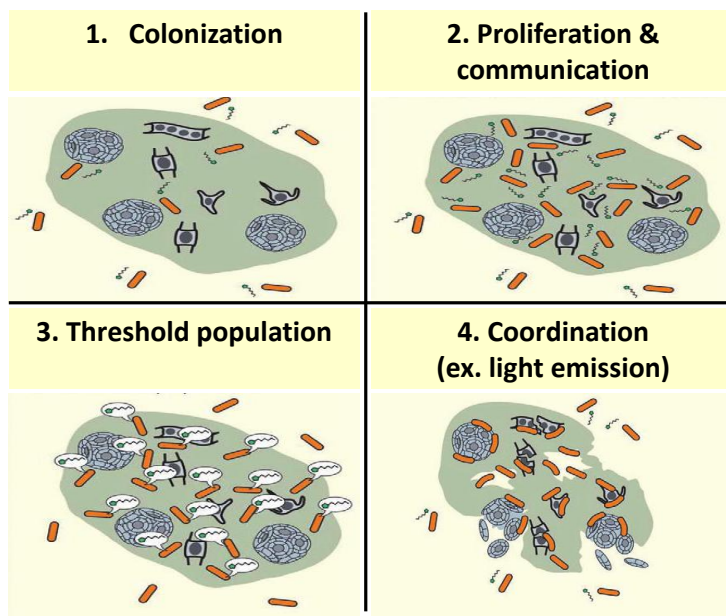


FIGURE (1.7) Quorum-sensing representation. 1: Bacteria are attached to sinking particles. 2: Population grows and the quorum-sensing signal increases. 3: Quorum-sensing signal reaches a threshold concentration. 4: Bacteria initiate a coordinated expression (bioluminescence for example). Modified from [Hmelo et al. \(2011\)](#).

The introduction of automated detectors for non-stimulated bioluminescence, the monitoring of biological activity into the deep sea and the description of the variability over time remain to be explored.

#### 1.1.4 Sensitivity of bioluminescence to environmental variables

##### Turbulence and current

Many studies focused on the action of mechanical stimulation on the bioluminescent planktonic organisms (mainly Dinoflagellates, considered as the most abundant phylogenetic group in bioluminescent coastal waters). [Cussatlegras and Le Gal \(2005\)](#) describe the effect of mechanical flow stimulation of water. [Latz et al. \(1994\)](#) describe the effect of a laminar flow. Then [Rohr et al. \(1998\)](#) describe effects of the turbulence created by the swimming dolphins on the luminescence emitted by these organisms. Unfortunately, few studies have quantified mechanical stimulation that is necessary to stimulate bioluminescence in deep-sea animals. However, [Hartline et al. \(1999\)](#) measure

the minimum force required to elicit bioluminescence reaction from *Pleuromamma xiphias*, a mesopelagic copepod species.

Bioluminescence emission for Dinoflagellates has been described in Cussatlegras (2006). These organisms are mechanically stimulated using accelerations or pressure from fluids. A turbulent flow is efficient to stimulate bioluminescent organisms and various bathyphotometers use this principle (Losee et al., 1985; Widder et al., 1993) for the light measurement. Laminar flux can also stimulate organisms. For bathyphotometers, most of the time, a grid stimulates organisms by generating a uniform and isotropic turbulence Cussatlegras (2006). Under mechanical stimulation, Dinoflagellates have been observed to emit light within less than 20 ms and with the light emission of a flash lasting 100 ms to about 250 ms. Copepods flash emission was measured during 50 to 150 ms.

It is worth noting that the bioluminescence in bacteria is not influenced by mechanical stimulation, current or turbulence (Bradner et al., 1987).

## Temperature

The joint action of temperature associated with mechanical stimulation was apprehended by Han et al. (2012). In a large volume of seawater, these authors were unable to determine the relationship between temperature, ranging from 15.8 to 19.2 °C, and bioluminescence emitted by *Noctiluca* sp.. Olga (2012) tested the effect of temperature on two species of Ctenophora. The author observes that the amplitude and duration of bioluminescence, chemically or mechanically stimulated, is also affected by the medium temperature with an optimum at 22 °C and 26 °C, for *Beroe ovata* and *Mnemiopsis leidyi*, respectively.

For bioluminescent bacteria, temperature has, by itself, an influence on the intensity of bioluminescence emission. However, this link is sometimes indirect since temperature will act on the growth of microorganisms and therefore impact the measure of bioluminescence. Temperatures limiting the emission of light are variable, depending on the studied bacterial strains (Harvey, 1952). However, the chemical bioluminescence reaction is limi-

ted by the inactivation temperature of luciferase, between 30 and 35°C (Dorn et al., 2003).

### pH

For bacterial bioluminescence, the study of Dorn et al. (2003) shows that temperature and pH of the medium can justify 98.1% of the intensity variation for bacteria grown on a salicylate substrate. consequently, these two variables have a major importance. The pH optima are variable depending on the bacterial strains. It is worth noting that the activation of luciferase is effective only between 6.0 and 8.5 pH units, outside this range, this system will not be activated. Moreover, Dorn et al. (2003) show that a small variation, of about 0.2 pH units, can impact bioluminescence.

### Salinity

For marine bacterial strains, culture-medium salinity is generally based on NaCl concentration similar to environmental conditions (Lee et al., 2001; Eley, 1972). The intensity of bioluminescence increases at this concentration ( $30 \text{ g L}^{-1}$ ) compared to a concentration of about  $10 \text{ g L}^{-1}$ . Indeed, with the ionic concentration too low, the osmotic pressure can not be maintained, leading to a disruption of the cell membrane (Vitukhnovskaya and Ismailov, 2001; Nunes-Halldorson and Duran, 2003). Furthermore, the increase in atomic weight of halogen anions, such as KCl , KI and KBr, causes lowering of the bacterial bioluminescence (Gerasimova and Kudryasheva, 2002; Kirillova and Kudryasheva, 2007).

### Hydrostatic pressure

In the marine environment, the hydrostatic pressure plays an important role with an increase of 0.1 MPa every 10 m. However, very few studies have examined the effect of hydrostatic pressure on bioluminescence. This parameter could strongly influence planktonic bioluminescent organisms in nyctemeral variations, or when water-masses movements occur.

Amongst the few studies, Strehler and Johnson (1954) show that the bioluminescence, emitted by an extract of *Achromobacter fischeri* or on living cells of *Photobacterium phosphoreum*, is related to the combined effect of temperature and pressure. An increase

in pressure, ranging from 0.1 to 55 MPa, will increase bioluminescence activity for a temperature higher than the optimum. In contrast the same variation in pressure will inhibit the bioluminescence activity at lower temperatures (Figure 1.8).

More recently, Ueda et al. (1994) were interested in the joint effect of the temperature and pressure of the firefly luciferase (Figure 1.8 B). In these experiments, a mixture of luciferase, luciferin and ATP is used. These authors have shown that an increase in pressure up to 40 MPa, increases bioluminescence at a temperature above the optimal temperature ( $22.5^{\circ}\text{C}$ ) and decreases it at temperatures below the optimum value.

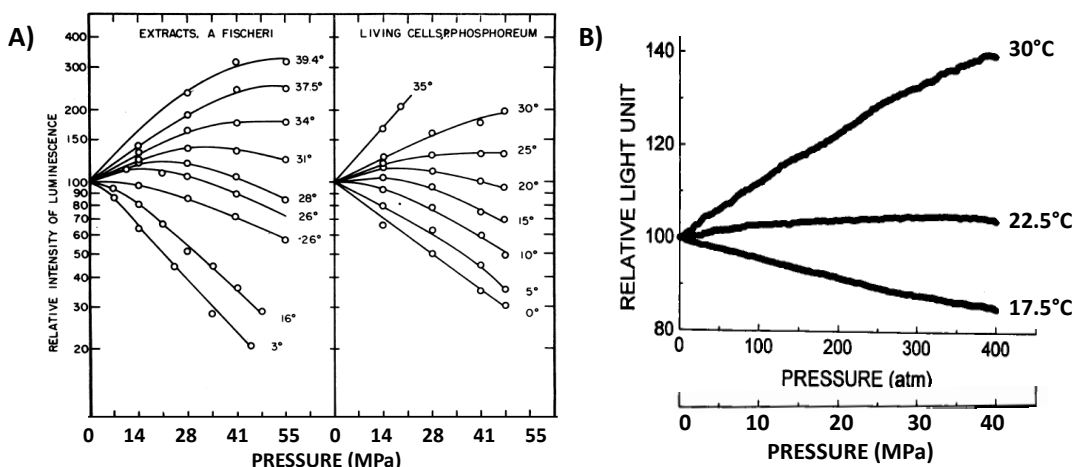


FIGURE (1.8) Effects of temperature and pressure conjointly on A) *Achromobacter fischeri* extract and *Photobacterium phosphoreum* living cells, from Strehler and Johnson (1954) and B) firefly luciferase, modified from Ueda et al. (1994).

In a completely different approach, Watanabe and Tanaka (2011) estimate the effect of hydrostatic pressure on the Dinoflagellate *Pyrocystis lunula* to determine the effect of breaking waves on bioluminescent organisms. The authors apply, to simulate the effect of increasing pressure, a water jet on a wall. They demonstrate that the imposed maximum pressure leads to a maximum bioluminescence.

### Bioluminescent bacteria and oxygen

In the chemical reaction of bioluminescence, oxygen plays a major role of electron donor (see Figure 1.3). The concentration of dissolved oxygen in the medium interacts with the

light emission of these organisms. Oxygen would be assigned, at first, to the respiratory chain and then to the light emission. As an example, Grogan (1984) shows that when the oxygen system is inhibited, there was a drop in bioluminescence and that this decrease is attenuated when the respiratory system is blocked with inhibitors. For species in symbiosis, with limited possibility to increase in biomass, energy from catabolic reactions is converted into light (Bourgois et al., 2001). Finally, the system, using luciferase to emit bioluminescence, is considered as an alternative electron transport. Lloyd et al. (1985) observed that after a long period in anaerobiosis, the aeration of the medium will result in a bioluminescence peak for a few seconds. This peak is due to the accumulation of luciferase-FMNH<sub>2</sub> complex and is not observed when aeration medium is progressive. According to Nealson and Hastings (1979) the amount of luciferase produced is identical between anaerobic and aerobic conditions.

Makemson (1986) estimates the oxygen consumption by the bioluminescent bacterial strains to be 50-120 nmol O<sub>2</sub> min<sup>-1</sup> 10<sup>9</sup> *Vibrio fischeri* cells and 80-120 nmol O<sub>2</sub> min<sup>-1</sup> for 10<sup>9</sup> *Vibrio harveyi* cells. These values range from 10 to 15 nmol O<sub>2</sub> min<sup>-1</sup> for 10<sup>9</sup> cells (Karl and Nealson, 1980) and can reach 120 to 300 nmol O<sub>2</sub> min<sup>-1</sup> for 10<sup>9</sup> cells in other publications (Watanabe et al., 1975).

The use of chemicals permit to discriminate the oxygen consumption attributed to the formation of bacterial growth and oxygen consumption dedicated to the issue of light. Amongst these compounds, the CCCP (Carbonyl Cyanide m-Chlorophenylhydrazone), the KCN or the cyanide were commonly used (Grogan, 1984; Karl and Nealson, 1980; Makemson, 1986). From these experiments, the proportion of oxygen consumed for bioluminescence is estimated to be about 11 to 17% with no difference between the various bacterial species tested. This percentage falls to 0.007% for non-symbiotic species. Makemson (1986) and Nealson and Hastings (1979) estimate this percentage to be 12% for *Vibrio harveyi* and 20% for *Vibrio fischeri*. However, Dunlap (1984) estimates this percentage as low as 3.4 %. Hastings and Balny (1975) estimate the production of 0.0001 to 0.1 photon per molecule of oxygen consumed. This production is also called 'quantum yield'<sup>3</sup>.

---

3. **Quantum yield :** the quantum yield *in vivo* of bioluminescence is the number of photons emitted

### ***In situ* environmental variables**

*In situ*, few studies have attempted to correlate the intensity of measured bioluminescence with environmental variables. Lapota et al. (1989); Cussatlegras et al. (2001) and Craig et al. (2010) show a correlation between the *in situ* bioluminescence and the chlorophyll concentration, using the later as a proxy for photosynthetic-Dinoflagellates biomass. Quantification of bioluminescent bacteria was correlated with certain environmental variables such as temperature, depth, salinity, nutrient limitations or sensitivity to photo-oxidation (Dunlap and Kita-Tsukamoto, 2006). However, the characterization of the relationship between environmental variables and bioluminescence intensity, seems very different from one study to another, with a strong dependence on the depth of the studied site. Similarly, the spatial scale of observation of these correlations is also very variable.

The links between the bioluminescence activity and environmental variables still need to be studied in a controlled environment laboratory or *in situ*. The establishment of *in situ* bioluminescence sensors, suitable for sampling the 'natural' bioluminescence, combined with sensors, dedicated to environmental variables, will determine the dynamics of these organisms and their sensitivity to the ecosystem changes.

### **1.1.5 Ecological roles in the marine environment**

#### **Communication between Eukaryotes**

Various light organs were identified in the bioluminescent eukaryotes: the scintillons (Dinoflagellates), the photocytes (Cnidaria, Ctenophora and Appendicularia) or the secretory cells (Ostracods) (Fogel and Hastings, 1972; Desa and Hastings, 1968). The photocytes can be distributed all over the body, or regrouped in light organs called photophores. In Dinoflagellates, the scintillons are cortical vesicles. These organelles migrate from the cytoplasm to the vacuole in which they discharge their luciferin and luciferase,

---

by O<sub>2</sub> molecule and used by the luciferase.

responsible for the bioluminescence reaction. Some species are not bioluminescent by themselves but are symbionts with bioluminescent bacteria, that they accumulate in specialized organs (Ruby and Nealson, 1976; Dunlap et al., 2009; Rader and Nyholm, 2012).

The emission of bioluminescence is an energy consuming biological reaction for organisms. Indeed, the light emission as flashes have duration time from few milliseconds to several seconds. This light is even emitted continuously for bioluminescent bacteria. A major question in the study of this phenomenon is to understand its role and the benefits obtained by bioluminescent organisms (Stabb, 2005). The light production has been proposed as being necessary to communication, predation, protection, and detection (Haddock et al., 2010; Widder, 2010; Rivers and Morin, 2012), Figure 1.9). Bioluminescence can alternatively be used for several or all of these functions depending on the circumstances (Mesinger and Case, 1992; Fleisher and Case, 1995; Roithmayr, 1970).

A different role in bioluminescence is directly related to the detection of this light in marine environment. Indeed, it is surprising to see the extent of the light emitted by these organisms, in an environment where the darkness is a major feature (Gillibrand et al., 2007). According to Priede et al. (2006), bioluminescence associated with 'food falls' could be observed up to ten meters away. If this sounds relatively low across the ocean, in an oligotrophic environment, it is still a significant increase in the probability of finding a source of nutrition, visible to a large number of 'scavenger' organisms (Warrant and Locket, 2004; Turner et al., 2009). A recent study also demonstrates the role of bioluminescence. Indeed, Vacquié-Garcia et al. (2012) found that the dives of elephant seals for food are positively correlated with recordings of the light emitted by organisms. These results have been demonstrated *in situ* and up to 1,050 m depth, showing that the presence of bioluminescence is actually an indicator of potential prey for predators in the deep sea.

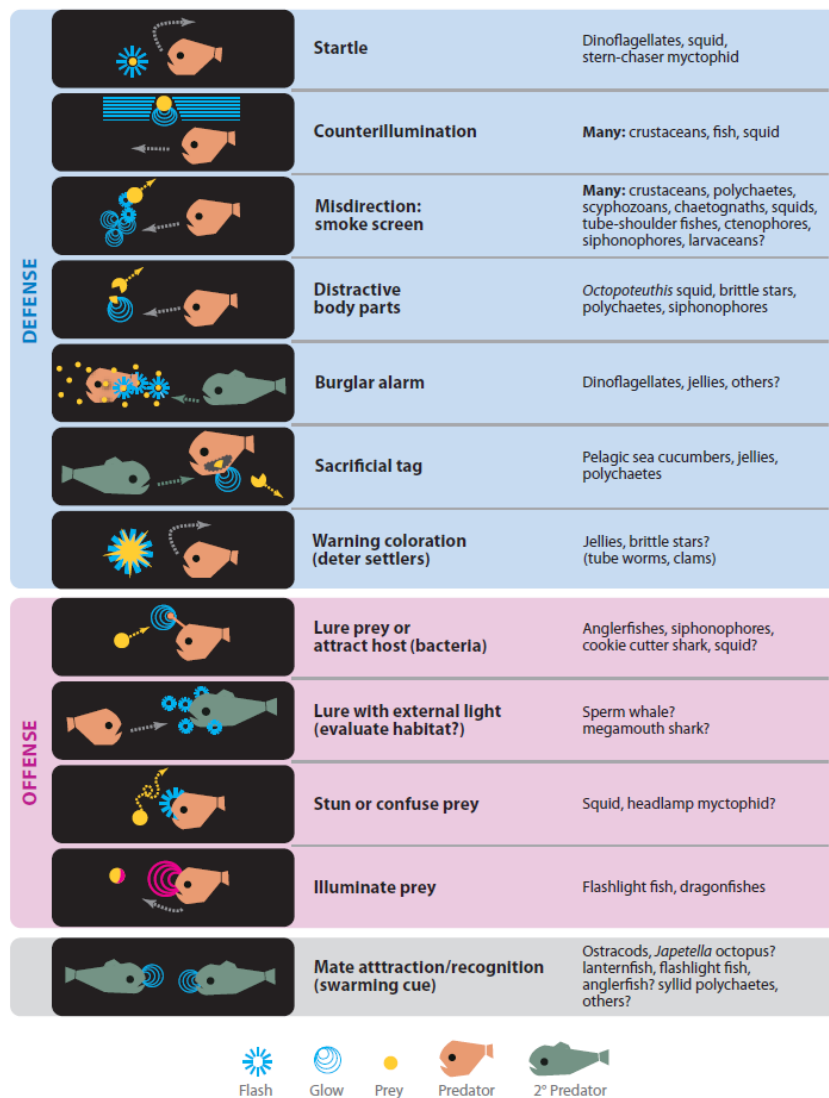


FIGURE (1.9) Ecological roles of bioluminescence activity, from Haddock et al. (2010)

## Communication in Bacteria

Regarding the role of bioluminescence for symbiotic bacteria with certain organisms (fish, squid ...) (Ruby and Nealson, 1976), the gain related to the light emission seems clear for each symbiont. Bacteria provide the host the necessary light for attracting preys or partners or to escape predators (Dunlap et al., 2009). The bacterial host provides an environment more favorable to their growth (nutrient sources, temperature ...). In the

case of non-symbiotic bioluminescent bacteria, the role of bacterial bioluminescence is less obvious.

The major hypothesis concerning the role of bioluminescent bacteria is directly related to the carbon cycle and called "bait hypothesis" (Hastings and Nealson, 1977; Robison et al., 1977; Ruby and Morin, 1979; Andrews et al., 1984). Indeed, bioluminescent bacteria colonize particles falling through the water column and the fecal pellets. The bioluminescence emitted would lead to a higher probability of visual detection of nutrient sources and therefore to the ingestion of these particles by zooplankton. The fecal pellets are more concentrated in essential minerals needed for the growth of organisms with a C: N: P ratio of 22: 2.8: 1, showing a high concentration of phosphorous components (Geesey et al., 1984).

This hypothesis was observed by Andrews et al. (1984) and recently demonstrated by Zarubin et al. (2012). Andrews et al. (1984) found that fecal pellets from copepods and particulate materials are luminescent. In Zarubin et al. (2012), the authors described and demonstrated each step of this theory. First of all, bioluminescence was tested as an attractor to the zooplankton. Then, the luminescence of zooplankton following ingestion of these bacteria was demonstrated. Finally, the consumption of the newly bioluminescent zooplankton was quantified. Once in the digestive tract of zooplankton and fish, microorganisms found favorable conditions to their development, as well as a means of effective dispersion.

A second hypothesis suggests that the role of bacterial bioluminescence is related to the response of the luciferase in the transport of oxygen. On the one hand, (Hastings et al., 1985; Meighen, 1993) show that, for bacterial symbionts in organs, metabolic function of bioluminescence is an alternative to the electron transport in this low oxygen medium. On the other hand, Baltar et al. (2013) indicate that an oxidative stress caused by H<sub>2</sub>O<sub>2</sub> might affects prokaryotic growth and hydrolysis of specific components of the organic matter pool. To counteract this process, the bioluminescence reaction could detoxifies molecular oxygen by its reduction Timmins et al. (2001).

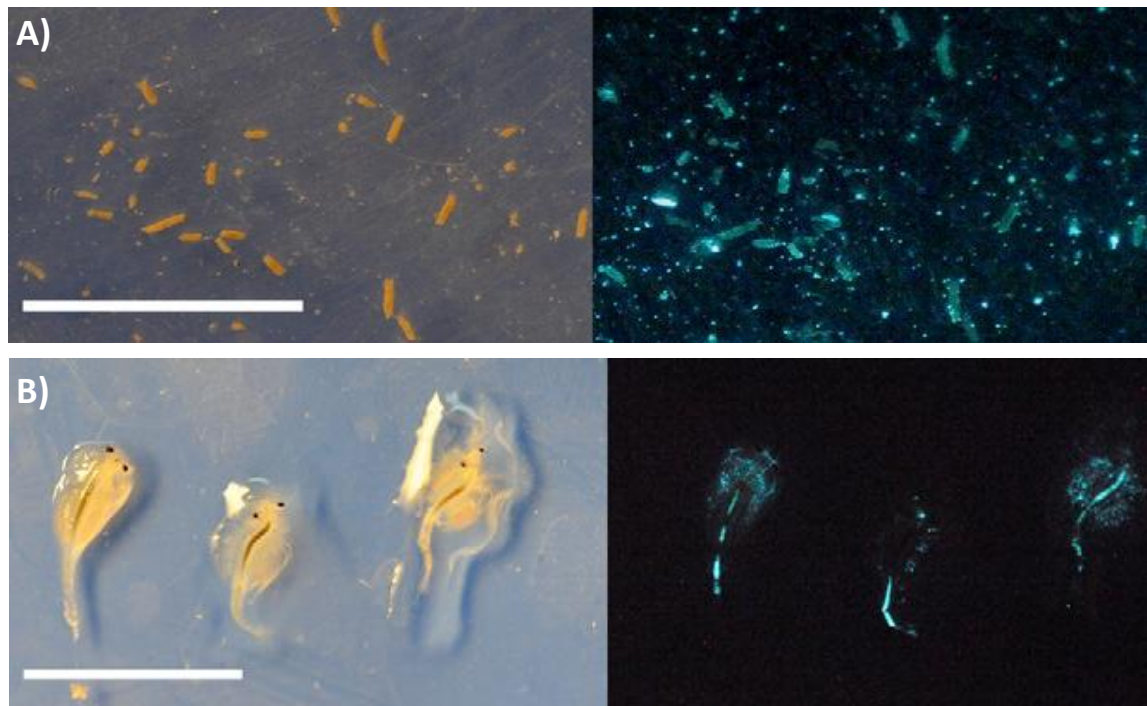


FIGURE (1.10) A) Fecal pellets of *Artemia salina* produced after swimming and feeding on small colony fragments of the bioluminescent bacterium *Photobacterium leiognathi* (visible in the background) photographed in room light (Left) and in darkness (Right) B) Glow of zooplankton (*Artemia salina*) after contacting and ingesting small particles broken off colonies of the bioluminescent bacterium *Photobacterium leiognathi*. The photograph on the left was taken in room light, and the photograph on the right was taken in darkness using long exposure (30 s). Scale bar: 1 cm. From Zarubin et al. (2012).

## 1.2 Afterthought and objectives of the study

### 1.2.1 Multidisciplinary objectives

The objectives of this thesis can be defined following two scientific questions:

- (i) Bioluminescence is described as "weak" in the deep sea, compared to the ocean surface, but are there variations in light intensity over time and how to explain them ?

The ANTARES neutrino telescope was used as a sentinel, in the deep sea, for marine bioluminescence. This observation site, with about 850 photomultipliers, on a surface of nearly 0.1 km<sup>2</sup>, allows the continuous detection of non-stimulated bioluminescence, at high frequency and in real time, since 2007. At immediate vicinity of this network, a mooring line is dedicated to the sampling of environmental variables. Chapter 2 describes the multivariate dataset. The use of a biological indicator (bioluminescence) in the deep sea, sampled automatically and at high frequency, will be validated at the end of this Chapter. Chapter 3 provides two different statistical methods appropriated to the analysis of changes in time and frequency of environmental time series, defined as non-linear and non-stationary. The work proposed in these two chapters allows understanding for oceanographic data at the ecosystem scale. In this section, all bioluminescent organisms will be considered.

**(ii) In the deep sea, what is the part of bacterial bioluminescence in the emission of light *in situ* ?**

The phenomenon of bioluminescence in Eukaryotes is widely studied. However, because of sampling difficulties and the lack of existing instrumentation, bacterial bioluminescence has only been poorly considered, so far. Indeed, the literature offers few studies characterizing or quantifying *in situ* bioluminescent bacterial communities. In addition, these studies are often old with the use of isolation techniques or bacterial culture allowing only partial detection of potentially bioluminescent strains (about 1% of the bacterial strains is defined as cultivable). In other studies, [Yetinson and Shilo \(1979\)](#), [Malave-Orengo et al. \(2010\)](#) and [Gentile et al. \(2009\)](#) perform a one-time sampling in time and space while [Asplund et al. \(2011\)](#) focus only on the ocean surface. Bacterial bioluminescence would be involved in the remineralization rate of organic matter in the deep sea according to the 'bait hypothesis' (see section 1.1.3), existing for thirty years but only recently demonstrated. Its description and its quantification seem an interesting approach not enough developed.

To reach the understanding of the part of bacterial bioluminescence into light emission,

two axes are proposed. First, environmental forcings, are they likely to influence the bacterial bioluminescence? Chapter 4 develops the effects of environmental variables (hydrostatic pressure, temperature, and carbon concentration) on bacterial bioluminescence, at the population scale. This laboratory work has been performed in a controlled environment, and with the use of a model strain isolated at the study site (*Photobacterium phosphoreum* ANT-2200). This is an intermediate step to answer the scientific objectives *in situ*. Finally, Chapter 5 will approach the question of the bacterial part in the emission of bioluminescence, through the use of the preliminary results of a survey over the year 2011, near the site ANTARES, and at 2,000 m depth. Total prokaryotic communities are described and bioluminescent ones are quantified using molecular biology methods. The part of bioluminescent bacteria within the bioluminescence signal detected by photomultipliers is also estimated and discussed.

The " Conclusions and Perspectives " part will give a critical summary of the objectives and contributions of this work and the prospects that will have to be developed after this work.

### 1.2.2 A study at several scales

The study of an ecosystem confronts with the choice of a characteristic observation scale. The observation of the community population dynamics and of the processes that are influencing them, requires to take into account variations in time and space. This will to the understanding of the observed phenomenon instantaneously, but also its spatio-temporal dynamics. The chosen scale will define variability associated with observed processes (Hewitt et al., 2007). The studied ecosystem varying into three dimensions (time, vertical and horizontal spatial variations), each of these dimensions has an inherent variability. Ecological studies suggest the concept of multi-scale theory to take into account a set of connections at different scales (Legendre et al., 1997; Anderson and Cribble, 1998). If the importance of the characteristic scales of studied processes in ecology is recognized, few studies take it into account in the measurements or in the result interpretation.

In this work, we try to keep a link between the different scales of studied processes. In Chapter 2 and 3, the spatial and temporal variations are taken into account at the ecosystemic level (annual observation and regional scale). Chapter 4 is devoted to a population level approach with the study of a bacterial strain (hourly observations and microscale). Finally, Chapter 5 provides an approach of the community level interacting in this ecosystem (daily observations and local scale).



# CHAPITRE 2

---

## *In situ* bioluminescence in the deep Mediterranean Sea (ANTARES site)

---

### Sommaire

---

<b>2.1</b>	<b>Introduction : interest of recording long time series in environmental science</b>	<b>31</b>
<b>2.2</b>	<b>Instrumentation and mathematical concepts for the observation of oceanographic variables</b>	<b>33</b>
2.2.1	ANTARES site and environmental context	33
2.2.2	Description of the IL07 instrumented line	34
2.2.3	Data description : the regression trees approach	37
<b>2.3</b>	<b>Multivariate survey at high frequency and real-time sampling</b>	<b>38</b>
2.3.1	Water masses proxies	38
2.3.2	Currentology	40
2.3.3	Bioluminescence interaction with current	42
2.3.4	Univariate and multivariate approaches using regression-tree method	43
2.3.5	Analysis of <i>in situ</i> images from bioluminescent organisms	46
<b>2.4</b>	<b>Article 1</b>	<b>51</b>

2.4.1	Foreword . . . . .	51
2.4.2	Deep-sea bioluminescence blooms after dense water formation at the ocean surface . . . . .	52
<b>2.5</b>	<b>Conclusions . . . . .</b>	<b>73</b>

---

## 2.1 Introduction: interest of recording long time series in environmental science

Time series are set of data obtained by consecutive measurements with time dependence. Historically, astronomers were first scientists to study such chronological data. However, in the XVIII<sup>th</sup> century, even if predictions were considered as competing with God, Halley was the first scientist to predict the next comet event, based on its periodicity. Nowadays, one admits that time series analysis is essential to understand, forecast, monitor or control systems.

Edwards et al. (2010) described, over the last 100 years, some of the longest international environmental and biological time series recorded in oceanography (Figure 2.1). Records of such time series are useful to detect episodic events in real time. They can be used to coordinate and provide a long term context for shorter duration scientific expeditions. At a different time-scale, long-term survey often lead to scientific strategies for marine-ecosystem management in order to face anthropogenic changes. These various objectives have led to the development of autonomous and remote instrumentation, as well as new sensors (biological, physical or chemical). Moreover, these infrastructures are often dedicated to multidisciplinary research in order to reduce costs and efforts. The increasing maturity of autonomous or mobile platforms enables adaptive observing systems and increases the access to more extreme environments such as open and deep sea.

The ANTARES observatory (Astronomy with a Neutrino Telescope and Abyss environmental RESearch) is a european project belonging to several observatory programs such as the European Seas Observatory NETwork (ESONET), EUROSITES (FP7, UE) or the international Global Ocean Observing System (GOOS). The ANTARES collaboration is composed of about 150 engineers, technicians and physicists and mainly financially supported by 6 countries (France, Netherlands, Spain, Italy, United Kingdom, Russia). The first aim of this program is the detection of high-energy particles with the immersion of a neutrino telescope in the deep Mediterranean Sea. Indeed, neutrinos are transformed, with the emission of a single photon, into muon particles when crossing the Earth

crust. This light emission is more easily detected in the sea due to water-transparency properties, using photons detectors, named photomultipliers. Astrophysicists are able to detect the trajectory of these single-photon emissions across the detector on a global volume of about  $0.1 \text{ km}^3$ . The use of the ANTARES telescope has been extended to a multidisciplinary objective by including oceanographers to the project. An instrumented line has been added to the observatory in order to record oceanographic long time series at this station.

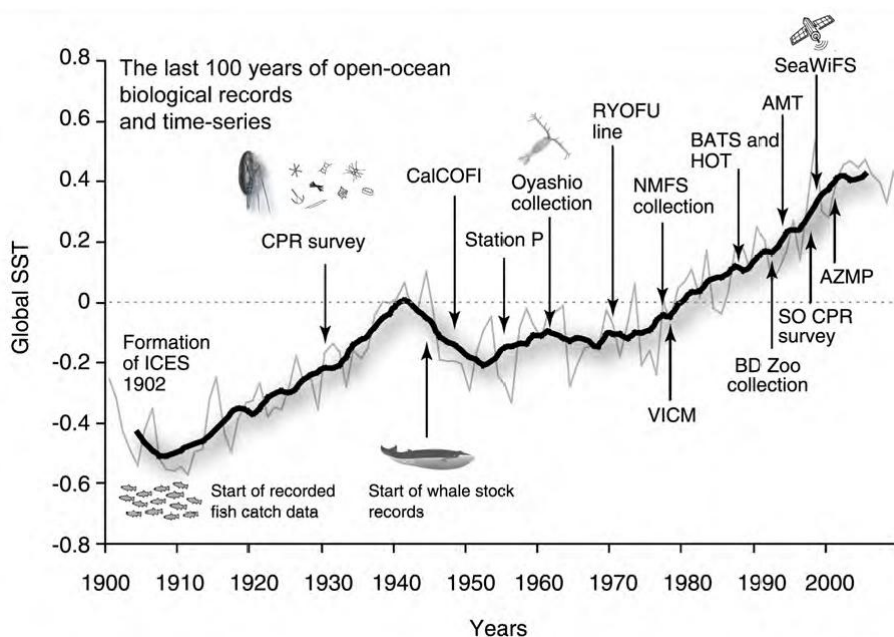


FIGURE (2.1) Representation of some of the international open-ocean biological records and time series since 1900. Station P (North Pacific), RYOFU line (west Pacific transect), VICM (Vancouver Island Continental Margin time series), NMFS (National Marine Fisheries Service collection), BATS (Bermuda Atlantic Time series Study), HOT (Hawaii Ocean Time series program), BD Zoo (North Coast of Spain), SO CPR survey (Southern Ocean CPR survey), AMT (Atlantic Meridional Transect), and AZMP (Atlantic Zone Monitoring Program). From Edwards et al. (2010).

## 2.2 Instrumentation and mathematical concepts for the observation of oceanographic variables

### 2.2.1 ANTARES site and environmental context

The ANTARES site is located in the North-Western Mediterranean Sea, 40 km off the french Provencal coast ( $42^{\circ}48'N, 6^{\circ}10'E$ ), at 2,475 m depth, down to the steep continental slope. The position and depth for the ANTARES station were optimized for various reasons (technical, geophysical...). The observatory had to be immersed at depth greater than the euphotic zone for light interference and below 1,000 m depth for space and volume reasons. The vicinity to the shore was also of major importance to connect the site to the coast. Moreover, the site location was optimized for the optical and transparency properties of the water as well as the low current speed to avoid sedimentation and biofilms on the structure (Amram et al., 1999, 2002) and (Aguilar et al., 2004).

Twelve mooring lines dedicated to photon detection are immersed at the ANTARES site (see Figure 2.2 A) close to an instrumented line, namely IL07 line, mainly dedicated to the sampling of oceanographic and environmental data (Figure 2.2 B). The IL07 is composed of 2 optical modules (containing photomultipliers tubes), 2 Acoustic Doppler Current Profilers (ADCP), 2 video cameras, 1 Conductivity Temperature Depth probe (CTD) and 1 Aanderaa<sup>®</sup> optode oxygen sensor. The telescope mooring lines are linked to the shore by a cable providing mechanical strength, electrical contact and optic-fiber readout. This cable is stored to the seabed by a dead-weight anchor and kept vertical by a buoy at the top of each mooring lines. This infrastructure allows the access to real-time data from the deep sea. The ANTARES telescope has been immersed, in its last configuration, in December 2007, with a break in the data acquisition from July to September 2008 due to maintenance operations. In October 2010, the instrumented line IL07 has been disconnected and taken off involving a stop in the survey until its re-immersion in March 2013.

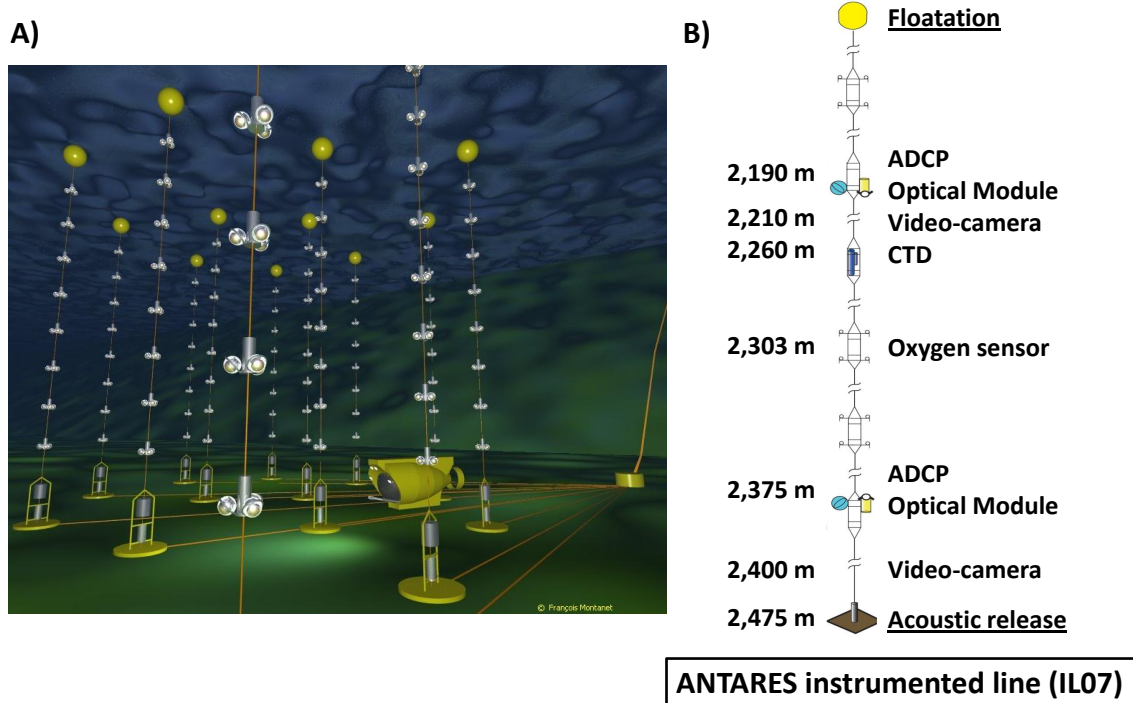


FIGURE (2.2) A) Artistic representation of the ANTARES neutrino telescope in the deep Mediterranean Sea. Each of the spherical globe protects a photomultiplier (PMT). All those 885 PMTs detect photon emission crossing the telescope and coming from various sources such as neutrino decomposition into muons,  $^{40}\text{K}$  decay of the water and from bioluminescent organisms. Image provided by the ANTARES collaboration. B) Schematic representation of the IL07 instrumented line immersed close to the ANTARES telescope. The mooring line is anchored to the seafloor by a dead weight and maintained vertically using a floating buoy, the line is connected to the junction box by a cable (not shown).

## 2.2.2 Description of the IL07 instrumented line

### Photomultiplier tubes

The ANTARES telescope is a net of 12 lines of 450 m length and horizontally separated by 70 m. These lines are vertically divided into 25 storeys of optical detectors separated by about 14.5 m and starting 100 m above the seabed. The lines are linked to an optical cable connected to a junction box (Ageron et al., 2009). Each storey is composed of three optical modules oriented downward,  $45^\circ$  from the vertical with a total number of about 885 optical modules (see Figure 2.3) over the telescope. This orientation prevents the particulate deposit (Amram et al., 2002). The optical-module position is controlled using a compass and a tilt meter. The optical modules are

spherical glass pressure vessels of 17 cm of diameter, 15 mm of thickness and containing a photomultiplier tube (PMT) 10" Hamamatsu PMT R7081-20. PMTs are sensitive to light emission ranging from 446 to 500 nm. The photon-counting rates of PMTs, expressed in Hertz (number of photons per second), are integrated over 13 ms for the IL07 instrumented line. The signal recorded by PMTs is a combination of several sources of photon emission. Firstly, the neutrino transformation into muon in the water emits a single photon. Then, a baseline with very low variations, between 40 and 50 kHz, is attributed to the  $^{40}\text{K}$  decay in the seawater. Finally, the main part of the signal is due to light emission from marine bioluminescent organisms. Hence, the photon-counting rate, higher than 50 kHz, will be associated to bioluminescence activity in the rest of this work.



FIGURE (2.3) Optical module from the ANTARES neutrino telescope. One photomultiplier is protected from high hydrostatic pressure inside the thick glass sphere.

### Video cameras

Two video cameras have been integrated into the IL07 between December 2007 and October 2010. The first objectives were to use simple, and easily available, video cameras as a primary step to record bioluminescent organisms crossing the ANTARES telescope. The detection of bioluminescent organisms, flowing through the telescope over several years, would permit to access to the ecological information, in order to understand and describe bioluminescent populations and communities. When such organisms cross the video-camera-detection area, they automatically trigger the camera and then, the data

are transferred in real time through the cable connected from the telescope to the shore. The camera AXIS221 (Figure 2.4 A) used on the IL07 line is optimized for light levels lower than  $10^{-5}$  lux. This camera has a large detection angle ( $90^\circ$ ) covering several cubic meters around. Time exposure is defined at 0.1 s. Cameras are located into spherical glass pressure vessels similar to the ones containing the photomultipliers. There are several differences between the two cameras. One camera is located on floor 1 at 2,400 m depth, 80 m above the seafloor and the second one is located on floor 5 at 2,210 m depth, 270 m above the seafloor (see Figure 2.4 B). The floor-1 camera has a detection field half the one of the camera on floor 5. The cameras are looking down to the deep-sea floor with a  $90^\circ$  angle for the camera on floor 1 and  $45^\circ$  for floor-5 camera. Moreover, it has been observed that floor-5 camera possibly detects cosmic-ray-photon emissions that are not detected by floor-1 camera due to their orientation differences.

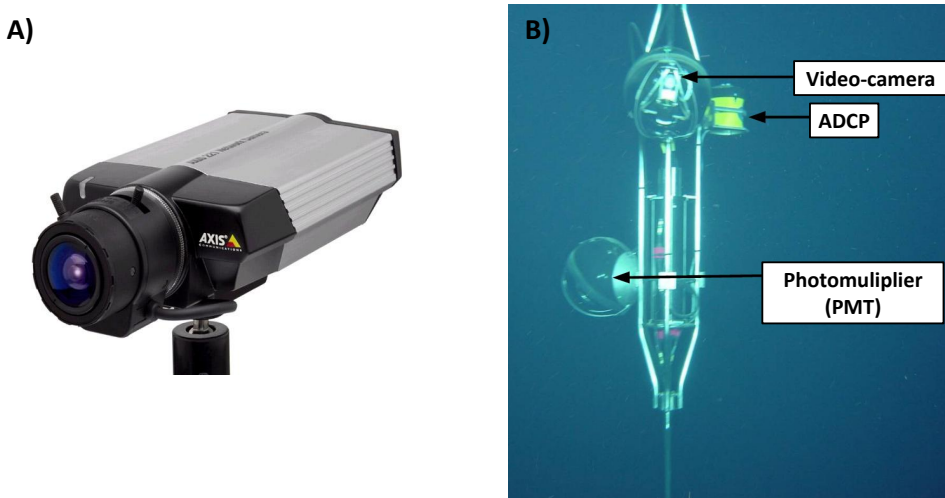


FIGURE (2.4) A) The AXIS 221 camera used on the instrumented line IL07. Two of those are placed on floor 1 (2,400 m depth) and on floor 5 (2,210 m depth). B) Floor 5 on the instrumented line IL07 of the ANTARES neutrino telescope. The video camera is located into the upper optical module. An ADCP looking downward (in yellow) and an optical module with photomultiplier (PMT) are also located on the same floor.

### Acoustic Doppler Current Profiler

Two Acoustic Doppler Current Profiler (ADCP), 300 kHz RDInstruments are located on the IL07 line. The first ADCP is located, on floor 1, at 2,397 m depth, and is looking

upward. The second one is located, on floor 5, at 2,207 m depth, and is looking downward. The ADCP detects particle sizes above  $3 \times 10^{-3}$  m. For each of those instruments, 125 m of the water column are sampled into 50 cells of 2.5 m length each. The detection of the two ADCP overlaps causing cross sampling on about 63 m of the water column. Turbidity values are determined by 4 beams of the ADCP and are averaged to smooth extreme or artifactual values. From the ADCP measurements, turbidity (dB), vertical and horizontal current speed ( $\text{cm s}^{-1}$ ) and current direction ( $^\circ$ ) are sampled. The vertical direction for current speed is not taken into account in this work due to the low signal-noise ratio of the dataset.

### **Conductivity-Temperature-Depth sensors**

The conductivity, temperature and depth are recorded using a Conductivity-Temperature Depth Microcat 37 SMP Sea-Bird®. Salinity has been computed based on conductivity values and EPS78 formula from [Fofonoff and Millard \(1983\)](#). Potential temperature is used and will be named "temperature" in further dataset and representations.

### **2.2.3 Data description: the regression trees approach**

#### **Threshold detection using regression trees**

As first representation of the oceanographic time series recorded between January 2009 and July 2010, regression and prediction trees have been performed to describe variability of the data over time. Regression trees are statistical models concerned with the prediction of a real response variable  $Y$  given a set of explanatory variables  $\mathbf{X}$ . Starting from a set of  $n$  *i.i.d.* observations  $\{(Y, \mathbf{X}), i = 1, \dots, n\}$  of  $(Y, \mathbf{X}) \in \mathbb{R} \times \Theta$ , they are constructed by partitioning the  $\mathbf{X}$  space into a set of hypercubes and fitting a simple model (a constant) for  $Y$  in each of these regions. The model can be displayed in the form of a binary tree containing  $q$  terminal nodes (the regions) where a predicted value of  $Y$  is given.

The construction of a tree-based model, the way to select the splits and the measure of

the accuracy are achieved using the following criterion called deviance defined for each node  $r$  of the tree as :

$$R(r) = \sum_{\mathbf{x}_i \in r} (y_i - \bar{y}_r)^2$$

where  $\bar{y}_r$  is the average of the observations of  $Y$  belonging to the region  $r$ . These models have been widely studied in machine learning and applied statistics and present many advantages like their representation in a form of a binary tree, working in high dimension and variable ranking. Moreover, it can be interesting to construct a regression tree when the predictor variable  $X$  is univariate or when observations are not *i.i.d.* In that case, the tree structure provides a nonlinear fitting of the time-series  $Y(X)$  by finding thresholds on the variable  $X$  and giving constant predicted values of  $Y$  in regions identified by these thresholds. The model can then be displayed as a piece wise constant function and allows to identify particular regions of the time series where values of  $Y$  change significantly.

## 2.3 Multivariate survey at high frequency and real-time sampling

In the following paragraphs ([2.3.2](#) to [2.3.5](#)), descriptive analyzes of bioluminescence activity linked to other oceanographic variables will be presented. More detailed description and analysis of all time series will be done in article 1 ([2.4.2](#)) and article 2 ([3.1.2](#)) for all variables independently and linked to bioluminescence activity.

### 2.3.1 Water masses proxies

Time series recorded at the ANTARES station are represented for bioluminescence, salinity, temperature and horizontal current speed from December 2007 to October 2010 (Figure [2.5](#)).

The scientific questions of this work focus on bioluminescence activity in the deep sea as an input to understanding the deep-ecosystem dynamics. Looking at the bioluminescence activity in Figure [2.5 A](#), a wide range of values, not expected in this deep environment

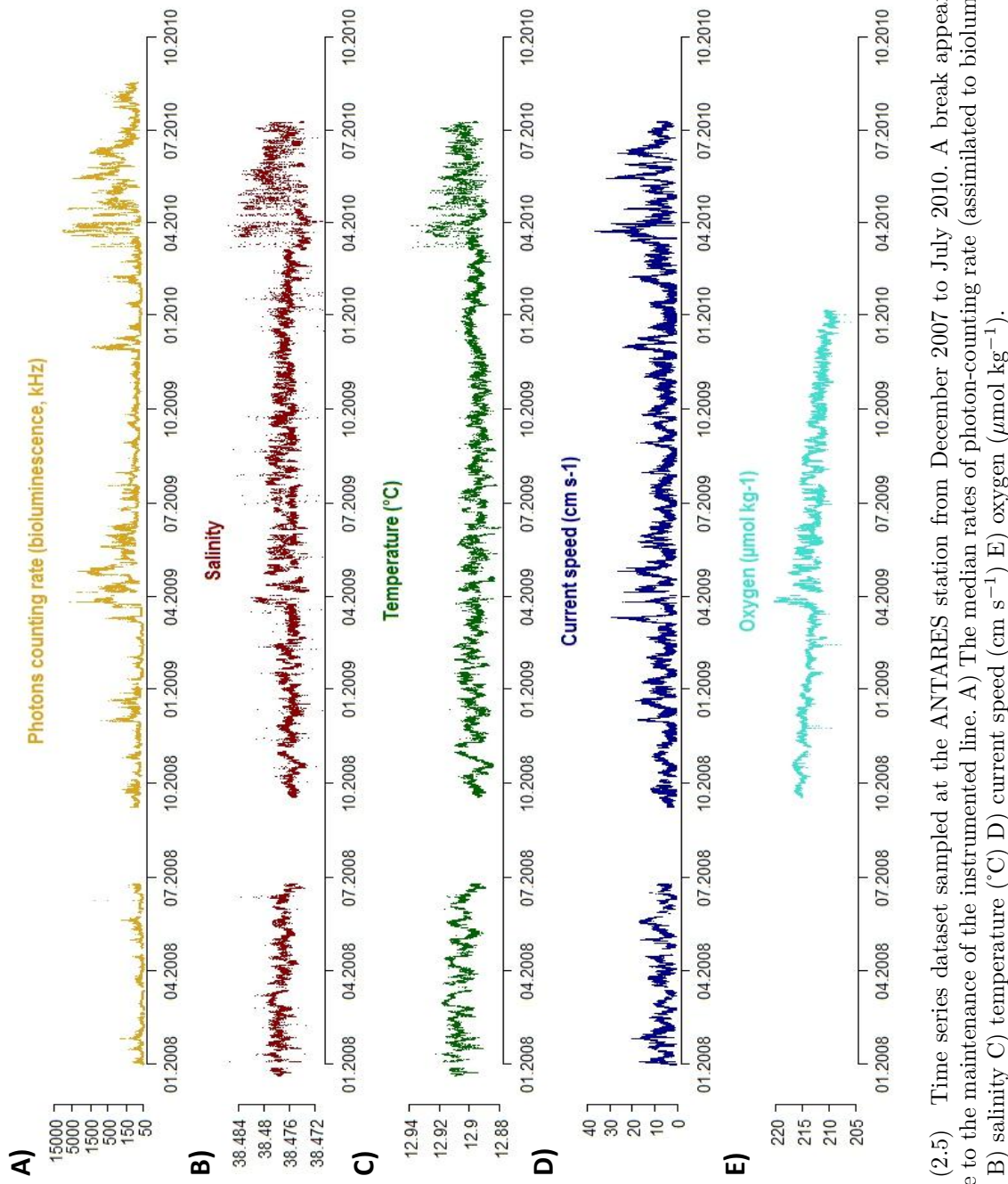


FIGURE (2.5) Time series dataset sampled at the ANTARES station from December 2007 to July 2010. A break appears in July 2008 due to the maintenance of the instrumented line. A) The median rates of photon-counting rate (assimilated to bioluminescence in kHz), B) salinity C) temperature (°C) D) current speed (cm s<sup>-1</sup>) E) oxygen (μmol kg<sup>-1</sup>).

(see 1.1.3), is observed over the considered time-period ranging from 40 to about 8,000 kHz. If this photon emission can not be described as high intensity, in absolute term, these values are altogether referring to unexpected level of bioluminescence in the deep sea and to intense variability. The bioluminescence activity shows an intermittent pattern with peaks above a baseline at about 40 kHz, known as the  $^{40}\text{K}$  decay in seawater. Two periods of very intense bioluminescence activity are distinct between March and July in 2009 and 2010. Moreover, in Figure 2.5 B and C, temperature and salinity have similar variations. In Figure 2.5 D, current speed shows moderate variations over time without clear distinct period of high intensity. In Figure 2.5 E, oxygen shows a clear linear decreasing trend with an important variation in March 2009, conjointly to salinity and bioluminescence time series.

### 2.3.2 Currentology

Figure 2.6 represents the horizontal current speed at the deep ANTARES station with direction, intensity and frequency information. Looking at the annual scale, in 2008, 2009 and 2010, a global East-West axis is dominant. Moreover, the current direction is more frequently, and with higher intensity coming from the West than from the East (current speeds up to  $20 \text{ cm s}^{-1}$  for Western currents and up to  $10 \text{ cm s}^{-1}$  for Eastern currents). Faster current speeds are observed in 2009 from the Western direction and in 2010 from the South-eastern direction (values above  $20 \text{ cm s}^{-1}$ ). No high current-speed values are observed in 2008.

Similar representation are drawn with a focus on March 2009 and March 2010 (Figure 2.7) referring to intense bioluminescence-activity events already described in Figure 2.5 A. Those two periods show similar current-direction pattern than the observation on annual scale (Figure 2.6), dominated by East-western direction. However, during those two periods, South-eastern currents are more frequent than during the whole year. March 2009 and 2010 are also periods of more intense current speed compared to the whole year (more than 15% above  $20 \text{ cm s}^{-1}$ ). In March 2009, the highest current-speed intensities

are essentially coming from the western direction whereas, in 2010, this direction is mainly South-East.

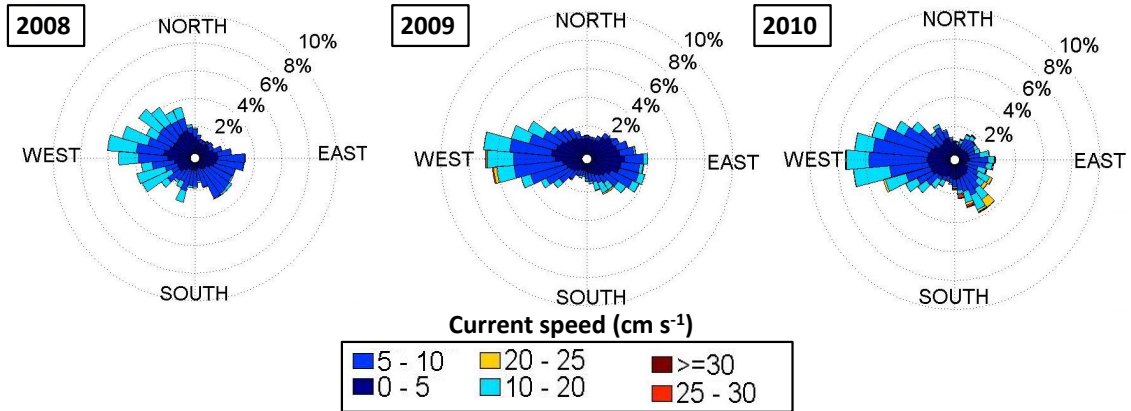


FIGURE (2.6) Current speed horizontal intensity, incoming direction and frequency representations for 2008, 2009 and 2010. Due to the stop of the instrumented line IL07 between July and September 2008, no data have been taken into account for that period in 2008. The total circle is subdivided into  $10^\circ$  angular sections. Color scale (from dark blue to dark red) represents the current speed ( $\text{cm s}^{-1}$ ) and dotted circles represent the frequency (% of occurrence).

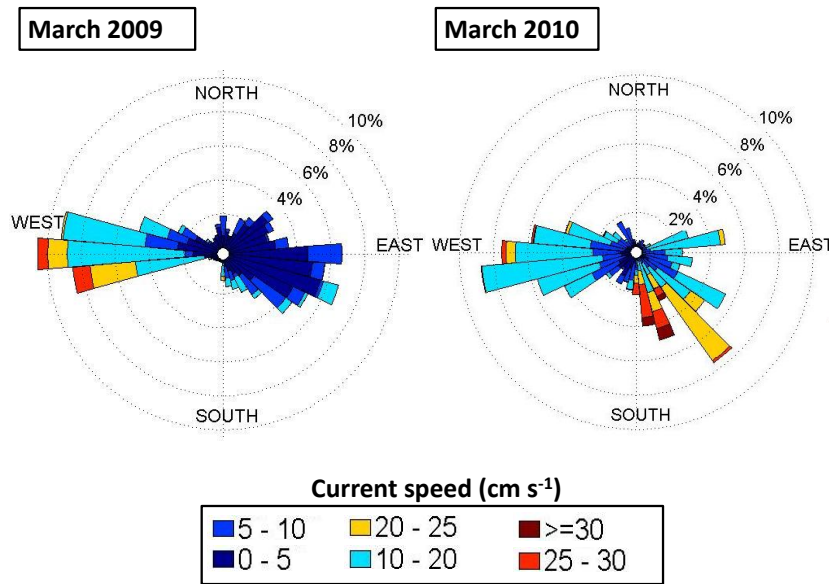


FIGURE (2.7) Current speed, horizontal intensity, direction and frequency representations focused on March 2009 and 2010. The total circle is subdivided into  $10^\circ$  angular sections. Color scale (from dark blue to dark red) represents the current speed ( $\text{cm s}^{-1}$ ) and dotted circles represent the frequency (% of occurrence).

### 2.3.3 Bioluminescence interaction with current

Such representation can be easily adapted in order to illustrate links between bioluminescence activity and current direction. In Figure 2.8, the median rate of bioluminescence (kHz) and frequency (% of occurrence) are plotted over current direction ( $^{\circ}$ ) recorded at the same time. An East-western axis is predominant with similar pattern as current speed in Figure 2.6. In 2008, 2009 and 2010, most of the bioluminescence activity is lower than 500 kHz. However, higher bioluminescence values occurring in 2009 and 2010 (above 1,500 kHz), are mainly related to South-eastern currents.

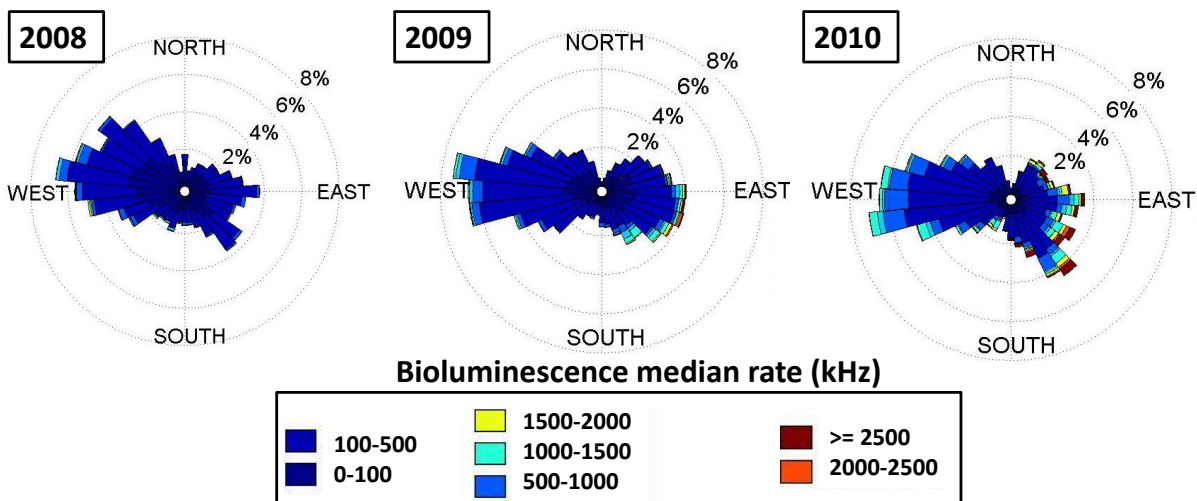


FIGURE (2.8) Bioluminescence representation over the years 2008, 2009 and 2010 depending on direction of current speed, intensity and frequency. Due to the stop of the instrumented line IL07 between July and September 2008, no data have been taken into account for that period in 2008. The total circle is subdivided each  $10^{\circ}$ . Color scale (from dark blue to dark red) represents the bioluminescence intensity (kHz) and dotted circles represent the frequency (% of occurrence).

A focus in March 2009 and March 2010 is represented (Figure 2.9). If March 2009 shows moderated bioluminescence activity, in March 2010, very high bioluminescence intensity (from 2,000 to 8,000 kHz) is recorded conjointly to a South-eastern current direction. Those two graphs (Figure 2.8 and 2.9) show similar pattern to current speed, frequency and direction (Figure 2.6 and Figure 2.7). The similarity between those representations highlights close links between current speed, current direction and bioluminescence activity. However, no discrimination can be made between the independent effect of the

current speed and that of the current direction on bioluminescence activity.

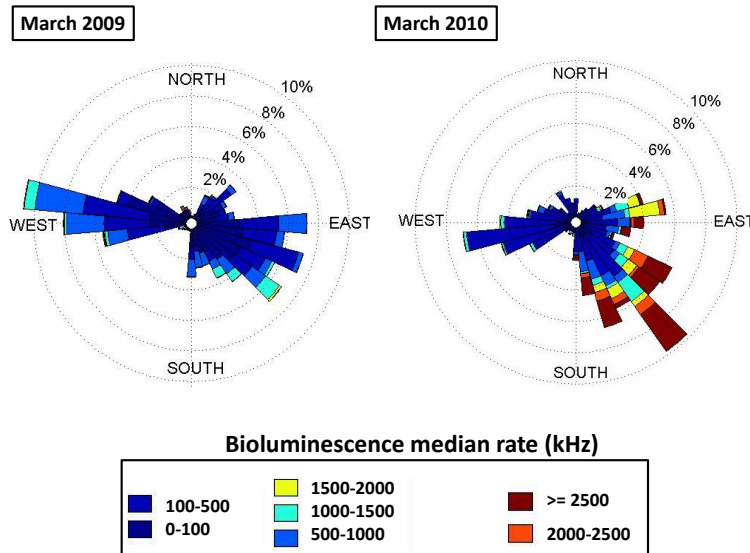


FIGURE (2.9) Bioluminescence representation in March 2009 and 2010 depending on direction of current speed, intensity and frequency. The total circle is subdivided each  $10^\circ$ . Color scale (from dark blue to dark red) represents the bioluminescence intensity (kHz) and dotted circles represent the frequency (% of occurrence).

### 2.3.4 Univariate and multivariate approaches using regression-tree method

For each variable independently, regression trees have been performed on dataset recorded between January 2009 and December 2010. This representation defines changes in intensity, taking into account time dependence. In Figure 2.10, on the left, the regression trees show time series partition into classes with mean value defined for the final leaves. On the right, the previously defined classes, performed by the regression trees, are represented on time series.

For bioluminescence (Figure 2.10 A), 5 classes are described, whereas for salinity (Figure 2.10 B) and temperature (Figure 2.10 C), 4 classes are discriminated over time.

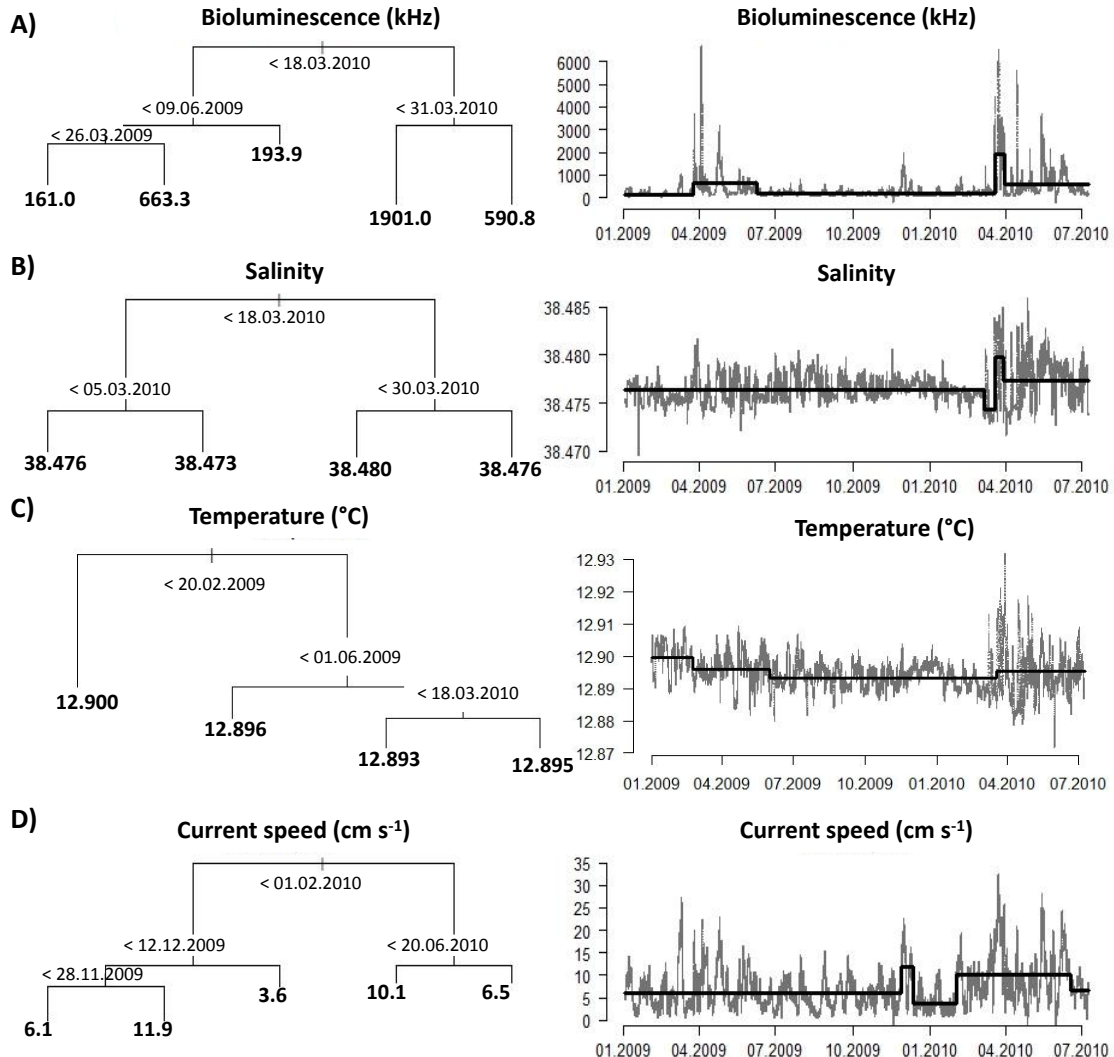


FIGURE (2.10) On the left, regression trees for A) bioluminescence, B) salinity, C) temperature and D) current speed. On the right, time series with the class mean values (black lines) defined by the leaves of regression trees. The regression trees give an overview of the occurrence of events inside the dataset by dividing the data into classes. The time series representation of these classes shows the variability over time.

Interestingly, the same period of time, between the 18<sup>th</sup> and 31<sup>st</sup> of March 2010 (the two first nodes), is highlighted for bioluminescence and salinity (Figures 2.10 A and B). These changes in variability over time are clearly observed with long branches and high-mean values (1,901 kHz for bioluminescence and 38.480 for salinity). The threshold corresponding to the 18<sup>th</sup> March 2010 also appears for temperature (last node in Figure

2.10 C) but not for current speed. This first observation highlights potentially common dynamics between bioluminescence activity, salinity and temperature on a global time scale.

From these results, a prevision tree, based on data acquisition from December 2007 to July 2010, has been performed (Figure 2.11). This prediction tree computes information from temperature, salinity, current speed in order to predict bioluminescence values.

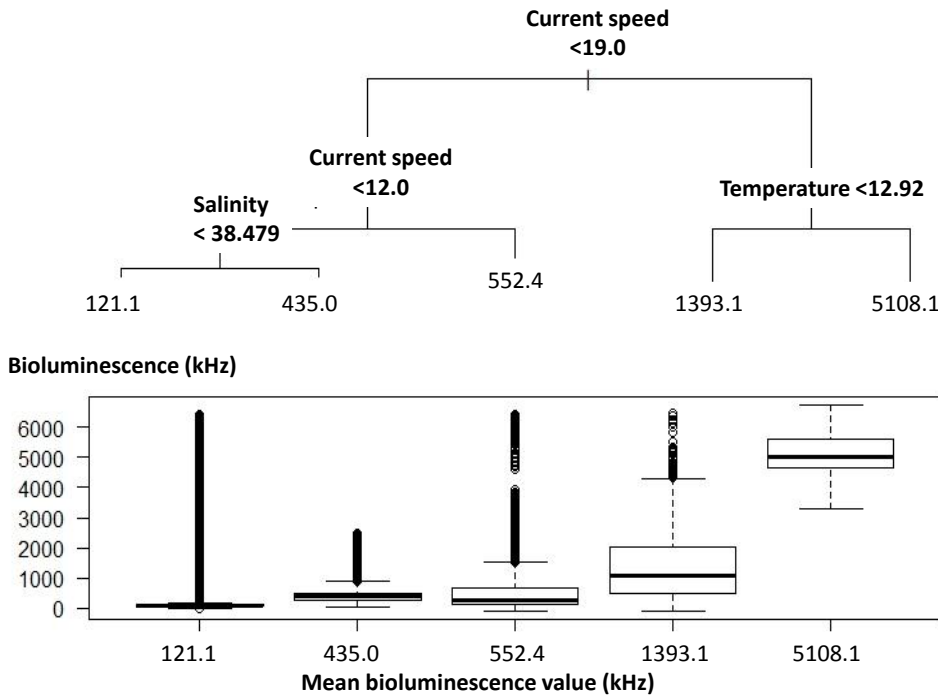


FIGURE (2.11) Regression tree for the prediction of bioluminescence activity using oceanographic variables (salinity, temperature and current speed) from December 2007 to July 2010. The top and bottom of each box-plot represent 75% (upper quartile) and 25% (lower quartile) of all values, respectively. The horizontal line is the median. The ends of the whiskers represent the 10<sup>th</sup> and 90<sup>th</sup> percentiles. Outliers are represented by empty dots. Modified from Tamburini et al. (2013), supplementary data.

The tree defines 4 nodes and 5 classes with an average bioluminescence intensity for each. Class 1 (mean 121.1 kHz), 2 (mean 435.0 kHz) and 3 (mean 552.4 kHz) gather low bioluminescence intensity mainly due to low sea-current speed (below 19.0 cm s<sup>-1</sup>). The branch length shows the strong dependence of bioluminescence to the current-speed threshold of

$19.0 \text{ cm s}^{-1}$ . Indeed, class 3 and 4 are firstly described by high current-speed intensity ( $>19.0 \text{ cm s}^{-1}$ ) but, as a second environmental condition, the temperature threshold of  $12.92^\circ\text{C}$  divides these two classes between high (class mean of  $1,393.0 \text{ kHz}$ ) and highest (class mean of  $5,108.0 \text{ kHz}$ ) bioluminescence values. Moreover, the boxplot representation of data within each class (Figure 2.11) reveals a straight range of values within the class of strongest bioluminescence activity ( $1^{\text{st}}$  and  $3^{\text{rd}}$  quantiles between  $4,500$  and  $5,200 \text{ kHz}$ ).

Similar variations are observed for bioluminescence activity and salinity (period between the  $18^{\text{th}}$  and the  $31^{\text{st}}$  of March 2010, in Figure 2.10 A and B). Time dependence seems to be of major importance for highlighting links between bioluminescence activity and environmental variables. Moreover, a current speed above  $19.0 \text{ cm s}^{-1}$  strongly discriminates the bioluminescence activity. However, intense bioluminescence activity also relies on temperature (threshold of  $12.92^\circ\text{C}$  in Figure 2.11).

This classification method is dependent on the variability threshold and on the final number of classes, both defined by the user. If some clues and hypotheses can be proposed using both time series observation and regression trees, more robust statistical-analysis methods have to confirm, or not, this first investigation. Such improvement will be proposed in article 1 (2.4.2) and article 2 (3.1.2).

### 2.3.5 Analysis of *in situ* images from bioluminescent organisms

#### Qualitative interpretations

The use of video camera for automatic detection is nowadays under development, with numerous recent studies. Such developments are done in various fields as for example the zooplankton detection (Stemmann et al., 2008), or other *in situ* organisms detection (Eye-in-the-sea, MARS observatory, USA or NEPTUNE, Canada, Aguzzi et al., 2011, 2009). To determine bioluminescent organisms crossing the ANTARES observatory, the ANTARES collaboration decided to immerse video cameras. In a first attempt, easily available and simple to use AXIS video-monitoring cameras were chosen to test the feasi-

bility (1) to connect them to the ANTARES telescope, (2) to trigger them in the presence of luminescent organisms detected by the ANTARES PMTs, (3) to real-time visualize and monitor the instrumentation, (4) to automatically transfer and stock images in the ANTARES data base and (5) to visualize luminescent organisms using only infrared light.

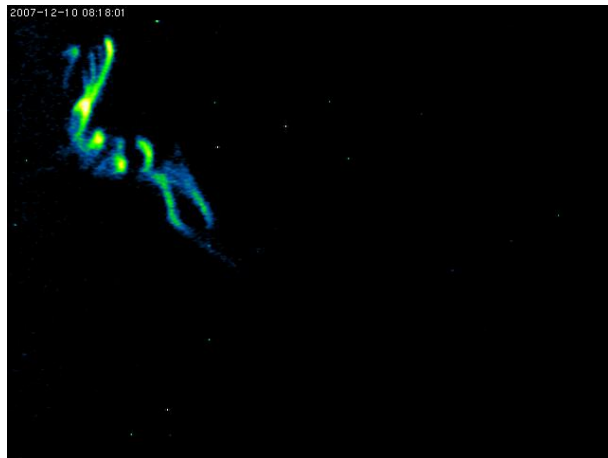


FIGURE (2.12) Example of colored images recording bioluminescent organism crossing the video-camera detection area, at the ANTARES site, on 10<sup>th</sup> December 2007.

While the first objectives were successfully achieved, the image quality obtained, using the 2 AXIS cameras placed on the IL07, does not permit an identification of bioluminescent objects (Figure 2.12). So, only the events detected by automatic triggers have been investigated in a quantitative approach and can be interpreted for now.

### **Quantitative analysis: number of events**

Between December 2007 and July 2010, a total number of 874 events has been recorded by the two video cameras on the IL07 line. Bioluminescence time series recorded by PMTs from the IL07 (Figure 2.13 A) and the number of detected events by the video cameras for both floor 1 and 5 (Figure 2.13 B) are represented. During July and August 2008, the video cameras were canceled due to the IL07 maintenance involving a gap into the dataset. A peak in the number of events is recorded from March to June 2010, with a maximum value occurring in March 2010 with 27 and 201 events detected on floor 1 and 5, respectively.

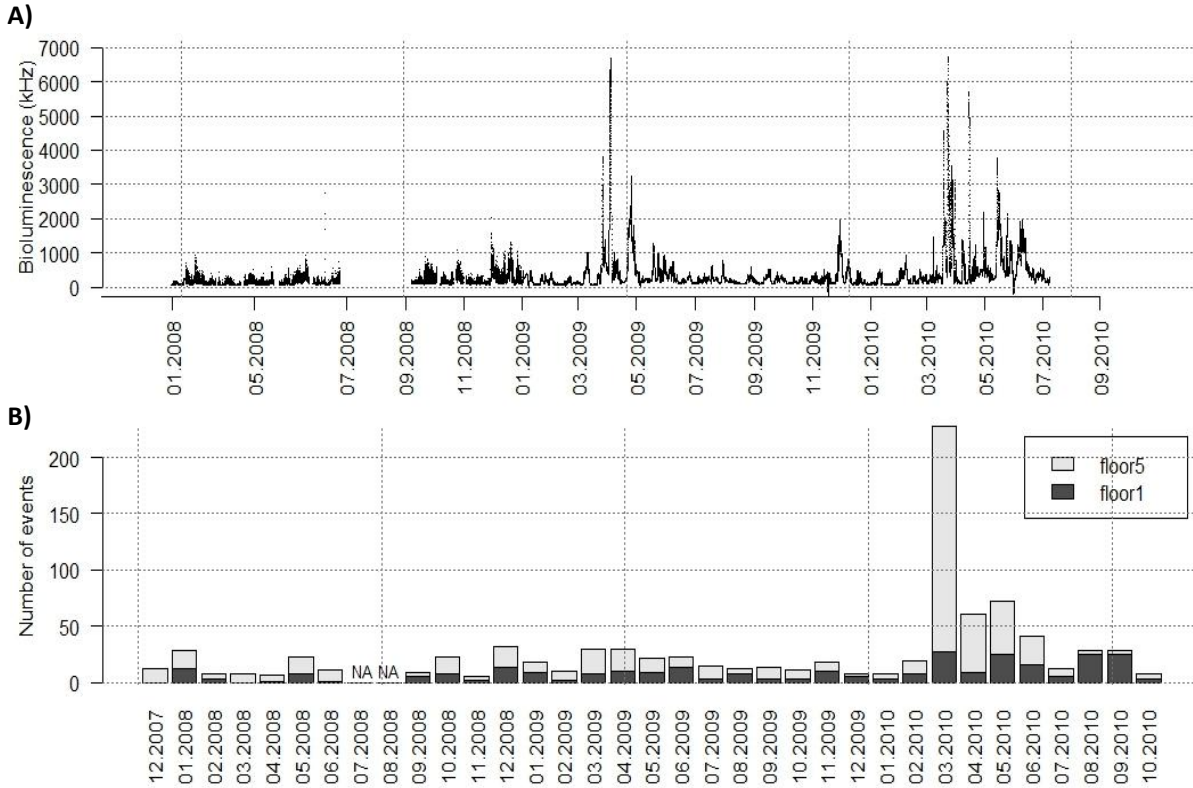


FIGURE (2.13) Bioluminescence emission and video records. A) The bioluminescence emission recorded from the ANTARES-IL07 photomultipliers. B) Bioluminescence events recorded from the two video-cameras using automatic detection on the ANTARES-IL07.

Video cameras detect less events at floor 1 than floor 5 (281 and 593 total events with median values of 7.0 and 9.0, respectively, see Figure 2.14). However, there is no significant difference between these two boxplot distributions corresponding to floor 1 and floor 5.

In order to quantify the bioluminescence activity detected by video cameras, the light emission recorded by the PMTs in Figure 2.13 A, was monthly integrated from January 2009 to July 2010. Correlation between the number of events and bioluminescence rate per month is represented (Figure 2.15). These results show a correlation (correlation coefficient of about 0.7) between the number of events detected and the bioluminescence rate recorded. On a monthly scale, the number of bioluminescent events from video

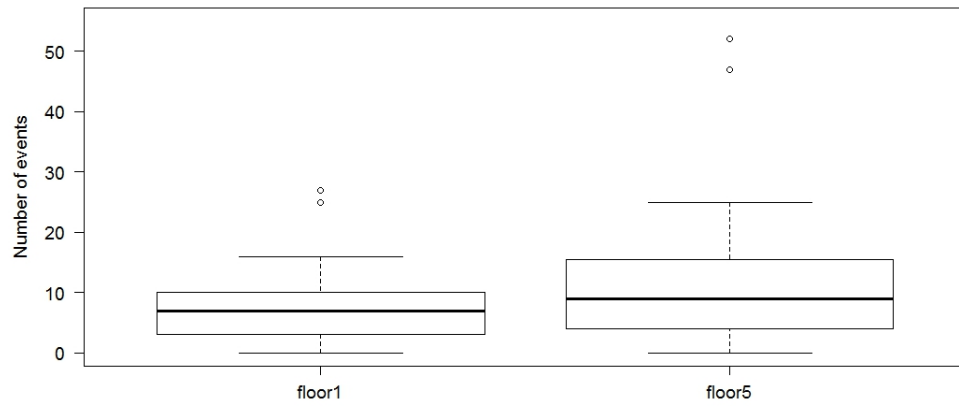


FIGURE (2.14) Representation of the video-event distribution between floor 1 and floor 5. The video camera at floor 1 is close to the seafloor and the one at floor 5 is assumed to be in the water column. Data recorded in March 2010, with 201 events detected, is not shown in this graph, since this data was considered as an extreme value out of the boxplot distribution. Total number of events are 281 and 593 for floor 1 and floor 5, respectively.

cameras reflects the variations in bioluminescence activity recorded at the ANTARES station. Exceptions occur in April 2009, and March 2010 (red crosses in Figure 2.15) that are outside the 95% confidence intervals. In April 2009, bioluminescence rate per month is high with a number of events detected by the video camera relatively low referring to the regression. However, in March 2010, a high number of events is recorded compared to the monthly bioluminescence rate also referring to the regression. This correlation is based on 19 months, with about 76% of the data in the lower part of the regression line (number of events lower than 35 and monthly bioluminescence lower than  $1 \times 10^6$  kHz, red dotted lines in Figure 2.15). According to this remark, the few events of high bioluminescence activity support heavy weight to determine the regression slope.

Organisms detected by the video-cameras can be mechanically stimulated by current speed, by turbulence or emit light when crashing to the optical module. Consequently, the bioluminescence activity is linked to the number of events detected by the video cameras. However, at some specific dates this relation is not confirmed (April 2009 and March 2010 in Figure 2.15). Other organisms, such as bacteria, are probably poorly detected in free living or when attached to particles and can probably modify the video-camera triggering.

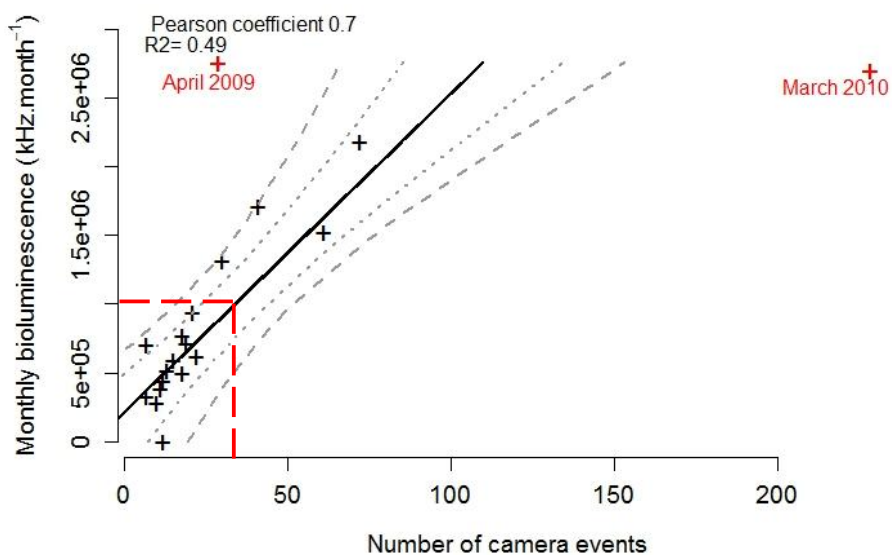


FIGURE (2.15) Correlation between the bioluminescence emission monthly integrated and the number of events recorded by video cameras at the same time scale. The data are studied from January 2009 to July 2010. The dotted lines represent the 95 and 75% of confidence intervals. In red, the data referring to April 2009 and March 2010 are considered as extreme couples of data. Red dotted lines represent 76% of the data.

## 2.4 Article 1

### 2.4.1 Foreword

Time series records at the ANTARES station lead to the observation of high variability in bioluminescence activity, especially in March 2009 and March 2010, that were unexpected in the deep sea. In the following article, these variations are described and explained at the regional scale of oceanographic processes observed in the Gulf of Lion (NW Mediterranean Sea). Indeed, the conjoint study of complementary time series, from monitored stations in the Gulf of Lion gave the opportunity to highlight the formation of new-water masses at the surface that are then exported to the deep sea. Such events explain changes observed on the ANTARES time series involving modifications of water-masses characteristics (temperature, salinity) but also of possible population changes in this deep ecosystem. These populations can be modified either by the input of organisms among them being bioluminescent (coming from the surface layers), or by the enrichment in carbon and energy of the deep sea due to the incoming of newly-formed water masses. This carbon, oxygen and nutrients input to the deep sea might involve an increase in the deep-sea biological activity and so higher bioluminescence activity.

*The ANTARES collaboration developed the underwater telescope and as members of the ANTARES collaboration, we have access to the data. C. Tamburini and S. Escoffier are the main authors for this publication. M. Canals, X. Durieu de Madron, L. Houpert, F. D'Ortenzio gave clues and interpretation for oceanographic data as well as data from the Gulf of Lion. D. Lefevre and A. Robert calibrated temperature and salinity data, thanks to the MOOSE monthly sea campaigns, as well as the supplementary data in Figure S3. I contributed to the time series representation, the statistical analyzes and the article understanding and writing.*

## 2.4.2 Deep-sea bioluminescence blooms after dense water formation at the ocean surface

Christian Tamburini<sup>1,2,\*</sup>, Stéphanie Escoffier<sup>3,\*</sup>, Miquel Canals<sup>3</sup>, Xavier Durrieu de Madron<sup>4</sup>, Loic Houpert<sup>4</sup>, Dominique Lefèvre<sup>1,2</sup>, Séverine Martini<sup>1,2</sup>, Fabrizio D'Ortenzio<sup>5</sup>, Anne Robert<sup>1,2</sup>, Pierre Testor<sup>6</sup>, and the ANTARES collaboration \*\*

<sup>1</sup> Aix Marseille Université , CNRS/INSU, IRD, Mediterranean Institute of Oceanography (MIO), UM 110, Marseille, France

<sup>2</sup> Université de Toulon, CNRS/INSU, IRD, Mediterranean Institute of Oceanography (MIO), UM 110, La Garde, France

<sup>3</sup> CPPM-Aix-Marseille Université , CNRS/IN2P3, Marseille, France

<sup>4</sup> GRC Geociències Marines, Departament d'Estratigrafia, Paleontologia i Geociències Marines, Facultat de Geologia, Universitat de Barcelona, Campus de Pedralbes, Barcelona, Spain

<sup>5</sup> Université de Perpignan, CNRS-INSU, CEFREM UMR5110, Perpignan, France

<sup>6</sup> Université Pierre et Marie Curie, CNRS-INSU, LOV UMR7093, Villefranche-sur-mer, France

<sup>7</sup> Université Pierre et Marie Curie, CNRS-INSU, Institut Pierre Simon Laplace, LOCEAN UMR 7159, Paris, France

\* Corresponding authors: [christian.tamburini@univ-amu.fr](mailto:christian.tamburini@univ-amu.fr) ; [escoffier@cppm.in2p3.fr](mailto:escoffier@cppm.in2p3.fr)

\*\* For easier reading, the complete list of authors belonging to the ANTARES collaboration has not been developed in this article. For a complete list, please refer to the PLoS ONE published version.

**Tamburini C, Canals M, Durrieu de Madron X, Houpert L, Lefèvre D, et al. (2013) Deep-Sea Bioluminescence Blooms after Dense Water Formation at the Ocean Surface. PLoS ONE 8(7): e67523. doi: 10.1371/journal.pone.0067523**

**Abstract**

The deep ocean is the largest and least known ecosystem on Earth. It hosts numerous pelagic organisms, most of which are able to emit light. Here we present a unique data set consisting of a 2.5-year long record of light emission by deep-sea pelagic organisms, measured from December 2007 to June 2010 at the ANTARES underwater neutrino telescope in the deep NW Mediterranean Sea, jointly with synchronous hydrological records. This is the longest continuous time-series of deep-sea bioluminescence ever recorded. Our record reveals several weeks long, seasonal bioluminescence blooms with light intensity up to two orders of magnitude higher than background values, which correlate to changes in the properties of deep waters. Such changes are triggered by the winter cooling and evaporation experienced by the upper ocean layer in the Gulf of Lion that leads to the formation and subsequent sinking of dense water through a process known as 'open-sea convection'. It episodically renews the deep water of the study area and conveys fresh organic matter that fuels the deep ecosystems. Luminous bacteria most likely are the main contributors to the observed deep-sea bioluminescence blooms. Our observations demonstrate a consistent and rapid connection between deep open-sea convection and bathypelagic biological activity, as expressed by bioluminescence. In a setting where dense water formation events are likely to decline under global warming scenarios enhancing ocean stratification, *in situ* observatories become essential as environmental sentinels for the monitoring and understanding of deep-sea ecosystem shifts.

## Introduction

The deep-sea ecosystem is unique because of its permanent darkness, coldness, high pressure and scarcity of carbon and energy to sustain life. Most of its biological activity relies on the arrival of carbon in the form of organic matter from surface waters. Ninety percent of the numerous pelagic organisms that inhabit the deep ocean are capable of emitting light (Robison, 2004) through the chemical process of bioluminescence, which appears to be the most common form of communication in this remote realm (Robison, 2004; Herring, 1987; Haddock et al., 2010). Deep-sea bioluminescence is also viewed as an expression of abundance and adaptation of organisms to their environment (Widder, 2010). Marine bioluminescent organisms include a variety of distinct taxa (Widder, 2010). When stimulated mechanically or electrically, eukaryotic bioluminescent organisms emit erratic luminous flashes, and also spontaneous flashes to attract prey and mates for recognition of congeners or for defence purposes (Robison, 2004; Haddock et al., 2010; Widder, 2010). In contrast, luminescent bacteria are unaffected by mechanical stimulation and can glow continuously for many days under specific growth conditions (Nealson and Hastings, 1979; Miller et al., 2005). Bioluminescent bacteria occur in marine waters as free-living forms, symbionts in luminous organs of fishes and crustaceans and attached to marine snow aggregates sinking through the water column (Nealson and Hastings, 1979; Andrews et al., 1984). During micro-algae blooms, strong bioluminescence produced by colonies of bacteria could even lead to spectacular marine phenomena such as 'milky seas' in surface waters (Miller et al., 2005).

Bioluminescence sources have been observed and quantified over the last three decades using a variety of observational platforms and instruments such as manned submersibles (Robison, 2004) and autonomous underwater vehicles (Shulman et al., 2005), *in situ* high sensitivity cameras (Widder et al., 1989), (Priede et al., 2006), underwater photometers (Andrews et al., 1984), (Swift et al., 1985), (Geistdoerfer and Vincendeau, 1999), and remote satellite imagery (Miller et al., 2005). In most cases, deep-sea bioluminescence is triggered and observed after external mechanical stimulation using, for instance, pumped flows through turbulence-generating grids (Widder et al., 1999) or downward moving grids that collide with the organisms (Priede et al., 2006). While these procedures provide

crucial information on the nature and distribution of deep-sea bioluminescent organisms in the water column ([Haddock et al., 2010](#)) and references therein, they are not suited to investigate the temporal variability of naturally occurring light production (i.e. non artificially triggered) at specific sites over long periods of time, which requires sustained high frequency *in situ* measurements.

An unanticipated application of underwater neutrino telescopes is to provide direct measurements of bioluminescence in the deep sea ([Bradner et al., 1987](#); [Aoki et al., 1986](#); [Amram et al., 2000](#)). A neutrino telescope aims at detecting the faint Cherenkov light emission radiated by elementary charged particles called muons that are produced by neutrino interactions. Darkness, transparency and water shielding against cosmic ray muons make the deep sea an ideal setting for a neutrino telescope. Here we make use of both the high frequency bioluminescence and hydrological time-series of the cabled ANTARES neutrino telescope ([Ageron et al., 2011](#)) located 40 km off the French coast (42°48'N, 6°10'E) at 2,475 m in the NW Mediterranean Sea (Fig. 2.16 a).

The NW Mediterranean Sea is one of the few regions in the world's ocean where both dense shelf water cascading and open-sea convection take place ([Mertens and Schott, 1998](#); [Marshall and Schott, 1999](#); [Canals et al., 2006](#); [Stabholz et al., 2013](#)) (Fig. 2.16 a). This results in the formation of deep water owing to the combination of atmospheric forcing and regional circulation that lead the water column to overturn ([Marshall and Schott, 1999](#); [Canals et al., 2006](#); [Béthoux et al., 2002](#)). Dense deep water formation occurs during late winter and early spring due to cold, strong and persistent northern winds (Mistral and Tramontane) causing surface cooling of the Modified Atlantic Water (MAW) both on the shelf and over the deep basin. When the cooled shallow waters on the shelf become denser than the ambient waters, they start sinking, overflow the shelf edge, and cascade downslope until they reach their density equilibrium depth, which may vary from 150 m to more than 2,000 m ([Canals et al., 2006](#); [Palanques et al., 2012](#)). At the same time, convection in the adjacent deep basin involves a progressive deepening of the upper ocean mixed layer, which first reaches the warmer and saltier underlying Levantine Intermediate Water (LIW) and eventually extends all the way

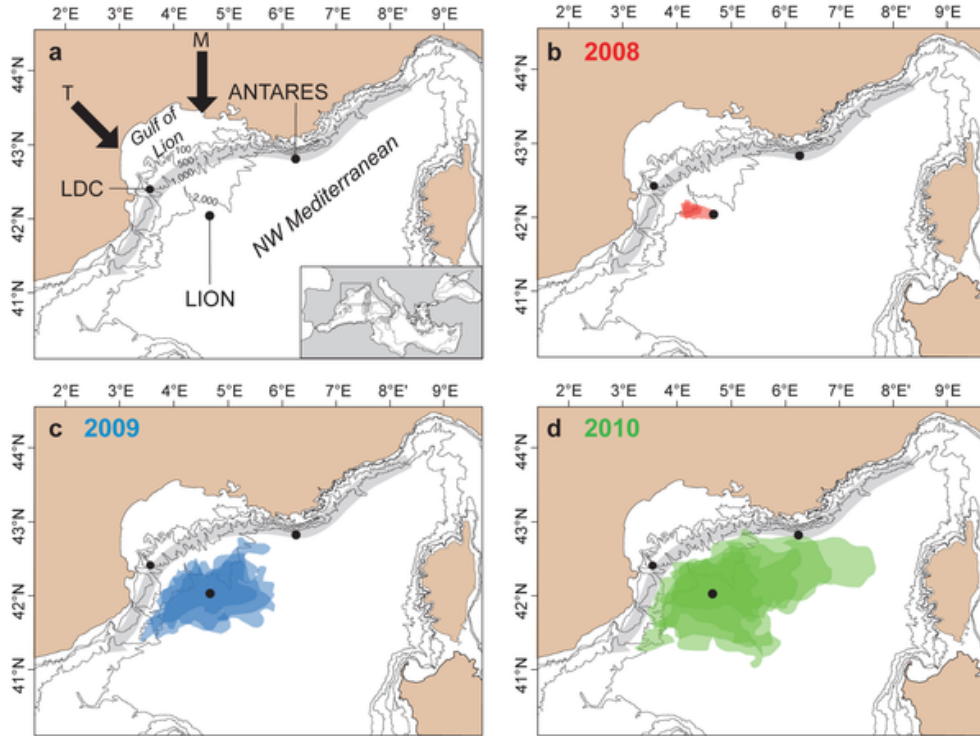


FIGURE (2.16) Map of the NW Mediterranean Sea showing the location of the ANTARES, LION and Lacaze-Duthiers Canyon (LDC) sites (a) as well as the extension of open-sea convection area in the Gulf of Lion and beyond from 2008 to 2010 (b-d). The boundaries of the convection area in winter 2008 (red in b), 2009 (blue in c) and 2010 (green in d) are derived from MODIS-Aqua satellite-based surface Chlorophyll-a concentration images. The limits of the convection area for each of the three successive winters correspond to their maximum extents during periods of deep water formation measured at the LION site (see Text S1 and Fig. 2.23). Black arrows indicate the direction of the two main continental winds leading to the cooling and subsequent sinking of surface waters: Mistral (M) and Tramontane (T). The grey arrow indicates the path of the cyclonic surface mesoscale Northern Current bordering the open-sea convection region.

down to the basin floor, should the atmospheric forcing be intense enough (Marshall and Schott, 1999). Both processes and the subsequent renewal of the Western Mediterranean Deep Water (WMDW) show a high interannual variability because of their sensitivity to atmospheric conditions (Mertens and Schott, 1998; Durrieu de Madron et al., 2013). The newly-formed deep water (nWMDW) resulting from both dense shelf water cascading and open-sea convection has been observed to spread over the deep basin floor within months (Béthoux et al., 2002; Durrieu de Madron et al., 2013; Schröder et al., 2006; Testor and Gascard, 2006). Studies about the response of deep ecosystems to such processes are scarce and focus on the impact of dense shelf water cascading on

benthic and epi-benthic organisms (Pusceddu et al., 2013; Company et al., 2008). Other recent works highlight how deep water formation triggers the resuspension of deep sea sediments, including organic matter (Stabholz et al., 2013), and the development and spreading of a thick bottom layer loaded with resuspended particulate matter across the NW Mediterranean Basin as a result of dense shelf water cascading (Puig et al., 2012).

Here we present compelling evidence of the quick response of the deep-sea pelagic ecosystem to seasonal atmospheric forcing leading to dense water formation and sinking, expressed by particularly intense bioluminescence events captured by neutrino telescope photomultiplier tubes. Observations on bioluminescence are supported by a two and a half years long unique and consistent record of hydrological and hydrodynamical variables obtained at the ANTARES deep-sea neutrino telescope itself but also at two independent mooring arrays equally located in the deep NW Mediterranean Sea.

## Results and Discussion

### Bioluminescence blooms at the ANTARES site

We report time-series measurements of light intensity expressed in median counting rates on photomultiplier tubes as well as temperature, salinity and current speed from December 2007 to June 2010 (Fig. 2.17 a), collected between 2,190 and 2,375 m depth in the ANTARES IL07 mooring line (see Methods and Fig. 2.20). While the light intensity background rate is predominantly between 40 and 100 kHz, which mainly includes the  $^{40}\text{K}$  rate (see Methods and Fig. 2.21), two remarkable bioluminescence events reaching up to 9,000 kHz were recorded between March and July in 2009 and 2010 (Fig. 2.17). Because of their high intensity and duration we call these events "bioluminescence blooms", defined here as periods with PMT median rates higher than 600 kHz, i.e. higher than the 96<sup>th</sup> percentile of the entire PMTs record.

Our records show that bioluminescence primarily increases with current speed, which is due to mechanical stimulation either by impacts of small-sized organisms and particles on the PMTs (Amram et al., 2000; Priede et al., 2008) or by the reaction of organisms to

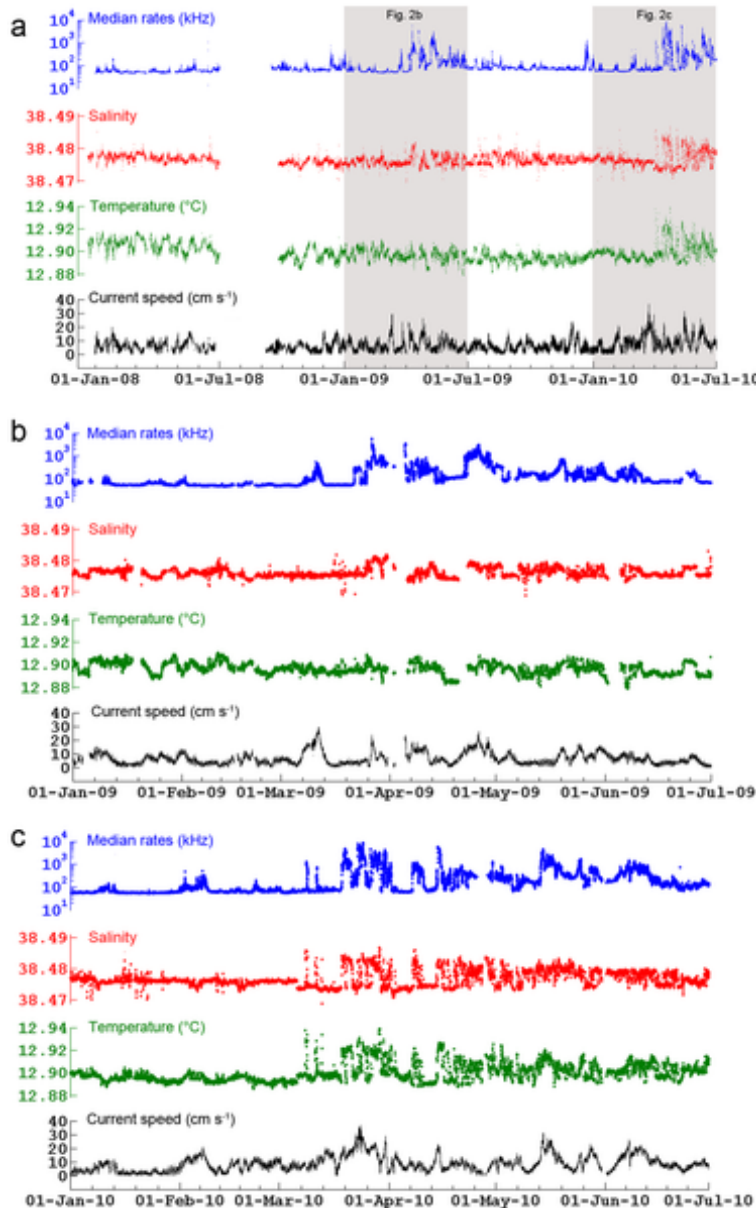


FIGURE (2.17) Time series measured at the ANTARES IL07 mooring line. (a) Median PMT counting rates (log scale), salinity, potential temperature and current speed from December 2007 to June 2010. Shading indicates periods (b) from January to June 2009 and (c) from January to June 2010, in which bioluminescence blooms were recorded. The lack of data from June 24 to September 6, 2008 is due to a cable technical failure.

enhanced turbulent motion in the wakes of the PMTs (Bradner et al., 1987; Aoki et al., 1986; Amram et al., 2000). However, current speed alone fails to explain the complete record of bioluminescent activity since, for moderate current speeds, differences in the median rates of up to one order of magnitude are observed in 2009 (Fig. 2.17 b) and 2010 (Fig. 2.17 c). For instance, on March 8, March 11 and April 8-12, 2010, bioluminescence peaks at 800 to 1300 kHz while current speeds are rather low, from 10 to 15 cm s<sup>-1</sup> (Fig. 2.17 c) a speed range usually associated to median rates of around 100 kHz. These bioluminescence bursts clearly correspond to significant increases in both potential temperature ( $\Delta\theta = 0.03 - 0.05^\circ C$ ) and salinity ( $\Delta S = 0.005 - 0.015$ ). As the deep water mass at the ANTARES site is the WMDW, characterized in 2008 by a narrow range of temperature and salinity ( $\theta = 12.89 - 12.92^\circ C, S = 38.474 - 38.479$ ), the increases above the normal range of variation observed in 2009 and 2010 are indicative of the intrusion of a distinct water mass (Fig. 2.17, see Text S1 and Fig. 2.22). It is noteworthy that neither deep-water thermohaline modification nor bioluminescence blooms were recorded in 2008 (Fig. 2.17 a).

To illustrate the link between the intrusion of newly formed deep water and high bioluminescence, we use a salinity threshold of 38.479 as marker of such intrusions at the ANTARES site. This value has been defined using a statistical decision tree (Fig. 2.11) and also corresponds to the 96<sup>th</sup> percentile of the entire salinity record. Bioluminescence data, divided into two groups above and below this salinity threshold, are presented as box-and-whisker plots versus current speed classes (Fig. 2.18). Close examination of Figure 2.18 shows that bioluminescent activity is enhanced by both increasing current speed and the renewal of the deep water. Indeed, on the one hand, the bioluminescence rates increase with current speed for each of the two bioluminescence data groups (grey and red box-and-whisker plots) and on the other hand, bioluminescence rates are always higher for new deep water (red boxes,  $S > 38.479$ ) than for pre-existing deep water (grey boxes,  $S < 38.479$ ). The Kruskal-Wallis test performed on the box-and-whisker plots attests that the red and grey boxes are significantly different ( $p < 0.001$ ) for current speeds up to 18 and 24 cm s<sup>-1</sup> in 2009 and 2010, respectively (Fig. 2.18 b-2.18 c), which means that bioluminescence rates are dependent on water mass properties too. This is

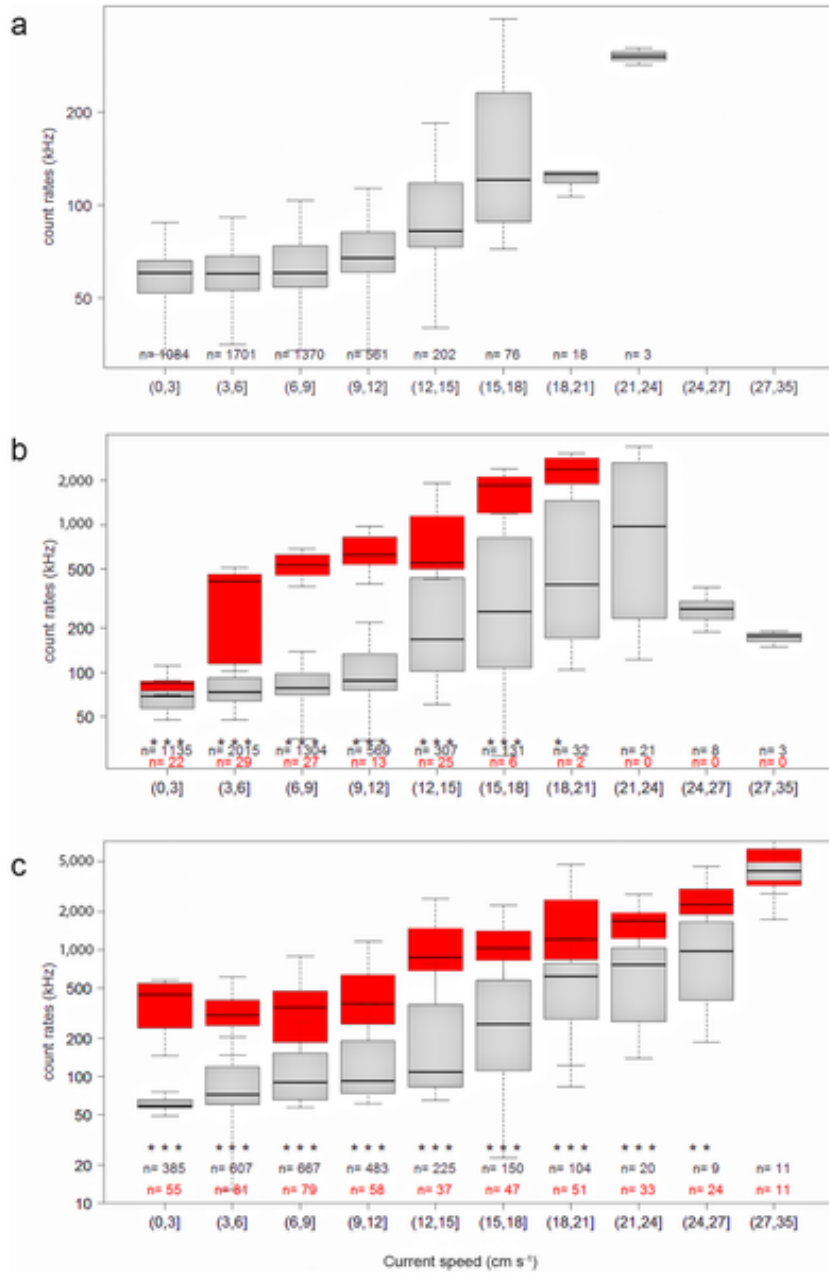


FIGURE (2.18) Links between bioluminescence, current speed and the modification of the properties of the Western Mediterranean Deep Water (WMDW). Box-and-whisker plot of median PMT counting rates (log scale) versus current speed classes for salinities higher (red) or lower (grey) than 38.479 for data recorded in (a) 2008, (b) 2009 and (c) between January and June 2010. The salinity threshold of 38.479 is used as a marker of the intrusion of newly formed deep water at the ANTARES site. While bioluminescence increases with current speed, it is also enhanced by the modification of WMDW (red box-plots). The top and bottom of each box-plot represent 75% (upper quartile) and 25% (lower quartile) of all values, respectively. The horizontal line is the median. The ends of the whiskers represent the 10th and 90th percentiles. Outliers are not represented. The statistical comparison between the two box-plots (red and grey) in each current class is given by the Kruskal-Wallis test: the observed difference between the two samples is significant beyond the 0.05 (\*), the 0.01 (\*\*) and the 0.001 (\*\*\*) levels. The absence of an asterisk in some current classes indicates that the difference between the two box-plots is not significant. The number of measurements for salinity lower or higher than 38.479 is given in black or in red, respectively. Note the different scales of figures a, b and c.

illustrated, for instance, by the 2010 record (Fig. 2.18c), which shows that the median bioluminescence rate for the  $0\text{--}3 \text{ cm s}^{-1}$  current range is about 60 kHz for the existing deep water (grey box-plots), while it reaches 400 kHz within the new deep water (red box-plots). Bioluminescent bacteria, which are not affected by mechanical stimulation (Nealson and Hastings, 1979; Bradner et al., 1987) and are able to glow continuously under specific conditions (Nealson and Hastings, 1979; Miller et al., 2005), are excellent candidates as main contributors to these bioluminescence blooms.

### **Deep-water convection in the NW Mediterranean Sea**

To determine the origin of the newly formed deep water observed at the ANTARES site in 2009 and 2010, we investigated whether dense shelf water cascading and/or open-sea convection occurred in winter months.

Instrumented mooring lines located at the center of the deep convection region (LION site at  $42^{\circ}02'9\text{N}$ ,  $04^{\circ}41'9\text{E}$ ; Fig. 2.16a) and in Lacaze-Duthiers Canyon (LDC site at  $42^{\circ}26'9\text{N}$ ,  $03^{\circ}33'9\text{E}$ ; Fig. 2.16 a) provided temperature, salinity and current speed time-series from different water depths (Fig. 2.19) synchronous to the ANTARES record. While no deep ( $>1,000 \text{ m}$ ) dense shelf water cascading took place during the study period (Fig. 2.19 a), bottom-reaching open-sea convection was observed in the basin down to 2,300 m depth during wintertime in 2009 and 2010, which led to the homogenization of the water column (Fig. 2.19 b). Increases in deep water temperature (Fig. 2.19 b) and salinity (Fig. 2.19 c) are due to the mixture of sinking cold surface water with warmer and saltier LIW. In winter 2008, open-sea convection only affected the upper 1,000 m of the water column and did not alter the deep water mass. Current measurements showed the strong barotropic character of horizontal velocities (Fig. 2.19 d) and high vertical velocities (Fig. 2.19 e) during intense mixing periods. Once the surface forcing abates, convection ceases and intense sub-mesoscale eddies carry discrete volumes of the newly formed deep water away from the convection area (Testor and Gascard, 2006). The delay between the appearance of the thermohaline anomalies at the LION site in late winter and their arrival at the ANTARES site in spring is compatible with the spreading of the

newly-formed deep water in the Gulf of Lion and subsequent mixing with pre-existing deep water (Béthoux et al., 2002; Durrieu de Madron et al., 2013; Schröder et al., 2006; Testor and Gascard, 2006). Further mixing could take place at the ANTARES site due to enhancement of vertical motion by the interaction of instabilities in the surface cyclonic Northern Current with the topography of the continental slope (Van Haren, 2011). The area of open-sea convection, as obtained from satellite imagery (see Fig. 2.23), was much smaller during winter 2008 than in 2009 and 2010 when it covered most of the deep Gulf of Lion (Figs. 2.16 b-d). Furthermore, it was larger and closer to the ANTARES site in 2010 than in 2009 (Fig. 2.16 c-d), which may explain why the signature of new deep-water recorded at the ANTARES site is stronger in 2010 than in 2009 (Fig. 2.17).

### Link between bioluminescence blooms and deep-water convection

All evidence points to deep-water formation by open-sea convection in the Gulf of Lion as the cause of the renewal of deep water at the ANTARES site that triggered the bioluminescence blooms observed in 2009 and 2010.

During and in the aftermath of the convection period large amounts of organic matter, both in particulate (POC) and dissolved (DOC) form, are exported from the productive upper ocean layer down to the deep (Stabholz et al., 2013; Martín et al., 2010; Santinelli et al., 2010). The resuspension of soft sediments covering the deep seafloor by bottom currents during the reported period could also inject organic matter into the deep-water mass (Stabholz et al., 2013; Martín et al., 2010). Changes in DOC concentration at the ANTARES site are shown by discrete measurements carried out at 2,000 m depth during oceanographic cruises from December 2009 to July 2010 (Fig. 2.24). DOC concentration significantly increased from  $42 \pm 1$  mM in December 2009, prior to the convection period, to  $63 \pm 1$  mM in March and May 2010 when the new deep water mass occupied the ANTARES site, concurrently with higher oxygen contents in bottom waters between March and mid-June 2010. Subsequently, DOC concentration decreased to 45 in mid-June and mid-July 2010 (Fig. 2.24). Such an injection of organic matter into the deep water mass has the potential to fuel the deep-sea biological activity, thus stimulating

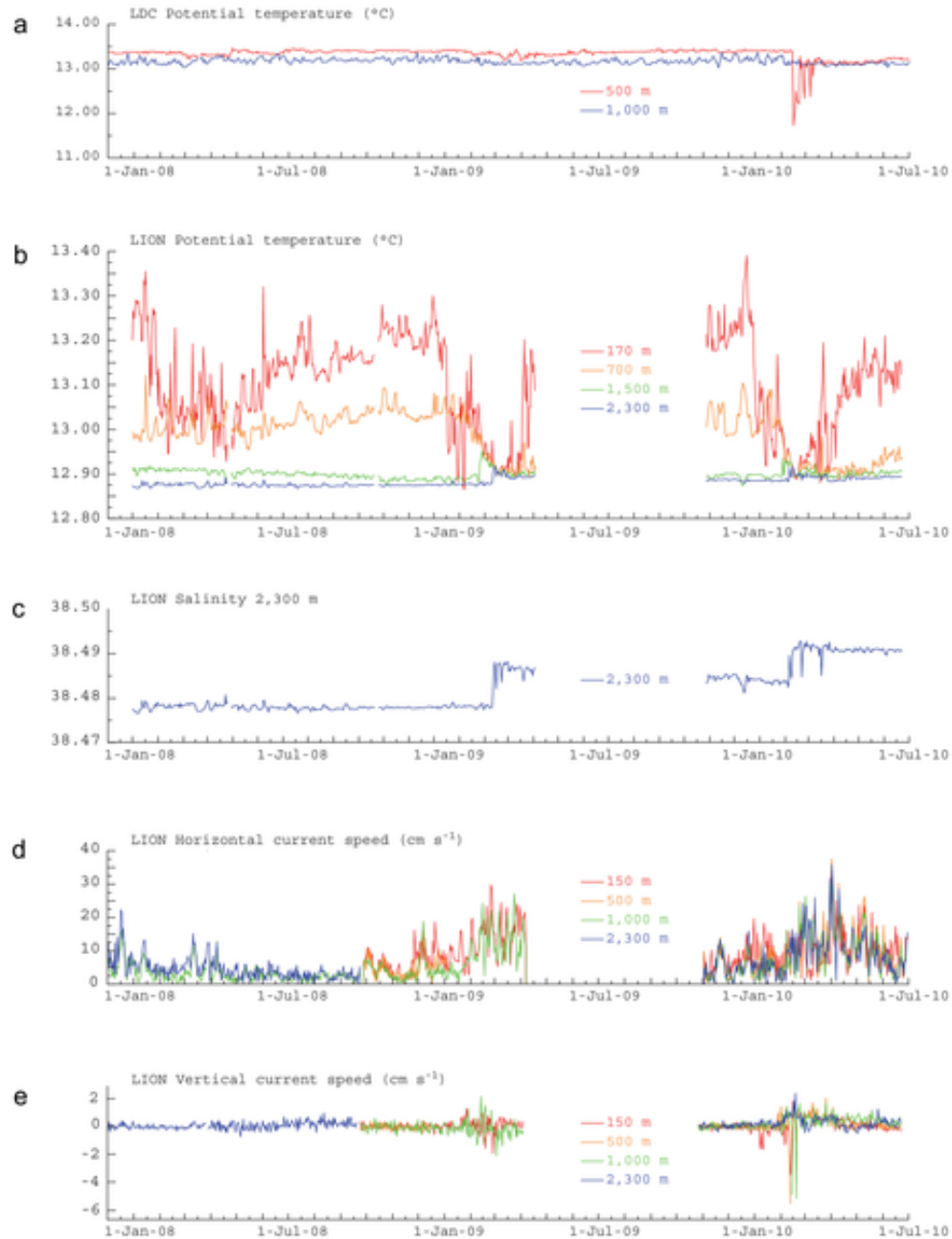


FIGURE (2.19) Time series of oceanographic parameters measured at the Lacaze-Duthiers Canyon (LDC) and the open-sea convection region in the Gulf of Lion (LION) from January 2008 to June 2010. (a) Potential temperature at 500 and 1,000 m depth at the LDC mooring site and (b) from various water depths at the LION site, jointly with (c) salinity at 2,300 m depth, (d) horizontal current speed and (e) vertical current speed from various water depths at the LION site. The four levels of temperature measurements at LION presented here are a sub-set of measurement depths (see Fig. 2.20). Essentially stable temperatures in the deepest layers in 2008 show that open-sea convection reached only 700 m and did not modify the deep water in the study area. In contrast, strong convection events, reaching 2,300 m depth, occurred during February-March 2009 and 2010 with an abrupt cooling of the upper water column and an increase in temperature and salinity in the deep layers. A concurrent increase in current speed was also noticed in winter 2009 and 2010. The 5-month long data gap in 2009 is due to a damaging of the mooring line during the April 2009 recovery, which induced a postponement of its redeployment to September 2009.

bioluminescence activity. The increase in DOC concentration matches with observations reported by (Santinelli et al., 2010) for different regions of the Mediterranean Sea where deep convection occurs. These authors showed a high mineralization rate of DOC in recently ventilated deep waters, which is mainly attributed to bacteria. Bioluminescent bacteria were isolated at the ANTARES site during a previous period of high bioluminescent activity in 2005 (Al Ali et al., 2010). Amongst them, we identified a piezophilic strain, *Photobacterium phosphoreum* ANT-2200 (Al Ali et al., 2010; Martini et al., 2013a), *P. phosphoreum* being the dominant bioluminescent species in the Mediterranean Sea (Gentile et al., 2009). These luminous bacteria likely represent the main organisms responsible for the higher level of bioluminescence detected at the ANTARES site. Such contribution is especially noticed when the current speed is low within the convection season (Fig. 2.18 b-2.18 c). Finally, the flow associated with deep convection events might likely carries significant amounts of bioluminescent organisms too, which can also contribute to the bioluminescence blooms observed in 2009 and 2010 due to their collision with PMTs and/or their stimulation by turbulent motion in the wakes of PMTs when current speed is high.

## Conclusions

We present evidence for seasonal episodes of dense water formation driven by atmospheric forcing being a major vector in fuelling the deep-sea pelagic ecosystem and inducing bioluminescence blooms after a fast transfer of the ocean surface signal. Since dense water formation occurs in other ocean regions worldwide (Marshall and Schott, 1999), we anticipate that an enhancement of the deep pelagic ecosystem activity similar to that observed in the NW Mediterranean Sea occurs there too, challenging our understanding of the carbon dynamics in the ocean. Dense water formation is likely to be altered by the on-going global warming. Recent models (Somot et al., 2006; Herrmann et al., 2008) based on the A2 IPCC scenario indicate a strong reduction in the convection intensity in the Mediterranean Sea for the end of the 21<sup>st</sup> century, which will induce a massive reduction in organic matter supply and ventilation of the deep basin. Hence changes in the deep Mediterranean ecosystem more intense than those already observed

in both the Eastern (Roether et al., 1996; Weikert et al., 2001) and the Western Mediterranean (Pusceddu et al., 2013) basins are forecasted for the near future, a situation that could also occur but remain unnoticed in other sensitive areas of the world ocean. Our results illustrate the potentially far reaching multidisciplinary scientific and societal benefits of the installation of cabled deep-sea observatories in critical ocean areas.

## Methods

The ANTARES neutrino telescope comprises a three-dimensional array of 885 Hamamatsu R7081-20 photomultiplier tubes (PMTs) distributed on 12 mooring lines (Ageron et al., 2011; Aguilar et al., 2005). These PMTs are sensitive to the wavelength range of 400-700 nm, which matches the main bioluminescence emission spectrum (440-540 nm) as reported in Widder (2010). An extra mooring line (named IL07) equipped with RDI 300 kHz acoustic Doppler current profilers, a conductivity-temperature-depth (SBE 37 SMP CTD) probe and PMTs was added to monitor environmental variables (Fig. 2.20). All moorings are connected to a shore-station via an electro-optical cable that provides real-time data transmission (Aguilar et al., 2007). A dedicated program of bioluminescence monitoring was implemented to measure the total number of single photons detected every 13 ms for each PMT. To consistently compare PMT counting rates (bioluminescence) with oceanographic data (temperature, salinity, current speeds) considering the acquisition interval of the later (15 minutes), we calculated the median rates as a mathematical estimator of PMT counting rates. The median was selected instead of the arithmetic mean because of its higher robustness and least disturbance by extreme values. Median rates were expressed in thousands of photons per second or kHz (see Text S1 and Fig. 2.21 a). The main light contributions recorded by PMTs result from dark noise, from Cherenkov radiation induced by the beta decay of  $^{40}\text{K}$  in seawater and from bioluminescence. The dark noise is about  $3 \pm 1$  kHz and remains constant with time (Aguilar et al., 2005). The Cherenkov radiation induced by the beta decay of  $^{40}\text{K}$  in seawater produces a background of about  $37 \pm 3$  kHz (Amram et al., 2002), found to be constant within the statistical errors over a period of a few years (Aguilar et al., 2006, 2010). Therefore, all light increases over this constant background ( $40 \pm 3$  kHz) can only

be due to bioluminescence. The records of light intensity at IL07 are representative of those collected by the whole array of ANTARES PMTs (see Text S1 and Fig. 2.21 b).

Potential temperature, salinity, horizontal and vertical current speeds (Fig. 2.20) at the LION mooring line were measured with SBE 37 SMP CTD probes and Nortek Aquadopp Doppler current-meters regularly spaced between the subsurface (150 m) and the seabed (2,350 m). Potential temperatures and vertical velocities were corrected for the current-induced tilting and deepening of the line. Hourly potential temperatures at the LDC mooring line were measured with the temperature sensor of Nortek Aquadopp Doppler current meters at 500 and 1,000 m depth.

Proper calibrations of the CTD probes were performed using the pre- and post-deployment calibrations made by the manufacturer. The inter-comparison of instruments complied with quality control procedures.

**Acknowledgments** The authors thank the captains and crews of R.V. Tethys II and L'Europe for cruise assistance. Technical support by Ifremer, Assistance Ingénierie Management (AIM) and Foselev Marine during sea operation and CCN<sub>2</sub>P3 for providing computing facilities is greatly appreciated.

#### Funding:

This work was partially funded by the ANR-POTES program (ANR-05-BLAN-0161-01), ANTARES-Bioluminescence project (INSU-IN2P3), AAMIS project (Univ. Méditerranée), EC2CO Biolux project (CNRS INSU), Excellence Research Groups (2009-SGR-1305, Generalitat de Catalunya), EuroSITES (FP7-ENV-2007-1-202955), MARINERA-REDECO (CTM2008-04973-E/MAR), HERMIONE (FP7-ENV-2008-1-226354), KM3NeT-PP (212525), ESONET NoE (FP6- GOCE-036851), DOS MARES (CTM2010-21810-C03-01) and CONSOLIDER-INGENIO GRACCIE (CSD2007-00067) projects. SM was granted a MERNT fellowship (Ministry of Education, Research and Technology, France). LH acknowledges the support of the Direction Générale de l'Armement (supervisor: Elisabeth Gibert-Brunet). The authors also acknowledge the

financial support of the funding agencies: CNRS, CEA, ANR, FEDER fund and Marie Curie Program, Régions Alsace and Provence-Alpes-Côte d’Azur, Département du Var and Ville de La Seyne-sur-Mer, France ; BMBF, Germany ; INFN, Italy ; FOM and NWO, the Netherlands ; Council of the President of the Russian Federation for young scientists and leading scientific schools supporting grants, Russia ; ANCS, Romania ; MICINN (FPA2009-13983-C02-01), PROMETEO (2009/026) and MultiDark (CSD2009-00064). The funders had no role in study design, data collection and analysis, decision to publish, or preparation of the article.

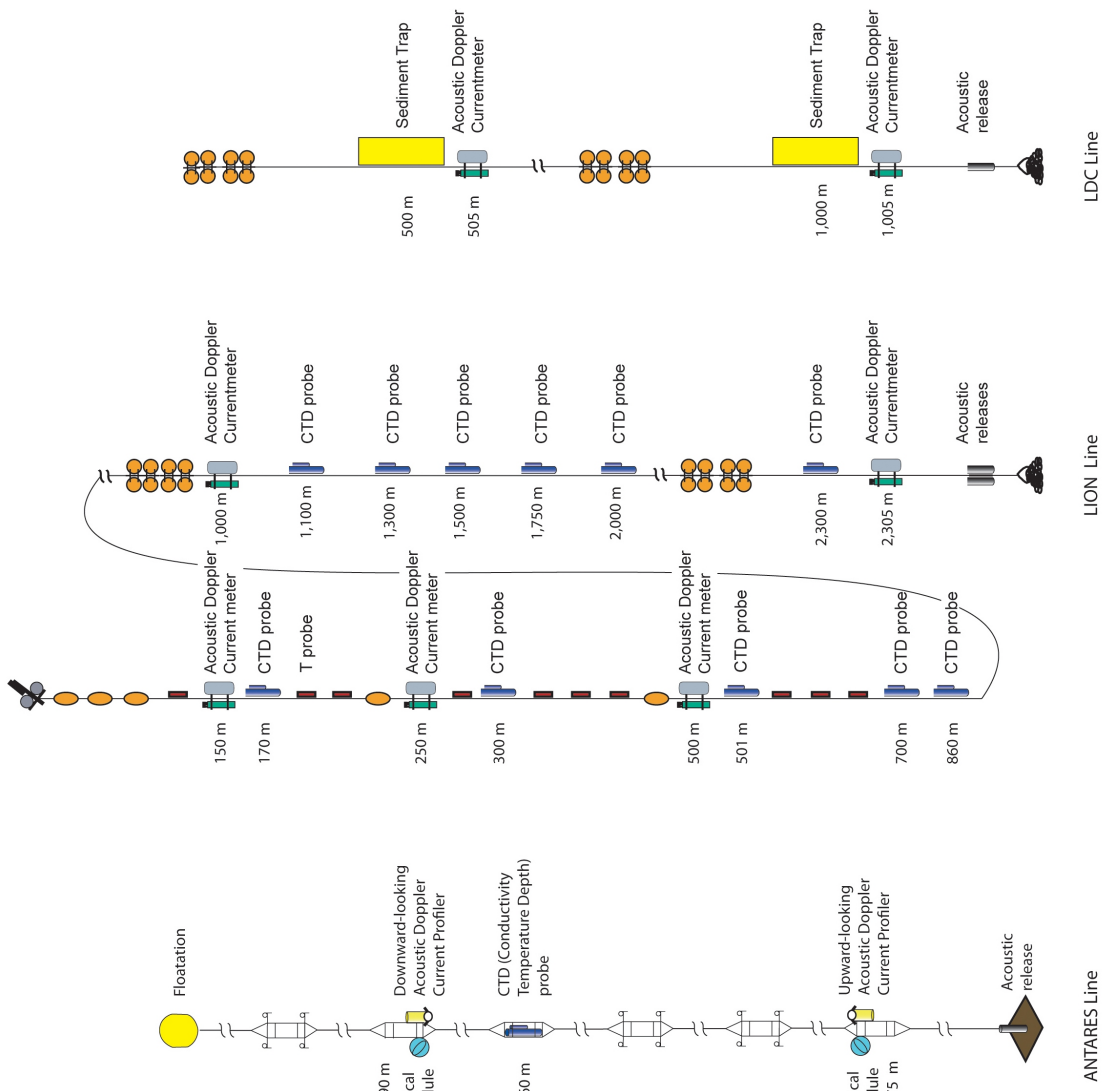


FIGURE (2.20) Supporting information. Configuration of the mooring lines from which the data presented in this study were obtained. They include the cabled IL07 ANTARES as well as the autonomous LION and Lacaze-Duthiers Canyon (LDC) mooring lines. Location is shown in Fig. 2.16.

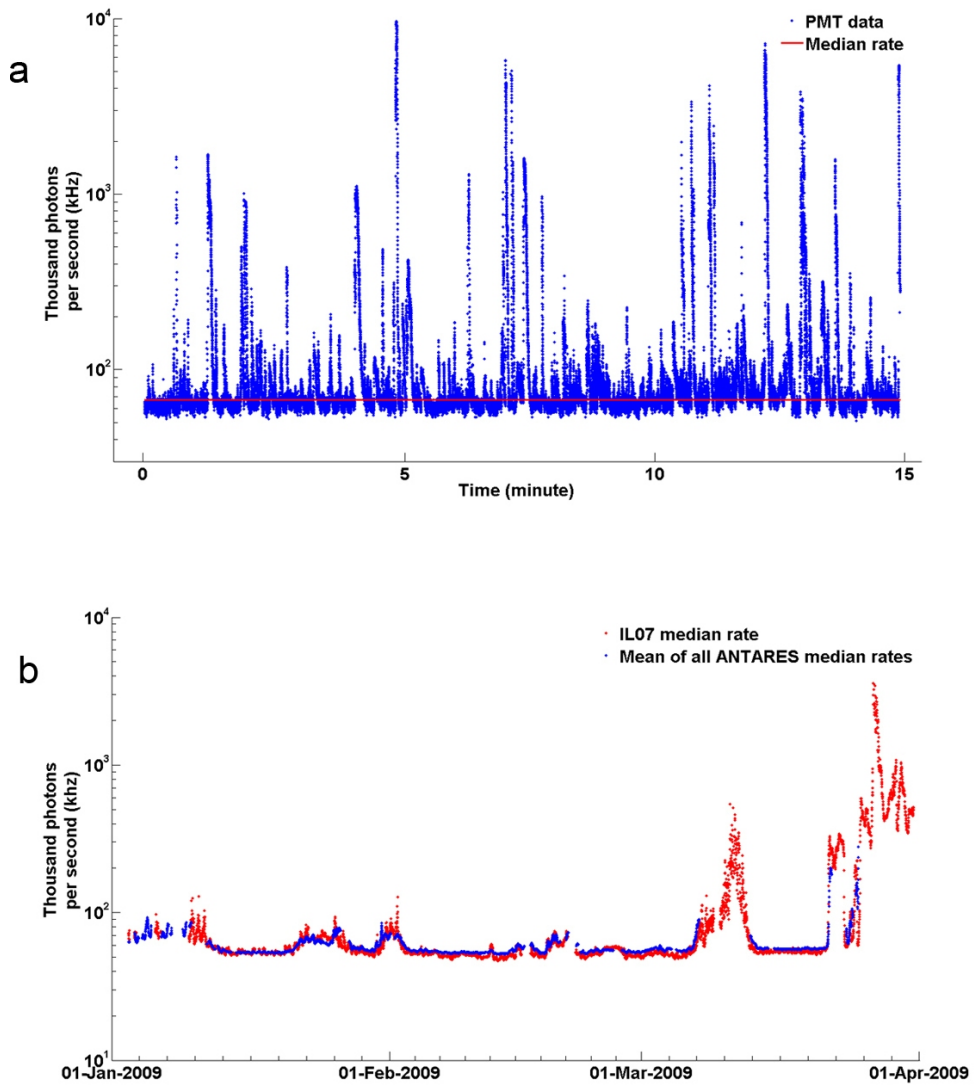


FIGURE (2.21) Supporting information. (a) Raw counting rates from one photomultiplier (PMT) on the IL07 line (ANTARES site). Counts are expressed in thousands of photons per second (kHz). The median rate is computed for each 15-minute data sample (red horizontal line). The dataset shown in the figure was recorded on March 28<sup>th</sup>, 2010 with a median rate of 68 kHz and a current speed of  $13 \text{ cm s}^{-1}$ . (b) Median rates from the IL07 PMT (red) and mean of all median rates of the 885 ANTARES PMTs (blue) from January to April 2009.

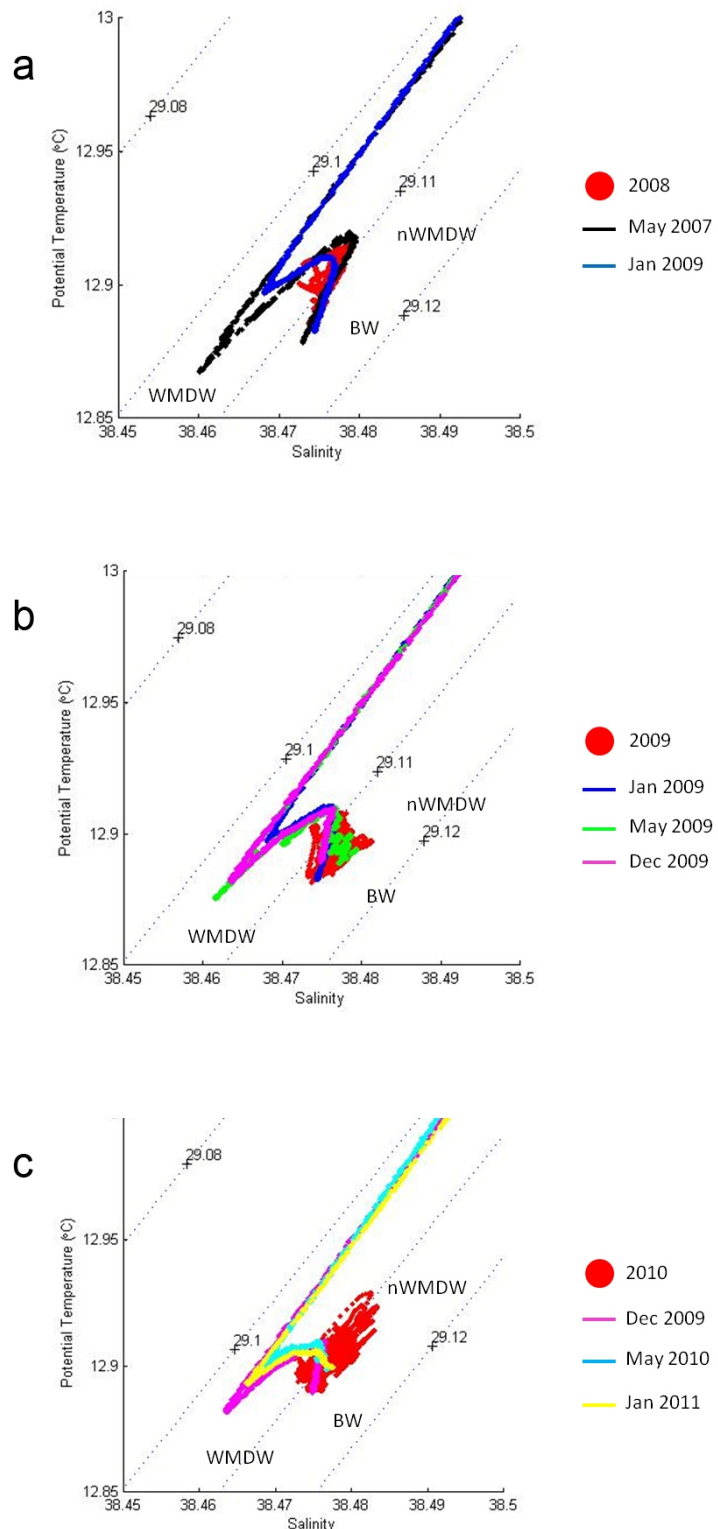


FIGURE (2.22) Supporting information. Potential temperature versus salinity diagram of near-bottom CTD time-series at the ANTARES site from the IL07 line (red dots) and CTD profiles (lines) collected close to the ANTARES site. (a) May 2007 to January 2009; (b) January to December 2009; and (c) December 2009 to January 2011. The data shown are from depths in excess of 1,000 m. Dotted lines correspond to potential density anomaly isolines in  $\text{kg m}^{-3}$ .

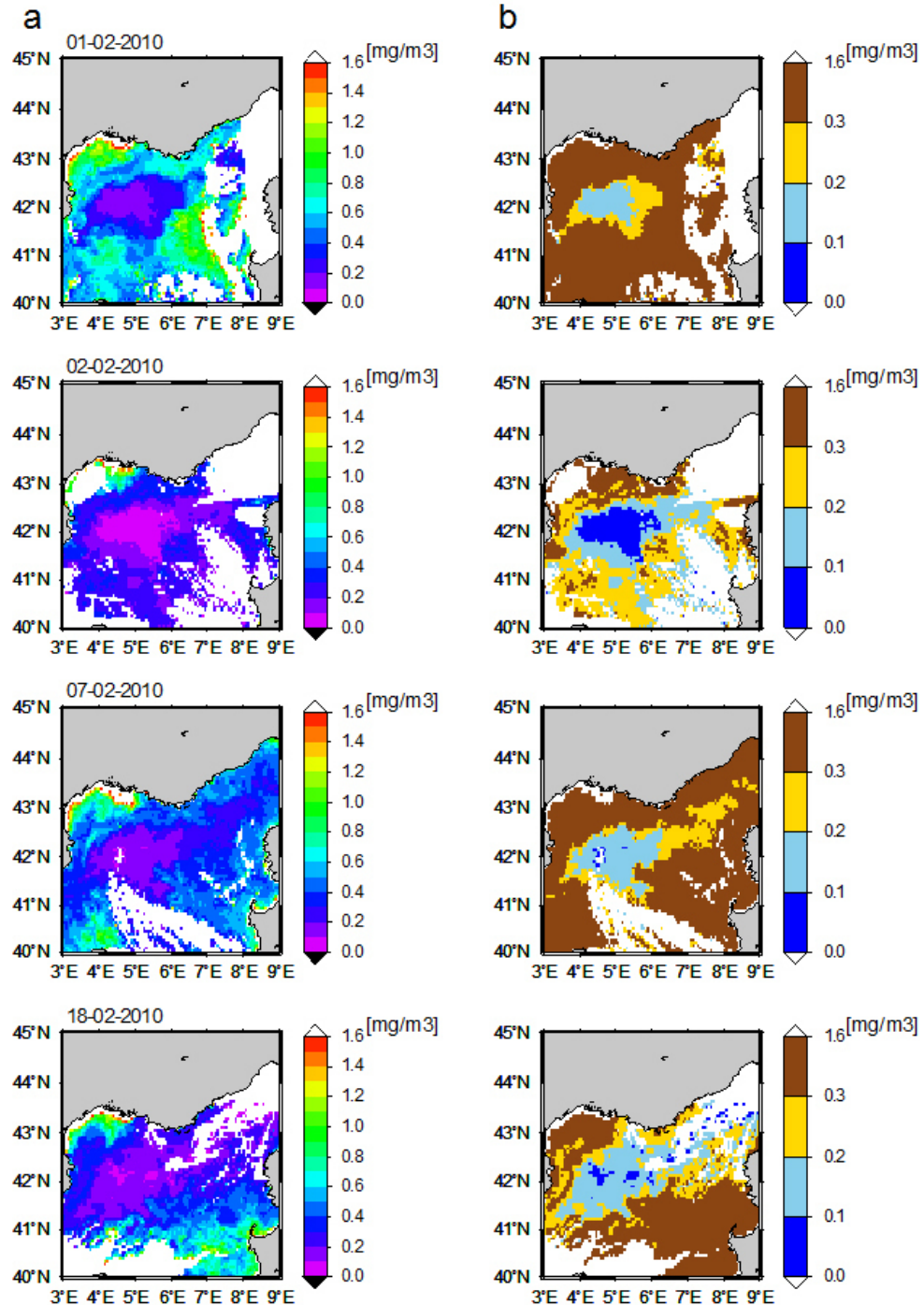


FIGURE (2.23) Supporting information. Illustrative ocean colour satellite images used to outline the limits of winter open-sea convection areas in the Gulf of Lion. (a) Images plotted with a classical, full range, linear palette. (b) Images plotted with a simplified four level palette. The images shown correspond to days 1, 2, 7 and 18 February 2010, which are also transferred into Fig. 2.16 b-d. White pixels are indicative of lack of data due to cloud coverage.

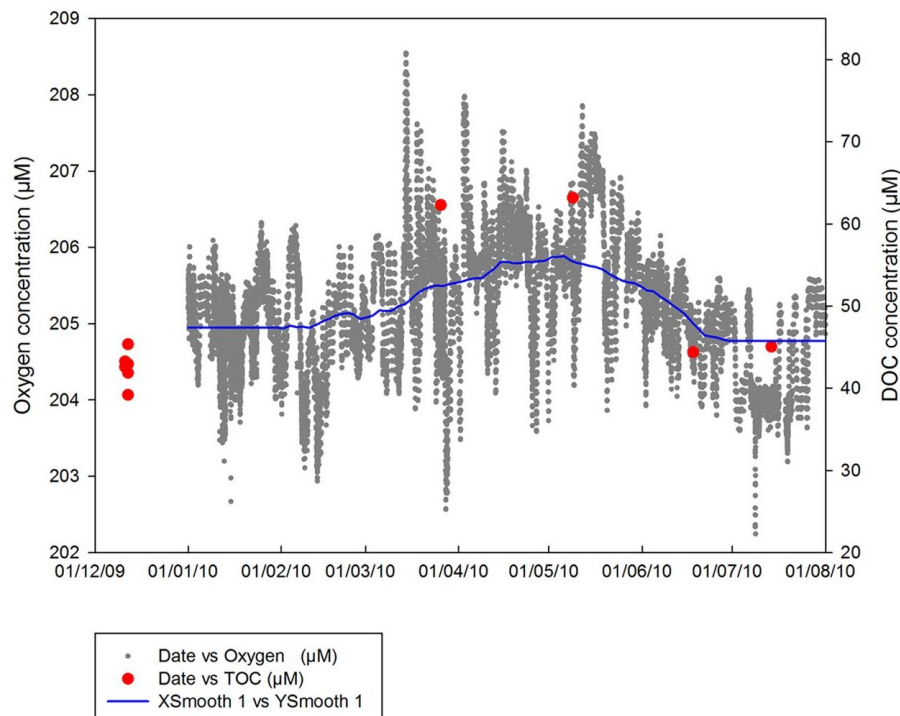


FIGURE (2.24) Supporting information. Dissolved organic carbon and oxygen concentrations at the ANTARES site in 2010. Dissolved Organic Carbon (DOC) was measured by high temperature combustion on a Shimadzu TOC 5000 analyzer (Sohrin and Sempéré, 2005). A four point-calibration curve was performed daily with standards prepared by diluting a stock solution of potassium hydrogen phthalate in Milli-Q water. Procedural blanks run with acidified and sparged Milli-Q water ranged from 1 to  $2\mu\text{M}$  C and were subtracted from the values presented here. Deep seawater reference samples (provided by D. Hansell; Univ. Miami) were run daily ( $43.5\mu\text{M}$  C,  $n = 4$ ) to check the accuracy of the DOC analysis. Oxygen concentration time-series was obtained using an oxygen optode Aanderaa fitted on the IL07

## 2.5 Conclusions

Through this chapter, the first analysis of multivariate time series at the ANTARES site, leads to the detection of several observations, despite a descriptive approach. The deep ANTARES site is characterized by current direction East-West with speed generally lower than  $20 \text{ cm s}^{-1}$ . This current direction is unexpectedly following the general path of the cyclonic surface mesoscale Northern Current (NC) ([Millot and Taupier-Letage, 2005](#); [Millot, 1999](#)). However, phenomena such as deep circulation, topography, and mesoscale eddies could possibly locally modify the expected current direction at this deep station ([Testor and Gascard, 2006](#)). To successfully explain such result, a detailed study is needed explaining the respective weight of local (NC instability forced by topographic effects) vs. regional circulations (downward propagating mesoscale variability of the NC, interactions with the spreading Western Mediterranean Deep Water...). The bioluminescence recorded on the instrumented line IL07 is representative of the whole telescope and generally lower than 1,500 kHz. Moreover, we found that the bioluminescence intensity is correlated with the event detection using cameras placed on the instrumented line.

However, high bioluminescence-activity events have been distinguished in March 2009 and March 2010. During these events, bioluminescence intensity is linked to current-speed values above a threshold of  $19 \text{ cm s}^{-1}$ , and determined using regression trees. Moreover, in 2009, the highest current-speed intensity is essentially coming from the western direction. On the contrary, in 2010, this direction is mainly South-East. Furthermore, a high bioluminescence activity is linked to similar current directions, West in 2009 and South-East in 2010. These similar informations do not permit to discriminate if the high bioluminescence activity observed is mainly due to current direction or current speed. Regression trees permit to detect changes in variability over time that occurred at the same time for bioluminescence, salinity and temperature. Noticeably, a threshold defined for the second event detected has been highlighted in March 18<sup>th</sup> 2010. These changes in variability have not been noticed for current speed. The highest values for bioluminescence are dependent on both current speed above  $19 \text{ cm s}^{-1}$  and temperature above  $12.92^\circ\text{C}$  (see regression trees Figure [2.11](#)) or with a salinity above à 38.479

(see Tamburini et al., 2013), depending on mathematical methods used. During these strong events, the study of video-camera images recorded using automatic detection demonstrates that the number of detected events is not anymore correlated to the bioluminescence activity.

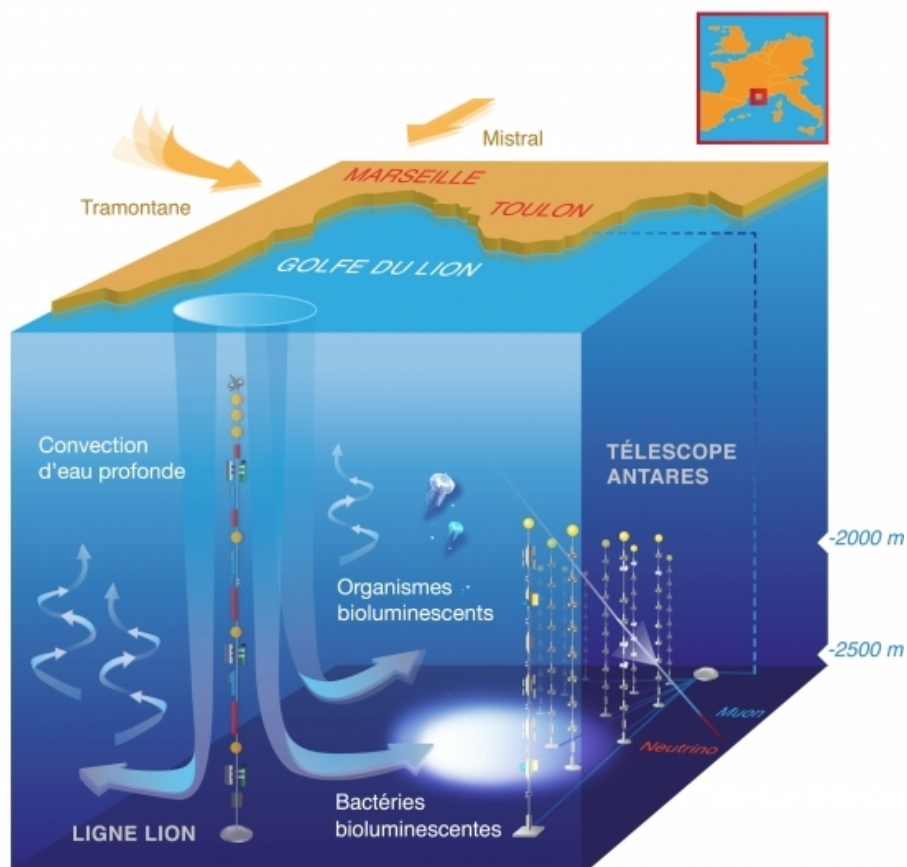


FIGURE (2.25) Artistic representation of newly-formed water mass in the Gulf of Lion and their impact on biological activity (bioluminescence) at the ANTARES station. Graphical design: [www.mathildedestelle.com](http://www.mathildedestelle.com).

The analysis of surrounding oceanographic data, at a regional scale, gave clues to explain such sudden changes in bioluminescence activity by new water-mass formation at the surface inducing a deep-sea convection (Figure 2.25). This phenomenon reaches

the ANTARES observatory in March 2009 and 2010, modifying both the activity and the presence of potentially bioluminescent populations. Possible links between (1) new water-mass input, enrichment of the environment, (2) duration of the emission of bioluminescence, (3) increase of the signal baseline as well as (4) photomultiplier ability to detect bioluminescent bacteria, led this work to focus on the characterization of bacterial bioluminescence. These first investigations highlighted the interest of developing methods for time series analysis, in order to detect such high bioluminescence-intensity events as well as discriminating possible links between environmental variables over time.



# CHAPITRE 3

---

*In situ* dataset analyzes using statistical methods adapted to time  
series

---

## Sommaire

---

<b>3.1 Article 2 . . . . .</b>	<b>78</b>
3.1.1 Foreword . . . . .	78
3.1.2 Relation between deep bioluminescence and oceanographic va- riables : a statistical analysis using time-frequency decompositions.	79
<b>3.2 Complementary data . . . . .</b>	<b>109</b>

---

## 3.1 Article 2

### 3.1.1 Foreword

Following the observation and description of two events of high bioluminescence intensity in March 2009 and March 2010, the use of appropriate statistical methods was needed for time series analysis. In signal processing, several methods exist and can be based on model approach (ARMA or ARIMA models for example), time-dependent methods (Markov chains, autocorrelation) or frequency-dependent methods (spectral analyzes, seasonality). In this work, a time-frequency analysis has been performed and developed on chronological data characterized as non-stationary and non-linear. A second objective of time series analysis from the ANTARES station is to discriminate bioluminescence events related to the current speed and those related to water-mass modifications. The necessity to cross informations of this multivariate dataset implies the comparison and the use of two conjoint methods such as the wavelet and the Hilbert-Huang decomposition methods.

*This work has been initiated during my master 2 and finalized during my PhD work. I performed the statistical analyzes supervised by D. Nerini. C. Tamburini took part in the result interpretation within an ecological context.*

### 3.1.2 Relation between deep bioluminescence and oceanographic variables : a statistical analysis using time-frequency decompositions.

Séverine Martini<sup>1,2,\*</sup>, David Nerini<sup>1,2</sup>, Christian Tamburini<sup>1,2</sup>

<sup>1</sup>Aix-Marseille Université, Mediterranean Institute of Oceanography (MIO), 13288, Marseille, Cedex 09, France

<sup>2</sup>Université du Sud Toulon-Var (MIO), 83957, La Garde cedex, France; CNRS/INSU, MIO UMR 7294; IRD, MIO UMR 235

\* Corresponding author : [severine.martini@univ-amu.fr](mailto:severine.martini@univ-amu.fr)

Submitted to Progress in Oceanography, under revision

**Abstract**

We consider the statistical analysis of a two-years high-frequency-sampled time series, between 2009 and 2010, recorded at the ANTARES observatory in the deep NW Mediterranean Sea (2,475 m depth). The objective is to analyze relationships between bioluminescence and environmental data (temperature, salinity and current speed). As this entire dataset is characterized by non-linearity and non-stationarity, two time-frequency-decomposition methods (wavelet and Hilbert-Huang) have been tested. These mathematical methods are dedicated to the analysis of oscillations within a signal at various time and frequency scales. Many applications of these methods dealing with only one variable may be found in the literature. The methodological contribution of this work is to propose some statistical tools dedicated to the study of relationships between two time series. Our study highlights three events of high bioluminescence activity in March 2009, December 2009 and March 2010. We show that the two events occurring in March 2009 and 2010 are correlated to the arrival of newly formed deep water masses at frequencies about  $4.8 \times 10^{-7}$  (period of 24.1 days). In contrast, the event in December 2009 is only correlated with current speed at frequencies about  $1.9 \times 10^{-6}$  (period of 6.0 days). The jointed use of wavelet and Hilbert-Huang decompositions has proved to be successful for the analysis of multivariate time series. These methods are well-suited in a context of increasing number of long time series recorded in oceanography.

## Introduction

The sampling and understanding of complex environmental systems aim at the detection of potential disturbances as a shift from the intrinsic variability of these systems. Marine systems are variable at all time and space scales (Hewitt et al., 2007) and their variability is still poorly understood due to sampling strategy, instrumentation and spatio-temporal-heterogeneity challenges. In response to this lack of knowledge, there is an international effort to capitalize oceanographic data and costs of autonomous and for mobile infrastructures that enable the detection of long term environmental context as well as episodic events or perturbations (Favali and Beranzoli, 2006). As an example, OceanSITES, and more generally the Global Ocean Observing System (GOOS), are the major scientific teams integrating a global network of more than 60 *in situ* observatories and acquiring long-term and high-frequency time series (Send and Lankhorst, 2011) over the world.

The ANTARES project (Astronomy with a Neutrino Telescope and Abyss environmental RESearch) developed one of those deep-sea-cabled observatory, in the North-Western Mediterranean Sea (Figure 3.1), since the end of 2007. This infrastructure is part of a global data network such as EMSO, KM3NeT, ESONET and EuroSITES for example. At first, the ANTARES observatory is dedicated to the search of high-energy particles such as neutrino (Amram et al., 2000; Aguilar et al., 2007; Ageron et al., 2011). About 885 photomultiplier tubes (PMTs) are installed between 2,000 and 2,400 m depth for the purpose of particle Physics. All the 12 ANTARES mooring lines are connected, via an electro-optical cable to a shore station providing real-time acquisition. With the installation of a specific line, namely IL07 (Tamburini et al., 2013), this deep observatory gives the opportunity to record simultaneously high frequency oceanographic data such as current speed, salinity and temperature (Figure 3.2). The IL07 is also equipped with PMTs devoted to the recording of bioluminescence activity. These datasets provide an extraordinary way to study the dynamics of the deep ecosystem in real time and at high frequency (Craig et al., 2009).

Recently, Tamburini et al. (2013) proposed an introductory and descriptive analysis of ANTARES oceanographic time series gathering both physical and biological variables. This has been jointly performed with synchronous hydrological records from a surrounding station located in the Gulf of Lion. They highlighted a link between high bioluminescence activity and changes in the properties of deep waters (temperature and salinity as proxies). Such changes attributed to an open-sea-convection event have renewed the deep waters (so called newly formed deep water) by the fall of upper ocean layer through the water column (Tamburini et al., 2013; Marshall and Schott, 1999; Stabholz et al., 2013; Béthoux et al., 2002). Then, open-sea convections represent a major vector in fueling the deep-sea ecosystem and inducing bioluminescence blooms.

The present study attempts to understand the mechanisms inducing deep-sea bioluminescence activity using temperature, salinity, current speed and bioluminescence time series on the same ANTARES dataset of Tamburini et al. (2013). The exploration of characteristic scales in time and frequency, in this high-frequency-sampled dataset, is achieved using statistical methods for signal processing. While most environmental data are non-stationary (Rao and Hsu, 2008; Cazelles et al., 2008; Ghorbani, 2013) most methods used in time-series analyzes are based on stationarity assumptions, as the Fourier decomposition does (Frazier, 1999). Firstly, we propose the use of two complementary mathematical methods (Wavelet and Hilbert-Huang decomposition) to deal with non-stationarity and to decompose each time series within time and frequency space. Secondly, we suggest original tools to quantify and illustrate links between bioluminescence time-frequency decomposition and other environmental variable time-frequency decompositions.

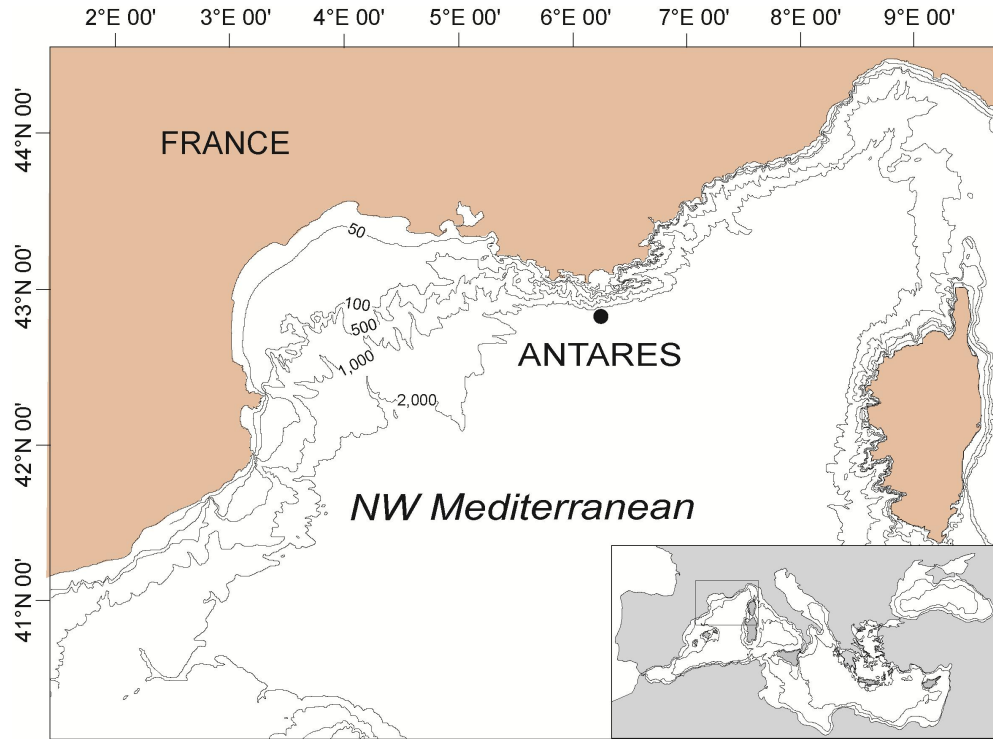


FIGURE (3.1) Map of the North-Western Mediterranean Sea and the ANTARES site (black dot) where the underwater neutrino telescope is immersed at 2,475 m depth. High-frequency-sampled time series of bioluminescence, temperature, salinity and current speed have been sampled between 2009 and 2010 at this station.

## Dataset for the deep bioluminescence study

The ANTARES site is located 40 km off the French Mediterranean coast ( $42^{\circ}48'N$ ,  $6^{\circ}10'E$ ) at 2,475 m depth (see Figure 3.1). This work focuses on multivariate time series sampled from the beginning of 2009 until October 2010, for oceanographic variables such as salinity, potential temperature ( $^{\circ}C$ ) and current speed ( $cm\ s^{-1}$ ) (Figure 3.2). Moreover, bioluminescence emission ( $kHz$ ) has been recorded in 2009 and 2010, from the IL07 instrumented line of the ANTARES telescope. The unit of bioluminescence activity ( $kHz$ ) refers to the photon-counting rate per second. We consider the bioluminescence time series as a variable response submitted to changes in environmental characteristics.

In Figure 3.2, each environmental variable is recorded with a high-frequency-sampling rate, involving the presence of a high level of noise. The base line of each signal is close to

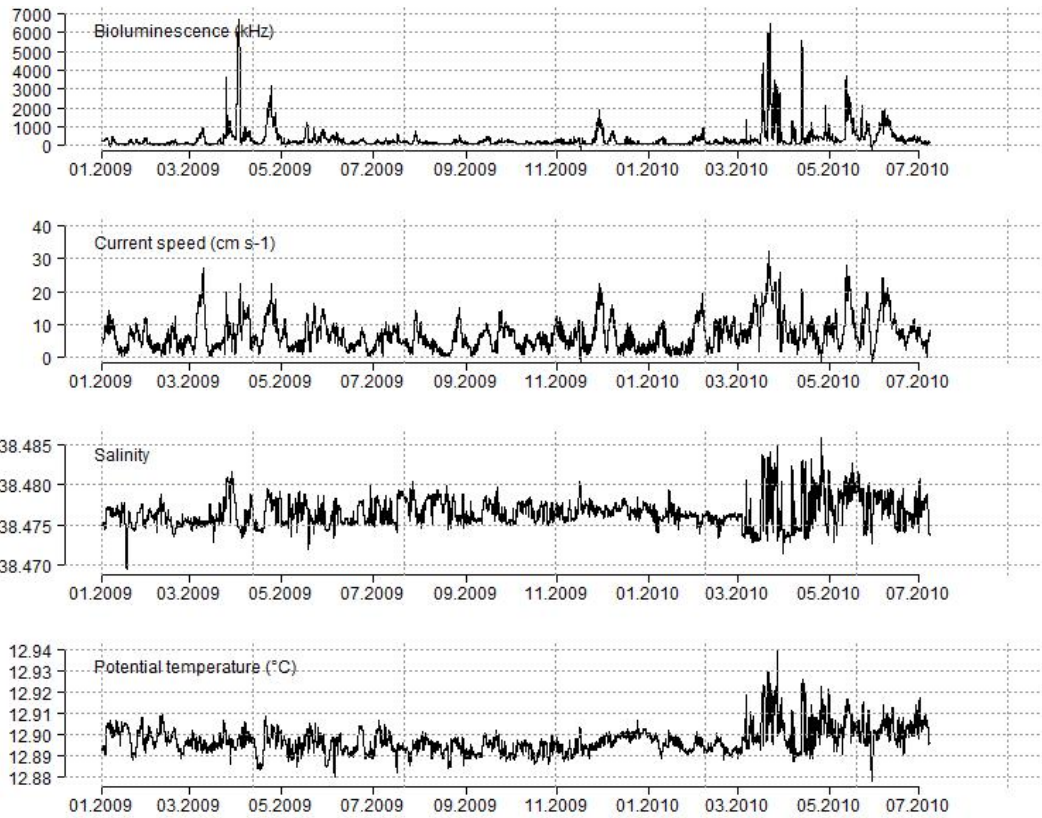


FIGURE (3.2) Time series recorded in the Mediterranean Sea, at the ANTARES station, between January 2009 and July 2010, for bioluminescence, current speed ( $cm\ s^{-1}$ ), salinity, and temperature ( $^{\circ}C$ ). Those high-frequency data, recorded each 1 to 15 minutes, are sampled at depth between 2,478 m and 2,169 m and transferred in real time to the database.

a constant background signal and does not show a clear trend, looking at low-frequency variations. However, some breaking sequences appear on each time series giving their non-linear and intermittent appearance. There is no clear time connection between those sequences from one time series to another. However, they are all characterized by a sudden increase in variability with two main events observed simultaneously occurring in April 2009 and from April to June 2010. If the connection between variables is relatively clear for the event in 2010, it is more tricky to conclude for the event in 2009 without adapted mathematical methods.

As shown previously the time series are not stationary. A time series  $X(t), t \in \mathbb{R}^+$  is said to be stationary if  $X(t)$  owns the same statistical properties (mean, variance,..) as the

TABLE (3.1) KPSS-test for testing stationarity of each time series.

Variable	KPPS value	p-value	Interpretation
Bioluminescence (kHz)	8.24	0.01	non-stationary
Current speed (cm s <sup>-1</sup> )	5.63	0.01	non-stationary
Temperature ( ° C)	8.50	0.01	non-stationary
Salinity	2.29	0.01	non-stationary

shifted time series  $X_{t+h}$  for  $h > 0$ . A Kwiatkowski-Phillips-Schmidt-Shin (KPSS) test, from [Kwiatkowski et al. \(1992\)](#), shows that all time series are non-stationary (Table 3.1).

## Methods dealing with non-stationary time series

Most methods in time-series analysis consist in an expansion of the studied signal  $X(t)$  into a linear combination of known basis functions. For the Fourier decomposition, the signal is expressed as a linear combination of trigonometric functions :

$$X(t) = \sum_{j=0}^{\infty} a_j e^{i\omega_j t}. \quad (3.1)$$

This decomposition provides an analytical expression of the function  $X(t)$  with amplitude coefficients  $a_j$  giving weight to frequencies  $\omega_j$ . Both coefficients  $a_j$  and  $\omega_j$  are independent of time providing a global decomposition of the signal in the space of frequencies.

The Hilbert-Huang (HHG) decomposition proposes a generalization of the Fourier decomposition by expanding  $X(t)$  such that :

$$X(t) = \sum_{j=1}^n a_j(t) e^{i2\pi \int \omega_j(\tau) d\tau} + R_{n+1}(t) \quad (3.2)$$

where both amplitude coefficients  $a_j(t)$  and frequency coefficients  $\omega_j(t)$  are functions of time. As further developed, this decomposition relies on a preliminary step in order to decompose the time series into  $n+1$  modes where  $R_{n+1}(t)$  is the trend of the time series.

Another decomposition with time-dependent parameters can be constructed using the

continuous wavelet decomposition

$$X(t) = \frac{1}{W_\psi} \int_{-\infty}^{\infty} \int_0^{\infty} W_X(a, b) \psi_{a,b}(t) \frac{1}{a^2} da db \quad (3.3)$$

In that case, the shape of the basis function,  $\psi_{a,b}(t)$ , is controlled by a scale parameter  $a$  which can be interpreted as a reciprocal of frequency and a shifting parameter  $b$ , both parameters varying continuously over  $\mathbb{R}^+$  and  $\mathbb{R}$  respectively. The analysis is conducted through the estimation of the coefficient  $W_X(a, b)$ , the wavelet transform, whose values are scale and time dependent and on the wavelet function  $\psi_{a,b}(t)$ . The constant  $W_\psi$  is an admissible value depending on the chosen wavelet function.

Once the basis expansion is achieved, each method gives the ability to analyze the distribution of energy over each frequency through the coefficient values of the decomposition. However, the Fourier analysis relies on a global expansion of the signal which can induce spurious harmonic components that cause energy spreading. This misinterpretation especially occurs when dealing with non-linear and non-stationary datasets as shown in Figure 3.3 B (see introduction of [Huang et al. \(1998\)](#) for more details) compared to stationary signal decomposed in Figure 3.3 A. Unlike Fourier decomposition, the continuous wavelet transforms and the HHG decomposition possesses the ability to construct a time-frequency representation as the coefficients of the decomposition are locally time dependent, which is well adapted to the analysis of non-stationary signals.

## Wavelet decomposition

### Decomposition into wavelet basis

The continuous wavelet decomposition is a consecutive pass-band filter through time series ([Torrence and Compo, 1998](#); [Addison, 2010](#)). The decomposition acts as a linear filter which extracts special features inside the signal through a projection over a wavelet basis  $\psi_{a,b}$  giving the coefficient

$$W_X(a, b) = \int_{-\infty}^{+\infty} X(t) \psi_{a,b}^*(t; a, b) dt \quad (3.4)$$

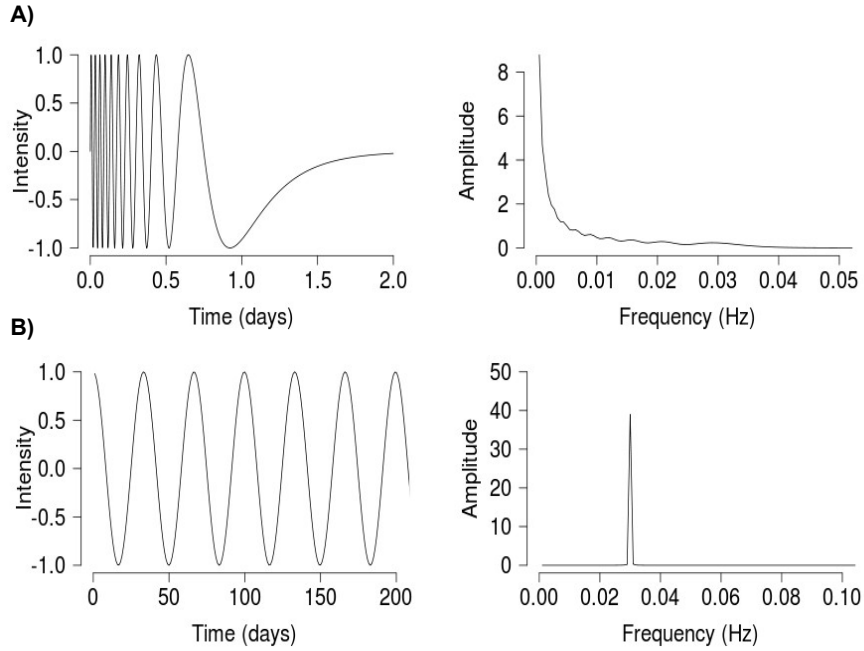


FIGURE (3.3) Two examples of signal decomposition. On the left, the signal represented over time, on the right, the periodogram over frequencies A) non-stationary and B) stationary signal. The non-stationarity spreads energy over frequencies in the periodogram representation.

where  $\psi_{a,b}^*$  denotes the complex conjugate of the basis wavelet. The peculiarity of that decomposition is the continuous dependency of the basis functions

$$\psi_{a,b}(t) = \frac{1}{\sqrt{a}}\psi\left(\frac{t-b}{a}\right) \quad (3.5)$$

regarding scale parameter  $a$  and location parameter  $b$ . The scale parameter  $a$  is inversely proportional to the frequency. The decomposition mainly relies on the choice of a mother-basis function. [Torrence and Compo \(1998\)](#) define some elements to choose the mother wavelet : orthogonality, real or complex function, shape of the mother wavelet related to shape of analyzed time series. In this study, we choose the Morlet wavelet function, commonly used in wavelet analysis. However, other choices can be relevant as well ([Ahuja et al., 2005](#); [Cazelles et al., 2008](#)). The Morlet wavelet is defined as :

$$\psi(t) = \frac{1}{\pi^{1/4}}e^{i2\pi f_0 t}e^{-t^2/2} \quad (3.6)$$

With  $\frac{1}{\pi^{1/4}}$  a normalization factor,  $e^{i2\pi f_0 t}$  the complex sinusoidal (referring to  $\cos(2\pi f_0 t + i\sin(2\pi f_0 t))$ ) and  $e^{-t^2/2}$  the Gaussian envelope. This periodic wavelet owns symmetrical properties ( $\int \psi(t)dt = 0$ ) and a unit norm ( $\int |\psi(t)|^2 dt = 1$ ). The decomposition of time series consists in coefficients for the real part of wavelet transform  $W_X(a, b)$ , at the position  $b$ . These coefficients are calculated by continuously moving the wavelet along the signal (modifying the position parameter  $b$ ) related to a specific scale parameter  $a$ . Then, a bi-dimensional surface of  $W_X(a, b)$  is constructed (Figure 3.4).

### Wavelet spectral representation

Using the wavelet decomposition, the time-frequency spectrum is plotted for bioluminescence time series in Figure 3.4 A, current speed in Figure 3.4 B, and salinity in Figure 3.4 C. For the bioluminescence spectrum (Figure 3.4 A), three distinct periods appear with high  $W_X(a, b)$  coefficients (in red). The two main periods in April 2009 and April 2010, appear with low excited frequencies, between  $4.8 \times 10^{-7} Hz$  (period of 24.1 days) and  $3.8 \times 10^{-6} Hz$  (period of 3.0 days). A third one in December 2009 is observed at about  $1.9 \times 10^{-6} Hz$  (period of 6.0 days). Moreover, frequencies at about  $2.0 \times 10^{-5} Hz$  (period of 0.6 days or 14 h) are also excited with high amplitude coefficients.

For the current speed spectrum (Figure 3.4 B), lower frequencies at about  $4.8 \times 10^{-7} Hz$  (period of 24.1 days) appear with high coefficients for the whole period. Moreover, a very distinct frequency band is highlighted at  $2.0 \times 10^{-5} Hz$  (period of 0.6 days or 14 h). This last range of excited frequencies is known to be linked to the "internal waves" (Huthnance, 1995). These periodic oscillations generated from the surface and transmitted to the deep sea have already been observed at periods about 17.6 h at the ANTARES station (Van Haren, 2011). The spectrum shows that if these waves are present during the whole sampled period, their frequency and amplitude coefficients vary over time. As an example, there are higher coefficients in January 2010 than in September 2009.

For salinity (Figure 3.4 C), two main events are distinct in April 2009 and April 2010 with very high coefficients, and excited frequencies at about  $9.5 \times 10^{-7}$  (period of 12.2

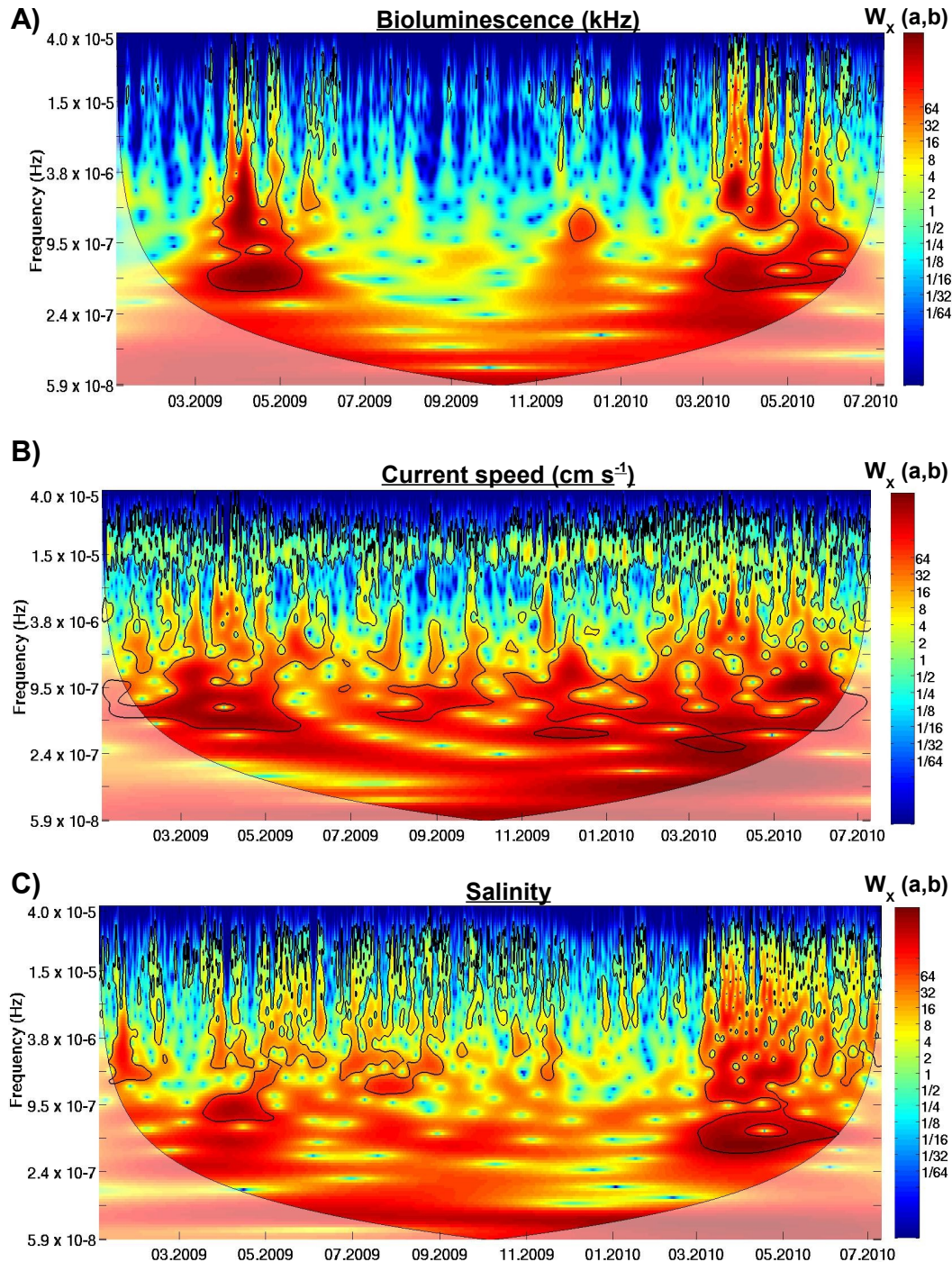


FIGURE (3.4) Time-frequency representation using the wavelet decomposition for A) bioluminescence B) current speed and C) salinity time series. The color scale for  $W_X(a, b)$  is from blue (low coefficient) to red (high coefficient). For the bioluminescence decomposition, three periods with high coefficients are distinct close to the dates 04.2009, 12.2009 and 04.2010. Black-contour lines represent the 5% significant level. The shaded part represents the cone of influence where edge effects appear.

days) and  $4.8 \times 10^{-7}$  (period of 24.1 days), respectively.

## Hilbert-Huang decomposition

Huang et al. (1998) proposed a second method for non-stationary and non-linear signal analysis (Huang et al., 1998; Huang and Wu, 2008; Huang et al., 2009a). The Hilbert-Huang decomposition (HHG) is based on the assumption that a signal  $X(t)$  is multi-component meaning that it can be expanded into a sum of  $n$  signals such that

$$X(t) = \sum_{j=1}^n C_j(t) + R_{n+1}(t), \quad (3.7)$$

where the  $C_j$  are called intrinsic mode functions (IMFs) and  $R_{n+1}$  is the trend of  $X(t)$ . Each IMF is supposed to be almost mono-component *i.e.* composed with only one instantaneous frequency, evolving with time, in a bounded range. The HHG decomposition is then realized in two main steps : the extraction of IMFs and their decomposition into instantaneous frequencies.

## Empirical mode decomposition

To constitute mono-component signals, the  $n$  IMFs must fulfill two conditions :

- (i) the number of times passing through the origin is identical to the number of extreme or differs by one for the most
- (ii) in any time, the mean between the local maximum and the local minimum is zero.

Following these conditions, the decomposition of  $X(t)$  into IMFs is based on the following steps :

**Step 1** - Identification of the extremes (minimum and maximum) of the signal  $X(t)$ .

**Step 2** - Connection of these extremes by natural cubic spline interpolation for the construction of the maximal envelope  $e_{max}(t)$ . Same process used for the lower envelope  $e_{min}(t)$ .

**Step 3** - Computation of the average of the two envelopes :  $m(t) = [e_{min}(t) + e_{max}(t)]/2$ ,

as shown in Figure 3.5.

**Step 4** - Computation of the locally centered time series with  $d(t) = X(t) - m(t)$ .

**Step 5** - Steps 1-4 are repeated on  $d(t)$  until convergence towards a time series with zero mean  $m(t)$  is sufficient. The convergence is controlled by a sifting criterion.

**Step 6** - If  $d(t)$  is zero mean then properties (i) and (ii) are checked and the function constitutes an IMF :  $C(t)$ .

**Step 7** - Construction of a new  $X(t)$  by subtracting  $C(t)$  to previous  $X(t)$ . Repeat steps 1 to step 6. Extracting IMFs is proceeded until rule (i) is broken.

**Step 8** - The last remainder constitutes the trend  $R_{n+1}(t)$  which is, by construction, a monotonic or a constant function.

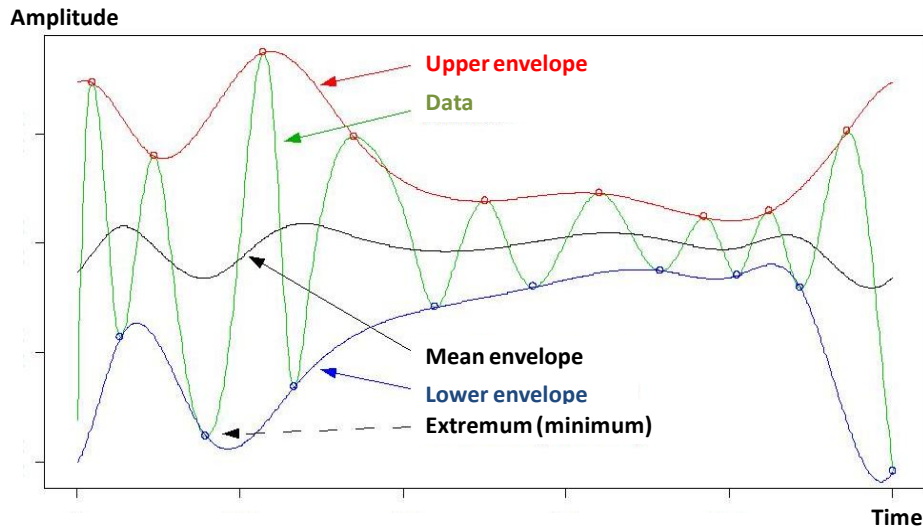


FIGURE (3.5) Schematic representation of the signal decomposition using the Hilbert-Huang method. The upper, and lower envelopes are represented by solid lines enclosing the signal. The mean is the centered line and the empty circles represent the extremes.

Decomposing the data into IMFs, an important question is to compare the signal decomposition with a white-noise decomposition. This would differentiate the decomposition using the Hilbert-Huang method from an artefactual decomposition due to random noise. The interpretation of physical processes embedded in the data will then be reinforced. Figure 3.6 represents the Hilbert-Huang decomposition of a hundred simulated

white-noise data (filled circles) and a partial set of data from the bioluminescence time series decomposition (empty circles). The log of energy (or squared amplitude coefficients) is represented over the log of mean frequency for each IMF. The empty circles outside the dark gray zones show that IMF decomposition is different from Gaussian noise.

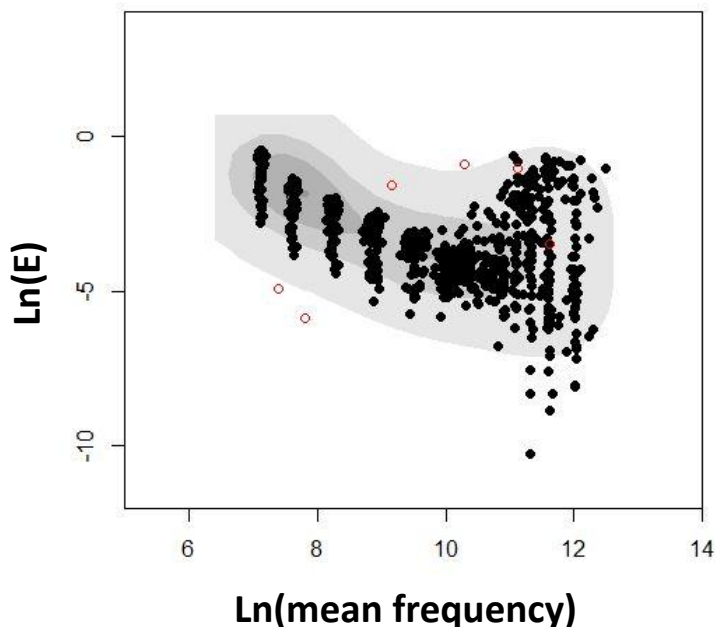


FIGURE (3.6) Example of significance for the IMFs decomposition from a partial set of data. The gray zones, from dark to light gray, represent high density regions containing respectively 0.01, 0.25, 0.75, 0.99 % of the data centered around local maximum. Empty circles, out of the area are the IMFs, significantly different from Gaussian noise. E is the energy into IMFs and mean frequency is the average frequency of each IMF band. This graph shows that HHG method removes the interpretation of IMF from a randomly artefactual decomposition.

### IMFs on ANTARES time series

All oceanographic variables recorded at the ANTARES site have been decomposed into IMFs using the HHG method. The empirical mode decomposition (EMD) extracts 10 IMFs and a trend for each time series. Figure 3.7 represents the IMFs for the bioluminescence time series with associated variability intervals. Variability intervals are

calculated by generating one hundred decompositions of each time series varying the sifting criterion, more or less 10%, to stop the process.

For the first IMFs (C1 to C5), the variability intervals are very low and can not be differentiated from the main IMF. They become more important for the last IMFs with, however, similar oscillations over time. By construction, the IMFs are first order stationary. The first extracted IMFs are high-pass filter and last IMFs are low-pass filter. The two bioluminescence events in 2009 and 2010 appeared on functions of higher frequencies (Figure 3.7 from C1 to C7). Once the linear decomposition achieved, the next step of the Hilbert-Huang method is to extract time-dependent frequencies (instantaneous frequencies) from each IMF.

### Instantaneous frequency using the Hilbert transform

The original signal  $X(t)$  is now expressed as a linear combination of IMFs which are supposed to be mono component. Considering an IMF  $C(t)$ , the function

$$Z(t) = C(t) + iY(t), \quad (3.8)$$

is constructed, where  $Y(t)$  is the Hilbert transform of the IMF  $C(t)$  with :

$$Y(t) = \frac{1}{\pi} P \int_{-\infty}^{\infty} \frac{C(t')}{t - t'} dt', \quad (3.9)$$

with  $P$  the Cauchy principal value (Paget and Elliott, 1972). The construction of  $Z(t)$  makes the decomposition of the IMF possible such that :

$$Z(t) = a(t)e^{i\theta(t)}, \quad (3.10)$$

where  $a(t)$  is the instantaneous amplitude and  $\theta(t)$  the instantaneous phase. The parameter  $a(t)$  reflects how the energy of the signal varies with time and is given with :

$$a(t) = [C(t)^2 + Y(t)^2]^{1/2}. \quad (3.11)$$

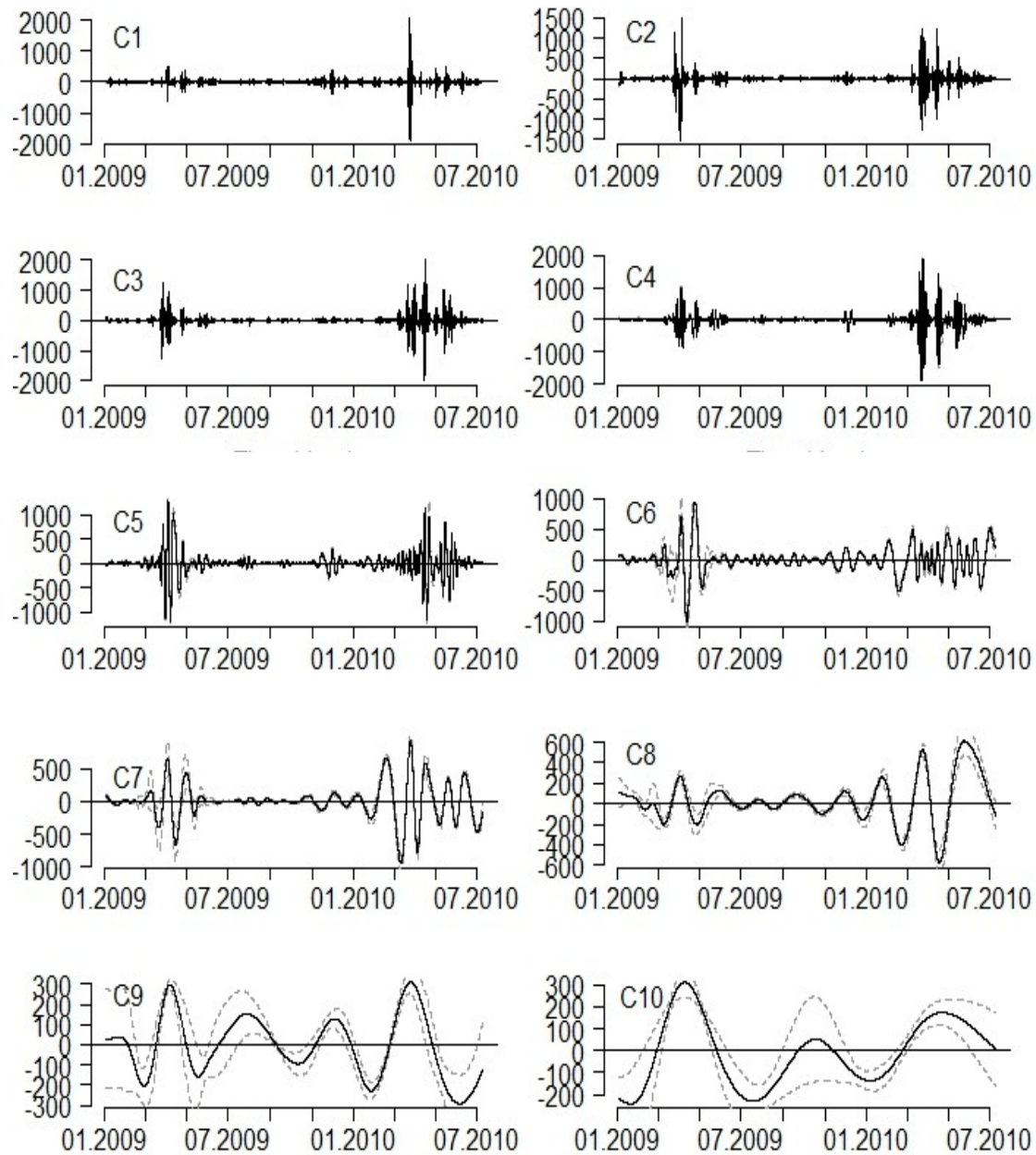


FIGURE (3.7) Hilbert-Huang decomposition for the bioluminescence signal into 10 intrinsic mode functions, from C1 to C10. These intrinsic mode functions are stationary for the first order. In gray, the variability intervals are plotted by moving the threshold defined to stop the sifting process. The trend of the data is not plotted.

The instantaneous phase  $\theta(t)$  computed with :

$$\theta(t) = \arctan \left( \frac{Y(t)}{C(t)} \right) \quad (3.12)$$

yields the instantaneous frequency  $w(t)$  such that :

$$w(t) = \frac{1}{2\pi} \frac{d\theta(t)}{dt}. \quad (3.13)$$

Applying the instantaneous frequency decomposition for each IMF  $C_j$  forms the HHG decomposition of the signal  $X(t)$ . It can be expressed as a linear combination of trigonometric functions with amplitude coefficients  $a_j(t)$  and frequency coefficients  $w_j(t)$  depending on time :

$$X(t) = \sum_{j=1}^n a_j(t) e^{i2\pi \int \omega_j(\tau) d\tau} + R_{n+1}(t) \quad (3.14)$$

### Dyadic frequency decomposition

In the literature, Huang et al. (2009a) give an empirical maximal number of IMFs between 6 and 12, depending on the complexity of time series. The IMF decomposition acts as a pass-band filter by separating frequency bands (Flandrin et al., 2004). A way to understand how the empirical decomposition takes place for the HHG method is to study the frequency narrow band for each extracted IMF. A linear relationship (using least-square method) between the logarithms of the IMF average frequencies and over the number of IMF, is defined empirically following an exponential law such as

$$\log(\omega_m(n)) \approx -n \log(\alpha) \quad (3.15)$$

with  $w_m(n)$  the mean frequency for the IMF  $n$  (Huang et al., 2009b). On this log-representation, the relation is linear with a slope coefficient  $\alpha$  and the  $R^2$  coefficient determined to characterize the quality of the fit.

Figure 3.8 represents the mean frequency and the standard deviation for the instantaneous frequencies calculated for each IMF from the time series of salinity, bioluminescence,

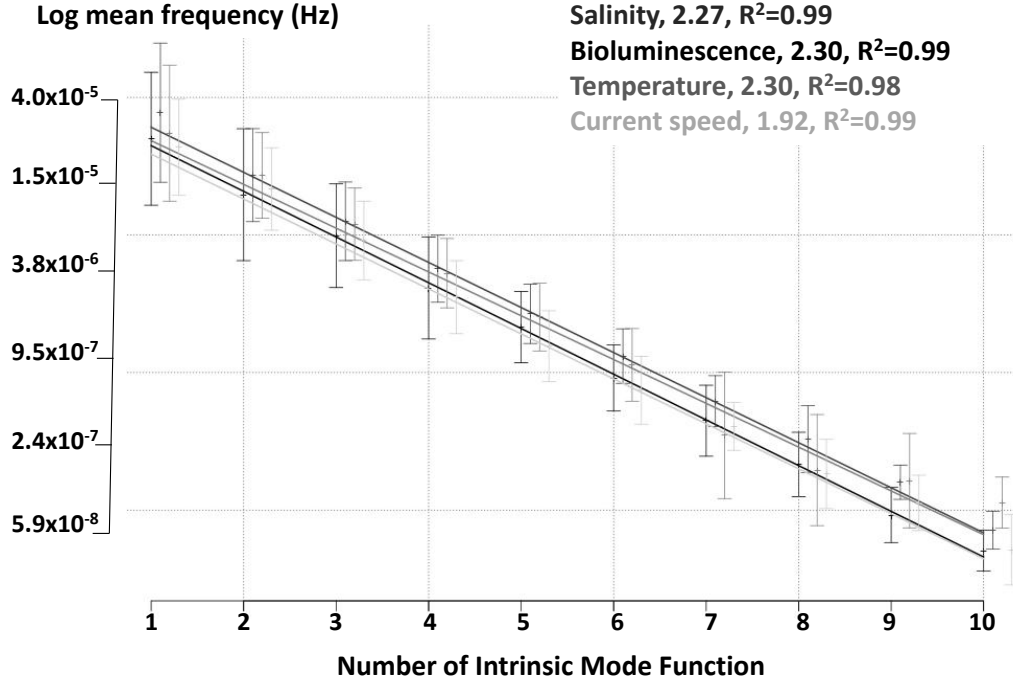


FIGURE (3.8) Representation of the empirical dyadic decomposition of the HHG method. The linear relation is fitted for the logarithm of the mean frequency of each intrinsic mode function, for each variable. Error bars are added for each intrinsic mode function. The slope coefficient close to 2 define a dyadic decomposition for all time series.

temperature and current speed. The  $\alpha$  coefficients from equation (3.15) estimated for each of the variables are between 2.27 and 2.30 except for the current speed for which the coefficient is lower (1.92). These relations define a dyadic decomposition. Each mean frequency from an IMF is about a half of the one extracted before. This is observed empirically in our case as well as in the literature (Flandrin et al., 2004; Huang and Wu, 2008), but no mathematical assumptions have been done at the beginning of the decomposition method (Huang et al., 2009a; Massei and Fournier, 2012). This observation differs from the wavelet decomposition for which a dyadic assumption is done using the set of scales  $b$  selected as a functional power of 2 :

$$b_i = b_0 \times 2^{i\delta}, i = 0, \dots, M \quad (3.16)$$

with  $M = \frac{1}{\delta} \log_2 \frac{(N\Delta t)}{b_0}$ , N the number of values in the time series,  $\Delta t$  the time sampling and  $\delta$  a scale factor (small values for  $\delta$  will give a finer definition).  $b_0$  is the initial parameter  $b$  and  $b_i$  the parameter at time  $i$ .

### Thin-plate spline smoothing

The evolution of instantaneous frequencies and amplitude over time can be represented as a time-frequency-amplitude plot. However, a HHG spectrum is discrete and cannot be cross-correlated between two variables. Indeed, the IMFs do not form a common basis where time-series could be expanded. The number of extracted IMFs is different from one time series to another, depending on the properties of the time series themselves. One way to cross time-frequency decompositions can be achieved by smoothing spectra over both time and frequency in order to obtain a continuous representation. This is done with thin plate regression splines (Bookstein, 1989; Mardia et al., 1996; Wood, 2003).

We dispose of  $n$  observations  $(y_i, \mathbf{x}_i)$  where  $\mathbf{x}_i = (\omega_i, t_i) \in \mathbb{R}^2$  is a position in the time-frequency space and  $y_i$ , the computed value of the discrete Hilbert spectrum from the IMFs decomposition. We want to estimate the regression surface  $H(\mathbf{x})$  as a continuous spectrum such that :

$$y_i = H(\mathbf{x}_i) + \varepsilon_i, \quad (3.17)$$

where  $\varepsilon_i$  is a random error term. Thin plate splines can be used to estimate  $H$  by finding the function  $g$  minimizing

$$\|\mathbf{y} - \mathbf{g}\|^2 + \lambda J(g), \quad (3.18)$$

where  $\mathbf{y}$  is the vector of data with entries  $y_i$ ,  $\mathbf{g} = (g(\mathbf{x}_1), \dots, g(\mathbf{x}_n))'$ ,  $J(g)$  is a penalty function

$$J(g) = \iint_{\mathbb{R}^2} \left( \frac{\partial^2 g}{\partial \omega^2} \right)^2 + 2 \left( \frac{\partial^2 g}{\partial \omega \partial t} \right)^2 + \left( \frac{\partial^2 g}{\partial t^2} \right)^2 d\omega dt, \quad (3.19)$$

giving a measure of roughness for  $g$  and  $\lambda$ , a parameter which controls the trade-off between the fit to data and the smoothness of  $g$ .

The value of  $\lambda$  is determined by cross-validation. The solution of the spline regression problem provides a continuous Hilbert spectrum  $H$  for a given variable. The Hilbert spectrum gives a measure of amplitude contributing to each frequency and one can calculate the associated marginal spectrum  $h(\omega)$  such that :

$$h(\omega) = \int_0^T H(\omega, t) dt \quad (3.20)$$

### HHG spectral representation

Figures 3.9 (from A to C) are the continuous spectral representations after smoothing the HHG spectra using thin plate splines for the bioluminescence (Figure 3.9 A), the current speed (Figure 3.9 B), and the salinity (Figure 3.9 C).

For bioluminescence, in Figure 3.9 A, three events are distinct. The two main occur from April to May 2009, and from March to June 2010 with high amplitude coefficients and at frequencies between  $4.8 \times 10^{-7}$  (period of 24.1 days) and  $1.0 \times 10^{-5} Hz$  (period of 1.2 days). The third one in December 2009 is defined with lower amplitude coefficients and at  $1.9 \times 10^{-6} Hz$  (period of 6.0 days). Frequency of  $2.0 \times 10^{-5} Hz$  (period of 0.6 days or 14 h) is not excited contrary to the Figure 3.4 A.

For current speed, in Figure 3.9 B, a large band of frequencies is excited between  $4.8 \times 10^{-7}$  (period of 24.1 days) and  $1.0 \times 10^{-5} Hz$  (period of 1.2 days). Another band of excited frequencies is defined at  $2.0 \times 10^{-5} Hz$  (period of 0.6 days or 14 h) (dotted box). These frequencies are linked to internal waves previously observed and described in Figure 3.4 B. The internal waves are mainly embedded in the two first IMF (Figure 3.8).

For salinity, in Figure 3.9 C, the two main events clearly appear in April 2009 and April 2010 at about  $9.5 \times 10^{-7}$  (period of 12.2 days) and at about  $3.8 \times 10^{-6}$  (period of 3.0 days).

These spectra are similar to those obtained using the wavelet decomposition Figure 3.4. Both wavelet and Hilbert-Huang decomposition methods result in a tri-dimensional continuous representation in the time-frequency domain. To quantify links in multivariate time series, the following step is to cross these spectra in pairs.

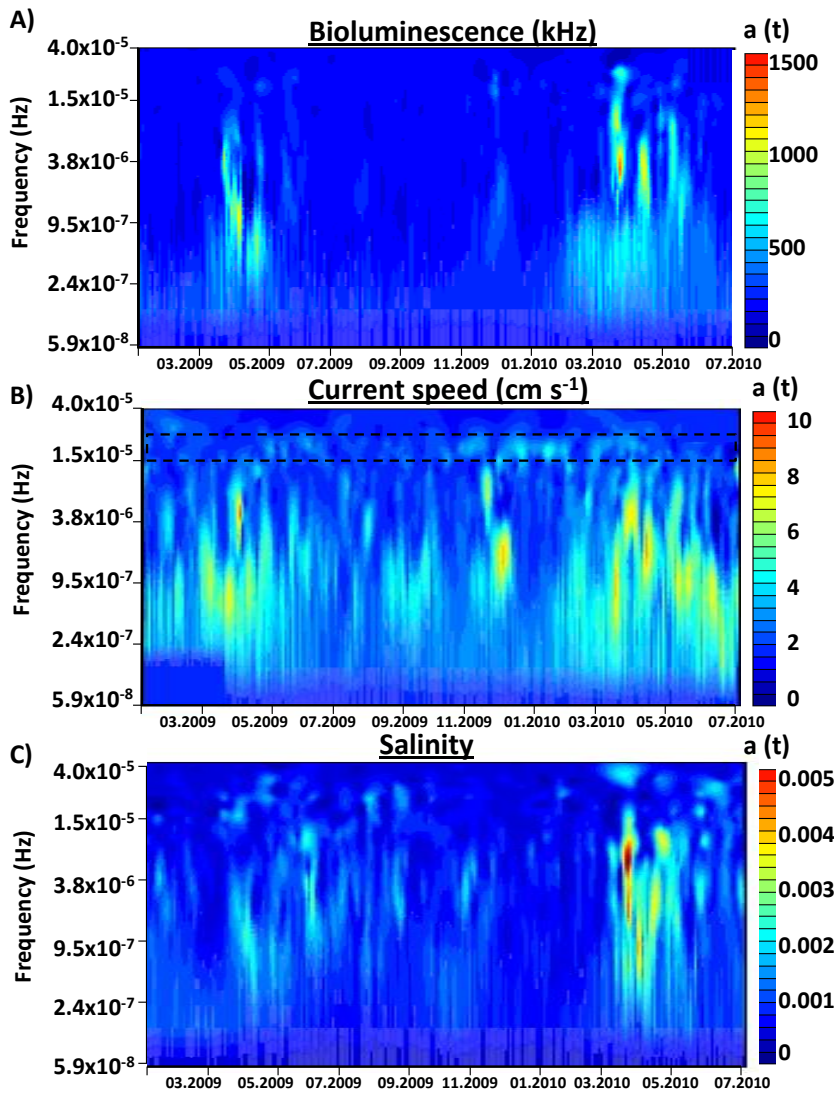


FIGURE (3.9) Spectral representation using HHG decomposition and thin-plate spline smoothing for A) bioluminescence, B) current speed and C) salinity from January 2009 to July 2010. The x-axis is the time, the y-axis the frequency (Hz) and the z-colored-scale is the amplitude coefficient value. In B) the dotted box highlights frequencies excited by internal waves.

## Bivariate time-frequency cross-analysis

### Wavelet coherence

One of the key issue for the analysis of the ANTARES time series is to compare decomposition spectra between variables. This point is well developed for the wavelet method using the cross-wavelet representation including both coherence-coefficient values and phase delays (Torrence and Compo, 1998; Addison, 2010). We consider two time series  $X(t)$  and  $Y(t)$  and their wavelet transforms  $W_X(a, b)$  and  $W_Y(a, b)$ , respectively. The coherence is a measure of the squared correlation between wavelet functions of time series for time and frequency instantaneously. This value allows to distinguish the higher coefficients for both crossed variables,  $W_X(a, b)$  and  $W_Y(a, b)$  (Grinsted et al., 2004; Torrence and Webster, 1999). The coherency corresponds to the square of the crossed and normalized spectra :

$$C^2(a, b) = \frac{S(W_{XY}(a, b))}{S(|W_X(a, b)|^2)S(|W_Y(a, b)|^2)}, \forall 0 \leq C^2(a, b) \leq 1. \quad (3.21)$$

$S$  is a smoothing operator on both time and scale of the wavelets, and  $W_{XY}(a, b)$  the cross-wavelet defined from :

$$W_{XY}(a, b) = W_X(a, b)W_Y^*(a, b). \quad (3.22)$$

### HHG cross analysis

In order to cross two continuous spectrograms using HHG, only few solutions have been proposed compared to the wavelet method (Chen et al., 2010). Considering smoothed time-frequency spectrum  $H_X(\mathbf{x})$  and  $H_Y(\mathbf{x})$  for variables  $X$  and  $Y$  (Figure 3.9), one way to analyze the links between variables is to summarize the dependence of the time-frequency spectrum across the only frequency argument. The computation of the correlation between both images is carried out by transformation of each time-frequency spectrum in a collection of curves.

Let  $\{t_1, \dots, t_n\}$  be an arbitrary regular fine grid over time such that  $t_1 < t_2 < \dots < t_n$ . The

construction of a collection of pairwise curves  $\{(X_k(f), Y_k(g)), k = 1, \dots, n\}$  with  $X_k(f) = X(t_k, f)$  and  $Y_k(g) = Y(t_k, g)$  is done taking slices of time-frequency spectra for fixed times with  $f$  and  $g$  specific frequencies. Starting with these pairs of functions considered as a sample, the marginal spectra is defined :

$$\bar{X}(f) = \frac{1}{n} \sum_{k=1}^n X_k(f) \quad (3.23)$$

and

$$\bar{Y}(g) = \frac{1}{n} \sum_{k=1}^n Y_k(g) \quad (3.24)$$

and associated variance functions are

$$V_X(f) = \frac{1}{n} \sum_{k=1}^n (X_k(f) - \bar{X}(f))^2 \quad (3.25)$$

and

$$V_Y(g) = \frac{1}{n} \sum_{k=1}^n (Y_k(g) - \bar{Y}(g))^2 \quad (3.26)$$

The cross-correlation between  $X_k(t)$  and  $Y_k(t)$  is given by :

$$C_{XY}(f, g) = \frac{1}{n} \sum_{k=1}^n \frac{(X_k(f) - \bar{X}(f))(Y_k(g) - \bar{Y}(g))}{\sqrt{V_X(f)}} \frac{1}{\sqrt{V_Y(g)}} \quad (3.27)$$

This bivariate function has the property that :  $-1 \leq C_{XY}(f, g) \leq 1, \forall f, g \in [0, f_{max}]$ . It gives a measure of links between variables  $X$  and  $Y$  in the space of frequency. This cross-correlation on frequencies gives clues on major frequencies in a different way than the wavelet-coherence spectrogram.

## Discussion

### Bioluminescence mechanically stimulated by current speed

The effects of current speed on bioluminescence activity have been well investigated in the literature (Cussatlegras and Le Gal, 2007, 2005; Fritz et al., 1990). This mechanical stimulation triggers more bioluminescent response enhancing cell membrane excitation in fluid motions (Cussatlegras and Le Gal, 2007; Blaser et al., 2002). Based on ANTARES time series, Tamburini et al. (2013) and Van Haren (2011) show that generally bioluminescence activity increases with current speed. This is thought to be due to either impacts of small-sized bioluminescent organisms and particles on the PMTs or the reaction of such organisms to enhance turbulent motion in the wakes of the PMTs.

In Figure 3.10 A, when crossing the bioluminescence and current speed spectra, from the wavelet decomposition method, coherence coefficients are between 0.6 and 0.95, most of the time, over a wide range of frequencies. Moreover, there is a high cross coherence coefficient of about 0.85 at frequency about  $2.0 \times 10^{-5} Hz$  (period of 0.6 days or 14 h), referring to the internal wave frequencies (Huthnance, 1995; Van Haren, 2011). These observations reinforce the well-understood link between current speed and bioluminescence already known as a mechanical stimulation of bioluminescent organisms by current speed. Since no phase delay is noticed (represented by the right direction of arrows in Figure 3.10 A) the light emission appears instantaneously after mechanical stimulation.

### Links between bioluminescence and new water masses

Tamburini et al. (2013) interpret salinity and temperature time series as proxies of newly formed deep water, spreading at the ANTARES site. The authors propose the use of a salinity threshold value to highlight links between water masses and bioluminescence activity. As shown by these authors, from an ecological point of view, deep-water formations impact bioluminescent organisms in two different ways. On the one hand, these water inputs carry significant amount of bioluminescent planktonic organisms

down from the surface. On the other hand, dissolved organic matter exports as well as re-suspension of particulate organic matter from sediment to the water column fuel deep-sea bioluminescent activity (Tamburini et al., 2013). In the present work, we explore the ANTARES time series using statistical analyzes taking into account non-stationarity and non-linearity properties of this multivariate dataset.

Figure 3.10 B displays results from the wavelet decomposition, crossing bioluminescence and salinity time series. Similar results are obtained crossing bioluminescence and temperature (Figure not shown). Both salinity and temperature variables represent proxies of newly formed deep water. Figure 3.10 B shows two spots of high-coherence values ranging from 0.8 to 0.9, from March to May 2009 and March to June 2010. In 2009, high-coherence coefficients are highlighted for frequencies of  $4.8 \times 10^{-7} Hz$  (period of 24.1 days). In 2010, high correlations are observed for frequencies between 2.4 and  $9.5 \times 10^{-7} Hz$  (periods of 48.2 and 12.2 days). This cross-spectra emphasized a similar range of excited frequencies at  $4.8 \times 10^{-7} Hz$  in both 2009 and 2010 with, in addition, a very high correlation between water-mass proxies and bioluminescence activity, for both time. Nevertheless, no hypothesis for the low frequency of  $4.8 \times 10^{-7} Hz$  can be validated.

Interestingly, a third bioluminescence event, occurring in December 2009, is observed on time series (Figure 3.2) and on spectrogram (Figure 3.4 A) at frequencies between 9.5 and  $1.9 \times 10^{-6} Hz$  (period of 6.1 days). While this event is correlated with current speed in Figure 3.10 A (coherence coefficient between 0.7 and 0.8), there is no changes in water masses (Figure 3.10 B, coherence values below 0.2). Consequently, in December 2009, current speed generates a mechanical stimulation of bioluminescent organisms and, by its only effect, increases the bioluminescence activity. The Figure 3.10 A and B clearly helps to discriminate the events of high bioluminescence intensity affected by newly formed deep water and current speed (April 2009 and 2010) and the events only affected by current speed (December 2009).

Figure 3.11 A and B, resulting from the HHG decomposition, illustrates cross-correlations between frequency spectrum of bioluminescence and those of environmental variables

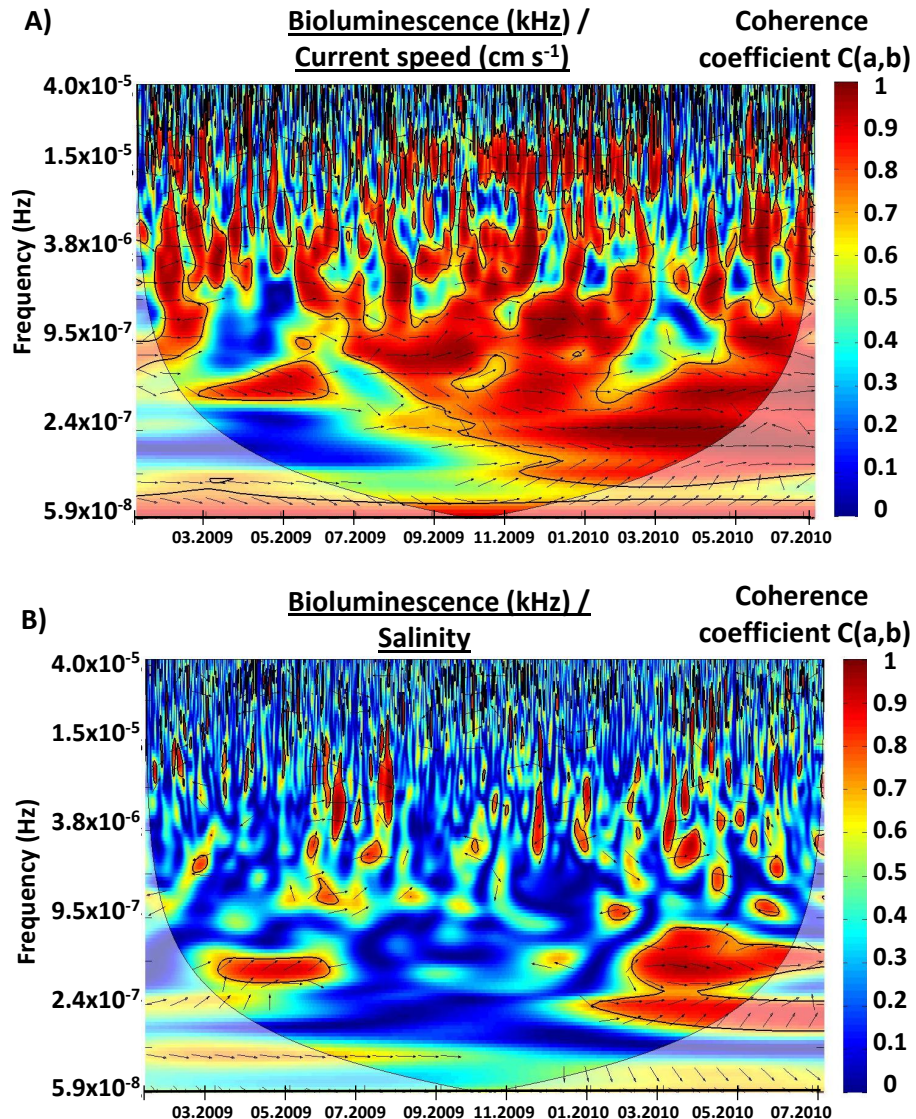


FIGURE (3.10) Cross spectrogram between bioluminescence and A) current speed and B) salinity, using the wavelet decomposition and coherence measurement. Black arrows represent the phase delay (right arrows mean no phase delay). Black line represents the edge effect for no significant results. The color-scale is the value for the coherence coefficient from 0 to 1 (blue to red).

(current speed and salinity). This representation is an original way to measure cross variations between two HHG spectra but induces a loss in time dependency. The correlation coefficients vary from -0.2 to 0.79 with higher coefficients on the diagonal (black line on Figure 3.11 for both A and B panels). This 1 :1 relation shows that highest excited

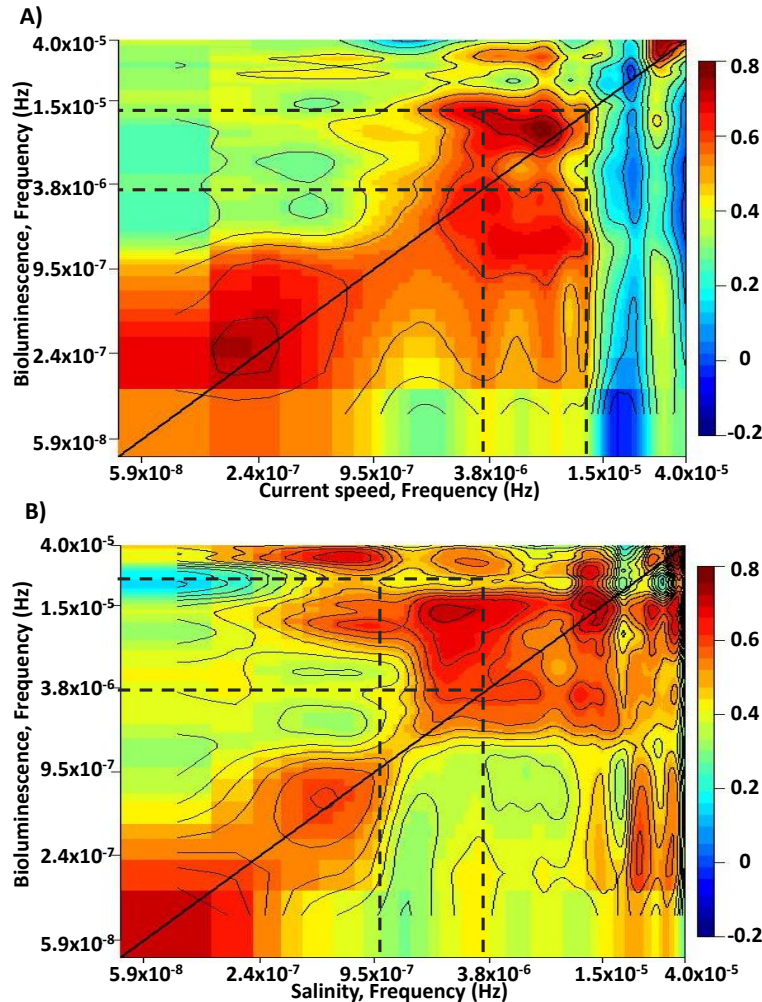


FIGURE (3.11) Cross spectrogram between bioluminescence and oceanographic variables. The cross-correlation coefficients (represented between -0.2 and 0.8) are plotted as isolines and color scale for bioluminescence with A) current speed and B) salinity. x and y axes represent frequencies for each variable. The dotted lines represent the range of frequencies of the most correlated intrinsic mode functions. These intrinsic mode functions are shown in Figure 3.12.

frequencies are the same for both variables (see Figure 3.8). Nevertheless, in Figure 3.11 B, crossing bioluminescence and salinity, some patterns of high cross coefficients occur out of the 1 :1 line. It shows that salinity (consequently newly formed deep water) and bioluminescence may be correlated at different frequencies. Then, in order to get back to a time-dependent representation, we isolate the IMFs referring to the higher correlation coefficients (black dotted lines in Figure 3.11). In Figure 3.11 A, the 3<sup>rd</sup> IMF for both current speed and bioluminescence are isolated and plotted simultaneously in Figure

**3.12 A.** The mean frequency of IMF 3 for bioluminescence is about  $6.1 \times 10^{-6}$  (period of 1.9 days) and for current speed  $5.7 \times 10^{-6}$  (period of 2.0 days). In Figure 3.11 B, the 5<sup>th</sup> IMF for salinity and the 2<sup>nd</sup> one for bioluminescence are represented together in Figure 3.12 B. This Figure shows that the high-correlation coefficient is mainly due to the two events of high bioluminescence activity with simultaneous oscillations induces. The mean frequency of IMF 5 for salinity is  $1.9 \times 10^{-6}$  (period of 6.1 days) and for IMF 2 for bioluminescence is  $1.1 \times 10^{-5}$  (period of 1.1 days). These results from the HHG decomposition are not easily detected in Figure 3.10.

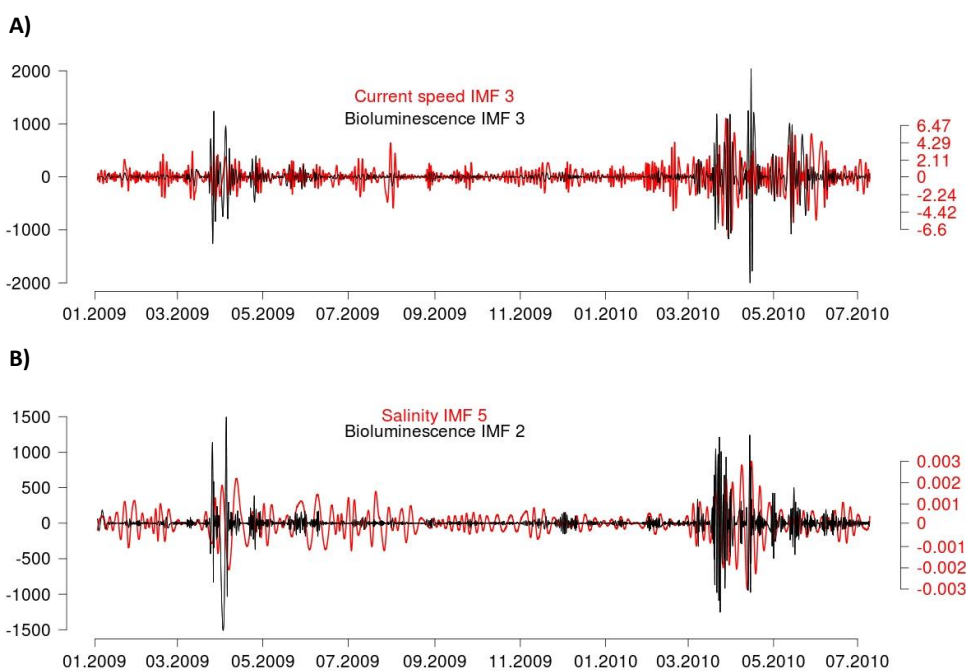


FIGURE (3.12) Representation of the most correlated intrinsic mode function for A) bioluminescence and current speed, B) bioluminescence and salinity. In A), mean frequency for bioluminescence IMF 3 is  $6.1 \times 10^{-6}$  (period of 1.9 days) and for current speed IMF 3 is  $5.7 \times 10^{-6}$  (period of 2.0 days). In B), mean frequency for bioluminescence IMF 2 is  $1.1 \times 10^{-5}$  (period of 1.1 days) and for salinity IMF 5 is  $1.9 \times 10^{-6}$  (period of 6.1 days).

## Two different mathematical methods

From a technical point of view, HHG and the wavelet decomposition provide complementary results. The HHG method is based on empirical decomposition which provides a basis expansion composed with IMFs. This decomposition only relies on the data itself without any assumption on time series shape. This is not the case for wavelet decomposition which relies on an arbitrary choice of the mother wavelet to decompose the signal. However, the bivariate analysis is more efficient using wavelet decomposition. Indeed, due to the different number of IMFs between variables, time-frequency cross spectra cannot be defined using HHG method. We propose in this study, a bivariate cross analysis which allowed to get the cross information between variables in only the frequency space.

## Conclusion

There is a clear interest in recording long time series to understand intrinsic variations in an ecosystem. High frequency samplings help to detect characteristic scales within a signal. Few time-frequency-decomposition methods are adapted to the analysis of non-stationary and non-linear signals and consequently, to the detection of frequencies excited during unusual events. Using Huang-Hilbert and wavelet decomposition, we show that current speed involves mechanical stimulation of bioluminescent organisms and increases light emission. The use of time and frequency-decomposition methods demonstrates that current speed stimulates bioluminescence at almost all frequencies and without delay. Their undeniable advantage is the possibility to highlight correlation between bioluminescence and the arrival of newly-formed deep waters at specific time (beginning in March 2009 and March 2010) for frequencies at about  $4.8 \times 10^{-7} Hz$  (period of 24.1 days). This excited frequency has no clear interpretation yet. Moreover, these statistical methods discriminate events due to newly-formed-deep-water spreading and events only due to variations in current speed. Finally, the use of those two methods applied to signal processing in oceanography for coherent dataset is definitely a way to better interpret variability, special events and links between variables.

**Acknowledgements**

SM was granted a MERNT fellowship (Ministry of Education, Research and Technology, France). The authors thank the Collaboration of the ANTARES deep-sea observatory for providing time series data. Authors especially thank S. Escoffier, M. Garel and C. Curtil for their comments and their inputs to this work. Cross wavelet and wavelet coherence software were provided by A. Grinsted.

## 3.2 Complementary data

Preliminary tests have been performed for Fourier, wavelets and Hilbert-Huang decomposition using well-defined time series. Dataset is the sea level record during a tsunami arrival in 2004 at the Jackson Bay, in New Zealand (data from NOAA <http://wcatwc.arh.noaa.gov/>). The signal is divided into two processes. The first one is the tidal periodic oscillation at low frequency and the second one is the tsunami arrival at higher frequencies. The second signal is starting at day 362 and with a modification of its amplitude over time (Figure 3.13 A).

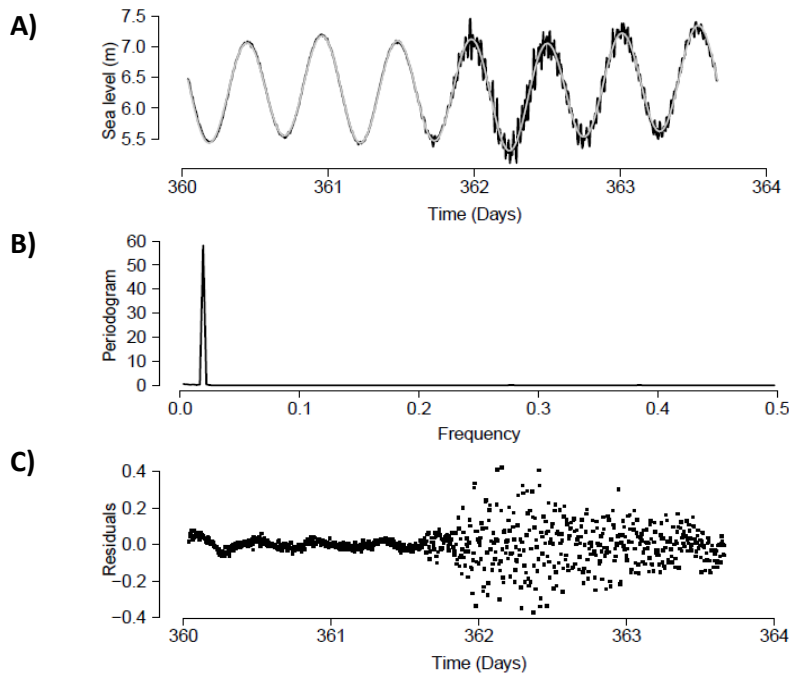


FIGURE (3.13) Fourier decomposition of the sea level dataset during a tsunami event. A) tidal periodic signal (grey line) extracted using Fourier decomposition, B) Periodogram with tidal frequency highlighted and C) Residuals from the signal.

In Figure 3.13 the Fourier decomposition is performed with 7 coefficients (see 3.2). This method easily define the periodic tidal wave in Figure 3.13 B, however, it does not permit to access to the tsunami arrival signal represented by residuals in Figure 3.13 C. This is mainly due to the non-stationarity problem highlighted in 3.1.2.

The decomposition of the dataset using the Hilbert-Huang method well-describe the two processes in Figure 3.14. A high frequency function and a low frequency one are extracted as the sum of Intrinsic Mode functions (IMFs). The time frequency spectra represented from this decomposition is shown with instantaneous frequency and amplitude coefficient evolving over time in Figure 3.16 a. Thin plate splines are applied on this dataset and represented after smoothing in Figure 3.16 b.

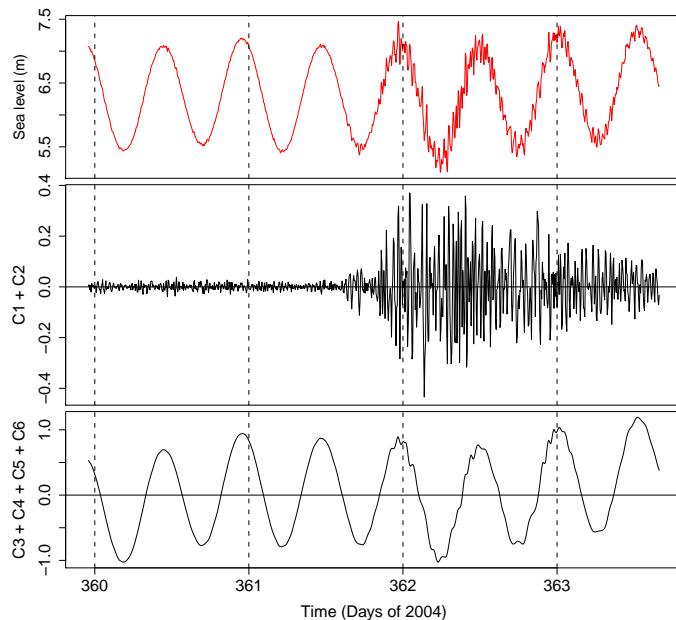


FIGURE (3.14) Time series decomposition within pass-band filter using the Hilbert-Huang decomposition method (see (Huang et al., 1998) and 3.1.2). On top time series of sea level during tsunami arrival is represented. The second plot represents the first extracted functions at high frequencies representing the tsunami arrival. The third plot represents the last functions extracted from data with low frequency and can be interpreted as the tidal periodic signal.

Similar pass-band filter should be represented using the wavelet decomposition method. Time series and time-frequency spectra are represented in Figure 3.16 A and B respectively.

This well-defined and already described example clearly illustrate problems of non-stationarity and advantages of time-frequency decomposition methods.

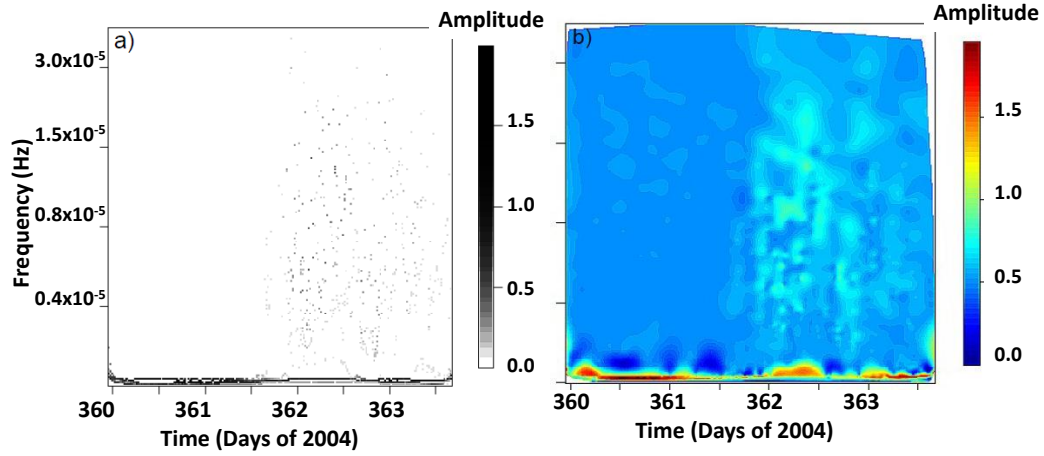


FIGURE (3.15) Time-frequency spectra representation using the Hilbert-Huang decomposition.  
a) Discrete representation before smoothing B) after thin plate spline smoothing method.

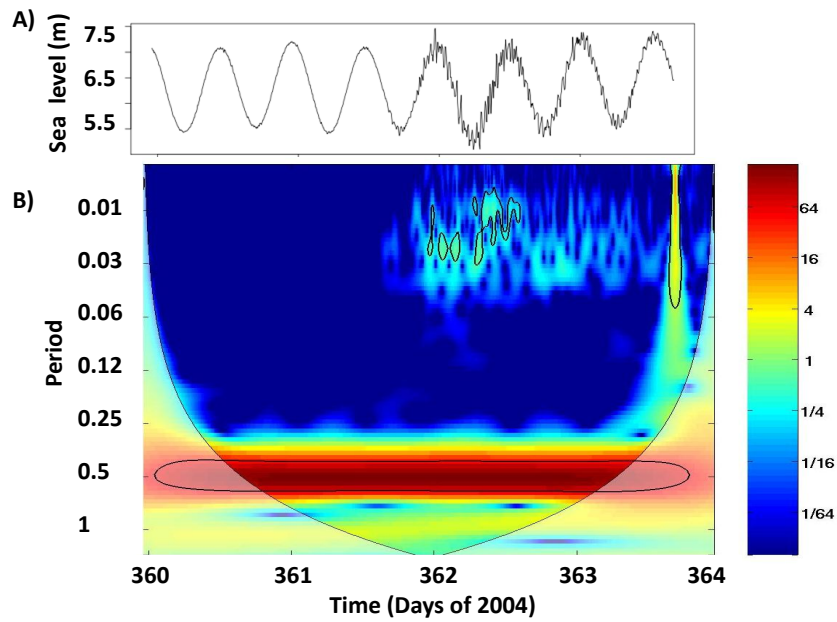


FIGURE (3.16) A) Tsunami arrival time series and B) time-frequency spectra (frequency is  $\frac{1}{\text{Period}}$ ). This graphical representation clearly define both signals with a low frequency periodic over the whole time considered (dark red band) and the tsunami event occurring at day 362 (blue patterns at high frequencies).



# CHAPITRE 4

---

In the laboratory, effects of forcing variables using a bioluminescent bacterial strain as a model.

---

## Sommaire

---

<b>4.1</b>	<b>Introduction : working with controlled variables and models.</b>	<b>114</b>
<b>4.2</b>	<b>Description of <i>Photobacterium phosphoreum</i> ANT-2200 strain</b>	<b>115</b>
<b>4.3</b>	<b>Article 3 . . . . .</b>	<b>117</b>
4.3.1	Foreword . . . . .	117
4.3.2	Effects of hydrostatic pressure on growth and luminescence of a moderately-piezophilic luminous bacteria <i>Photobacterium phosphoreum</i> ANT-2200 . . . . .	118
<b>4.4</b>	<b>Effects of hydrostatic pressure and growth medium on growth, luminescence and oxygen consumption . . . . .</b>	<b>138</b>
4.4.1	Growth medium . . . . .	138
4.4.2	High-pressure and oxygen consumption system . . . . .	139
4.4.3	Data acquisition into High Pressure Bottles . . . . .	141
<b>4.5</b>	<b>Conclusions . . . . .</b>	<b>145</b>

---

## 4.1 Introduction : working with controlled variables and models.

In previous chapters, high bioluminescence events, observed in March 2009 and 2010, have been explained to be linked to newly-formed-water masses sinking to the deep ocean. Bioluminescent organisms might be involved in this hydrological phenomenon into two different ways. First, bioluminescent organisms could be brought from the surface by physical transport and spread to the deep sea before reaching the ANTARES site. Secondly, newly-formed-deep-water inputs into the deep sea involve modifications in dissolved oxygen or carbon availability. Small variations, such as those observed in temperature and salinity, can not rationally influence growth and physiology of organisms or involve modifications in their bioluminescence activity. However, pressure effect on sinking organisms or carbon content are more foreseeable to affect growth, physiology and then bioluminescence activity.

Amongst the diversity of bioluminescent organisms, and due to a global lack of knowledge on *in situ* bacterial bioluminescence, we investigated bioluminescent bacteria as a part of the light signal. To validate or not this assumption, an intermediate step is to evaluate the potential bioluminescence activity of such bacteria under various environmental conditions. The bacterial strain *Photobacterium phosphoreum* ANT-2200 has been isolated in 2005, at the ANTARES station during a high bioluminescence event (Al Ali et al., 2010). Moreover, *Photobacterium phosphoreum* has been described as the main bioluminescent bacterial species in the deep Mediterranean Sea (Gentile et al., 2009). For those two major reasons, this strain is used as model for experiments in the laboratory. In this Chapter, we will apprehend the effects of high pressure, temperature, and carbon availability on both growth and bioluminescence activity. The results from these experiments will permit to criticize our hypotheses under controlled conditions and extrapolate such results at *in situ* scale. To reach such an aim, we divide laboratory experiments into two intermediate steps.

- In 4.3, *Photobacterium phosphoreum* ANT-2200 is cultivated into a carbon rich growth

#### 4.2. DESCRIPTION OF *PHOTOBACTERIUM PHOSPHOREUM* ANT-2200 STRAIN115

medium (Sea Water Complete medium) under various temperature and pressure conditions to determine optimal growth conditions for this strain and potential effects on bioluminescence activity. Moreover, logistic-growth model has been applied to those experiments.

- Finally, in 4.4, *Photobacterium phosphoreum* ANT-2200 is cultivated into a growth medium closer to environmental composition (ONR7a) and as close as possible to *in situ* conditions under high pressure (22 MPa) and *in situ* temperature (13°C). The instrumentation has been developed in the laboratory and these experiments are validating the ability to measure both bioluminescence and oxygen consumption over time.

Part 4.3 has been investigated and major results published into an article (Martini et al., 2013a). Then, 4.4 validates the instrumentation, methods and the ability to record bioluminescence and bacterial growth as well as physiological parameters close to environmental conditions. The part 4.4 is preliminary and still need to be improved and replicated in order to robustly interpret the results. However, these experiments are presented given the originality of the methods and the ability to record the data at high frequency and in an automatic way.

## 4.2 Description of *Photobacterium phosphoreum* ANT-2200 strain

The bioluminescent bacterial strain *Photobacterium phosphoreum* ANT-2200 has been isolated in the laboratory in 2005. At sea, 500 mL of water have been sampled at 2,200 m depth, at the ANTARES station and filtered. After cultivation on a solid medium, one luminous UFC (Unit Forming Colony) has been isolated. A 16S-rRNA-gene sequence defines the strain close to *Photobacterium phosphoreum* (100%) strain IFO 13896. Based on phylogeny, the isolate has been named *Photobacterium phosphoreum* ANT-2200 (Figure 4.1). For more details, see Al Ali et al. (2010).



FIGURE (4.1) *Photobacterium phosphoreum* ANT-2200 strain emitting bioluminescence in liquid growth medium and solid medium. Bioluminescent bacteria emit light at wavelength about 490 nm (blue-green emission).

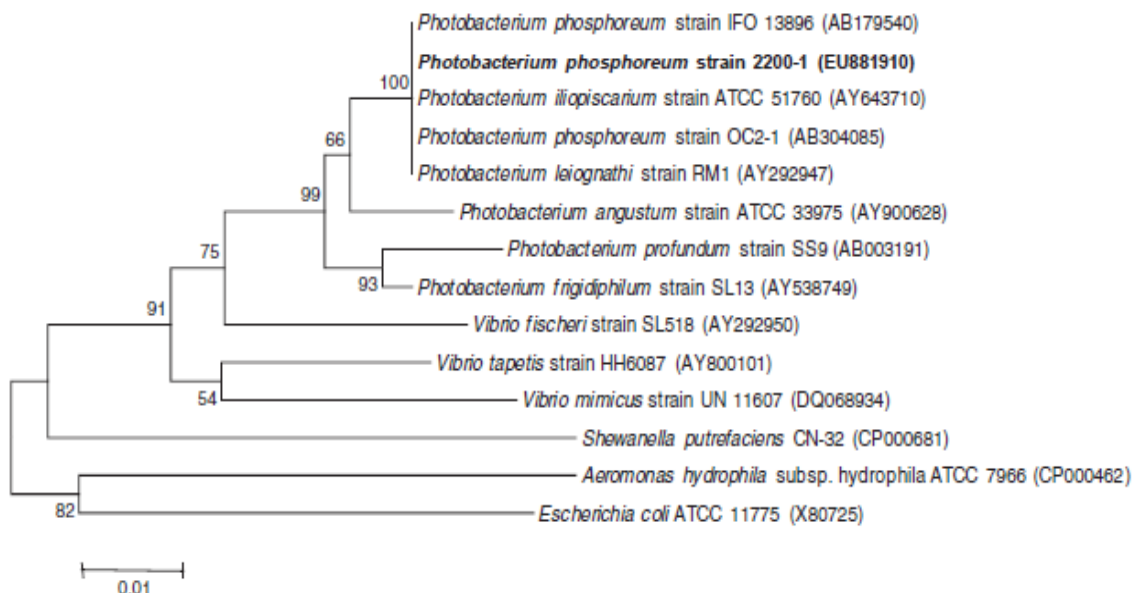


FIGURE (4.2) Neighbor-joining tree showing the phylogenetic position of *Photobacterium phosphoreum* ANT-2200 strain and related taxa based on 16S rDNA sequences. Numbers at nodes are levels of bootstrap support (%) based on neighbor-joining analyzes of 1,000 re-sampled datasets. Only values above 70% are given. Bar 0.01 substitutions per nucleotide position. From Al Ali et al. (2010).

## 4.3 Article 3

### 4.3.1 Foreword

In this article, the effects of environmental variables (hydrostatic pressure and temperature) on the activity of *Photobacterium phosphoreum* ANT-2200 strain have been studied. This bacterial strain, isolated at the ANTARES site, has been used as a model. This work has been started during B. Al Ali PhD (2010) with a part of the data acquisition for growth and bioluminescence, and has been finalized during my PhD work.

*This work granted by EC2CO-BIOLUX. C. Tamburini is the PI for the project. B. Al Ali, M. Garel, C. Tamburini and me performed the experimental part on the high pressure platform. I joined the bioreactor platform with S. Davidson, Y. Combet-Blanc, and R. Auria, for an experimental part using bioreactors (see Perspective part 6.2.1). L. Casalot, S. Isart and me worked using the pure culture of the bacterial strain. I did the modelisation part supervised by D. Nerini and M. Garel also join us for data analysis. V. Grossi, P. Cuny and M. Pacton have performed the physiological analyzes. M. Garel and C. Tamburini developed the hyperbaric system as well as the bioluminescence and oxygen measurement systems under high pressure.*

#### 4.3.2 Effects of hydrostatic pressure on growth and luminescence of a moderately-piezophilic luminous bacteria *Photobacterium phosphoreum* ANT-2200

Martini S.<sup>1,2</sup>, Al Ali B.<sup>1,2,◊</sup>, Garel M.<sup>1,2</sup>, Nerini D.<sup>1,2</sup>, Grossi V.<sup>3</sup>, Pacton M.<sup>3</sup>, Casalot L.<sup>1,2</sup>, Cuny P.<sup>1,2</sup> and Tamburini C.<sup>1,2,\*</sup>

<sup>1</sup> Aix-Marseille Université, Mediterranean Institute of Oceanography (MIO), 13288, Marseille, Cedex 09, France ;

<sup>3</sup> Université du sud Toulon-Var (MIO), 83957, La Garde cedex, France ; CNRS/INSU, MIO UMR 7294 ; IRD, MIO UMR 235.

<sup>4</sup> Université Lyon1, CNRS, Laboratoire de Géologie de Lyon, UMR5276 Villeurbanne, France

<sup>5</sup> ETH Zurich, Geological Institute, CH-8092 Zurich, Switzerland

◊Present address : Tishreen University, High Institute of Marine Research, P.O. Box 2242, Ministry of Higher Education, Syrian Arab Republic

\* Corresponding author : [christian.tamburini@univ-amu.fr](mailto:christian.tamburini@univ-amu.fr)

**Martini S, Al Ali B, Garel M, Nerini D, Grossi V, et al. (2013) Effects of Hydrostatic Pressure on Growth and Luminescence of a Moderately-Piezophilic Luminous Bacteria *Photobacterium phosphoreum* ANT-2200. PLoS ONE 8(6) : e66580. doi :10.1371/journal.pone.0066580**

**Abstract**

Bacterial bioluminescence is commonly found in the deep sea and depends on environmental conditions. *Photobacterium phosphoreum* ANT-2200 has been isolated from the NW Mediterranean Sea at 2200-m depth (*in situ* temperature of 13°C) close to the ANTARES neutrino telescope. The effects of hydrostatic pressure on its growth and luminescence have been investigated under controlled laboratory conditions, using a specifically developed high-pressure bioluminescence system. The growth rate and the maximum population density of the strain were determined at different temperatures (from 4 to 37°C) and pressures (from 0.1 to 40 MPa), using the logistic model to define these two growth parameters. Indeed, using the growth rate only, no optimal temperature and pressure could be determined. However, when both growth rate and maximum population density were jointly taken into account, a cross coefficient was calculated. By this way, the optimum growth conditions for *P. phosphoreum* ANT-2200 were found to be 30°C and, 10 MPa defining this strain as mesophile and moderately piezophile. Moreover, the ratio of unsaturated vs. saturated cellular fatty acids was found higher at 22 MPa, in agreement with previously described piezophile strains. *P. phosphoreum* ANT-2200 also appeared to respond to high pressure by forming cell aggregates. Its maximum population density was 1.2 times higher, with a similar growth rate, than at 0.1 MPa. Strain ANT-2200 grown at 22 MPa produced 3 times more bioluminescence. The proposed approach, mimicking, as close as possible, the *in situ* conditions, could help studying deep-sea bacterial bioluminescence and validating hypotheses concerning its role into the carbon cycle in the deep ocean.

## Introduction

The deep sea, under 1,000 m depth, is characterized by a high hydrostatic pressure ( $\geq 10$  MPa), with, generally, a low temperature and a low organic-matter concentration. Laboratory experiments using pure cultures of piezophilic Bacteria have highlighted microbial adaptations to high hydrostatic pressure. The adaptive traits include those related to growth (ZoBell and Johnson, 1949; Abe and Kato, 1999), membrane (Yayanos, 1995), and storage lipids (Grossi et al., 2010), membrane and soluble proteins (Bartlett et al., 1989; Kato, 2008), the respiratory-chain complexes (Abe and Kato, 1999; Yamada et al., 2000), replication, transcription and translation (Bartlett et al., 1995; Lauro et al., 2008). Most isolated piezophilic Bacteria belong to the genera : *Carnobacterium*, *Desulfovibrio*, *Marinitoga*, *Shewanella*, *Photobacterium*, *Colwellia*, *Moritella*, and *Psychromonas* within the Gammaproteobacteria subclass reviewed by Bartlett et al. (2007).

Darkness is another major characteristic of this deep-sea environment that can be disturbed by a biological phenomenon named bioluminescence. Bioluminescence is the process by which living micro- or macro-organisms emit light. Among the bioluminescent organisms, marine luminous bacteria are ecologically versatile and can be found as free-living forms, epiphytes, saprophytes, parasites, symbionts in the light organs of fishes and squids, and commensals in the gut of various marine organisms (Ruby et al., 1980; Hastings, 1983; Herring, 1987). Metagenomic analysis from deep eastern-Mediterranean water samples shows a surprising high number of *lux* genes directly involved in bioluminescence (Martin-Cuadrado et al., 2007). As far as we know, all-known marine bioluminescent bacteria are phylogenetically affiliated to the *Vibrio*, *Photobacterium* and *Shewanella* genera within the Gammaproteobacteria subclass (Kita-Tsukamoto et al., 2006). Among them, *Photobacterium phosphoreum* is the predominant species found in the Mediterranean Sea (Gentile et al., 2009).

Those of the most studied micro-organisms are, for piezophily, *Photobacterium profundum* SS9 (e.g. Vezzi et al., 2005), not known as luminous, and for bioluminescence, *P. phosphoreum* (e.g. Dunlap and Kita-Tsukamoto, 2006). Up to date, little information is

available concerning potential physiological-adaptation mechanisms of luminous bacteria to hydrostatic pressure, especially for both piezophily and bioluminescence. In this study, we used a bioluminescent strain isolated from Mediterranean deep-sea waters (sampled at 2,200-m depth) and identified as *Photobacterium phosphoreum* ANT-2200 (Al Ali et al., 2010). At this depth, the *in situ* conditions of pressure and temperature are about 22 MPa and 13°C, respectively. The purpose of this study is (1) to define temperature and pressure optima for growth and (2) to study pressure effect (0.1 versus 22 MPa, 13°C) on growth and bioluminescence activities of *P. phosphoreum* ANT-2200 using a new laboratory controlled hyperbaric system dedicated to high-pressure and bioluminescence studies.

## Material and methods

### Growth parameters of *P. phosphoreum* ANT-2200 under various temperature and hydrostatic-pressure conditions

*P. phosphoreum* ANT-2200 (GenBank accession number EU881910) was isolated from sea water collected in the Northwestern Mediterranean Sea at the ANTARES neutrino-telescope site (42°54'N, 06°06'E) at 2200-m depth (13°C) (see Al Ali et al., 2010 for details). Phenotypic and enzymatic characterizations are available in Supporting Information (Table S1). Procedures for pre-culturing were performed as described by Al Ali et al. (2010). For the determination of growth rate and maximum population density as a function of pressure and temperature, mid-log cultures were inoculated 1:10 into 5 mL sterilized syringes supplied with 3/4 of seawater complete medium (SCW medium) and with 1/4 oxygen-saturated Fluorinert<sup>TM</sup> FC-72 (3M<sup>TM</sup>). The impoverished SCW liquid medium contained per liter (pH 7.5) : 3 mg of yeast extract, 5 mg of bio-peptone, 3 mL of glycerol, 250 mL of distilled water, and 750 mL of old sea water (Nealson, 1978). Fluorinert<sup>TM</sup> FC-72 was used as oxygen supplier to ensure the growth and the luminescence of the bacterial strain in closed conditions (Kato et al., 1994, 1995; Yanagibayashi et al., 1999).

Triplicates cultures were incubated at pressures of 0.1, 10, 22, 30 and 40 MPa and

for temperatures of 4, 13, 20, 30 and 37°C. Syringes were placed into high-pressure bottles (HPBs). In order to avoid decompression-recompression of the samples, each HPB corresponded to one incubation time. Bacterial growth was estimated by measuring the optical density ( $OD_{600nm}$ ) using a spectrophotometer (Perkin Elmer, Lamda EZ201 UV/Vis spectrophotometer).

Direct counting was also performed using epifluorescence microscopy with DAPI-staining procedure, according to (Porter, 1980). This counting method was used to define the link between total-cell counts (DAPI counts) and optical density ( $OD_{600nm}$ ) according to the equation (1). For DAPI-cell counts, to avoid possible artefact due to the aggregates, the samples were sonicated (3 min), vortexed (1 min), diluted with milliQ-water, then, sonicated (2 min), vortexed (1 min) and finally filtered on 0.2- $\mu\text{m}$ -pore-size polycarbonate filters. The data have been, firstly, treated separately for atmospheric-pressure (0.1 MPa) and high-pressure (22 MPa) conditions. Since no significant difference has been observed between the two sets of data, a common relation has been defined as following :

$$\text{Number of DAPI-stained cells mL}^{-1} = 6.7 \times 10^8 \times OD_{600nm} - 2.3 \times 10^7 \quad (1)$$

$$(R^2 = 0.79, N = 14)$$

Traditionally, a linear regression is used to determine the growth rate of a strain during the logarithmic phase. The logistic (or Verhulst) model (Verhulst, 1838) was used in this study to determine both the growth rate ( $r$ ) and the maximum population density ( $K$ ). This model gives a continuous function of optical density, fitting discrete experimental data measured during the bacterial growth. Its hypotheses take into account limited resources in the medium and are defined as :

The birth rate :

$$n(x) = \alpha - \beta x \quad (4.1)$$

The mortality rate :

$$m(x) = \gamma - \delta x \quad (4.2)$$

$n(x)$  and  $m(x)$  are linear functions with  $\alpha, \beta, \gamma, \delta$  four real numbers and  $x$  is the population density. The birth and mortality rates are supposed to be constant during time :

$$\frac{dx}{dt} = nx - mx \quad (4.3)$$

Meaning that the logistic model is written as :

$$\frac{dx}{dt} = rx_1 - \frac{x}{K} \quad (4.4)$$

Where :

$$K = \frac{\alpha - \gamma}{\beta - \delta} \quad (4.5)$$

$K$ , being the maximum population density (expressed in optical density, OD<sub>600nm</sub>) that *P. phosphoreum* ANT-2200 can reach according to the growth conditions (temperature, pressure...) and  $r$ , being the growth rate, defined as :

$$r = \alpha - \gamma \quad (4.6)$$

Biologically, the intrinsic growth rate ( $r$ , expressed in  $h^{-1}$ ) is supposed to be positive (meaning that  $\alpha > \gamma$ ).

A cross coefficient ( $C_{r,K}$ ) has been calculated for both temperature and pressure effects on growth. If  $R$  and  $K$  are two matrices with  $n$  the number of temperature and  $m$  the number of pressure conditions tested, the  $C_{r,K}$  is defined as :

$$C_{r,K} = \left( \frac{R}{\max(R)} \right) \left( \frac{K}{\max(K)} \right) \quad (4.7)$$

With  $0 < C_{r,K} < 1$

The values for growth rate ( $r$ ,  $h^{-1}$ ), maximum population density ( $K$ , OD<sub>600nm</sub>) and cross coefficient ( $C_{r,K}$ ) were used to construct extrapolated-contour plots for the pressure-temperature dependency using R software (Team, 2012).

### Scanning electron and transmission electron microscopes

Cultures of *P. phosphoreum* ANT-2200 were performed at 0.1 and 22 MPa at 13°C. Cells were harvested at the end of the logarithmic phase and prepared for electron microscopy in order to observe cellular morphology and structure according to the pressure conditions.

Scanning Electron Microscopy (SEM) was performed according to two different procedures. On the one hand, cells were fixed with 0.2 % glutaraldehyde, filtered on 0.2- $\mu\text{m}$ -pore-size nucleopore membranes, washed with filtered and sterilized seawater with 2 % osmic acid, and then with Milli-Q water. Washed cells were dehydrated and observed using SEM (FEI Quanta 250 FEG, Centre Technologique des Microstructures, University Claude-Bernard, Lyon 1). On the other hand, cells were rapidly frozen in liquid nitrogen and lyophilized for 48 h using a CHRIST beta 2-4 LT+LD lyophilizator, operated at a temperature of -50°C and a pressure of 4 Pa. After complete dehydration, samples were attached onto stubs with double-sided adhesive (carbon type) and sputter coated, in a Baltec MED020 Sputter Coater, with a thin film of platinum to improve electrical conductivity of the sample surface. Samples were subsequently observed using SEM (FEI Quanta 250 FEG, Centre Technologique des Microstructures, University Claude-Bernard, Lyon 1).

Transmission Electron Microscopy (TEM) was carried out using cells fixed with 2% glutaraldehyde, buffered with PBS and embedded in 2% agar. Cells were post-fixed in 1% osmium tetroxide, dehydrated in a graded series of ethanol and embedded in Epon. Sections of 70 nm were realized using an ultramicrotome (Leica ultracut S), contrasted with uranyl acetate and lead citrate, and observed under a Philips CM 120 Transmission Electron Microscope at 80 kV.

### Cellular fatty-acid composition of *P. phosphoreum* ANT-2200 grown at 0.1 and 22 MPa (13°C)

Cultures of *P. phosphoreum* ANT-2200 were grown in 300-mL completely-filled polyethylene bottles (188 mL of culture + 62 mL of oxygenated Fluorinert<sup>TM</sup> FC-72), at 13°C and at 0.1 or 22 MPa (into high-pressure bottles). The bottle stoppers were equipped with a septum through which the pressure was applied. Cells in the late logarithmic stage of growth were harvested by centrifugation (20 min, 5,500 rpm at 0°C). Bacterial pellets were immediately frozen at -20°C and lyophilized. Lipids were extracted using the modified method of Bligh and Dyer (1959) with dichloromethane/methanol/water (DCM/MeOH/H<sub>2</sub>O, 1:2:0.8, v/v/v) under sonication. Following the addition of DCM and water to allow phase separation (final DCM/MeOH/H<sub>2</sub>O ratio of 1/1/0.9), the lower DCM layer was collected and the upper aqueous phase was further extracted with DCM ( $\times 2$ ). The combined lipid extracts were concentrated, dried over anhydrous sulfate and evaporated to dryness (N<sub>2</sub> flux) before being trans-esterified (50°C, 2h) with 2% sulfuric acid in MeOH in the presence of toluene (Christie, 1989). Individual fatty acids were identified and quantified by gas-chromatography-mass spectrometry (GC-MS), using an Agilent 6890N gas chromatograph interfaced to an Agilent 5975 mass spectrometer (electronic impact at 70 eV). The GC was equipped with a splitless injector and a HP5-MS capillary column (30 m  $\times$  0.25 mm  $\times$  0.25  $\mu$  m). Helium was used as the carrier gas (constant flow of 1 mL min<sup>-1</sup>) and the oven temperature was programmed from 70 to 130°C at 20°C min<sup>-1</sup>, and then at 4°C min<sup>-1</sup> from 130 to 300°C at which it was held for 20 min.

### Bioluminescence of *P. phosphoreum* ANT-2200 at 0.1 and 22 MPa (13°C)

Bioluminescence (photons sec<sup>-1</sup>) was monitored with a high-pressure bioluminescence system shown in Figure 4.3 A. Luminous bacteria were cultivated within a culture chamber placed inside a high-pressure tank (Fig. 4.3 B). The hydrostatic pressure is transmitted (via the HP-chamber valve) from the high-pressure tank to the culture chamber via a floating piston (Fig. 4.3 B). Sub-sampling is done by opening the

culture-chamber valve, while the pressure is monitored, using a piloted pressure generator (Tamburini et al., 2009) connected to the HP-chamber valve. The culture chamber is made in ertalyte (chemically and biologically inert material, white for light reflection) and sustains a plexiglass cone which transmits photons emitted by luminous bacteria by the way of an optical fiber (Fig. 4.3 B). Photon counting was obtained by integrating signals during 10 seconds using a photomultiplier (H7155, Hammamatsu) linked to its counting unit (C8855, Hammamatsu). Temperature was regulated using an external housing of tubing around the high-pressure bioluminescence tank. Temperature was controlled with a thermo chiller and monitored using a K-type thermocouple directly fitted within the high-pressure tank. More details of the high-pressure bioluminescence tank can be found in (Al Ali et al., 2010). Experiments were performed three times for 0.1 and 22 MPa.

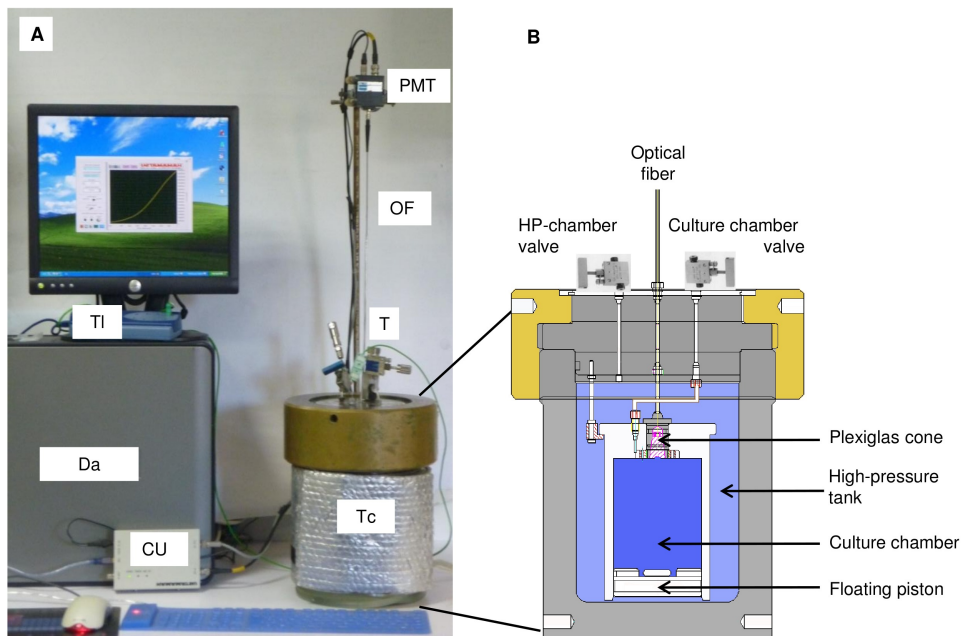


FIGURE (4.3) High-pressure bioluminescence system. (A) Photography of the high-pressure bioluminescence system and (B) schematic section diagram of the high-pressure bioluminescence tank. PMT : photomultiplier tube ; OF : optical fiber ; CU : photomultiplier counting unit ; T : high-pressure temperature sensor ; Tc : Tubing around tank for temperature control connected to a thermo chiller (not shown) ; TI : Data logger for temperature sensor ; Da : PC for data acquisition of bioluminescence and temperature

## Results and discussion

### Growth temperature and pressure optima of *P. phosphoreum* ANT-2200

Using the logistic model, growth-rate ( $r$  expressed as  $h^{-1}$ ) and maximum-population-density ( $K$  expressed as  $OD_{600nm}$ ) parameters were defined for each temperature (4, 13, 20, 30, 37°C) and pressure (0.1, 10, 22, 30, 40 MPa) conditions (Fig. 4.5). Figure 4.4 presents the model curves fitting with empirical data obtained at 13°C and 30°C, for all tested pressures. The model parameters have been estimated qualitatively using the confidence interval of the logistic growth curves.

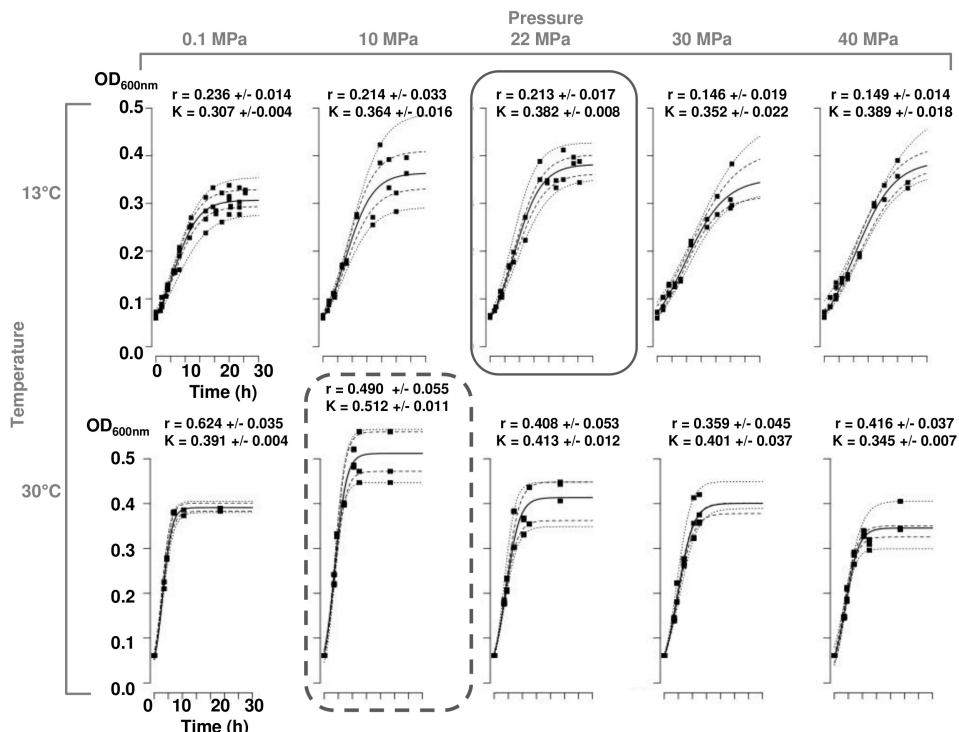


FIGURE (4.4) Example of logistic model fitting empirical growth data of *P. phosphoreum* ANT-2200. Experiments were done at pressures of 0.1, 10, 22, 30 and 40 MPa and at temperatures of 13°C and 30°C. The logistic model (line) improves the  $r$  and  $K$  parameter estimation on empirical growth data (dots). Dashed lines are levels of confidence for the 0.05 and 0.95 quantile curves and the 0.25 and 0.75 quantile curves. Mean  $\pm$  standard deviation for growth rate ( $r$ ,  $h^{-1}$ ) and maximum population density ( $K$ ,  $OD_{600nm}$ ) parameters are indicated. The dotted frame is the growth curve under optimum pressure and temperature conditions using both  $r$  and  $K$  parameters. The solid line frame is the growth curve under *in situ* conditions, at 22 MPa and 13°C. N is the number of replicates done for the same pressure and temperature conditions.

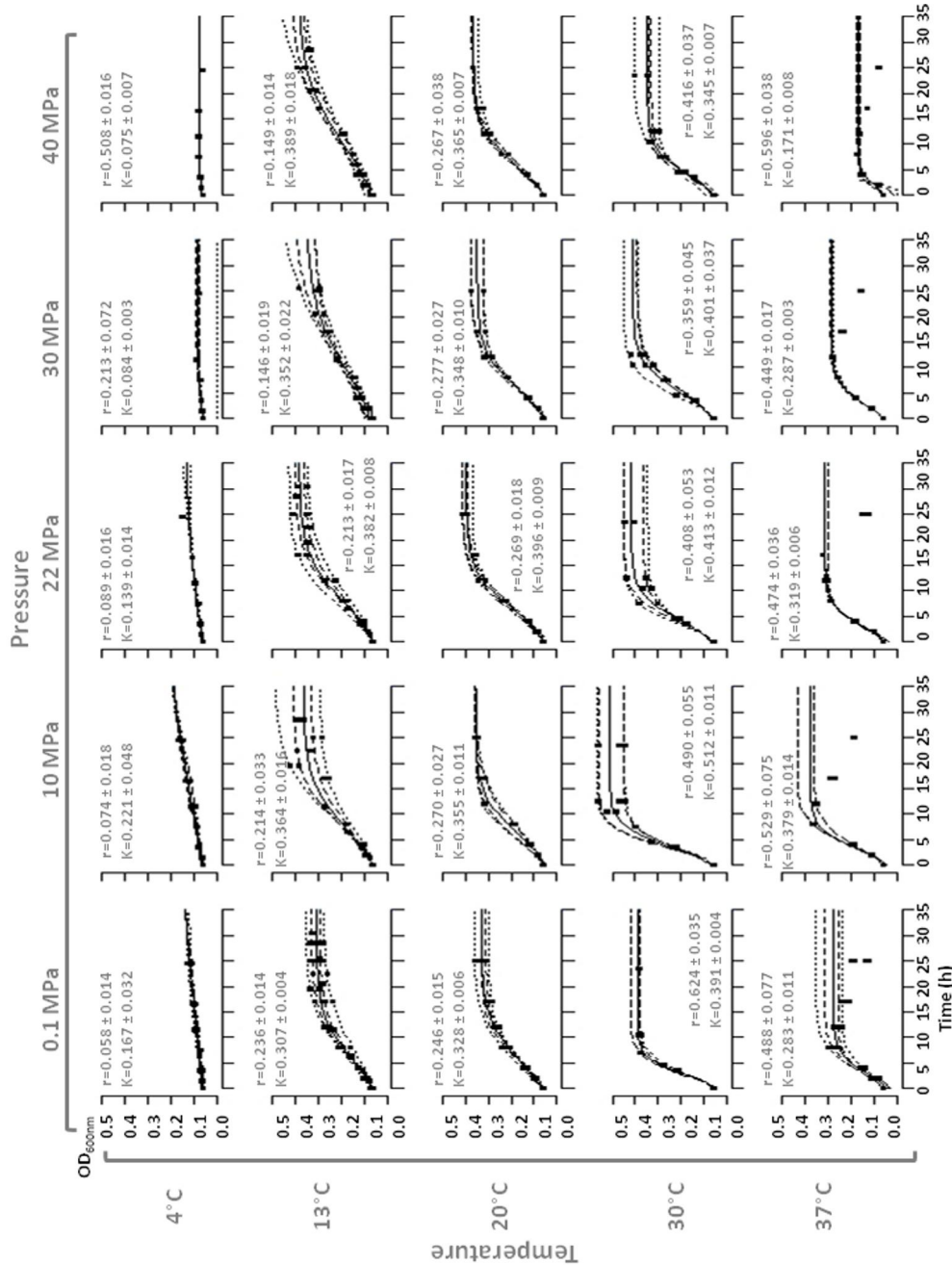


FIGURE (4.5) Representation of growth curves for temperatures of 4, 13, 20, 30 and 37°C and for pressure of 0.1, 10, 20, 30, and 40 MPa. The logistic model (line) improves the  $r$  and  $K$  parameter estimation on empirical growth data (dots). Dashed lines are levels of confidence for the 0.05 and 0.95 quantile curves and the 0.25 and 0.75 quantile curves. The growth rate ( $r$ ,  $\text{h}^{-1}$ ) and maximum population density ( $K$ ,  $\text{OD}_{600nm}$ ) parameters are indicated.

The  $r$  and  $K$  parameters were used to construct the extrapolated-contour diagram of their temperature-pressure dependence (Fig. 4.6 A and Fig. 4.6 B, respectively). *P. phosphoreum* ANT-2200 was able to grow at hydrostatic pressures ranging from 0.1 to 40 MPa and at temperatures ranging from 4 to 37°C.

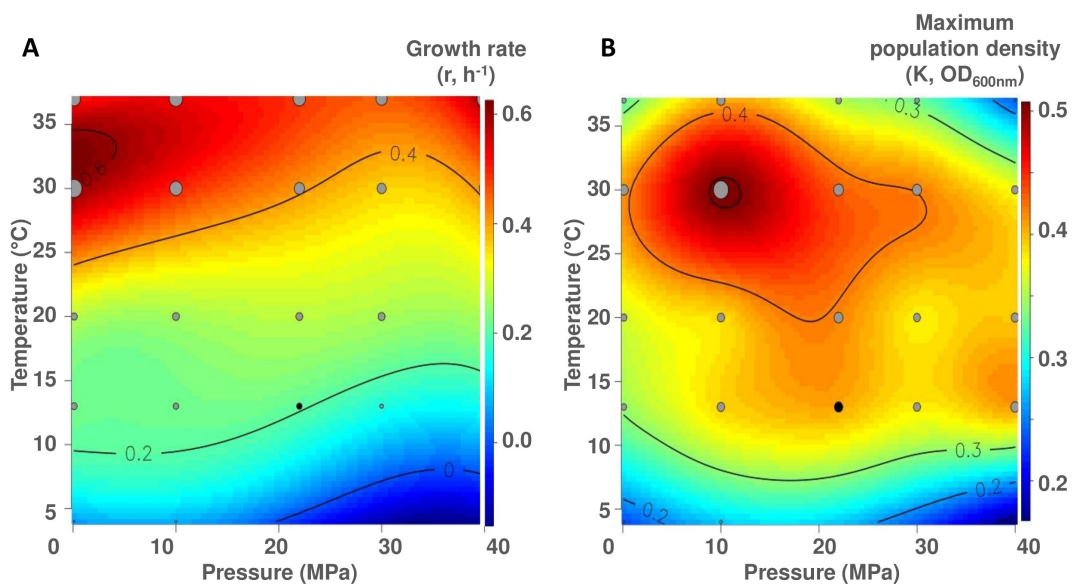


FIGURE (4.6) Extrapolated-contour diagram of the temperature-pressure dependence of *P. phosphoreum* ANT-2200. The diagrams are plotted for (A) the growth rate ( $r$ ,  $\text{h}^{-1}$ ) and (B) the maximum population density ( $K$ ,  $\text{OD}_{600\text{nm}}$ ). The gray circles indicate parameter values used to extrapolate the contours. Size is proportional to their value. The black circle corresponds to the *in situ* conditions for the strain. Isolines define zones with same level of parameter values.

The strain grew very slowly at 4°C, with a minimum  $r$  value obtained at 0.1 MPa ( $0.058 \pm 0.014 \text{ h}^{-1}$ ) and a low  $K$  of  $0.167 \pm 0.032$  (Fig. 4.6 A). The higher  $r$  values were observed at 30°C / 0.1 MPa and at 37°C / 40 MPa ( $0.624 \pm 0.035 \text{ h}^{-1}$  and  $0.596 \pm 0.038 \text{ h}^{-1}$  respectively, Fig. 4.6 A). While growth rates appeared to depend on temperature, pressure did not clearly affect it, at least in the tested range (Fig. 4.6 A). Furthermore, the stationary phase was very short with fast and strong cell lyses at 37°C for all pressures (Supporting Information, Fig. 4.5). In opposition to what is generally observed (Yayanos, 1995; Eloë et al., 2011), it was not possible to define the pressure affinity of

strain ANT-2200 using the growth rate only. Therefore, we also used the same approach to overlook the effect of temperature and pressure conditions on maximum population density reached by strain ANT-2200. Interestingly, both influenced  $K$  and for all tested conditions, the highest value ( $0.512 \pm 0.011$  OD<sub>600nm</sub>) was observed at 30°C and 10 MPa (Fig. 4.6 B). While the growth rate is commonly the main growth parameter used in microbiology, our experiments show that the maximum population density has a strong influence on the definition of the optimal conditions for growth. So, we propose to cross the  $r$  and  $K$  parameters (using the  $C_{r-K}$  coefficient) in order to define these optima (in our case, temperature and pressure).

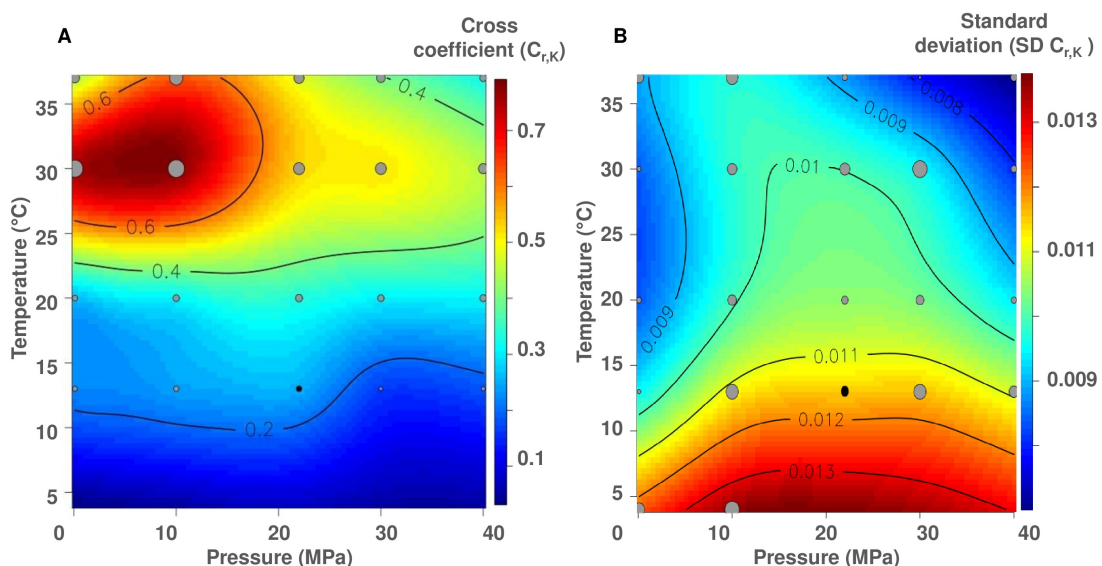


FIGURE (4.7) Cross diagram of the temperature-pressure dependence of *P. phosphoreum* ANT-2200. (A) Extrapolated-contour diagram of the temperature-pressure dependence for both the growth rate ( $r$ ,  $h^{-1}$ ) and the maximum population density ( $K$ , OD<sub>600nm</sub>) for *P. phosphoreum* ANT-2200. The cross coefficient  $C_{r-K}$  is defined as :  $0 < C_{r-K} < 1$ . (B) Standard deviation associated to the  $C_{r-K}$  coefficient. The gray circles indicate parameter values used to extrapolate the contours. Size is proportional to their values. The black circle corresponds to the *in situ* conditions for the strain. Isolines define zones with same level of values.

An extrapolated-contour diagram was drawn for the cross coefficient  $C_{r-K}$  (Fig. 4.7 A). The standard deviation, associated to the  $C_{r-K}$  coefficient, was calculated using the confidence-interval estimation on parameters from the logistic model and illustrated in

Figure 4.7 B. The standard-deviation values were one order below the cross-coefficient values, meaning that the cross-coefficient interpretation was robust. The highest  $C_{r-K}$  coefficient value (0.78) was found at 30°C and 10 MPa (Fig. 4.7 A). These optima allowed characterizing strain ANT-2200 as mesophile and moderately piezophile (Fang et al., 2010). As previously observed (Yayanos, 1995), the optimal pressure for piezomesophiles is often found lower than their habitat pressure, while their optimal temperature is higher than their habitat temperature. Different hypotheses can be evoked to explain the temperature shift (Yayanos, 1986) (1) inheritance from ancestors who lived in a warmer environment or (2) life in warmer temperatures in the gut of deep-sea animals. Even if we identified optimal conditions for growth at 30°C and 10 MPa, we decided to perform further experiments at in situ conditions (13°C) and to compare atmospheric pressure (0.1 MPa) to high pressure (22 MPa). This allowed to checking the piezophilic character of strain ANT-2200 and studying its morphology and its fatty-acid composition, known to be affected by hydrostatic pressure (Lauro et al., 2008; Bartlett et al., 1992; Bartlett, 2002). The pressure-dependent (0.1 versus 22 MPa, 13°C) bioluminescence activity of *P. phosphoreum* ANT-2200 was also characterized.

### Morphology of *P. phosphoreum* ANT-2200

*P. phosphoreum* ANT-2200 was observed by SEM and TEM after cultivation at 0.1 and 22 MPa (Fig. 4.8). *P. phosphoreum* ANT-2200 is a rod-shaped bacterium. The size of the cells is in average equal to  $2.4 \pm 1.4 \times 10^{-1}\mu\text{m}$  long and  $0.8 \pm 0.7 \times 10^{-1}\mu\text{m}$  wide at atmospheric pressure (Fig. 4.8 A1-3). Cells at 22 MPa display a smaller size (*i.e.*, less than 2  $\mu\text{m}$  long) and contain numerous intracellular inclusions (Fig. 4.8 B1-3). The exact nature of these inclusions has not yet been determined. Such inclusions may serve as energy reserve, may contribute directly to the metabolic capabilities of the cell, and/or may be involved in the cell ability to cope with changing environmental conditions (Shively et al., 2011; Campbell and Dower, 2003). In any case, this confirms an adaptation strategy of *P. phosphoreum* ANT-2200 cells to high hydrostatic pressure. Besides, cells also appear to aggregate more at 22 MPa than at 0.1 MPa (Fig. 4.8 A1-B1).

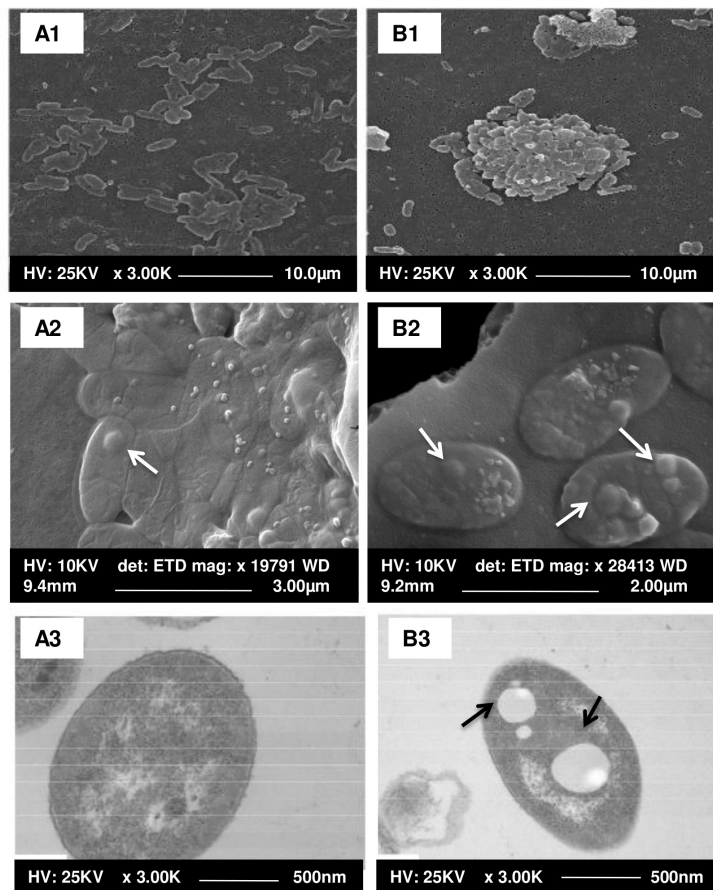


FIGURE (4.8) Micro-photographs of *P. phosphoreum* ANT-2200 cells by electron microscopy. Observation at 0.1 MPa (A1 on dehydrated samples, A2 on freeze-dried samples) and 22 MPa (B1 on dehydrated samples, B2 on freeze-dried samples) using SEM and at 0.1 MPa (A3) and 22 MPa (B3) using TEM. Intracellular inclusions are indicated by arrows.

### Pressure effects on the cellular fatty-acid composition of *P. phosphoreum* ANT-2200

The effect of hydrostatic pressure on the cellular fatty-acid composition of *P. phosphoreum* strain ANT-2200 was determined for cultures grown at 0.1 and 22 MPa at 13°C (Fig. 4.9). The main fatty acid was C16:1, representing 40.8 and 43.1% of the total cellular fatty-acid at 0.1 MPa and 22 MPa, respectively. Growth at 22 MPa also induced an increase in the relative proportions of C16:1, C17:0, C17:1, C18:1 and C18:2 fatty acids. The ratio of total unsaturated vs. total saturated fatty acids (UFA/SFA) was 1.9

at 0.1 MPa and 2.3 at 22 MPa. These values are similar to those found by DeLong and Yayanos (1985) for the piezophilic bacterium CNPT-3 grown under similar pressures. The increase in the relative proportions of mono-unsaturated fatty acids at elevated pressure is in good agreement with previous studies (Kamimura et al., 1993; Yano et al., 1998), indicating that many piezophilic bacteria respond to an increase in hydrostatic pressure by modifying their membrane lipid composition. This homeoviscous adaptation allows to tailor the membrane to environmental conditions with suited physical properties (Bartlett, 2002).

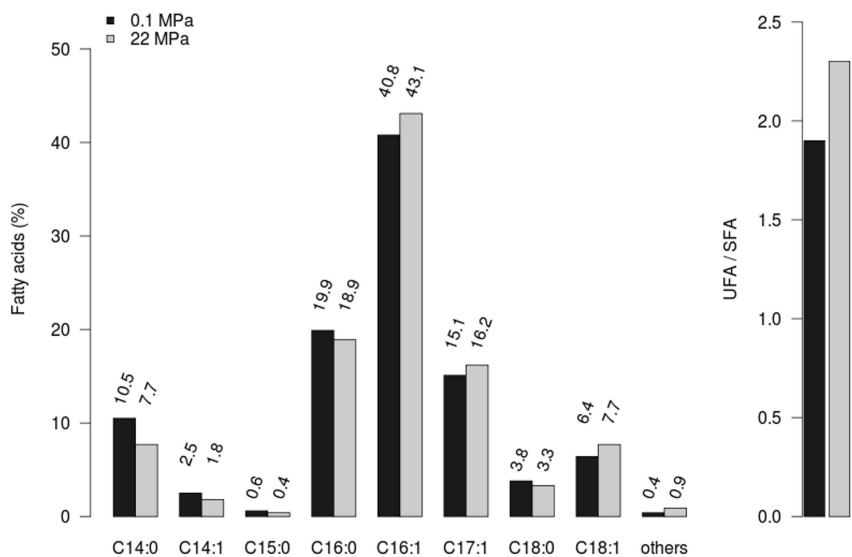


FIGURE (4.9) Relative total fatty-acid composition (%) of *P. phosphoreum* ANT-2200. Strain ANT-2200 is grown at 0.1 (black bar) and 22 MPa (gray bar). Others: sum of C17:0, C18:2 and C 19:1 fatty acids ; UFA: unsaturated fatty acids ; SFA: saturated fatty acids.

The results obtained with *P. phosphoreum* ANT-2200 further argue for the piezophilic character of this bioluminescent strain. It is noteworthy that the poly-unsaturated C20:5 fatty acid (C20:5 PUFA or eicosapentaenoic acid) was not detected in this strain. DeLong et al. (1997) suggested that C20:5 PUFA could be used to define strains originating from low temperature and high pressure environments. Nevertheless, the absence of such PUFA in *P. phosphoreum* ANT-2200 may be due to its origin from warmer deep-sea waters

(Mediterranean Sea, average temperature about 13°C), and to its optimal temperature of growth (30°C).

### Pressure effects on bioluminescence of *P. phosphoreum* ANT-2200

Three successive experiments using the high-pressure bioluminescent tank were carried out in order to quantify the luminescence produced by *P. phosphoreum* ANT-2200, at 0.1 MPa and 22 MPa, 13°C. Our results showed that the higher maximum cell density at 22 MPa than at 0.1 MPa is associated to higher luminescence intensity. Maximum luminescence intensity is reached, in average, at 17.6 h at 22 MPa and at 13.3 h at 0.1 MPa (Fig. 4.10 A). The average value of the maximum luminescence for the three replicates is three times higher at 22 MPa ( $3.5 \pm 0.1 \times 10^6$  photons sec $^{-1}$ ) than at 0.1 MPa ( $1.2 \pm 0.2 \times 10^6$  photons sec $^{-1}$ ). When bioluminescence is maximal, the total cell number is  $1.40 \pm 0.01 \times 10^8$  cells mL $^{-1}$  at 0.1 MPa and  $1.90 \pm 0.01 \times 10^8$  cells mL $^{-1}$  at 22 MPa (Fig. 4.10 B). At this time, the light emission capacity represents  $8.4 \times 10^{-3}$  photons cell $^{-1}$  mL $^{-1}$  at 0.1 MPa and  $19.0 \times 10^{-3}$  photons cell $^{-1}$  mL $^{-1}$  at 22 MPa. Noticeably, the ratio of photons emitted per cell and volume unit is higher at 22 MPa than at 0.1 MPa, clearly indicating the pressure dependence of bioluminescence. Since strain ANT-2200 is characterized as piezophile, its light emission appeared to be an adaptive trait more than a stress response to pressure as suggested by Czyz et al. (2000).

Actually, during the growth, the respiration and the bioluminescence emission are two processes competing for the consumption of oxygen (Nealson et al., 1970; Nealson and Hastings, 1977; Bourgois et al., 2001; Grogan, 1984). To explain the differences in light emission between high pressure and atmospheric conditions, the oxygen availability has been checked. An oxygen optode (PreSens GmbH) permitted to control the remaining presence of enough oxygen at the end of the growth (oxic condition) both under atmospheric and high-pressure conditions (data not shown). The oxygen concentration seems not to explain the differences in bioluminescence emission per cell described in these experiments. A second explanation to these results is based on the ecological aim of the bioluminescence emission. Metabolic processes, such as the increase of

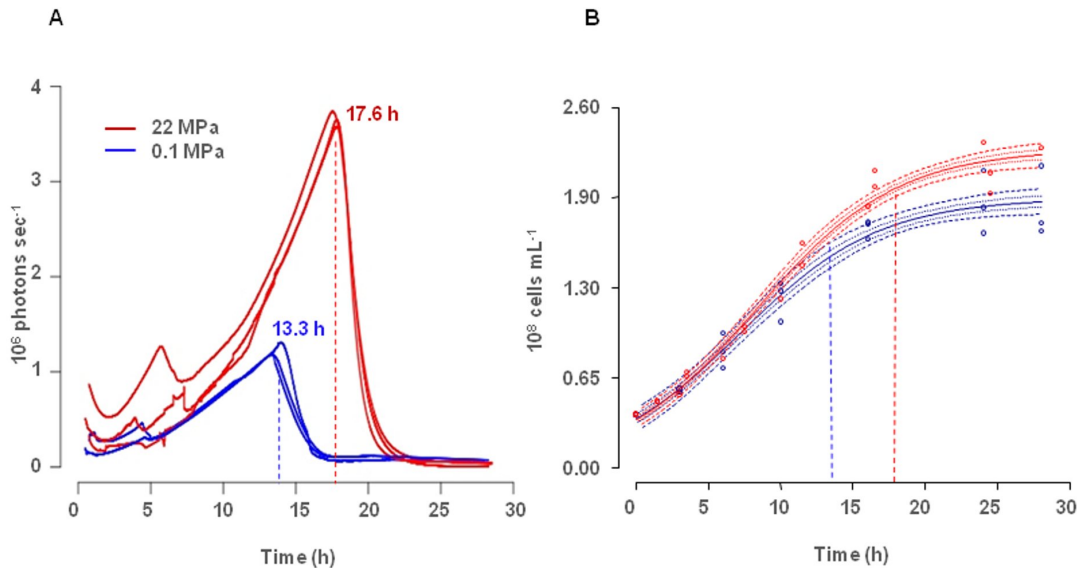


FIGURE (4.10) Bioluminescence and growth of *P. phosphoreum* ANT-2200. (A) Bioluminescence ( $\text{photons sec}^{-1}$ ) of *P. phosphoreum* ANT-2200 at 0.1 MPa (blue lines) and 22 MPa (red lines). (B) Fitted logistic growth curves for 0.1 MPa experiments (blue lines) and 22 MPa experiments (red lines). The dashed lines represent levels of confidence for the 0.05, 0.95 and 0.25, 0.75 quantile curves. Cell number is estimated using equation (1). On (A) and (B) blue and red dotted lines represent the mean time of the bioluminescence peak for both pressure conditions.

bioluminescent-bacterium biomass, will increase the luminescence by an autoinduction phenomenon. Many bacteria use this cell-density-dependent signaling system, also called quorum sensing, to coordinate the expression of the genes involved in biofilm formation and luminescence production (Hmelo et al., 2011). In our study, the aggregates formed at 22 MPa (Fig. 4.8 B1) keep the cells close together, miming a higher cell density, and this could possibly induce a quorum-sensing response leading to higher bioluminescence intensity. This is in agreement with previous hypotheses from Pooley (2011).

Three different ecological niches with high cell density, enhancing quorum sensing and indirectly bioluminescence, have been described in the literature so far. Firstly, light organs of marine squids or fish contain up to  $10^{11} \text{ cells mL}^{-1}$  of luminescent bacteria. This symbiosis provides an advantage for the host (prey or partner attraction...) and an ideal growth environment for bacteria (Haddock et al., 2010; Widder, 2010). Secondly, marine

snows are millimetre- to centimetre-size aggregates of macroscopic flocculent particles consisting of detritus, inorganic particles and phytoplankton on which micro-organisms grow (Azam, 1998; Azam and Long, 2001; Alldredge and Cohen, 1987). Bacteria can develop swimming behavior to colonize this sinking organic material, therefore reaching a cell density 100 to 10,000 times higher than in the water column (up to  $10^8$  to  $10^9$  cells  $\text{mL}^{-1}$ ) (Schweitzer et al., 2001; Ploug and Grossart, 2000). At this density, they are able to emit light in order to attract preys. Then, they might be ingested by macro-organisms to live in a better-growing environment (Ruby and Morin, 1979; Andrews et al., 1984). Thirdly, luminous bacteria are known to be present in the gastro-intestinal tracts of marine organisms. Their expelled faecal pellets are enriched in micro-organisms, including bioluminescent bacteria, up to  $10^5$  to  $10^6$  times more than the surrounding waters (Ruby and Morin, 1979; Andrews et al., 1984; Zarubin et al., 2012). Ingestion rate and cycling of pellet constituents are affected by bioluminescence phenomenon (Zarubin et al., 2012), suggesting that bioluminescence bacteria might play an important role in the carbon cycle in the deep ocean.

## Conclusion

The strain *P. phosphoreum* ANT-2200 was isolated from a deep-water sample (2,200 m, 13°C, 22 MPa) close to the ANTARES site in the Mediterranean Sea. It has been shown that, using only growth rate, it was not possible to characterize the strain growth optima. However, using both growth rate and maximum population density of strain ANT-2200, optimal temperature and pressure have been estimated at 30°C and 10 MPa. As observed in other deep-sea strains, the ratio of total unsaturated vs. total saturated fatty acids is higher at elevated pressure. All these points converge to characterize this strain as mesophile and moderately piezophile. The strain ANT-2200 produces higher luminescence intensity at high pressure (22 MPa) than at atmospheric pressure (0.1 MPa). To our knowledge, this is the first time that such phenomenon is described. Genetic determinism and corresponding ecological benefit of this pressure-controlled bioluminescence still have to be determined.

**Acknowledgements**

Authors thank S. Escoffier, and the ANTARES collaboration. Authors are also grateful to Mrs A. Rivoire and C. Boulé (Centre Technologique des Microstructures, Université Lyon 1) for electron microscopy. Comments from two anonymous reviewers allowed to significantly improving a previous version of the article.

**Fundings**

This work was funded by the ANR-POTES program (ANR-05-BLAN-0161-01) supported by the Agence Nationale de la Recherche, by the AAMIS program (Aix-Marseille Université) and by EC2CO BIOLUX program (CNRS). SM was granted a MERNNT fellowship (Ministry of Education, Research and Technology, France). BAA was supported by a fellowship funded by the Syria Ministry of Higher Education.

## 4.4 Effects of hydrostatic pressure and growth medium on bacterial growth, luminescence and oxygen consumption

### 4.4.1 Growth medium

Based on these first experiments and results, growth medium has been modified to get closer to *in situ* environmental water composition. The initial medium compositions (see SWC mediums composition in Table 4.1) were based on literature contents (Hastings and Nealson, 1977; Karl and Nealson, 1980; Pooley et al., 2004). These mediums were optimized for fast bacterial growth (about 24 h for *Photobacterium phosphoreum* ANT-2200) and intense bioluminescence activity with high yeast extract, bio-polypeptone and glycerol concentrations.

The growth medium has been modified with reduced yeast extract, no bio-polypeptone and lower glycerol concentration (see ONR7a composition in Table 4.2). These changes lead to fewer carbon sources but easier to detect and measure during the growth. Both NH<sub>4</sub>Cl and Na<sub>2</sub>HPO<sub>4</sub> 2H<sub>2</sub>O concentrations have been increased to avoid nutrients limitation. The ONR7a growth medium involves slower bacterial growth (about 70 h in ONR7a compared to 24 h in SWC medium to reach the stationary phase). Cultures

TABLE (4.1) Composition of the rich Sea Water Complete medium (SWC) and impoverished SWC medium. SWC is described as rich due to its high carbon content (yeast extract, bio-polypeptone and glycerol concentrations). pH is set at 7.5.

chemical component	SWC medium rich	SWC medium impoverished
Old seawater	750 mL L <sup>-1</sup>	750 mL L <sup>-1</sup>
Distilled water	250 mL L <sup>-1</sup>	250 mL L <sup>-1</sup>
Bio-polypeptone	5 g L <sup>-1</sup>	5 mg L <sup>-1</sup>
Yeast extract	3 g L <sup>-1</sup>	3 mg L <sup>-1</sup>
Glycerol	3 mL L <sup>-1</sup>	3 mL L <sup>-1</sup>

TABLE (4.2) Composition of the ONR7a medium with low carbon concentration. Before mixing, solutions 1 and 2 are autoclaved separately to avoid precipitation and solution 3 is filtered on 0.2 µm. pH is set at 7.5

Chemical component	ONR7a medium
Solution 1	(in 700 mL)
NaCl	22.79 g L <sup>-1</sup>
Na <sub>2</sub> SO <sub>4</sub>	3.98 g L <sup>-1</sup>
KCl	0.72 g L <sup>-1</sup>
NH <sub>4</sub> Cl	0.8 g L <sup>-1</sup>
Na <sub>2</sub> HPO <sub>4</sub> 2H <sub>2</sub> O	0.2 g L <sup>-1</sup>
NaBr	83 mg L <sup>-1</sup>
NaF	2.6 mg L <sup>-1</sup>
NaHCO <sub>3</sub>	31 mg L <sup>-1</sup>
H <sub>3</sub> BO <sub>3</sub>	27 mg L <sup>-1</sup>
Glycerol	2 mL L <sup>-1</sup>
Yeast extract	50 mg L <sup>-1</sup>
Solution 2	(in 300 mL)
MgCl <sub>2</sub> 6H <sub>2</sub> O	11.18 g L <sup>-1</sup>
CaCl <sub>2</sub> 2H <sub>2</sub> O	1.46 g L <sup>-1</sup>
SrCl <sub>2</sub> 2H <sub>2</sub> O	24 mg L <sup>-1</sup>
Solution 3	(prepared in 10 mL, add 1 mL)
FeSO <sub>4</sub> 7H <sub>2</sub> O	0.025 g L <sup>-1</sup>

performed under similar experimental conditions show higher *K* and lower *r* parameters for ONR7a than SWC medium (data not shown). These changes in *K* and *r* parameters involving a higher carrying capacity<sup>1</sup> with a lower growth rate.

#### 4.4.2 High-pressure and oxygen consumption system

The final aim of this experimental Chapter is to cultivate a bioluminescent bacterial strain potentially active at the ANTARES site as close as possible to environmental conditions. In order to sample oxygen during growth and under high hydrostatic pressure, new instrumentation dedicated to the measure of the bacterial oxygen consumption has been developed in the laboratory (Figure 4.11) and is under validation (Figure 4.12). This led

1. Carrying capacity is the maximum population size that the environment or medium can sustain based on food or habitat available in the environment

to the improvement of new technology and adapted protocols. In this experimental part, we present first results of the measure of bacterial oxygen consumption during growth. These experiments take into account hydrostatic pressure (22 and 0.1 MPa), temperature (13°C) and carbon availability (ONR7a medium) to describe oxygen consumption and bioluminescence activity of *Photobacterium phosphoreum* ANT-2200.

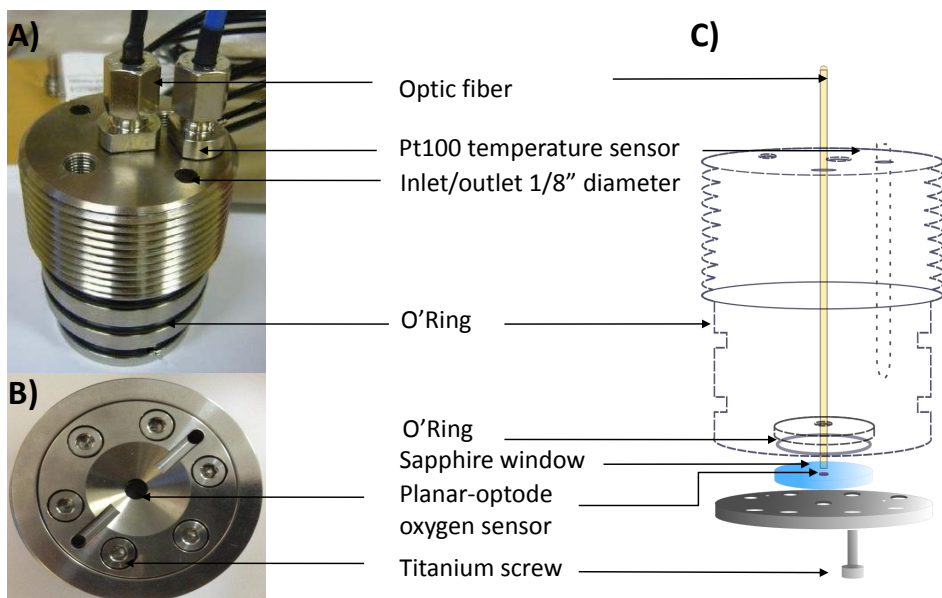


FIGURE (4.11) A) and B) Representation of the end cap for High Pressure Bottles (HPBs) with top end cap dedicated to oxygen consumption measurements. The end cap is made with titanium mater and both temperature and oxygen probes can be connected for direct measurements. Probes are connected with oxygen and temperature fiber to a computer, for data acquisition. A) Photograph of the external part, from above B) Photograph of the external part, from below. C) Photograph of the internal part. Schematic representation of the end cap for High Pressure Bottles (HPBs) with oxygen and temperature fibers and connections.

High-Pressure Bottles (HPBs), described in [Bianchi et al. \(1999\)](#) and [Tamburini et al. \(2003\)](#), are composed by a APX4 stainless steel cylinder with a PEEK coating for biological compatibility closed by two end caps. One end-cap in 316 L stainless steel is covered with a sheet of PEEK. The second end-cap has been modified in order to support

the oxygen sensor as described below and in Figure 4.11. A PEEK floating piston permit to transmit the pressure inside the HPB and to perform sub-sampling if necessary. The modified end cap has been built in Titanium (grad 4, biologically and chemically compatible) and modified as following : four pecking, two for fluid pathway, one for Pt100 temperature sensor, and one stopped by sapphire window to measure dissolved oxygen concentration. The sapphire window is 2 mm thickness and 4 mm diameter and permit to support an optical fiber (OXY4 PreSens®). On the end cap three Viton® O'ring allow to insure etancheity and to prevent organic carbon contamination.

The measurement of dissolved oxygen is based on oxygen luminescence quenching of a platinum porphyrine complex caused by the collision between the excited luminophore and the quencher (oxygen) resulting in radiationless deactivation, called dynamic quenching. The decrease in fluorescence intensity and/or change in fluorescence decay lifetime can be used as a measure of oxygen concentration. The luminophore was contained in polymer support coated on sapphire and was sterilized by autoclave before use, in order to avoid contamination during experiments.

HPBs are filled with milli-Q water before sterilization. Oxygen and temperature sensors are then screwed to the end cap and a first high pressure input up to 40 MPa is transmitted to the HPBs. This necessary pre-conditioning involves a peak in the oxygen measurement due to high pressure input (Figure 4.12). After this pre-conditioning step, similar high pressure level will not modify oxygen measurement above the noise level. Culture medium is oxygen saturated by intense stirring before bacterial inoculation and saturated Fluorinert is used as oxygen supplier in HPBs. Inoculated culture medium and Fluorinert (25% of total volume) are transferred to the HPB under high pressure.

#### 4.4.3 Data acquisition into High Pressure Bottles

Following experiments led to the measure of growth, bioluminescence activity and oxygen consumption with temperature and pressure-controlled conditions. In this part, we

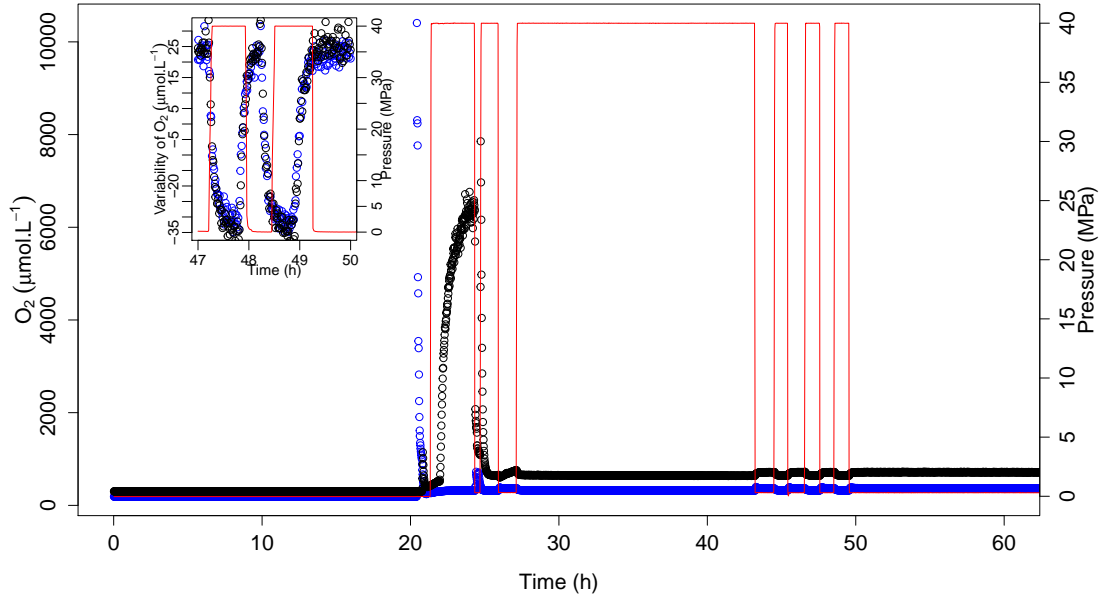


FIGURE (4.12) Test for oxygen measurement before inoculation and conditioning for high pressure experiment. Two channels (blue and black dots) are connected to the HPB for noise level comparison. Hydrostatic pressure involved to the system is plotted over time (red line). The first high pressure transmission, at 40 MPa involves a burst in oxygen measure. Then after this first conditioning, fairly low modifications of oxygen measure appear with similar high pressure transmission. Thanks to this test, the HPBs are pre-conditioned with higher pressure transmission (40 MPa) before experiments. Data and representation from M. Garel.

aimed at understand bioluminescence-bacterial answer as close as possible to the *in situ* conditions. Experiments have been performed under atmospheric conditions (0.1 MPa) (Figure 4.13 A 1-3) and similarly under *in situ* pressure conditions (22 MPa) (Figure 4.13 B 1-3).

### Growth measurements

Growth measurements ( $OD_{600nm}$ ) are triplicates for each pressure condition (0.1 vs 22 MPa). A logistic model (see Martini et al., 2013a and Verhulst, 1838) has been applied to this dataset and is plotted (red and blue lines, Figure 4.13 A-1 and B-1) with confidence intervals (dashed lines Figure 4.13 A-1 and B-1). Higher  $r$  and lower  $K$  values are observed under atmospheric conditions than under high pressure (0.079/0.43 and

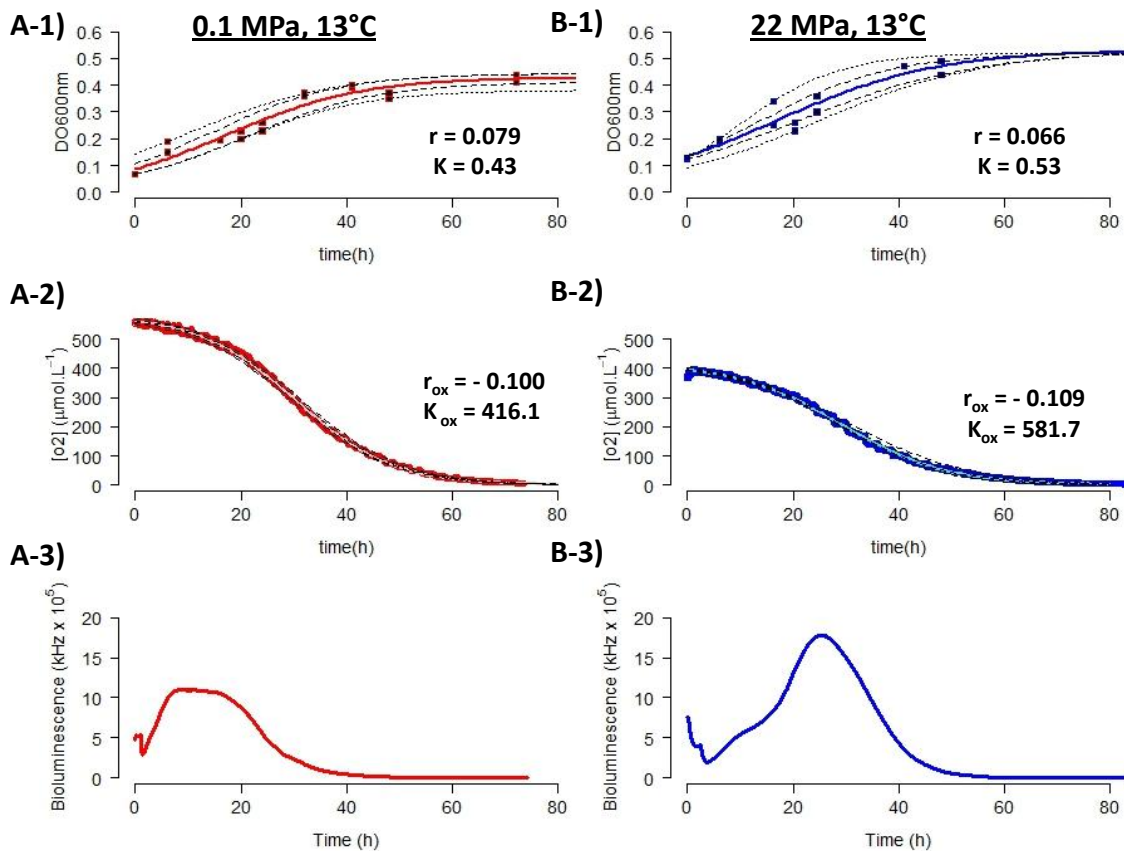


FIGURE (4.13) *Photobacterium phosphoreum* ANT-2200 is cultivated in ONR7a growth medium and experiments are performed at 13°C and A) Atmospheric pressure (0.1 MPa) B) High pressure (22 MPa). 1) Bacterial growth (DO<sub>600nm</sub>) 2) Oxygen consumption (μmol L<sup>-1</sup>) 3) Bioluminescence emission. Dashed lines are levels of confidence for the 0.05 and 0.95 quantile curves and 0.25 and 0.75 quantile curves. A logistic model is fitted for both growth and oxygen consumption dataset and the model defined the two characteristic parameters  $r$  (h<sup>-1</sup>) and  $K$  (OD<sub>600nm</sub>) for bacterial growth and  $r_{ox}$  (h<sup>-1</sup>) and  $K_{ox}$  (μ mol L<sup>-1</sup>) for oxygen consumption.

0.066/0.53 respectively). Furthermore,  $r$  and  $K$  parameters have been measured with higher values in ONR7a than SWC growth medium. However, the observation of higher  $r$  and  $K$  parameters under atmospheric pressure is similar to the variations observed for SWC medium at 13°C and between similar pressure conditions (see Figure 4.5). These observations confirm the effects of high pressure on bacterial physiology independently of the culture conditions.

## Oxygen consumption

Using the newly-developed setup to record O<sub>2</sub> concentration within HPBs, we measured the oxygen consumption for *Photobacterium phosphoreum* ANT-2200 (Figure 4.13 A-2 and B-2). For bioluminescent bacteria, oxygen consumption is dedicated to both bacterial respiration and bioluminescence reaction. The data have been represented using a model as follow :

$$x_t = \frac{K_{ox}}{1 + \exp((xmid - t)/scal)} \quad (4.8)$$

with  $x_t$  the oxygen concentration,  $xmid$  the value at the inflection time  $t$ ,  $scal$  a negative scale parameter,  $K_{ox}$  the asymptotic parameter represented as the initial oxygen concentration, and  $t$  the time. The oxygen-consumption rate is defined as  $r_{ox} = 1/scal$ .

Oxygen consumption is closely related to the biomass during bacterial growth, this last variable following the logistic model hypotheses (see [Martini et al. \(2013a\)](#) and [Verhulst \(1838\)](#) for details). The oxygen-consumption model performed is close to the logistic one with a negative coefficient for oxygen consumption. Similar  $r$  and  $r_{ox}$  values were expected between bacterial growth and oxygen consumption (increase in bacterial growth will linearly increases the oxygen consumption). However, higher  $r_{ox}$  than  $r$  values have been measured for both pressure conditions meaning that oxygen consumption is faster than bacterial growth. These differences can possibly be explained by oxygen consumption dedicated to the bioluminescence reaction.

For both pressure conditions, a similar  $r_{ox}$  negative coefficient is computed (-0.100 and -0.109 for atmospheric and high pressure conditions respectively) meaning that similar oxygen consumption occurs. Then, for similar oxygen consumption between both pressure conditions, there is a higher bioluminescence activity and higher biomass under high pressure condition. This result possibly led to a better oxygen efficiency under high pressure than atmospheric one. Such results would be in accordance with expected ones

for this moderately piezophile bacterial strain. However, due to experimental constraints, the initial oxygen values are not similar between those two experiments (416.1 and 581.7  $\mu\text{mol O}_2 \text{ L}^{-1}$  for atmospheric and high pressure conditions respectively). Such differences in initial-oxygen concentrations could possibly lead to misinterpretation and need to be fixed in further experiments.

### Bioluminescence activity

Bioluminescence activity has been measured for both pressure conditions (Figure 4.13 A-3 and B-3). The maximum bioluminescence intensity is lower at atmospheric than at high pressure conditions ( $1.0 \times 10^6$  kHz and  $1.9 \times 10^6$  kHz respectively). Under atmospheric pressure (0.1 MPa), the bioluminescence peak is long, occurring between 7 and 18 h whereas under high pressure (22 MPa), the peak is very straight and occurs few hours later, between 22 and 25 h. The photon emission per cell has been estimated for both pressure conditions with  $2.0 \times 10^{-2}$  and  $2.1 \times 10^{-2}$  photons  $\text{cell}^{-1}$  for 0.1 and 22 MPa respectively. From these results, only weak differences are observed between both pressure conditions. However, we still observe higher photon emission per cell for high-pressure conditions (22 MPa) compared to atmospheric ones (0.1 MPa).

## 4.5 Conclusions

From these successive sets of experiments under various pressure conditions (0.1 and 22 MPa) and growth medium composition with different carbon content (SWC and ONR7a growth mediums), several results have been highlighted.

### Pressure effects

Firstly, *Photobacterium phosphoreum* ANT-2200 strain has been defined as moderately piezophile. This strain isolated from the ANTARES station seems to be adapted to this deep environment. Moreover, higher pressure affects the bioluminescence emission by increasing the number of photons per cell (see Table 4.3). The effects of high pressure

TABLE (4.3) Summary of results measured in High Pressure Bottles. SWC : Sea Water Complete medium.

Growth medium	P condition	Photons cell <sup>-1</sup> s <sup>-1</sup>
SWC	0.1 MPa	$8.4 \times 10^{-3}$
SWC	22 MPa	$1.9 \times 10^{-2}$
ONR7a	0.1 MPa	$2.0 \times 10^{-2}$
ONR7a	22 MPa	$2.1 \times 10^{-2}$

on bioluminescence activity have been clearly demonstrated for SWC growth medium (Martini et al., 2013a), however, this is less obvious for ONR7a medium with low variations between both pressure conditions. These photons emission per cell are very low compared to the data from the literature. Makemson (1986) estimates about  $1.0 \times 10^3$  and  $3.0 \times 10^3$  photons cell<sup>-1</sup> s<sup>-1</sup> for *Vibrio harveyi* and *Vibrio fischeri* respectively. However, in these experiments, the maximal values for OD<sub>600nm</sub> are measured between 0.5 and 4. Such units refer to about  $10^7$  to  $10^8$  total cells in the culture medium. These values are fairly low for quorum sensing threshold known to activate the bioluminescence reaction at about  $10^8$  to  $10^9$  bacterial cells. The difference in bacterial strain, in growth medium and the maximal cell concentration can explain these very low values.

### Carbon availability

Then, carbon availability for bacterial growth has been investigated between a carbon-rich medium (Sea Water Complete) and a lower carbon-content medium (ONR7a). For the two pressure conditions (0.1 and 22 MPa), the photons per cell per second are higher for lower carbon-content than rich carbon-content mediums. The rich carbon-content medium (SWC medium) is possibly well adapted for faster bacterial growth but probably limited in mineral-content available for growth (NH<sub>4</sub>Cl and NaHPO<sub>4</sub>·2H<sub>2</sub>O). This probably happens before the carbon-limitation. The low carbon-content medium (ONR7a) is limited in carbon under constant oxygen saturation. However, in HPBs, without constant input of oxygen, the bacterial growth is limited by oxygen availability (Figure 4.13 A-2 and B-2).

Further investigations on physiological processes have to be pursued using the low carbon

content growth medium (ONR7a). Indeed, physiology is altered for *Photobacterium phosphoreum* ANT-2200 strain as observed in [Martini et al. \(2013a\)](#), meaning that oxygen efficiency for respiration or bioluminescence reaction can be altered within high pressure. Therefore, the difference in dissolved O<sub>2</sub> saturation at the beginning of the experiment between both conditions (*K* values, 416.1 and 581.7 for 0.1 and 22 MPa respectively) has to be fixed. Then, the part of oxygen dedicated to the respiration and the one involved into the bioluminescence reaction have to be estimated. Several methods can be used and these estimations in the literature have been achieved using inhibitors for the bioluminescence reaction such as CCCP or cyanide (see [1.1.4](#)) components. Similar experiments can be performed with *Photobacterium phosphoreum* ANT-2200 to define this percentage.

### Illustrated conclusion

To conclude, catabolic and anabolic pathways in aquatic bacteria have been summarized (Figure [4.14](#) from [del Giorgio and Cole \(1998\)](#)) and this schematic representation has been implemented with bioluminescence activity. From this schematic representation (Figure [4.14](#)) bioluminescence (process in orange) appears as a positive feedback on the biomass/storage and product compartments and a negative action on the oxygen consumption for cell.

Firstly, the part of oxygen dedicated to the substrate oxidation is modified due to the oxygen taking for bioluminescence reaction ('m' and 'n' rates in Figure [4.14](#)). Moreover, the bioluminescence reaction involving ATP (rate 'o' on Figure [4.14](#)) influences the ATP uptake rate for catabolic and anabolic pathway (rates 'a', 'b', 'c', 'd' on Figure [4.14](#)). Consequently, bioluminescence reaction is costly for the bacterial cell and the benefice back is the major issue to investigate. To explain such benefice, in the ocean, [Baltar et al. \(2013\)](#) indicate that oxidative stress caused by H<sub>2</sub>O<sub>2</sub> affects prokaryotic growth and hydrolysis of specific components of the organic matter pool. Thus, the authors suggest that oxidative stress may have important consequences on marine carbon and energy fluxes. Bioluminescence could be, in these cases, an ecological advantage by the detoxification of molecular oxygen due to its reduction during the chemical reaction ([Timmins et al., 2001](#)).

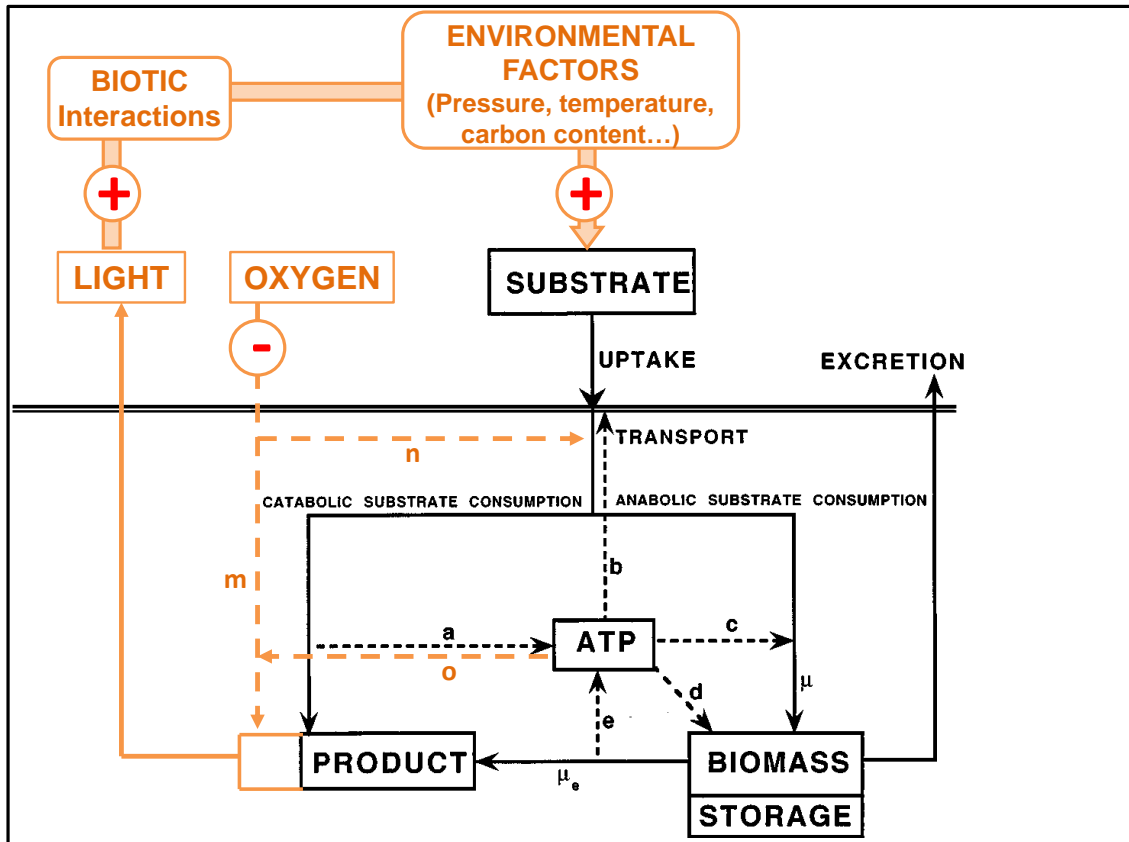


FIGURE (4.14) Bacterial metabolic and anabolic pathways within and without the cell. "+" are positive action of light emission on substrate availability and biotic interactions, "-" negative action on oxygen consumption for the cell. Products are cell expenditure for maintenance.

a : rate to which oxidation of organic compounds contributes to the energy pools as ATP.

b : rate to which energy is required for active transport of substrates into the cell.

c : rate to which ATP is utilized for anabolic reaction.

d : rate to which ATP is utilized for maintenance expenditure.

$\mu$  : growth rate

$\mu_e$  : endogenous metabolism by biomass decomposition in absence of substrate

e : rate to which ATP is supplied in the absence of exogenous substrates by degradation of biomass.

m : rate to which oxygen is attributed to the bioluminescence reaction.

n : rate to which oxygen is attributed to the substrate oxidation.

o : rate to which ATP is consumed during the bioluminescence reaction.

Adapted from [del Giorgio and Cole \(1998\)](#)

Then, indirectly, the light emission influences the cellular mechanisms by its ecological role. Indeed, on the one hand, bacterial bioluminescence will act positively on substrate availability and oxygen by improving environmental factors (better growth condition

for example in symbiotic association). As demonstrated by Zarubin et al. (2012), bioluminescent bacteria are more attractive for other organisms and would be more easily consumed on fecal pellets, this leading to the symbiosis between such organisms involving a better growing environment considering the carbon, temperature or oxygen conditions. On the other hand without bioluminescence reaction there is no impact on carbon availability and consequently, possibly no positive contribution to the biomass/storage and product compartments.

Further work can be investigated, based on these results. On the one hand, using the high pressure equipment, it is possible to adapt experimental protocol to test the pressure effect on bioluminescent bacteria attached to particles sinking from the surface waters to the deep sea. On the other hand, we only investigated bacteria as possible organisms involved in the bioluminescence activity recorded during intense events at the ANTARES station. It could be of interest to test the hypothesis that newly formed water masses bring other bioluminescent organisms from the surface to the deep. Such organisms also undergo pressure effects that probably affect their physiology and bioluminescence.



# CHAPITRE 5

---

## *In situ* prokaryotic survey, quantification and bacterial bioluminescence: estimation at the ANTARES station

---

### Sommaire

---

<b>5.1</b>	<b>Introduction : from laboratory to <i>in situ</i> measurements . . . . .</b>	<b>152</b>
<b>5.2</b>	<b>Article 4 . . . . .</b>	<b>155</b>
5.2.1	Temporal survey of prokaryotic communities, presence and activity of bioluminescent bacteria at the deep ANTARES station (North-western Mediterranean Sea) . . . . .	155
<b>5.3</b>	<b>Conclusions . . . . .</b>	<b>178</b>

---

## 5.1 Introduction: from laboratory to *in situ* measurements

In Chapter 4, experimentations have been performed, in the laboratory, under controlled growth conditions and with a pure culture, using the bioluminescent bacterial strain *Photobacterium phosphoreum* ANT-2200 as a model. This necessary first step gave us some clues, using experimental results, to validate or not the relevance of considering bioluminescent bacteria as inducers of the intense bioluminescence events detected at the ANTARES station, as we proposed in Chapters 2 and 3. Laboratory experiments were efficient to define independent effects of hydrostatic pressure, temperature and growth medium on oxygen consumption, growth and bioluminescence activity. We demonstrate that high hydrostatic pressure (22 MPa) compared to atmospheric pressure (0.1 MPa), increases bioluminescence activity for this bacterial strain, defined as moderately piezophile. Moreover, several physiological adaptations, better yield for both oxygen consumption and photon emission, have been highlighted under *in situ* conditions compared to atmospheric ones. Furthermore, physiological aspects still need to be defined.

As far as we know, until the present study, milky sea were the only large phenomena of high bioluminescence activity detected *in situ*. Such phenomenon has been observed by naked eye and by satellites. Miller et al. (2005), Nealson and Hastings (2006) and Lapota et al. (1988) attribute these phenomena to bioluminescent Bacteria and give an estimation for their concentration of about  $2.8 \times 10^8$  cells  $\text{cm}^{-2}$ . However, these phenomena were described from satellite images or seamen opportunist observations and recorded at the surface of the oceans. Using neutrino telescope and, more generally, PMTs as bioluminescence detectors, such surprising events will be more easily observed, quantified, and explained even in extreme environments such as the dark ocean. To validate such an aim, the part of bacterial bioluminescence has to be quantified and differentiated from the total bioluminescence signal.

In the next Chapter, we aim at answering the question of bioluminescent bacteria abundance, variability and their possible implication in the signal recorded from PMTs.



FIGURE (5.1) Milky sea detection from satellite observation in the Indian Ocean. The bioluminescent feature (lower right) is to scale, but has been colorized and enhanced, so it appears much brighter in relation to the scene than it would naturally. The glowing area has been estimated about 15,400 km<sup>2</sup> and attributed to bioluminescent Bacteria (*Vibrio harveyi*) associated to *Phaeocystis* (Haptophyte, Eukaryotes). From <http://biolum.eemb.ucsb.edu/organism/milkysea.html>.

As first objective, we describe the prokaryotic community over one-year survey at the ANTARES station. At the same time, discrete sampling for environmental variables (temperature, salinity, DOC, NO<sub>3</sub><sup>-</sup>, PO<sub>4</sub><sup>3-</sup>, Si(OH)<sub>4</sub>, and dissolved oxygen) are performed during MOOSE and CASCADE cruises. Unfortunately, the stop of the IL07 instrumented line, at the end of 2010, does not permit to access to high frequency dataset for temperature and salinity. From these data, the bioluminescent bacterial contribution, its activity and variability over the year are quantified thanks to molecular biology methods and analyzed conjointly with environmental data obtained monthly by discrete profiles and water sampling. This sampling strategy involving instrumentation at sea, meteorology hazards have been one of the major constraint. However, from this preliminary work, presented as an "article in preparation", first results and perspectives will be proposed.

Conjointly to this survey, the CASCADE cruise was conducted in 2011, from March 1<sup>st</sup> to 30<sup>th</sup>, in the Gulf of Lion and at the ANTARES site aiming at the description of deep

convection phenomena. During this cruise, hydrological data show a winter convection in March 2011, reaching 1,600 m depth (X. Durieu de Madron pers. com., M. Boutrif PhD thesis 2012). Hence, this phenomenon observed in 2011 is much less intense and less deep than the previous ones described in Chapter 1, ([Tamburini et al., 2013](#)), [2.4.2](#) reaching 2,300 m depth in 2010 (see Figure [2.19](#)) and consequently not directly impacting the ANTARES station.

*This work has been granted by EC2CO-BIOLUX. C. Tamburini is the PI for the project. D. Lefèvre, M. Garel, C. Tamburini and me performed the sampling at sea at the ANTARES station during both MOOSE and CASCADE campaigns. L. Casalot and et S. Isart elaborated the beginning of the study with lux gene sequence determination and preliminary work. V. Michotey and S. Guasco performed the experimentations and the interpretation of the results for molecular biology. I summarized, interpreted and wrote the results.*

## 5.2 Article 4

### 5.2.1 Temporal survey of prokaryotic communities, presence and activity of bioluminescent bacteria at the deep ANTARES station (North-western Mediterranean Sea).

Martini S.<sup>1,2\*</sup>, Michotey V.<sup>1,2</sup>, Guasco S.<sup>1,2</sup>, Casalot L.<sup>1,2</sup>,  
Garel M.<sup>1,2</sup>, Tamburini C.<sup>1,2</sup>

<sup>1</sup> Aix-Marseille Université, Mediterranean Institute of Oceanography (MIO), 13288, Marseille, Cedex 09, France ;

<sup>2</sup> Université du sud Toulon-Var (MIO), 83957, La Garde cedex, France ; CNRS/INSU, MIO UMR 7294 ; IRD, MIO UMR 235.

\* Corresponding author: [severine.martini@univ-amu.fr](mailto:severine.martini@univ-amu.fr)

**Abstract**

The ANTARES station is indirectly used as an observatory for the bioluminescence record in the deep (2,000 m depth) North-western Mediterranean Sea. In this study we describe the prokaryotic community, at the deep ANTARES site, over one-year survey in 2011. Relatively stable prokaryotic abundance and diversity have been recorded during the year with the detection of *Chloroflexi* and *Proteobacteria* as the most active members. Conjointly to these data, environmental conditions are characterized using water samplings (temperature, salinity, nutrients, dissolved organic carbon and oxygen). During this survey, no hydrological particularities affecting the ANTARES station have been observed with minor variability in temperature, salinity, nutrients, dissolved organic carbon and oxygen. Then, the final objective was to focus on bioluminescent-bacterial variability over the year and during a low bioluminescence event, recorded in the deep sea. Using the *luxF* gene, about 0.1 to 1% of bioluminescent bacteria have been detected in the sampling period. These bacteria were mainly belonging to *Photobacterium* genus. Moreover, bioluminescent bacteria have been found to be mainly active cells even during a low bioluminescence event.

## Introduction

Bioluminescence is the production of light by organisms as a result of a chemical reaction. In the ocean, this process is the primary source of light (Haddock et al., 2010). Bioluminescent organisms are spread within 14 phyla (Widder, 2002) covering eukaryotic and prokaryotic domains. Within evolution, the distribution of bioluminescence ability does not appear to follow any obvious phylogenetic distribution. In the mesopelagic zone, from 500 to 1,000 m, Herring (2002) estimate that 90% of deep-sea fish, 65% of decapods, 20-30% of copepods as well as ostracods are bioluminescent. This wide variety and abundance of species using bioluminescence as well as the pattern of light emission, decreasing with depth, have lead to the assumption that bioluminescence-activity records could be used as a relative proxy of the marine-organisms abundance (Moline et al., 2009; Tokarev et al., 1999).

In the literature, the *in-situ* bioluminescence emission is mainly attributed to eukaryotic organisms such as dinoflagellates (Cussatlegras and Le Gal, 2005; Widder, 2010), or zooplankton (Craig et al., 2010). Correlations have been shown, above 1,000 m depth, between the concentration of chlorophyll-*a* (Craig et al., 2010; Lapota et al., 1989) or dinoflagellates (Piontkovski et al., 2003) and the bioluminescence emission (Haddock et al., 2010). Some studies assert that bioluminescence intensity reflects zooplankton abundance. In Craig et al. (2010), this relation was not supported below 1,000 m depth suggesting the possible implication of other organisms. Bioluminescent bacteria could explain part of this signal during special events of deep convection as suggested by Tamburini et al. (2013). However, bioluminescence from bacteria does not respond to mechanical stimulation. In most studies, bioluminescence is estimated by bathyphotometers using mechanical stimulation of bioluminescent eukaryotic organisms (Cussatlegras and Le Gal, 2007). Consequently, the use of only bathyphotometers does not permit to detect bacterial bioluminescence. This technical approach probably leads to an underestimation of bacterial contribution to the bioluminescence activity.

Dark ocean represents about 95% of the oceans and accounts for 55% of all prokaryotes

(Archaea and Bacteria) found in aquatic habitats (Whitman et al., 1998; Aristegui et al., 2009; Carlson et al., 2010). Within the biological pump process, these organisms contributes to the carbon cycle by being active in the remineralization of organic matter in the deep sea (Aristegui et al., 2009; Nagata et al., 2010; Cho and Azam, 1988) and by feeding back nutrients and dissolved inorganic carbon by respiration. Amongst these deep-sea prokaryotes, bioluminescent bacteria attached to particles are known to play a role in the degradation of particulate carbon. However their *in situ* importance is still unclear (Zarubin et al., 2012). Described bioluminescent bacteria belong, so far, to the Gammaproteobacteria subclass and are affiliated to *Vibrio*, *Photobacterium* and *Shewanella* genera (Kita-Tsukamoto et al., 2006). Bioluminescence activity is driven by the product of the *luxICDABFEG* genes belonging to one operon. For a cellular concentration, estimated at about  $10^7$  to  $10^8$  cells in liquid culture, bioluminescent genes are activated by quorum-sensing phenomenon (Nealson et al., 1970; Eberhard and Hastings, 1972). Such high cellular concentration can be reached in symbiotic association, and most probably for bacteria attached to sinking particles or "marine snow" (Azam, 1998; Alldredge and Cohen, 1987). At the surface, bioluminescent bacteria have frequently been recorded. They can be responsible for large and intense emission of bioluminescence referred as "milky sea" (Miller et al., 2005, 2006). Bacterial bioluminescence has been intensively studied from punctual *in-situ* samplings (Malave-Orengo et al., 2010) or from experiments at laboratory (Hastings, 1983). However, only few studies have dealt with *in-situ* temporal dynamic of such bacteria, due to time-consuming and expensive reasons (Ruby and Nealson, 1978; Yetinson and Shilo, 1979; Orndorff and Colwell, 1980). Within these few studies, seasonal changes in bioluminescent bacteria have been recorded in surface layers and a correlation between *Vibrio harveyi* and the surface temperature has been demonstrated (Ruby and Nealson, 1978). Yetinson and Shilo (1979) and Orndorff and Colwell (1980) also investigate, over time, links between bioluminescent bacterial strains and environmental variables at the surface, such as salinity or temperature. In the deep layer of the ocean (below 1,000 m depth), less information on the *in-situ* bioluminescence and presence of organisms is available due to technical constraints. Gentile et al. (2009) recorded bioluminescent bacteria in the deep Mediterranean Sea (Thyrrenian Sea), based on the *luxA*-gene detection from environmental DNA. These

authors found unexpected high number of *luxA* lineages mainly belonging to the *Photobacterium* cluster. Furthermore, at the deep Mediterranean ANTARES site (2,000 m depth), Tamburini et al. (2013) proposed bioluminescent bacteria to be the main contributors to the intense bioluminescence activity recorded during periods of deep convection occurring in the Gulf of Lion. The presence, at this station, of bioluminescent bacterial strain (*Photobacterium phosphoreum* ANT-2200), isolated during a previous event of deep convection and high bioluminescence activity, also supports this hypothesis (Al Ali et al., 2010; Martini et al., 2013a).

The recent development of neutrino underwater telescope (Amram et al., 2000) gives access to long time series luminescent records in real time. Such structures use photomultiplier tubes (PMTs) as photon detector for high-energy particles. This instrumentation is used by oceanographers as a bioluminescence sensor (Tamburini et al., 2013; Craig et al., 2010) with no direct mechanical stimulation (excepted from current speed), compared to bathyphotometers. In this study, we use the ANTARES neutrino telescope, in the North-western Mediterranean Sea, as one of those observatory possibly able to detect no only bioluminescence emissions from eukaryotes but also from bacteria. A one-year water sampling conjointly to that continuous luminescence record, at 2,000 m depth, were used (1) to analyze the composition of the global prokaryotic community at this site on qualitative, quantitative, activity aspects based on ribosomal information, (2) to investigate the bioluminescent bacterial counterpart using *lux* genes, (3) and to estimate possible links between *in-situ* bioluminescence activity and bioluminescent bacteria.

## Methods

### Site location and continuous record of deep bioluminescence

The ANTARES project (Astronomy with a Neutrino Telescope and Abyss environmental RESearch) developed, since the end of 2007, a deep-sea cabled observatory, in the North western Mediterranean Sea. The ANTARES site is located 40 km off the French Mediterranean coast (42°48'N, 6°10'E) at 2,475 m depth. At first, this site was dedicated to

the search of high energy particles such as neutrino (Amram et al., 2000), (Aguilar et al., 2007). About 885 PMTs are located between 2,000 and 2,400 m depth for the purpose of particle Physics. All the 12 ANTARES mooring lines are connected, via an electro-optical cable to a shore station providing real-time acquisition. These PMTs sample photons emission at high frequency (0.013 s), and are connected to the ANTARES-transmission cable, delivering real-time data. The bioluminescence activity analyzed in this study is the mean rate of PMTs recorded at the ANTARES telescope, at 2,000 m depth, and sampled on a 7-days period around the sampling day (period from  $n - 3$  to  $n + 3$  with  $n$  the water-sampling day). Current speed has been sampled using an Accoustic Doppler Current Profile 300 kHz RDInstruments.

### Sample collection and on-field processing

The monitoring strategy for the biogeochemical sampling has been established in the framework of the MOOSE and CASCADE programs. The ANTARES site has been visited in January, March, May, June, August and October 2011. A 12-Niskin-bottle rosette of 8 L was used to sample water at 2,000 m depth. These water samplings give access to: potential temperature, salinity, Dissolved Organic Carbon (DOC), nitrates ( $\text{NO}_3^-$ ), phosphates ( $\text{PO}_4^{3-}$ ), silicates ( $\text{Si(OH)}_4$ ), and dissolved oxygen ( $\text{O}_2$ ).

Potential temperature and salinity have been sampled from a CTD probe SBE 9+. The dissolved oxygen has been recorded using an oxygen sensor SBE 43 cross-calibrated by oxygen Winkler measurements (Gaarder and Gran, 1927; Bryan et al., 1976; Williams, 1981).

DOC content was determined using a Shimadzu model TOC-V Total Carbon Analyzer with a quartz combustion column filled with 1.2% Pt on silica pillows. Standardization of the instrument was performed daily using Milli-Q water as blank and potassium hydrogen phthalate diluted in Milli-Q water (range 0-125 mM) prepared just before sample analysis as a standard (Sohrin and Sempéré, 2005). The running blank injected in triplicate after every 4 samples corresponding to the peak area of the Milli-Q water acidified with

$\text{H}_3\text{PO}_4$ . The DOC concentration was determined from 3 to 4 independent analyzes after subtracting the running blank. Low-carbon water (LCW) and deep-seawater reference (DSR) were kindly provided by the Bermuda Biological Station and were measured daily to monitor the accuracy and the stability of the TOC analysis. The nominal analytic precision of the analysis procedure was within 2%.

The water samples, for  $\text{NO}_3^-$ ,  $\text{PO}_4^{3-}$ ,  $\text{Si}(\text{OH})_4$  determinations, were collected with Niskin bottles and preserved at -20°C until analysis, according to Aminot and Kérouel (2004, 2007). Nutrient concentrations were determined colorimetrically with an automated method, using a semi automatic Technicon Autonanalyser II (detection limit=0.05  $\mu\text{moles L}^{-1}$ ), according to Treguer and Le Corre (1975).

For DNA and RNA analyzes, between 6 and 17 L have been gently filtered, using a peristaltic pump, on autoclaved 0.22  $\mu\text{m}$  GPWP 47 mm filters (Millipore<sup>®</sup>). For RNA analyzes, filtration time was limited to 15 min resulting in a filtered volume from 0.4 to 1.6 L. All filters were stored with 1 mL of RNAlater (Sigma-aldrich<sup>®</sup>) into liquid nitrogen directly after filtration.

### DNA and RNA extraction

DNA was extracted from filters using ultra clean water DNA kit (MO BIO<sup>®</sup>, CA) according to the manufacturer's instructions. The DNA was stored at -20°C. Total RNA was extracted from 0.4 to 1.6 L of water collected by gentle filtration on 0.22  $\mu\text{m}$  filter using RNeasy minikit (Qiagen, Germany). Putative traces of DNA were removed by the Turbo DNase-free digestion (AMBION<sup>®</sup>, Austin, Texas). The RNA was stored at -80°C. Synthesis of cDNA was performed from about 50 ng of RNA using GOscript reverse transcriptase (Promega) and reverse primer of PCR for bacterial (907R) or archaeal (915R or 1100R) SSU RNA and *luxF* gene (*luxF* 572R).

### Screening and quantification of communities

The quantification of bacterial, archaeal 16S rRNA and 16S rDNA gene and *luxF* gene and mRNA copy numbers were determined by qPCR with Sso Advanced<sup>TM</sup> SyberGreen Supermix using a CFX96 Real Time System (C1000 Thermal Cycler, Bio-Rad Laboratories, CA, USA) with a calibration curve using a plasmid harboring corresponding gene fragment. For bacterial 16S rRNA, quantification was performed with primer sets (GML5F-Uni516R) (Takai and Horikoshi, 2000; Michotey et al., 2012). Archaeal 16S rRNA gene and cDNA were quantified with two sets of primer: 1100R-931f (Einen et al., 2008) and 300-516 (Michotey et al., 2012).

For bioluminescent bacteria, different candidate genes were tested (*luxA*, *luxG*, *luxF*). From the literature, *luxA* codes for two sub-units of the bacterial luciferase. The *luxG* codes for a protein close to the flavin reductase enzym. As far as we know, the *luxF* function has not been precisely determined ; However, it is detected in all mesopelagic and bathypelagic species, known so far, suggesting a major role for deep bioluminescent species (Meighen, 1993).

Three sets of degenerated primers for amplifying *luxA*, *luxF* and *luxG* genes were designed by aligning sequences available in the databases. Eight sequences from marine bacteria were used for *luxF* (AY849520, AY849502, AB367391, AY849504, DQ988874, AY849485, AY341064 and DQ790856). Eight sequences were used for *luxG* (AB261992, AY341064, AY849485, DQ988874, AY849502, AB367391, AY849504 and AY849486). Twelve sequences were used for *luxA* (KC332289, X58791, AB058949, AY456753, AY341064, DQ988874, AY849504, AY345887, AY849502, AY849520). The primers were chosen according to various characteristics: optimum size for PCR product between 150 and 200 bp (range 75-250 bp), 25 bp primers (range 20-30 bp), optimal  $T_m$  at 60°C (range 57-63°C), GC% between 30 and 70% and no more than 3 identical consecutive nucleotides.

Classical PCR gave better results on *Photobacterium phosphoreum* DNA and on environmental DNA with primer sets amplifying *luxF* (*luxF*-385F ATGTTACATGTCAATG-

TYAATGAGG, *luxF*-527R AATTACCAGCAAGATTGCTACAT) or *luxG* (*luxG*-179F AGTTACATGTTGGAGTTCGGTAAA, *luxG*-349R ATAACCCTGTACCTCCAG-CIATAAG) compared to *luxA* (*luxA*-598F AARAAAGCICARATGGAACTITATAATG, *luxA*-784R TATTGGTNGCATTIACGTAIGAITC), in consequence these primers were kept for qPCR tests. As qPCR parameters were much better for *luxF* than *luxG* (threshold templates number corresponding to 40 versus 4750, PCR efficiency corresponding to 101% versus 61%), *luxF* was chosen to detect bioluminescent bacteria. The program consists of a denaturing step of 10 s, an hybridization step of 10 s at 57.3°C, with an elongation step of 10 s. At the end of the PCR reaction, the specificity of the amplification was checked from the first derivative of their melting curves and by electrophoresis analysis.

### Molecular fingerprinting analysis of microbial community

Denaturing Gradient Gel Electrophoresis (DGGE) analysis was used to screen samples prior to barcoding experiment. Ribosomal fragment were amplified using the GML5F 907MR primer set for Bacteria (Bonin et al., 2002; Goregues et al., 2005) and 344f 915R primer-set for Archaea (Casamayor et al., 2002). To improve resolution of DGGE analyzes, primers GML5F-GC or 344f-GC contained a 40-nucleotide GC-rich sequence at the 5' end. PCR amplifications were carried out in 20  $\mu$ L reaction mixtures containing 1-2 ng of template DNA, 1.5 mM MgCl<sub>2</sub>, 0.2 mM of dNTP, 1.25 or 0.31  $\mu$ M of each primer for Bacteria and Archaea respectively, and 1 U of Hot start polymerase plus 1  $\mu$ L of solution Q (Qiagen, Germany). The thermal cycling programs were similar to those previously described (Casamayor et al., 2002; Michotey et al., 2012). DGGE was performed using a D-code Universal Mutation Detection System (Bio-Rad Laboratories Inc.). Equal amounts of PCR products were loaded in each lane (~300 ng SSU rRNA gene fragment). The 1 mm thick, 6% (wt. /vol) polyacrylamide gels presented a denaturing gradient of 30%-50% for SSU rRNA gene fragment analysis.

Pyrosequencing of bacterial cDNA ribosomal gene of May and October samples were performed on fragment generated with the 16S universal Eubacterial primers (bact 343F,

bact 806R) by MR DNA (Texas, USA). A single-step PCR using HotStarTaq Plus Master Mix Kit (Qiagen, Valencia, CA) were used under the following conditions: 94°C for 3 minutes, followed by 28 cycles of 94°C for 30 seconds ; 53°C for 40 seconds and 72°C for 1 minute ; after which a final elongation step at 72°C for 5 minutes was performed. Following PCR, amplicon products were purified using Agencourt Ampure beads (Agencourt Bioscience Corporation, MA, USA). Samples were sequenced utilizing Roche 454 FLX titanium instruments and reagents according to manufacturer's instructions. Sequence data derived from the sequencing process were processed using a proprietary analysis pipeline ([www.mrdnalab.com](http://www.mrdnalab.com), MR DNA, Shallowater, TX). Sequences were depleted of barcodes and primers. Short sequences < 200 bp sequences with ambiguous base calls, and sequences with homopolymer runs exceeding 6 bp were removed. Subsequently a denoising step and chimeras check were performed. Operational Taxonomic Units (OTU) were defined after removal of singleton sequences, clustering at 3% divergence (97% similarity) (Dowd et al., 2008a,b; Edgar, 2010; Capone et al., 2011; Dowd et al., 2011; Eren et al., 2011; Swanson et al., 2010). OTUs were then taxonomically classified using BLASTn against a curated GreenGenes database (De Santis et al., 2006) and ambiguous affiliations on species level were checked manually and compared with environmental clones.

## Results and discussion

### Environmental conditions at the ANTARES station

During the year 2011, potential temperature, salinity, Dissolved Organic Carbon (DOC),  $\text{NO}_3^-$ ,  $\text{Si}(\text{OH})_4$ , and oxygen concentrations have been sampled over vertical profiles, using discrete water sampling, at the ANTARES station (see Figure 5.2). Continuous profiles have been represented, over the water depth, for each variable and smoothed, using a local polynomial regression (loess method Cleveland and Grosse 1991) based on dataset (Figure 5.2). Then, the annual mean values at 2,000 m depth are summarized (Table 5.1). Only low variations are detected over the water column, as well as at 2,000 m depth

suggesting a stability of environmental conditions. In comparison with other bathypelagic regions already studied in the literature (Nagata et al., 2010), the deep-sea waters at the ANTARES station (NW Mediterranean Sea) present higher temperature (12,896 / 0.4-5.4), lower nitrate (8.1 / 16-43), phosphate (0.35 / 1-3.2) and silicate concentrations (8.1 / 10-177). The recorded values at the ANTARES station are in the range of already observed ones in the deep Mediterranean Sea (Santinelli et al., 2010; Hansell and Carlson, 2001; Hansell et al., 2009).

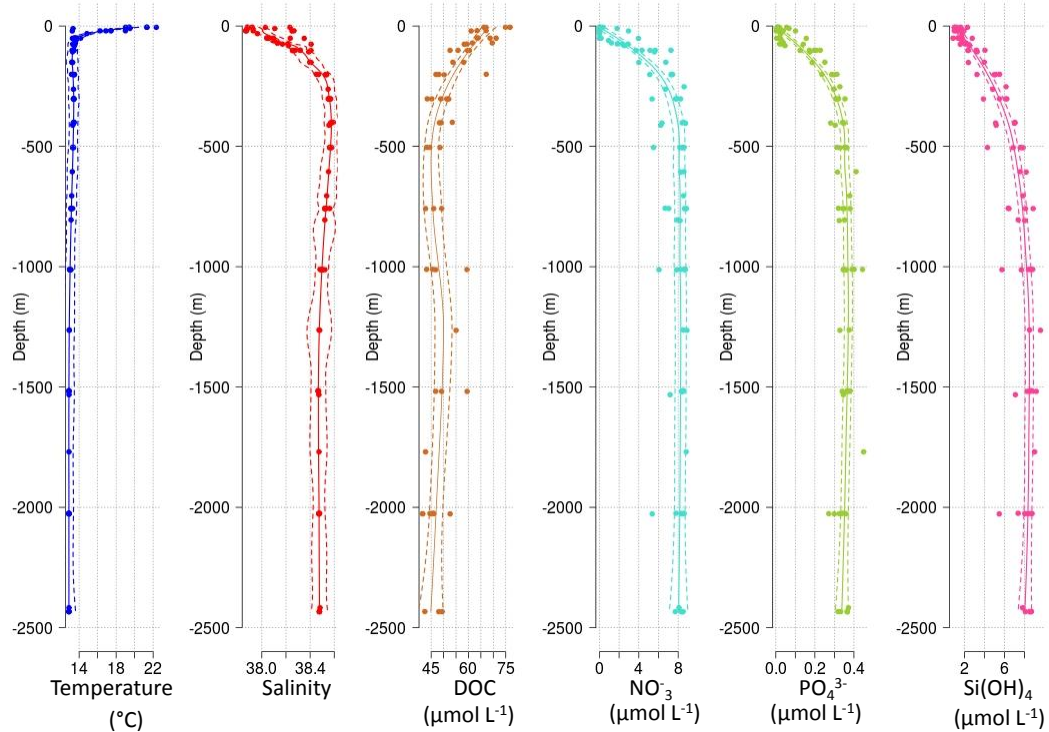


FIGURE (5.2) Vertical profiles for temperature, salinity, DOC,  $\text{NO}_3^-$ ,  $\text{PO}_4^{3-}$ , and  $\text{Si(OH)}_4$  using water sampling. Dots are samples values from the 6 sampling times, continuous lines are the profile using a local polynomial regression (loess method Cleveland and Grosse 1991) and dotted lines are the standard error for each profile.

The Mediterranean Sea has long been described as a low nutrient concentration basin. Measurements of C:N:P ratios are useful to describe the functioning of the ecosystem and the 105:16:15:1 Redfield ratios proposed in the North-Atlantic for C:N:Si:P are still used as a reference (Redfield, 1963; Sterner et al., 2008; Arrigo, 2004) to examine these changes

TABLE (5.1) Average and standard deviation for the main environmental variables over the year 2011, sampled at 2,000 m depth. T = potential temperature. S = salinity. DOC = Dissolved Organic Carbon.

T (°C)	S -	DOC ( $\mu\text{mol L}^{-1}$ )	$\text{NO}_3^-$ ( $\mu\text{mol L}^{-1}$ )	$\text{PO}_4^{3-}$ ( $\mu\text{mol L}^{-1}$ )	$\text{Si(OH)}_4$ ( $\mu\text{mol L}^{-1}$ )	Oxygen ( $\text{mol kg}^{-1}$ )
12.896 (0.003)	38.474 (0.003)	49.2 (4.8)	8.1 (0.7)	0.35 (0.03)	8.1 (0.7)	202.5 (3.1)

in nutrient limitation. During this survey, at the ANTARES station, the N:P ratio varies between 21.6 and 26.6 and the Si:N ratio is stable between 0.9 and 1 (see Table 5.1). The deep Western Mediterranean basin (under 1,000 m depth) is characterized by nutrient ratios different from the Redfield ratio and are estimated at about N:P~20 and Si:N≤1.0 (Santinelli et al., 2010; Moutin and Raimbault, 2002).

CTD profiles, for both temperature and salinity, give information on water-masses modifications. Using these set of data, a Theta-S diagram (Figure 5.3) allows to identify hydrological changes for the different sampling times, below 1,200 m depth (and until 2,400 m depth). This representation highlights relatively stable water masses with however an intense hydrological event in March (pink dots) due to incursions of water masses from the surface and spreading to the ANTARES site (De Madron, pers. com.). However, these modifications of water characteristics returned to the previous stable state in May (orange dots). Water depth sampled for microbiological studies (2,000 m depth) were highlighted using bigger dots in Figure 5.3. This shows that the water masses modifications clearly occur above 2,000 m, i.e above our sampling depth and above the ANTARES telescope, with no impact on the ANTARES telescope.

Consequently, during this survey, environmental conditions at the deep ANTARES station can be defined as relatively stable in nutrients, and without water mass input.

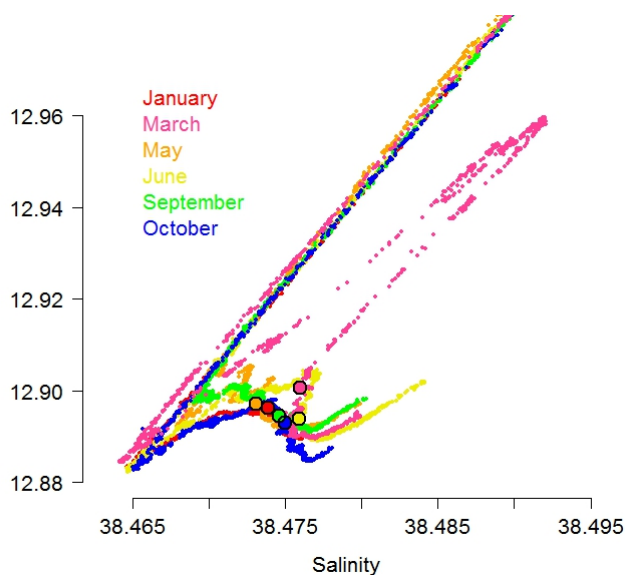


FIGURE (5.3) Potential temperature versus salinity diagram of CTD time series at the ANTARES site in January, March, May, June, September, and October 2011. Data shown are above 1,200 m. Colored dots represent data point sampled at 2,000 m depth. Changes in water masses occur at depth below 2,000 m with a come back to the stable state in May 2011.

## Annual dynamic of the prokaryotic community in the deep Mediterranean Sea

The prokaryotic community was analyzed during this one-year-survey through ribosomal information (Figure 5.4 A and B).

Archaeal 16S rDNA appeared not to be abundant ranging from  $0.4 \times 10^2$  to  $4.7 \times 10^2$  genes  $\text{mL}^{-1}$  (Figure 5.4 A). To investigate the possibility of underestimation due to primers selectivity, another primer set (primer 931F-1100R) was used for qPCR quantification. Results obtained with the second primer set were in good accordance with the previous one (see Table 5.2) and confirmed the low values obtained. These values are extremely low for deep-sea environment. Indeed, it has been previously observed that Archaea were nearly as abundant as Bacteria in meso- and bathypelagic systems (Church et al., 2003; Herndl et al., 2005; Karner et al., 2001; Tamburini et al., 2009; Teira et al., 2006) with about  $10^4$  cells  $\text{mL}^{-1}$ . At the ANTARES station, in April 2005, Al Ali et al. (2010) refer to values of about  $5 \times 10^4$  cells  $\text{mL}^{-1}$  and about 40% of DAPI counts belonging

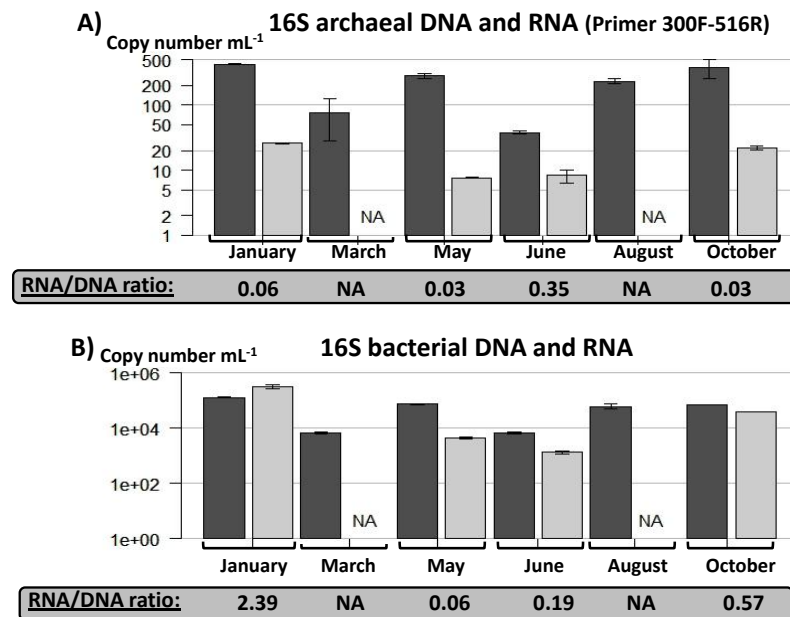


FIGURE (5.4) Quantitative estimation of A) 16S archaeal DNA (black bars) and RNA (grey bars) B) 16S bacterial DNA (black bars) and RNA (grey bars) among the year 2011, at the ANTARES station (2,000 m depth). NA: no sampling for RNA.

to Archaea detected by CARD-FISH method. At this stage, an underestimation due to cell lysis problem could not be excluded. However, methodological differences between CARD-FISH method and qPCR are noticed and can possibly modify the archaeal detection between those methods. Then, the activity of this community was estimated by 16S rRNA abundance. A weak activity with very few archaeal 16S rRNA was detected and rRNA/rDNA ratios ranging from 0.03 to 0.35 corresponding to October and June respectively (Figure 5.4 A).

Abundance of bacterial 16S rDNA was higher than archaeal counterpart and varied from  $0.7 \times 10^4$  to  $13.3 \times 10^4$  genes mL<sup>-1</sup> (Figure 5.4 B and Table 5.2). These results for bacterial 16S rDNA quantification are in good accordance with previous data obtained using FISH method at this station (Al Ali et al., 2010 and see references above). As for Archaea, the bacterial activity was estimated by 16S rRNA abundance. Bacteria appeared more active than Archaea although overall rRNA/rDNA ratios were not very high ranging from 0.06 to 2.39 in May and January respectively (Figure 5.4).

TABLE (5.2) Values of molecular analysis survey in 2011 at the ANTARES station for both Archaea and Bacteria. ND: Not Determined.

		January	March	May	June	August	October
<b>Bacterial 16S rDNA</b>	13.35 gene mL <sup>-1</sup> × 10 <sup>4</sup>	0.69 (± 0.31)	7.53 (± 0.05)	0.68 (± 0.24)	6.24 (± 0.03)	7.06 (± 1.34)	7.06 (± 0.08)
<b>Archaeal 16S rDNA</b>	4.25 gene mL <sup>-1</sup> × 10 <sup>2</sup> (Primer 300F-516R)	0.76 (± 0.06)	2.81 (± 0.48)	0.38 (± 0.20)	2.34 (± 0.02)	3.78 (± 0.20)	3.78 (± 1.23)
<b>Archaeal 16S rDNA</b>	4.72 gene mL <sup>-1</sup> × 10 <sup>2</sup> (Primer 931F-1100R)	0.77 (± 0.29)	2.42 (± 0.19)	0.28 (± 0.16)	2.90 (± 0.01)	2.73 (± 0.1)	2.73 (± 0.49)
<b>Bacterial 16S rRNA</b>	31.95 gene mL <sup>-1</sup> × 10 <sup>4</sup>	ND (± 5.40)	0.46 ND (± 0.04)	0.13 (± 0.01)	ND ND (± 0.01)	4.00 ND (± 0.07)	4.00 (± 0.07)
<b>Archaeal 16S rRNA</b>	0.258 gene mL <sup>-1</sup> × 10 <sup>2</sup>	ND (± 0.005)	0.093 ND (± 0.002)	0.134 (± 0.018)	ND ND (± 0.018)	0.104 ND (± 0.018)	0.104 (± 0.018)
<b>Lux DNA</b>	1.4 gene mL <sup>-1</sup> × 10 <sup>2</sup>	2.6 (± 0.2)	1.8 (± 2.9)	5.0 (± 1.2)	7.2 (± 2.2)	72.0 (± 7.7)	72.0 (± 5.3)
<b>Lux mRNA</b>	5.5 gene mL <sup>-1</sup> × 10 <sup>-2</sup>	ND (± 0.1)	7.7 ND (± 0.1)	7.0 (± 0.3)	ND ND (± 7.0)	15.4 ND (± 7.0)	15.4 (± 7.0)

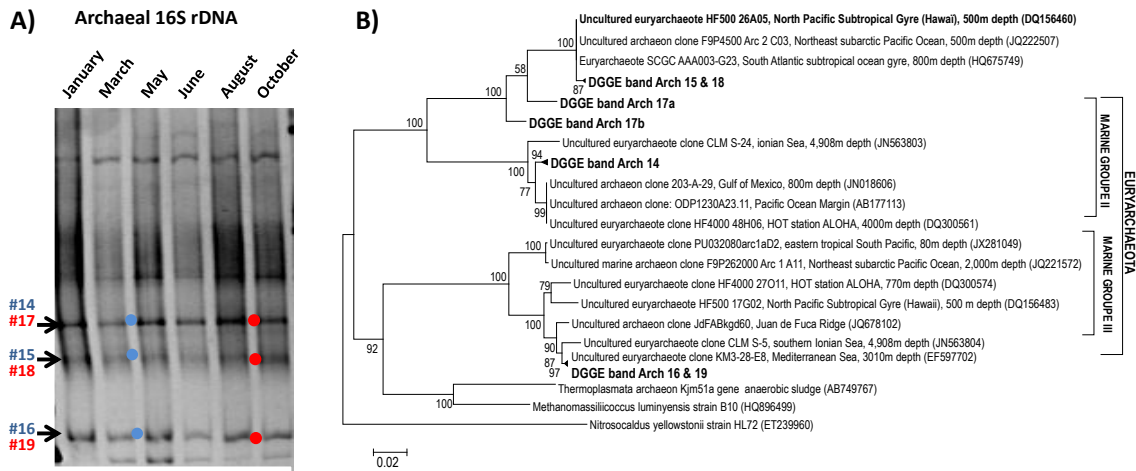


FIGURE (5.5) A) Denaturing Gradient Gel Electrophoresis (DGGE) analysis estimation of 16S archaeal rDNA among the year 2011, at the ANTARES station. Blue dot (# 14) represents the sampled band in May and red dot (# 17) the sampled band in October. # 16, # 19 and # 15, # 18 are similar sequences sampled into two different DGGE bands. B) Phylogenetic tree of the archaeal 16S rDNA gene sequence from the clones from DGGE bands. Values at nodes represent bootstrap value using neighbor joining. Scale bar denotes 0.02 substitution per nucleotide position.

The diversity of total and active prokaryotes has been firstly analyzed by DGGE. Archaeal 16s rDNA DGGE profiles present similar patterns over the year 2011 (Figure 5.5). Five clear bands are visible on the gel and sequences from the 3 most intense ones were obtained. These organisms are affiliated to the Euryarchaeota phylum in marine groups 2 and 3 cluster (Figure 5.5 B). The low quantity of archaeal 16S rRNA does not allow enough PCR material to analyze active archaeal community using DGGE.

DGGE profiles of bacterial 16S rDNA show a major band (# S1) at all sampling periods (Figure 5.6 A), surrounded by numerous other fainter bands. The sequence of this intense band fell within *Chloroflexi* phylum (Figure 5.7), and is closely related to *Chloroflexi bacterium* SCGC AAA240-O15, belonging to SAR 202 group, retrieved at 770 m depth at the HOT ALOHA station, subtropical ocean gyre (99% similarity, HQ975645, Swan et al., 2011). *Chloroflexi bacterium* was also observed over the water column, between 200 and 4,000 m at the ALOHA station (DeLong et al., 2006) and in other mesopelagic and bathypelagic areas of various oceans (Nagata et al., 2010). Moreover, concentration of this phylum has been observed to increase over the water

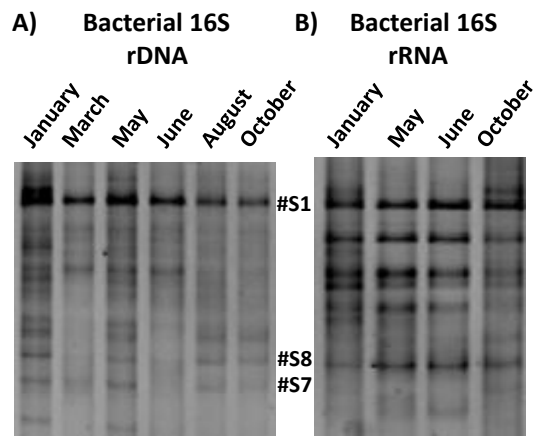


FIGURE (5.6) Denaturing Gradient Gel Electrophoresis (DGGE) analysis estimation of A) 16S bacterial rDNA and B) 16S bacterial rRNA among the year 2011, at the ANTARES station. No sampling for 16S rRNA have been performed in March and June.

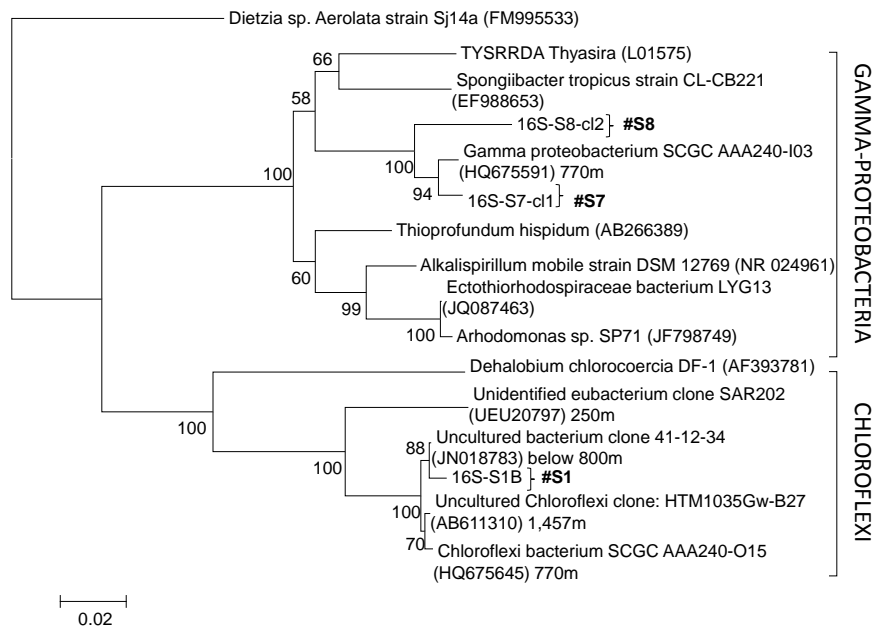


FIGURE (5.7) Phylogenetic tree of the bacterial 16S rDNA gene sequence from the clones DGGE bands. Values at nodes represent bootstrap values using neighbor joining. Scale bar denotes 0.02 substitution per nucleotide position.

column (mainly for SAR202, Varela et al., 2008). Since qPCR results indicate that most of the cells are inactive, the diversity of the active members was investigated firstly by DGGE on RT-PCR fragment (see Figure 5.6 B). About 8 intense bands are

visible with similar patterns for January, May and June samples, and slightly different for October sample presenting less contrasted bands. The most intense band (# S1) previously observed on DNA profiles also appear on all RT-RNA counterparts. This observation suggests a highly active strain in abundance all year round. Other active members visible although the corresponding bands on DNA DGGE gel show relatively lower intensity, such as # S7 and # S8 (identified as Gammaproteobacteria). In order to further investigate the diversity of active member, pyrosequencing was performed on cDNA of 16S rRNA of May and October samples, presenting different DGGE patterns.

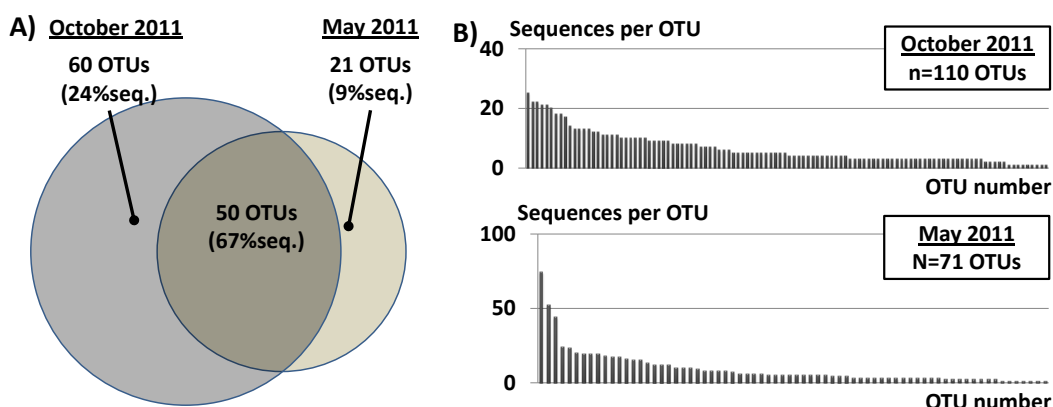


FIGURE (5.8) A) Venn diagram representation of total number of OTUs in October (110 OTUs) and in May (71 OTUs) and OTUs shared in between. About 50 OTUs (67% of sequences) are shared between those two samples. The Venn diagram depicts the percentage of present sequences. B) Number of sequences per OTU for May and October samples showing a higher diversity for October than May with 3 major OTU in May sample.

For May and October samples 662 and 735 sequences were obtained respectively, spread in 133 OTUs with 3% divergence cutoff. Their lengths vary between 200 and 480 nucleotides but are mainly about 400 nucleotides long. October sample appear more diverse with 110 OTUs detected in contrast to 71 for May (Figure 5.8 A). In accordance with DGGE analysis, May sample presents structured active community with 3 OTUs of major abundance whereas for October, the abundance within OTU is less contrasted (Figure 5.8 B). Amongst both samples, 50 OTUs are shared accounting for 67% of all sequences (Figure 5.8 A). The affiliation of these OTUs showed that most of them belong to *Chloroflexi* and *Proteobacteria* with percentages reaching 58 and 33% for May and 37 and 46% for October, respectively (Figure 5.9). The *Chloroflexi* sequence identified

as major member on DGGE analysis is also found by pyrosequencing as one of the abundant OTU (data not shown). Beside these phyla, the lower abundant OTUs fell in *Bacteroides*, *Cyanobacteria*, *Synergistetes*, *Nitrospirare*, *Firmicutes*, *Planctomycetes*, *Actinobacteria* phyla, and candidate division ksb1 (Figure 5.9).

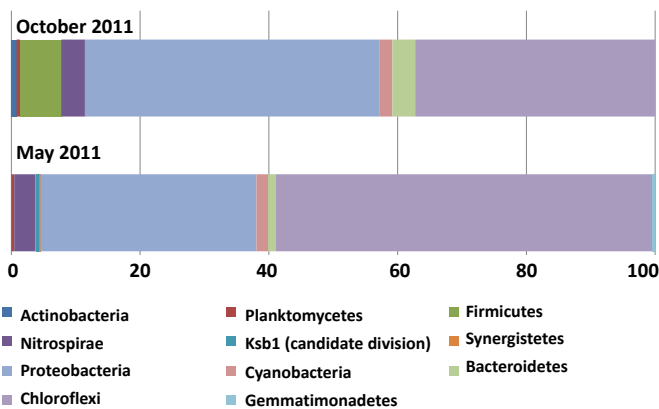


FIGURE (5.9) Diversity percentages representation among major phyla for October and May samples. *Chloroflexi* and *Proteobacteria* are the main contributors to the diversity at the ANTARES station for those two samples.

## Quantification and dynamic of bioluminescent bacteria in a deep environment

In parallel, current speed (Figure 5.10 A) and bioluminescence activity (Figure 5.10 B) were recorded continuously through the ANTARES telescope.

Relatively low bioluminescence activity (Figure 5.10 B) was observed in comparison to data previously monitored at that site (Tamburini et al., 2013). It is worth noting that, at sampling times, the recorded current speeds were low with values of about  $7 \text{ cm s}^{-1}$ . In consequence, bioluminescent eukaryotes that emit light under mechanical stimulation are not stimulated and their contribution to the signal is probably not an important part of the signal. This observation might make easier the determination of bacterial bioluminescence within the signal. During these periods of low bioluminescence and without extreme events of water-mass input, the abundance of bioluminescent bacteria

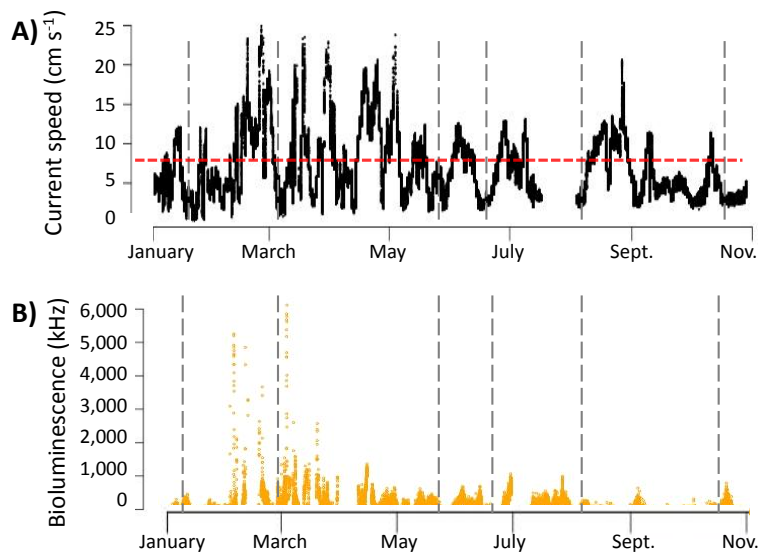


FIGURE (5.10) A) Current speed time series B) Bioluminescence time series recorded by photomultiplier tubes at the ANTARES station over the year 2011.

was investigated based on *lux* genes detection, to monitor bioluminescent bacteria. Indeed, from ribosomal analysis, no genera are known to harbor bioluminescent bacteria and that it is known from the literature that this character does not fit with phylogenetic affiliation (Haddock et al., 2010).

While most of the year, the abundance of *lux* gene attained around  $10^2$  genes mL<sup>-1</sup> (Table 5.2) it corresponds to 0.1-1% of the bacterial community (*lux* gene DNA/bacterial 16S rDNA ratio) most of the year. In October sample, *lux* genes concentration increased and reached  $7.2 \times 10^3$  genes mL<sup>-1</sup>. The activity of *lux* bacteria has been estimated by *lux* RNA quantification. Their concentrations were in the same range than that of the DNA counterpart (about  $10^2$  *lux* mRNA mL<sup>-1</sup>) showing the bioluminescence activity for some of them. Bioluminescent bacteria seemed more active than the overall bacterial community since *lux* RNA/DNA ratio (range 1.4 to 4.2) was higher than the 16S bacterial counterpart (0.06 to 2.39 range). *Lux* population did not follow similar trend as the overall bacterial community. The highest specific activity estimated by RNA/DNA ratio (ratio of 4.2) was observed in May (Figure 5.11) whereas it corresponds to January for 16S bacterial ratio (ratio value of 2.39), in Figure 5.4.

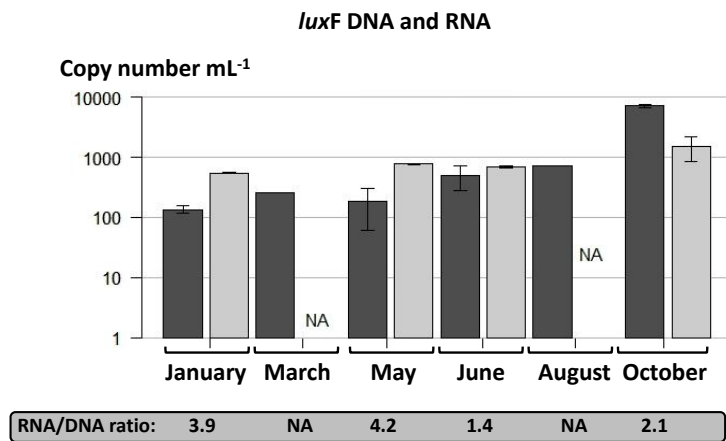


FIGURE (5.11) Quantitative estimation of *luxF* genes for bacterial DNA (black bars) and RNA (grey bars) among the year 2011, at the ANTARES station. NA: no sampling for RNA.

Despite the small size of the *lux* RT-qPCR fragment, sequences obtained in May and October, permit to affiliate the harboring organisms to *Photobacterium* genera since all sequences fell in *luxF* cluster including *P. phosphoreum*, *kishitanii* and *leiognathi* (Figure 5.12). Interestingly, this observation is similar to data reported in Gentile et al. (2009) in Tyrrhenian Sea, at 2,750 m depth and for which numerous *luxA* gene fell in *Photobacterium* cluster. Furthermore, a *Photobacterium* strain was also isolated at the ANTARES station (Al Ali et al., 2010).

Finally, we estimate, possible links between bioluminescent bacteria and bioluminescence total activity. In Figure 5.13, bioluminescence activity has been integrated over 7 days and active bioluminescent bacteria are described using a *luxmRNA* / bacterial rRNA ratio. Using data from PMTs, integrated during water sampling periods, bioluminescence activity is relatively low with only few variations over the year. Bioluminescence recorded in January and October are very close to background and higher values were observed for the other months (March, May, June and August). March and August samples correspond to highest values whereas no RNA data was available for these sample. Over

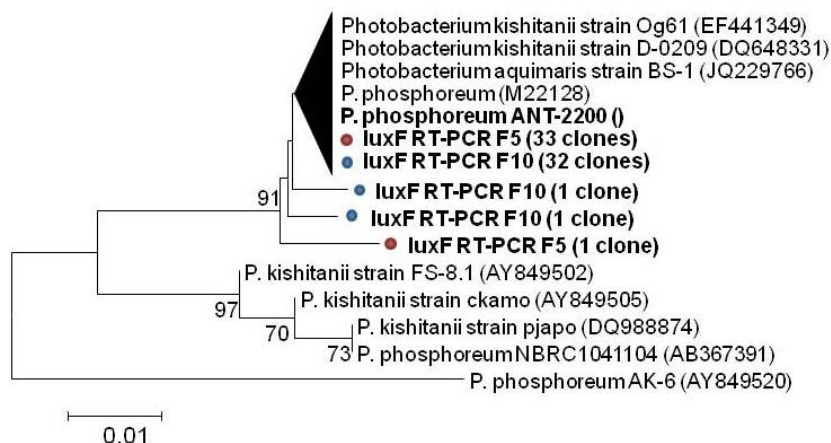


FIGURE (5.12) Phylogenetic tree of the *lux* genes sequence from the clones DGGE bands. Values at nodes represent bootstrap value using neighbor joining. Scale bar denotes 0.01 substitution per nucleotide position. Blue dots are selected band from May sample and blue ones are selected from October sample.

the 4 available samples *Lux* mRNA/bacterial 16S rRNA ratios ranged from  $0.2 \times 10^{-2}$  to  $53.8 \times 10^{-2}$ . The two highest ratios ( $16.7 \times 10^{-2}$  and  $53.8 \times 10^{-2}$ ) were obtained for May and June samples respectively. The lack of replicate due to technical reason did not allow to perform statistical tests. However, it should be noticed that similar trend is observed between bioluminescence activity and *lux* mRNA/bacterial 16S rRNA ratios.

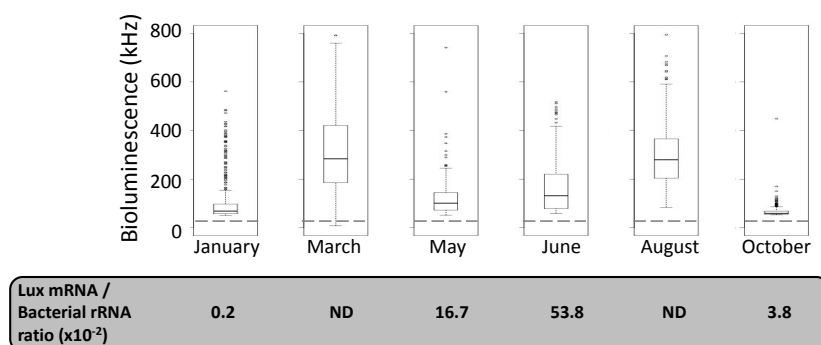


FIGURE (5.13) Box-and-whisker plot of bioluminescence 7 days around water sampling periods. The top and bottom of each box-plot represent 75% (upper quartile) and 25% (lower quartile) of all values, respectively. The horizontal line is the median. The ends of the whiskers represent the 10<sup>th</sup> and 90<sup>th</sup> percentiles. Outliers are represented by empty dots. The  $^{40}\text{K}$  baseline at about 40 kHz is represented as a dashed line. *Lux* mRNA/bacterial rRNA ratio are presented as part of active bioluminescent bacteria over the total active bacteria.

## Conclusion

The aim of this work is to describe total prokaryotic communities in the deep Mediterranean Sea, and to focus on bioluminescence activity conjointly to the detection of bioluminescent bacteria. During this survey, stable hydrological and physico-chemical conditions were observed with no input of water masses from the surface. In this context, prokaryotic community appeared relatively stable over the year. On a quantitative and qualitative aspect, *Chloroflexi* and *Proteobacteria* appeared as the most active members. In consequence, bioluminescence from eukaryotic organisms was limited due to the absence of mechanical stimulation and the identification of the bacterial part in light emission was probably easier to determine. Moreover, *luxF* genes and transcripts were detected all over the year demonstrating the presence and activity of bioluminescent bacteria affiliated to *Photobacterium* genus.

This study increases the interest to use similar approach during high bioluminescence activity events already detected in real-time by the ANTARES observatory in 2010 and 2009 ([Tamburini et al., 2013](#); [Martini et al., 2013a](#)). On the one hand, short sampling cruises should be managed during high bioluminescence events detection to compare both prokaryotic communities and bioluminescent bacteria quantification and activity. On the other hand, as continuous record of bioluminescence emission is already done by real-time data from the ANTARES cabled observatory. Automatic sampler for prokaryotic sampling might be an innovative tool to follow, understand and, at the end, predict extreme bioluminescence events in the deep sea.

## Acknowledgements

This work has been founded by the EC2CO-BIOLUX program. SM was granted a MENRT fellowship (Ministry of Education, Research and Technology, France). Authors thank N. Garcia, P. Raimbault for the nutrients analysis, B. Charrière for the DOC analysis, D. Lefèvre for the environmental data availability, S. Isart for her laboratory work, the crew of the N/O Thetys and the CASCADE-team. Authors thank the Collaboration of the ANTARES deep-sea observatory for providing time series data.

### 5.3 Conclusions

In Chapter 2 and 3, bioluminescence and new water masses events were related (see Tamburini et al., 2013; Martini et al., 2013b) in 2009 and 2010 impacting the deep ANTARES station. In this Chapter 5, we focused on year 2011. The CASCADE cruise occurs from 1<sup>st</sup> to 30<sup>th</sup> of March 2011 in the Gulf of Lion and sampling data from this expedition, show that no deep convection occurs below 1,600 m depth. This weak convection does not lead to deep water formations influencing bioluminescence activity at the ANTARES observatory (2,000 m) meaning that no links between water masses and bioluminescence activity can be highlighted during this period. This survey was an opportunity to describe the ANTARES site characteristics and the prokaryotic community over the year within stable hydrological conditions.

Between October 2010 and March 2013, the IL07 instrumented line has been turned off. The bioluminescence-activity data presented in this work have been extracted from one of the PMTs located in the whole observatory. Contrarily to the ones located on the IL07, during too high bioluminescence-intensity events, these PMTs are turned off. Such technical constraint induces gaps in time series record. However, these periods of high bioluminescence activity are shorter than those observed in 2009 and 2010 and does not occur during the sampled period.

The bioluminescence activity continuously recorded at the deep ANTARES station during this survey is relatively low and does not show high and long-time variation in bioluminescence activity in 2011, as previously observed by Tamburini et al. (2013) and Martini et al. (2013b). To conclude from this survey, without deep-sea convection or cascading phenomena, bioluminescent bacteria have been estimated at about 0.1 to 1% with high rate of active cells compared to total prokaryotes. Moreover, bioluminescent bacteria can not be excluded as a potential contributor of high level of bioluminescence activity already described in the deep sea. Sampling during high bioluminescence events are still

needed to describe the bacterial role during high bioluminescent activity detected at the ANTARES station. Thanks to the real time data acquisition on the ANTARES observatory, adapted water sampling must be adapted to reach that goal in further investigations.

As perspective work, from this Chapter 5, firstly, the *lux* genes analyzes might be improved. *LuxF* gene was the most efficient at laboratory and has been used to detect bioluminescent bacteria. The *luxF* function is identified for all meso and bathypelagic species involving a major role for deep-bioluminescent-species but with no clear identification. In further investigations, *LuxA* primers coding for two sub-units of the bacterial luciferase has been used however the results were not decisive to improve our results robustness.

Moreover, during this survey, seasonal spring bloom has been observed in March 2011, at the surface of the ANTARES station, using chlorophylle-a observations.

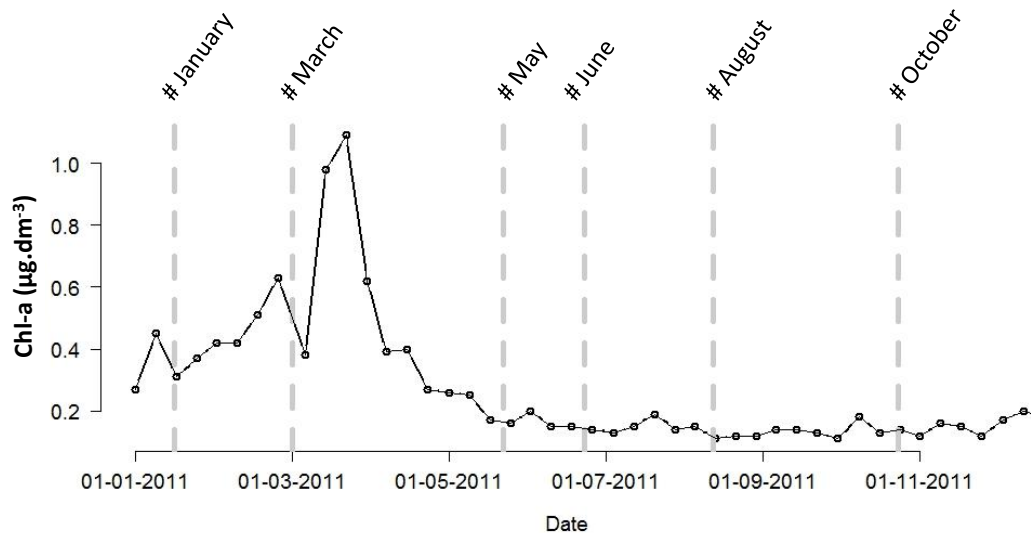


FIGURE (5.14) Chlorophyll-a time series recorded at the ANTARES station from satellite data, data acquisition in collaboration with F. D'Ortenzio. Grey bars represent the discrete water sampling.

Such bloom is already known to involve an increase in POC and DOC sinking to the deep sea. Indeed, it is known that 1 to 40% of the photosynthetically fixed carbon is exported

into the dark realm where it is remineralized (Ducklow et al., 2001) by prokaryotes. Such seasonal spring blooms could involve higher abundance of bioluminescent bacteria fueling the deep sea and, by the end, an increase in bioluminescence activity. Using a suitable sampling survey, this phenomenon has to be distinguished from newly formed deep water events. However, to reach such information, it is necessary to sample after the occurrence of such bloom, and at high frequency, DOC, POC as well as prokaryotic communities and bioluminescence activity.

# CHAPITRE 6

---

## Conclusions and Perspectives

---

### Sommaire

---

<b>6.1 Conclusions . . . . .</b>	<b>182</b>
6.1.1 Is bioluminescence a proxy ? . . . . .	182
6.1.2 Is bioluminescence linked to biological activity ? . . . . .	185
6.1.3 Does bioluminescence play a major role in the deep sea ? . . . . .	187
<b>6.2 Perspectives . . . . .</b>	<b>188</b>
6.2.1 Physiological parameters determination using bioreactor culture	189
6.2.2 Proposal for the detection of bioluminescent organisms . . . . .	193

---

## 6.1 Conclusions

The aim of this thesis was to investigate if bioluminescence can be defined as a proxy of biological activity in the deep sea. To reach this goal, we follow two main axes:

**(i) Bioluminescence is described as "weak" in the deep sea, compared to the ocean surface, but are there variations in light intensity over time and how to explain them ?**

**(ii) In the deep sea, what is the part of bacterial bioluminescence in the emission of light *in situ* ?**

The first axis has been mainly developed in Chapter 2 and 3, the second axis in Chapter 4 and 5. Moreover, in Chapter 1, (Introduction part) the interest of taking into account the different scales to defined processes has been highlighted. In this "Conclusions and Perspectives" section, results will be summarized, at various scales, into a more global view in order to answer to the general question.

### 6.1.1 Is bioluminescence a proxy ?

A proxy is an intermediate with the ability to mimic the behavior of something else. In this work, the bioluminescence was investigated as a proxy of biogeochemical processes, as well as a proxy of prokaryotic communities.

Photomultipliers have been used as detectors of 'natural' bioluminescence. In this work, the ability of such apparatus to record *in situ* duration and intensity of bioluminescence events, with continuous, automated, and high-frequency data, has been validated ([Tamburini et al., 2013](#)). Only few detectors dedicated to biological-variable recording exist, and such instrumentation is of importance to the global network of ocean observation. Moreover, the instrumented line, used at the ANTARES, station led to the conjoint record of physical variables, at high frequency and continuously. Discrete water

samplings have also been performed over one-year survey for both physical and biological descriptions.

At a regional scale, due to time dependence of those data, only one replicate (time series) is available to study those processes. Well-adapted methods were needed in order to analyze and interpret those multivariate time series. For such an aim, the Hilbert-Huang and wavelet methods have been used to interpret these time series. Our results demonstrated that the bioluminescence is, at all time and frequency, linked to current speed due to mechanical stimulation. Moreover, we highlighted that in peculiar conditions, the bioluminescence is strongly linked to changes in water-mass properties and this is mainly observed for the highest bioluminescence intensity. Such high bioluminescence events are mainly linked to current speed faster than  $19 \text{ cm s}^{-1}$ , temperature above  $12.92^\circ \text{C}$  and salinity higher than 38.479 and explained by deep convection flowing through the ANTARES observatory. During these events, water masses could carry to the site significant amounts of bioluminescent organisms and/or could fuel the deep sea with particulate and dissolved organic matters. These hydrological movements could induce, at the end, an increase in the bioluminescence activity. Moreover, those threshold values are of great interest for the prediction of events of high bioluminescence activity in the future. For astrophysicists, these results are also of interest to protect photomultipliers from too high light activity, that could damage these photon detectors. The survey of these water-mass changes requests a more global survey at the Mediterranean Sea level since the convection of newly formed water masses, described in the Gulf of Lion, will spread into the deep-sea and impact the ANTARES station few days later.

At a local scale, in Chapter 4, discrete water samplings have been performed every 2 months and over a one-year period in 2011, depending on the meteorological conditions. This sampling protocol was well adapted for the local description of the ANTARES site, as we observed only few variations in hydrological variables and prokaryotic communities. Moreover, the year 2011 was characterized by no deep convection reaching the seafloor (contrary to 2010) and represents a relatively "calm" period in term of bioluminescence activity, at the ANTARES station. Besides, during this survey, the

sampled bioluminescence (integrated over 7 days for discrete information) and the bacterial abundance were too limited discrete observations to be correlated and therefore to interpret bioluminescence as a proxy. To reach this information, there is a need of higher frequency or rather longer survey, including a sampling during newly formed deep sea waters, to evaluate the increase in bioluminescent bacteria. Indeed, longer survey describing variations in bioluminescence intensity, as well as in bacterial abundances, will give more reliability on a possible correlation.

Finally, bioluminescence has been efficiently used as a proxy at the regional scale for hydrological processes. However, to validate the use of bioluminescence as a proxy of bacterial abundance at a local scale, longer investigations are needed. Consequently to these results, the observation scale (local or regional) was strongly dependent on the process to be described (water masses and bacterial communities). So is the use of bioluminescence as a proxy.

The ANTARES station, at first, was dedicated to astrophysics. Therefore, environmental sciences only have a minor weight within the ANTARES collaboration which sometimes leads to go against scientific decisions for oceanographic goals and to the loss of the necessary continuity of time series. This is a major limit for recording long time series. For example, the IL07 instrumented line has been shut down in October 2010 and it was not possible to re-immerse it before March 2013. Another major constraint is the huge amount of stored data to be analyzed. For discrete water samplings, major limits are the meteorology uncertainties as well as the low frequency records. The development of automatic water sampling and filtration would be a great improvement for scientific community. As an example, the deep-ESP (deep Environmental Sample Processor), developed at the MBARI (Monterey Bay Research Aquarium), is dedicated to automatic samplings that permit water filtration at relatively high frequency into bathypelagic environment. Moreover, this automated molecular biology laboratory can detect microorganisms using their genetic material. Such device can transmit informations in real time. For *in situ* observatories, the sampling frequency of oceanic observations might be adapted, using real-time monitoring. This will lead to define oceanographic processes

acting at various observation scales and to limit the quantity of data stored.

### 6.1.2 Is bioluminescence linked to biological activity ?

Bioluminescence is a reaction produced by both Eukaryotes and Bacteria. We investigated this phenomenon as a biological activity correlated with the physiological state of these organisms.

At first, from time series records at the regional scale, this work describes *in situ* variations of bioluminescence over time. Three main events of high bioluminescence activity (in March 2009, December 2009 and March 2010) were detected. These bioluminescence events have been defined as intense compared to the global fluctuations recorded over time. Such high variations were unexpected.

Furthermore, looking at the local scale, in Chapter 5, prokaryotic survey over the year 2011 led to a first link of bioluminescence with the activity of bioluminescent bacteria. This was based on *lux* genes quantification. In particular, this work demonstrates that bioluminescent bacteria (belonging to *Photobacterium* genus) were active. This was observed even during a period of low bioluminescence at the ANTARES site.

In Chapter 4, at the microscale in the laboratory, bioluminescence has also been demonstrated to be involved in bacterial activity. The bacterial strain used as a model, *Photobacterium phosphoreum* ANT-2200, has been isolated during an event of high bioluminescence activity in 2005. In Martini et al. (2013a), we demonstrated that the bioluminescence of *Photobacterium phosphoreum* ANT-2200 strain is influenced by environmental growth conditions (carbon availability, temperature, and pressure). Higher activity of bioluminescence has been recorded at high pressure *vs.* atmospheric pressure, showing that it does not have an inhibitory effect on the bioluminescence activity. On the contrary, bioluminescent bacteria potentially involved in the bioluminescence activity are adapted to extreme conditions encountered in the deep sea. This shows that

bioluminescence is an important physiological response for bacterial activity.

All these results allowed to validate that bioluminescence is associated to the physiological state of these organisms. However, questions remain concerning the type of organisms emitting light and recorded by photomultipliers. Indeed, photomultipliers are still inefficient to discriminate bacterial and eukaryotic bioluminescence. In this work, we focused on bioluminescent bacteria due to the lack of *in situ* informations in the literature. The wide diversity of bioluminescent organisms involved in the bioluminescence activity detected by the ANTARES telescope, has to be further explored. Bathyphotometers have been developed to enhance turbulence and mechanical stimulation on eukaryotic bioluminescent organisms. Photomultipliers, detect *a priori* all light emission. The combined use of both devices should allow to measure the global and the eukaryotic bioluminescence and, therefore, to estimate the prokaryotic part in the signal. An efficient protocol has to be developed given the different sampling strategies between those instruments. Comparison between records over time will probably lead to the description of organisms, as well as the ability and limits of those complementary methods.

Moreover, the use of adapted video cameras nearby a photomultiplier could give interesting information describing each bioluminescent organisms. The successive record of images using a camera with an active lighting, followed by red lighting (invisible for most of organisms) could permit to identify organisms. The photomultiplier will measure the bioluminescence intensity and shape of emission over time. These couples of characteristics could help to discriminate automatically bioluminescent organisms crossing the ANTARES observatory. Detection methods are widely developed and image processing easily automatized as shown by Stemmann et al. (2008), Aguzzi et al. (2009) and the Eye-in-the-Sea project [www.mbari.org/mars/science/eits.html](http://www.mbari.org/mars/science/eits.html). By the end, using a network of about 885 photomultipliers will be a fascinating way to detect organisms crossing the entire 3D-telescope over space and time in the deep sea. Indeed, spatial analyzes can be performed using all photomultipliers within a total volume of 0.1 km<sup>3</sup> and would permit to estimate spatial dynamics of bioluminescent organisms through the observatory.

### 6.1.3 Does bioluminescence play a major role in the deep sea ?

About 95% of the hydrosphere (deeper than 200-300 m) is characterized by its darkness and the deep sea (under 1,000 m depth) is also defined by high hydrostatic pressure. The interest of the question "Does bioluminescence play a major role in the deep sea ?" is to evaluate possible roles of bioluminescence in such environment and to investigate how high pressure would impact organisms in the deep sea.

At the regional scale, in Chapter 2, we demonstrated the input of newly formed deep waters from the surface to the deep, increasing, in an unexpected way, the bioluminescence activity (see [Tamburini et al. \(2013\)](#) for details). Moreover, it has been observed that seasonal spring blooms of chlorophyll-*a* occur at the surface of the ANTARES station. Such blooms are known to involve an increase in POC and DOC sinking into the deep sea. Moreover, as we described all over this work, bioluminescent bacteria can be attached to particles and therefore be transported to the deep. Such blooms can also involve bioluminescent eukaryotic organisms, sinking into the deep sea. In this work, first investigations do not permit to identify links between bioluminescence and surface seasonal spring blooms. However, in further work, using a suitable sampling survey, this phenomenon and its impact on bioluminescence activity and, by the end on bioluminescent organisms, has to be distinguished from newly formed deep-water-mass effects.

At the local scale, in Chapter 4, we have estimated between 0.1 to 1%, the part of bioluminescent bacteria among the total bacterial community at 2,000 m depth. This percentage proved the presence of such bacteria at the deep ANTARES station and do not exclude them as a part of the bioluminescence signal. But this survey has been done out of intense-bioluminescence-activity periods and further investigation during these events are needed. Sinking particles are known to be hot spot of microbial activity in the dark ocean ([Cho and Azam, 1988](#); [Turley, 2002](#); [Long and Azam, 2001](#); [Azam and Long, 2001](#)). Indeed, prokaryotic abundance in particles is up to 3 order of magnitude higher than the abundance of free-living prokaryotes in the same volume of sea water ([Turley](#)

and Mackie, 1995). Focusing on sinking particles or marine snow for investigating *lux* genes might be of interest for defining the role of bioluminescent bacteria into the carbon cycle, and in the deep sea.

At the microscale, in Chapter 3, bioluminescent bacterial physiology has been investigated in relation to temperature and pressure, as the two main characteristics of the deep Mediterranean Sea. Their effects have been analyzed on both growth rate and maximum population density for the bioluminescent bacterial strain *Photobacterium phosphoreum* ANT-2200. This study defined an innovative way to describe bacterial optimal conditions for growth and permitted to characterize this strain as moderately piezophile. Moreover, we highlighted the increase in bioluminescence for this bacterial strain under high pressure conditions. Then, the first results also demonstrated that under high pressure conditions, this model strain allocated a better yield for oxygen consumption than under atmospheric pressure.

To conclude from the results of this thesis work, we investigated the bioluminescence as a proxy of biological activity using two sets of indicators : scales and levels. On the one hand, observation scales were ranging from micro to local and to regional. On the other hand, ecological levels were defined from population to communities and to ecosystem. We demonstrated that bioluminescence can be used as a proxy of biological activity for some levels (population and ecosystem) and some scales (micro and regional). For local scale and community level, we can not yet conclude and several perspective works have been proposed in this conclusion part.

## 6.2 Perspectives

A first perspective developed hereafter proposes to investigate the cultivation of the bacterial strain in a bioreactor, under controlled and monitored conditions. Using this method, physiological parameters described in Chapter 4 could be improved at atmospheric pressure before going back to high pressure system. Finally, a project concerning

the implementation of video cameras on the ANTARES site and the concomitant analysis of data from photomultipliers is presented.

### 6.2.1 Physiological parameters determination using bioreactor culture

#### Bioreactor platform

The *Photobacterium phosphoreum* ANT-2200 pre-culture is inoculated into a bioreactor fairmentec (total volume 2.2 L and working volume of 1.5 L) with an erthalite culture chamber (biologically and chemically neutral mater of white color and reflecting light). The bioreactor is autoclaved within 121°C for 20 min into an autoclave system Federagi FVG. The bioreactor is equipped with sensors controlling automatically the temperature (Julabo F25, France), the pH (InPro 3253, Mettler Toledo, Suisse), the redox-potential (InPro3253, Mettler Toledo, Suisse), and the dissolved oxygen (InPro6800, Mettler Toledo, Suisse). The transmitter for both pH and redox electrods is a Mettler Toledo PH2100e. The transmitter for oxygen is a Mettler Toledo O2 4100e. Sensors are calibrated before each experiment and a verification is done at the end, to validate measurements. On the outlet gas stream line, a CO<sub>2</sub> probe (Vaisala GMT 221, Finland) was fitted downstream from the glass exhaust water cooler to enable on-line measurement of CO<sub>2</sub> concentration. To control the gaz-mix for the oxygenation into the bioreactor, a debimeter (Bronkhorst, el flow, Netherlands) has been used. The debit injected was from 0 to 200 mL min<sup>-1</sup>. An HPLC (shimadzu RID6A refractometer and colonne HPX87H) allow the control of glucose consumption throughout the experiment. The bioluminescence is recorded using an optical fiber (FVP600660710 Photon Lines) plugged to the bioreactor end cap and connected to a photomultiplier (H7155, Hammamatsu) linked to a counting box (C8855). Photons counting rate is recorded automatically on a computer, with an integrating rate of 10 s. In order to simplify the photon acquisition, experiments have been performed into dark room.

Bioreactor liquid volume and NaOH consumption, regulating the pH, were monitored

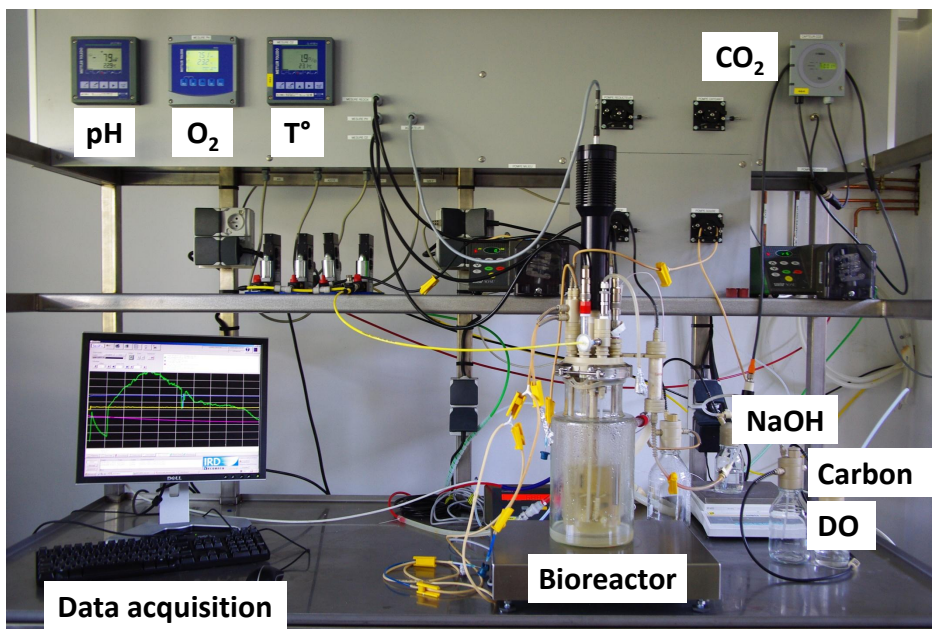


FIGURE (6.1) The bioreactor platform with pH, O<sub>2</sub>, temperature and CO<sub>2</sub> data acquisition and control in real time and high frequency sub-sampling. Glycerol consumption and Optical Density (OD) are measured with culture sub-sampling over time. The culture room was completely dark during bioluminescence measurements.

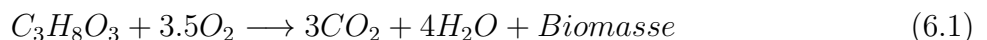
by two balances (respectively Combics 1 and BP 4100, Sartorius, France). Temperature, pH, gas flow rates and stirrer speed were regulated through control units (local loops). All this equipment was connected to an automat (Wago, France) via either a serial link (RS232/RS485), a 4-20 mA analog loop, or a digital signal. The automat was connected to a computer and a BatchPro software (Decobecq Automatismes, France) was used to monitor, acquire data and manage the processes with good flexibility and accuracy.

### Data acquisition into bioreactor

The bioreactor is an optimal system for the bacterial cultivation under controlled conditions and to the record of variables simultaneously. Moreover such instrumentation is dedicated to the cultivation of a large volume of bacterial culture. In this experiment, *Photobacterium phosphoreum* ANT-2200 has been cultivated for 70 h. Dissolved oxygen

concentration was set at 100 % of saturation (oxygen dissolved in the medium) to avoid limitation, temperature regulated at 13°C and pH at 7.5. During the growth, air input ( $O_2$ ) (by bacterial consumption), glycerol consumption (by bacterial metabolism), bioluminescence emission,  $CO_2$  (by bacterial respiration), and Optical Density ( $OD_{600nm}$ ) (linked to bacterial biomass) are recorded (see Figure 6.2). Contamination has been tested, from culture sub-sampling dedicated to the OD measurement, by microscopy observation. High  $OD_{600nm}$  values have been recorded due to stirring conditions, bioreactor volume and air input.

The chemical equation for glycerol respiration is defined as :



The glycerol concentration shows a limitation in carbon content occurring at 65 h of growth (reaching 0 g L<sup>-1</sup>). This limitation involves the end of bacterial population growth with the end of exponential phase ( $OD_{600nm}$  value about 5),  $CO_2$  release and  $O_2$  consumption, as well as a spontaneous stop of the bioluminescence activity.

Thanks to this continuous record and variable acquisition, oxygen consumption, bioluminescence emission, growth, and glycerol consumption helped to determine the medium limitations and to a first estimation of physiological parameters. [del Giorgio and Cole \(1998\)](#) defined Bacterial Growth Efficiency (BGE) as the amount of new bacterial biomass produced per unit of organic C substrate assimilated. BGE can be estimated using the bacterial Biomass Production (BP) and the Bacterial Respiration (BR) with  $CO_2$  production as  $BGE=BP/(BP+BR)$ . In natural ecosystems, BGE is estimated between 0.01 and 0.6 for oligotrophic to eutrophic environments ([del Giorgio and Cole, 1998](#)). These BGE values are higher in batch setup at laboratory with BGE values between 0.3 and 0.9 ([del Giorgio and Cole, 1998](#)). In this work, the experimental BGE value is 0.86 showing an important biomass production per unit of organic carbon. In this work, the experimental BGE value can be estimated with both glycerol and  $O_2$  consumption, the  $OD_{600nm}$  / dry weight ratio and the  $CO_2$  production. However, this value has to be dis-

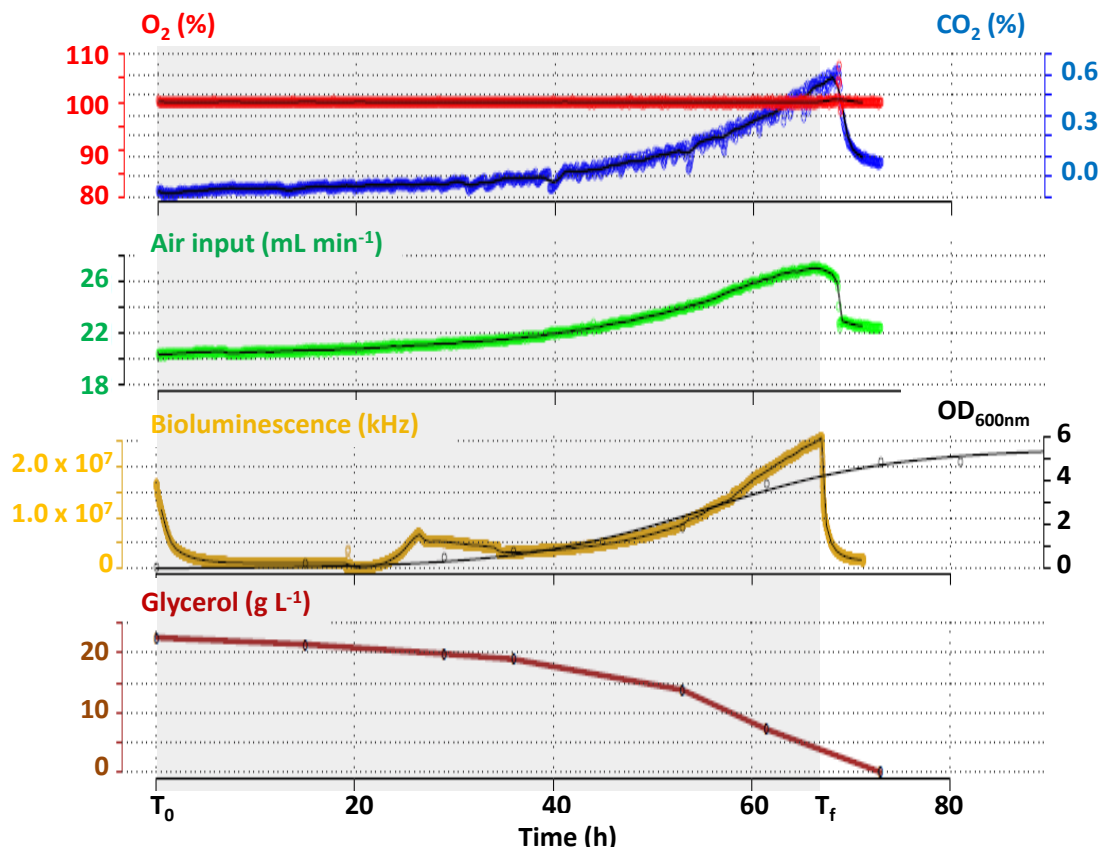


FIGURE (6.2) Data acquisition from the bioreactor. *Photobacterium phosphoreum* ANT-2200 strain has been cultivated in an ONR7a growth medium under controlled conditions. Oxygen concentration has been controlled to be non-limitant at 100% of saturation (red dots), temperature is 13°C and pH is 7.5. CO<sub>2</sub> (blue dots), air input to the medium (green dots), bioluminescence activity (yellow dots) are recorded at high frequency and in real time. Culture has been sampled each 4 to 12 hours for both optical density (OD<sub>600nm</sub>, black dots) and glycerol measurements (brown line). Black lines are the data continuous fit for each variable. The OD<sub>600nm</sub> has been plotted using a logistic model (see Martini et al., 2013a and Verhulst, 1838). Grey area represents the bacterial growth duration.

cussed with caution because the computation is based on only one experiment. There is a need of replicates for robust interpretation. Moreover, further investigations with several replicates will lead to the computation of physiological parameters for this bacterial strain.

### 6.2.2 Proposal for the detection of bioluminescent organisms

#### Importance of bioluminescence into the carbon cycle

Following this work, we propose to deploy autonomous PMTs through the water column in order to check bioluminescent organisms at the upper and lower level of the mesopelagic zone as well as "bioluminescent" fecal pellets flux.

#### PMTs acquisition and calibration in the laboratory.

The Centre de physique des Particules de Marseille (CPPM) is one of the main institutes of the ANTARES collaboration, in charge of ANTARES PMTs development. Recently, in the framework of the MEUST project (Mediterranean Eurocentre for underwater sciences and technologies), the CPPM develops autonomous PMTs dedicated to the survey of a new site for the future km<sup>3</sup> neutrino telescope. In close collaboration with the CPPM, we could ask the development of specific PMTs dedicated to the bioluminescence study. Indeed, using this first experiment, we are able to define the need of two different data sampling rates, in order to increase memory space acquisition and the efficiency of PMTs data acquisition.

#### First essays of PMTs deployments on mooring line.

In the framework of the site survey dedicated to the MEUST project, a deep mooring line has already been deployed. We plan to reproduce the schema of this mooring line also in the upper and lower part of the mesopelagic zone, adding UVP and LISST instruments. First essays will be done to choose the best implementation of all instruments, first data acquisition and cross-data calibration. More precisely, two sampling rates have to be improved with first deployments. Firstly, a low frequency sampling rate (about minutes) will be dedicated to the record of bioluminescence intensity linked to environmental variables. Then, at other periods, higher frequency sampling rate will be dedicated to the organisms' recognition spectra. Modulation in frequency sampling rate is a good compromise between data acquisition interest and data storage.

### Time-frequency analyzes of bioluminescence time-series and oceanographic variables (temperature, salinity, currents, oxygen, POC fluxes)

One of the approaches proposed for further investigations, is to understand links between bioluminescent organisms and carbon supply in the mesopelagic and bathypelagic environment. To do so, we could use the previously described mooring line (PMTs, UVP, LISS, CTD, current meter at different depths). Time series analysis using statistically adapted and developed mathematical methods is a crucial point to access to a better ecological understanding. Indeed, such time series are statistically defined as non-linear and non-stationary. If the Fourier method has been traditionally used for time-series decomposition it is not well adapted to non-stationary data. Since the 80's two different methods named the wavelet and the Huang-Hilbert decomposition methods have been developed to counteract this gap ([Huang et al., 1998](#); [Torrence and Compo, 1998](#)). These decompositions methods are defined in the time-frequency domain. From the ANTARES time-series analysis, using both the wavelets and Hilbert-Huang methods, bioluminescence intensity has been found to be clearly sea-current-intensity dependent but also highly correlated with modification of deep-water masses (using salinity and temperature as proxies) ([Martini et al., 2013b](#)). These mathematical methods represent an appropriate way to provide new insight from time-series and would be applied in future work.

### Bioluminescence spectra analysis and automatic classification of organisms

Using this instrumented-mooring line, a perspective of ecological interest in the mesopelagic and bathypelagic could also be approached. As already described, bioluminescence is a phenomenon produced by very wide range of organisms. We focused on links between biology and the environmental changes aiming at the definition of populations or organisms involved. Bioluminescence spectra analysis is a way to determine what kind of organisms are present close to the mooring line and, eventually, to detect some shifts in populations over time. Indeed, different organisms have already been described to emit

different light pattern (see Figure 6.3, Widder et al., 1989; Nealson et al., 1986).

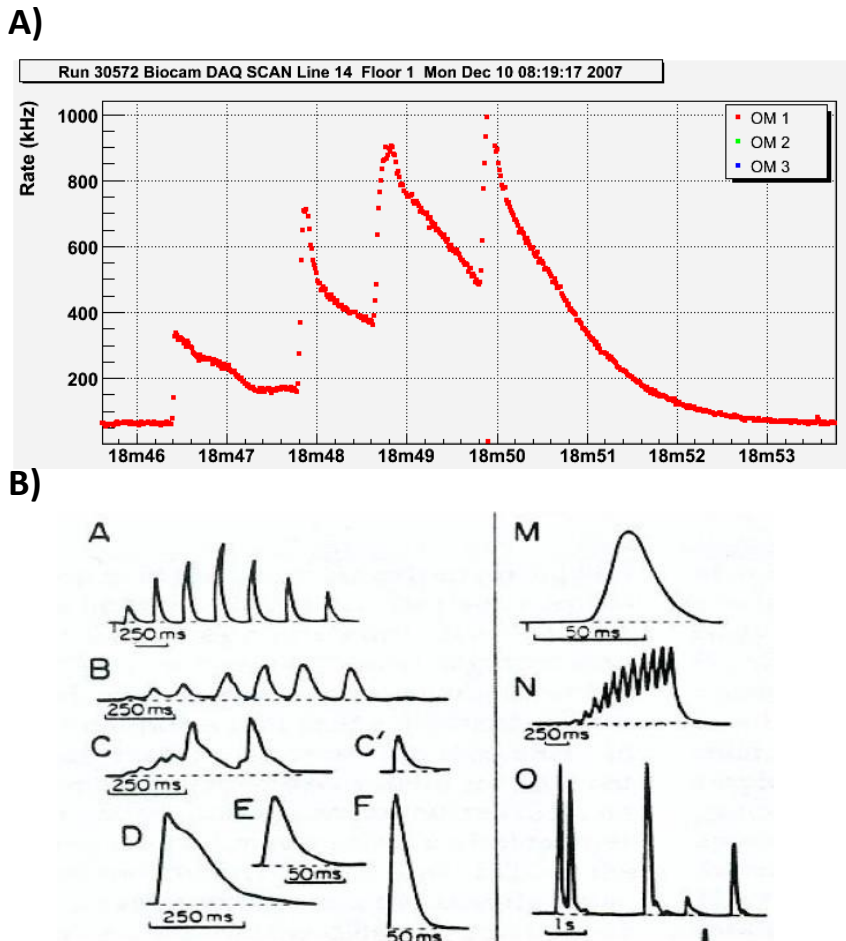


FIGURE (6.3) Example of bioluminescence emission patterns. A) From the ANTARES observatory, B) In the literature (Hastings and Morin, 1991).

These signatures can be used to describe populations crossing the mooring line. Bioluminescence spectra as a signature of organisms has been approached by Nealson et al. (1986), which only used ten species. In this part, the proposed approach is the use of mathematical unsupervised classification for population detection. Emission intensity can be recorded as curves for individuals crossing the detector. The shape, length and area of the curves are several potential descriptors that can be used for the classification method. Depending on the variability between these criteria, each bioluminescence

emission curve is attributed to one class. At the end of the process, each class defines similar curves with the same pattern of light emission, potentially, the same class of organisms.

This classification method is already used into several fields such as cytometry ([Mal-kassian et al., 2011](#)) or hydrological prediction ([Nerini et al., 2000](#)). In a final aim, crossing this automatic classification method for bioluminescence intensity (recorded at high-frequency sampling rates) with the UVP, we should define an image of organisms for each class defined. In order to recognize organisms that have been classified with video camera and bioluminescence spectra, collaborations with international experts in bioluminescent organisms have to be envisaged. This support would be of great importance to determine higher level identification for observed organisms.

---

## Bibliographie

---

- Abe, F., Kato, C., 1999. Barophysiology (piezophysiology). In : Extremophiles in Deep-Sea Environments. Springer, pp. 227–248. (cite page 120)
- Addison, P. S., 2010. The illustrated wavelet transform handbook : introductory theory and applications in science, engineering, medicine and finance. CRC Press. (cite page 86, 100)
- Ageron, M., Aguilar, J., Al Samarai, I., Albert, A., Ameli, F., André, M., Anghinolfi, M., Anton, G., Anvar, S., Ardid, M., et al., 2011. ANTARES : the first undersea neutrino telescope. Nuclear Instruments and Methods in Physics Research 656 (1), 11–38. (cite page 55, 65, 81)
- Ageron, M., Aguilar, J., Albert, A., Ameli, F., Anghinolfi, M., Anton, G., Anvar, S., Ardid, M., Aubert, J.-J., Aublin, J., et al., 2009. Performance of the first ANTARES detector line. Astroparticle Physics 31 (4), 277–283. (cite page 34)
- Aguilar, J., Al Samarai, I., Albert, A., Anghinolfi, M., Anton, G., Anvar, S., Ardid, M., Assis Jesus, A., Astraatmadja, T., Aubert, J.-J., et al., 2010. Measurement of the atmospheric muon flux with a 4 GeV threshold in the ANTARES neutrino telescope. Astroparticle Physics 33 (2), 86–90. (cite page 65)
- Aguilar, J., Albert, A., Ameli, F., Amram, P., Anghinolfi, M., Anton, G., Anvar, S., Ardellier-Desages, F., Aslanides, E., Aubert, J.-J., et al., 2005. Study of large hemispherical photomultiplier tubes for the ANTARES neutrino telescope. Nuclear Instruments and Methods in Physics Research Section A 555 (1), 132–141. (cite page 65)
- Aguilar, J., Albert, A., Ameli, F., Anghinolfi, M., Anton, G., Anvar, S., Aslanides, E., Aubert, J.-J., Barbarito, E., Basa, S., et al., 2006. First results of the instrumentation line for the deep-sea ANTARES neutrino telescope. Astroparticle Physics 26 (4), 314–324. (cite page 65)
- Aguilar, J., Albert, A., Ameli, F., Anghinolfi, M., Anton, G., Anvar, S., Aslanides, E., Aubert, J.-J., Barbarito, E., Basa, S., et al., 2007. The data acquisition system for the

- ANTARES neutrino telescope. Nuclear Instruments and Methods in Physics A 570 (1), 107–116. (cite page 65, 81, 160)
- Aguilar, J., Alleyne, H., Ameli, F., Amram, P., Anghinolfi, M., Anton, G., Anvar, S., Ardellier-Desages, F., Aslanides, E., Aubert, J.-J., et al., 2004. The ANTARES neutrino project. Physics of Atomic Nuclei 67, 1172–1176. (cite page 33)
- Aguzzi, J., Costa, C., Fujiwara, Y., Iwase, R., Ramirez-Llordà, E., Menesatti, P., 2009. A novel morphometry-based protocol of automated video-image analysis for species recognition and activity rhythms monitoring in deep-sea fauna. Sensors 9 (11), 8438–8455. (cite page 46, 186)
- Aguzzi, J., Mànuel, A., Condal, F., Guillén, J., Nogueras, M., Del Rio, J., Costa, C., Menesatti, P., Puig, P., Sardà, F., et al., 2011. The new seafloor observatory (OBSEA) for remote and long-term coastal ecosystem monitoring. Sensors 11 (6), 5850–5872. (cite page 46)
- Ahuja, N., Lertrattanapanich, S., Bose, N., 2005. Properties determining choice of mother wavelet. In : Vision, Image and Signal Processing, IEE Proceedings. Vol. 152. IET, pp. 659–664. (cite page 87)
- Aiken, J., Kelly, J., 1984. A solid state sensor for mapping and profiling stimulated bioluminescence in the marine environment. Continental Shelf Research 3 (4), 455–464. (cite page 11)
- Al Ali, B., Garel, M., Cuny, P., Miquel, J. C., Toubal, T., Robert, A., Tamburini, C., 2010. Luminous bacteria in the deep-sea waters near the ANTARES underwater neutrino telescope (Mediterranean Sea). Chemistry and Ecology, 26 (1), 57–72. (cite page 64, 114, 115, 116, 121, 126, 159, 167, 168, 175)
- Alldredge, A. L., Cohen, Y., 1987. Can microscale chemical patches persist in the sea ? microelectrode study of marine snow, fecal pellets. Science 235 (4789), 689–691. (cite page 14, 136, 158)
- Aminot, A., Kéroutil, R., 2004. Hydrologie des écosystèmes marins : paramètres et analyses. Editions Quae. (cite page 161)
- Aminot, A., Kéroutil, R., 2007. Dosage automatique des nutriments dans les eaux marines : méthodes en flux continu. Editions Quae. (cite page 161)
- Amram, P., Anghinolfi, M., Anvar, S., Ardellier-Desages, F., Aslanides, E., Aubert, J.-J., Azoulay, R., Bailey, D., Basa, S., Battaglieri, M., et al, 2002. The ANTARES optical module. Nuclear Instruments and Methods in Physics A 484 (13), 369 – 383. (cite page 33, 34, 65)
- Amram, P., Anvar, S., Aslanides, E., Aubert, J., Azoulay, R., Basa, S., Benhammou, Y., Bernard, F., Berthier, R., Bertin, V., et al., 1999. The ANTARES project. Nuclear Physics B-Proceedings Supplements 75 (1), 415–417. (cite page 33)
- Amram, P., Anvar, S., Aslanides, E., Azoulay, R., Basa, S., Benhammou, Y., Bernard, F., Bertin, V., Billault, M., Blanc, et al., 2000. Background light in potential sites for the ANTARES undersea neutrino telescope. Astroparticle Physics 13 (2), 127–136. (cite page 55, 57, 59, 81, 159, 160)

- Anderson, M., Cribble, N., 1998. Partitioning the variation among spatial, temporal and environmental components in a multivariate data set. *Australian Journal of Ecology* 23 (2), 158–167. (cite page 26)
- Andrews, C. C., Karl, D. M., Small, L. F., Fowler, S. W., 1984. Metabolic activity and bioluminescence of oceanic faecal pellets and sediment trap particles. (cite page 23, 54, 136)
- Aoki, T., Kitamura, T., Matsuno, S., Mitsui, K., Ohashi, Y., Okada, A., Cady, D., Learned, J., O'Connor, D., Dye, S., et al., 1986. Background light measurements in the deep ocean. *Il Nuovo Cimento C* 9 (2), 642–652. (cite page 55, 59)
- Aristegui, J., Gasol, J. M., Duarte, C. M., Herndl, G., 2009. Microbial oceanography of the dark ocean's pelagic realm. *Limnol. Oceanogr* 54 (5), 1501–1529. (cite page 158)
- Arrigo, K. R., 2004. Marine microorganisms and global nutrient cycles. *Nature* 437 (7057), 349–355. (cite page 165)
- Asplund, M., Rehnstam-Holm, A.-S., Atnur, V., Raghunath, P., Saravanan, V., Härnstrom, K., Collin, B., Karunasagar, I., Godhe, A., 2011. Water column dynamics of *Vibrio* in relation to phytoplankton community composition and environmental conditions in a tropical coastal area. *Environmental Microbiology* 13 (10), 2738–2751. (cite page 25)
- Azam, F., 1998. Microbial control of oceanic carbon flux : the plot thickens. *Science*, 694–695. (cite page 14, 136, 158)
- Azam, F., Long, R. A., 2001. Oceanography : Sea snow microcosms. *Nature* 414 (6863), 495–498. (cite page 136, 187)
- Baltar, F., Reinthaler, T., Herndl, G. J., Pinhassi, J., 2013. Major effect of hydrogen peroxide on bacterioplankton metabolism in the Northeast Atlantic. *PloS one* 8 (4), e61051. (cite page 23, 147)
- Bartlett, D., 2002. Pressure effects on in vivo microbial processes. *Biochimica et Biophysica Acta (BBA)-Protein Structure and Molecular Enzymology* 1595 (1), 367–381. (cite page 131, 133)
- Bartlett, D., Kato, C., Horikoshi, K., 1995. High pressure influences on gene and protein expression. *Research in Microbiology* 146 (8), 697–706. (cite page 120)
- Bartlett, D., Wright, M., Yayanos, A. A., Silverman, M., 1989. Isolation of a gene regulated by hydrostatic pressure in a deep-sea bacterium. *Nature* 342 (6249), 572–574. (cite page 120)
- Bartlett, D., et al., 1992. Microbial life at high pressures. *Science progress* 76 (301-302 Pt 3-4), 479. (cite page 131)
- Bartlett, D. H., Lauro, F. M., Eloe, E. A., 2007. Microbial adaptation to high pressure. *Physiology and Biochemistry of Extremophiles*. American Society for Microbiology Press, Washington, DC, 333–348. (cite page 120)

- Béthoux, J., Durieu de Madron, X., Nyffeler, F., Tailliez, D., 2002. Deep water in the western Mediterranean : peculiar 1999 and 2000 characteristics, shelf formation hypothesis, variability since 1970 and geochemical inferences. *Journal of Marine Systems* 33, 117–131. (cite page 55, 56, 62, 82)
- Bianchi, A., Garcin, J., Tholosan, O., 1999. A high-pressure serial sampler to measure microbial activity in the deep sea. *Deep Sea Research Part I* 46 (12), 2129–2142. (cite page 140)
- Bivens, J., Geiger, M., Bird, J., 2002. Interpreting bathyphotometer signals. In : OCEANS'02 MTS/IEEE. Vol. 3. IEEE, pp. 1705–1710. (cite page 11)
- Blaser, S., Kurisu, F., Satoh, H., Mino, T., 2002. Hydromechanical stimulation of bioluminescent plankton. *Luminescence* 17 (6), 370–80. (cite page 102)
- Bligh, E., Dyer, W. J., 1959. A rapid method of total lipid extraction and purification. *Canadian journal of biochemistry and physiology* 37 (8), 911–917. (cite page 125)
- Bonin, P. C., Michotey, V. D., Mouzdaire, A., Rontani, J.-F., 2002. Anaerobic biodegradation of squalene : using DGGE to monitor the isolation of denitrifying Bacteria taken from enrichment cultures. *FEMS microbiology ecology* 42 (1), 37–49. (cite page 163)
- Bookstein, F. L., 1989. Principal warps : Thin-plate splines and the decomposition of deformations. *IEEE* 11 (6), 567–585. (cite page 97)
- Bose, J. L., Rosenberg, C. S., Stabb, E. V., 2008. Effects of *luxCDABEG* induction in *Vibrio fischeri* : enhancement of symbiotic colonization and conditional attenuation of growth in culture. *Archives of microbiology* 190 (2), 169–183. (cite page 12)
- Bourgois, J.-J., Sluse, F., Baguet, F., , Mallefet, J., 2001. Kinetics of light emission and oxygen consumption by bioluminescent Bacteria. *Journal of bioenergetics and biomembranes* 33 (4), 353–363. (cite page 19, 134)
- Bradner, H., Bartlett, M., Blackinton, G., Clem, J., Karl, D., Learned, J., Lewitus, A., Matsuno, S., O'Connor, D., Peatman, W., et al., 1987. Bioluminescence profile in the deep Pacific Ocean. *Deep Sea Research A* 34 (11), 1831–1840. (cite page 9, 14, 16, 55, 59, 61)
- Bryan, J., Rlley, J., Williams, P. l., 1976. A Winkler procedure for making precise measurements of oxygen concentration for productivity and related studies. *Journal of Experimental Marine Biology and Ecology* 21 (3), 191–197. (cite page 160)
- Buskey, E., 1992. Epipelagic planktonic bioluminescence in the marginal ice zone of the greenland sea. *Marine Biology* 113 (4), 689–698. (cite page 11)
- Campbell, R., Dower, J., 2003. Role of lipids in the maintenance of neutral buoyancy by zooplankton. *Marine Ecology Progress Series* 263, 93–99. (cite page 131)
- Canals, M., Puig, P., Durieu de Madron, X., Heussner, S., Palanques, A., Fabres, J., 2006. Flushing submarine canyons. *Nature* 444 (7117), 354–357. (cite page 55)
- Capone, K. A., Dowd, S. E., Stamatas, G. N., Nikolovski, J., 2011. Diversity of the human skin microbiome early in life. *Journal of Investigative Dermatology* 131 (10), 2026–2032. (cite page 164)

- Carlson, C. A., Hansell, D. A., Nelson, N. B., Siegel, D. A., Smethie, W. M., Khatiwala, S., Meyers, M. M., Halewood, E., 2010. Dissolved organic carbon export and subsequent remineralization in the mesopelagic and bathypelagic realms of the north atlantic basin. Deep Sea Research Part II 57 (16), 1433–1445. (cite page 158)
- Casamayor, E. O., Massana, R., Benlloch, S., Øvreås, L., Díez, B., Goddard, V. J., Gasol, J. M., Joint, I., Rodríguez-V, F., Pedrós-Alió, C., 2002. Changes in archaeal, bacterial and eukaryal assemblages along a salinity gradient by comparison of genetic fingerprinting methods in a multipond solar saltern. Environmental Microbiology 4 (6), 338–348. (cite page 163)
- Cazelles, B., Chavez, M., Berteaux, D., Ménard, F., Vik, J., Jenouvrier, S., Stenseth, N. C., 2008. Wavelet analysis of ecological time series. Oecologia 156 (2), 287–304. (cite page 82, 87)
- Chen, X., Wu, Z., Huang, N., 2010. The time-dependent intrinsic correlation based on the empirical mode decomposition. Advances in Adaptive Data Analysis 2 (02), 233–265. (cite page 100)
- Cho, B. C., Azam, F., 1988. Major role of bacteria in biogeochemical fluxes in the ocean's interior. Nature 332 (6163), 441–443. (cite page 158, 187)
- Christie, W. W., 1989. Gas chromatography and lipids. (cite page 125)
- Church, M. J., DeLong, E. F., Ducklow, H. W., Karner, M. B., Preston, C. M., Karl, D. M., 2003. Abundance and distribution of planktonic Archaea and Bacteria in the waters west of the Antarctic Peninsula. Limnology and Oceanography 48 (5), 1893–1902. (cite page 167)
- Clarke, G. L., Kelly, M. G., 1965. Measurements of diurnal changes in bioluminescence from the sea surface to 2,000 meters using a new photometric device. Limnology and Oceanography, 54–66. (cite page 11)
- Cleveland, W. S., Grosse, E., 1991. Computational methods for local regression. Statistics and Computing 1 (1), 47–62. (cite page 164, 165, 222)
- Company, J., Puig, P., Sardà, F., Palanques, A., Latasa, M., Scharek, R., et al., 2008. Climate influence on deep sea populations. PloS ONE 3 (1), e1431. (cite page 57)
- Craig, J., Jamieson, A. J., Bagley, P. M., Priede, I. G., 2011. Naturally occurring bioluminescence on the deep-sea floor. Journal of Marine Systems 88 (4), 563–567. (cite page 10)
- Craig, J., Jamieson, A. J., Heger, A., Priede, I. G., 2009. Distribution of bioluminescent organisms in the Mediterranean Sea and predicted effects on a deep-sea neutrino telescope. Nuclear Instruments and Methods in Physics Research Section A 602 (1), 224–226. (cite page 81)
- Craig, J., Jamieson, A. J., Hutson, R., Zuur, A. F., Priede, I. G., 2010. Factors influencing the abundance of deep pelagic bioluminescent zooplankton in the Mediterranean Sea. Deep Sea Research I 57 (11), 1474–1484. (cite page 20, 157, 159)

- Cussatlegras, A.-S., 2006. Dynamique spatio-temporelle de la bioluminescence marine en mer d'alboran et sur le plateau continental atlantique français. Ph.D. thesis, Atelier national de reproduction des thèses. (cite page 16)
- Cussatlegras, A.-S., Geistdoerfer, P., Prieur, L., 2001. Planktonic bioluminescence measurements in the frontal zone of Almeria–Oran (Mediterranean Sea). Oceanologica acta 24 (3), 239–250. (cite page 20)
- Cussatlegras, A.-S., Le Gal, P., 2005. Dinoflagellate bioluminescence in response to mechanical stimuli in water flows. Nonlinear Processes in Geophysics 12 (3), 337–343. (cite page 15, 102, 157)
- Cussatlegras, A.-S., Le Gal, P., 2007. Variability in the bioluminescence response of the dinoflagellate *Pyrocystis lunula*. Journal of Experimental Marine Biology and Ecology 343 (1), 74–81. (cite page 102, 157)
- Czyz, A., Wrobel, B., Wegrzyn, G., 2000. *Vibrio harveyi* bioluminescence plays a role in stimulation of DNA repair. Microbiology 146 (2), 283–288. (cite page 134)
- De Santis, T., Hugenholtz, P., Larsen, N., Rojas, M., Brodie, E. L., Keller, K., Huber, T., Dalevi, D., Hu, P., Andersen, G. L., 2006. Greengenes, a chimera-checked 16s rRNA gene database and workbench compatible with ARB. Applied and environmental microbiology 72 (7), 5069–5072. (cite page 164)
- del Giorgio, P. A., Cole, J. J., 1998. Bacterial growth efficiency in natural aquatic systems. Annual Review of Ecology and Systematics, 503–541. (cite page 147, 148, 191)
- DeLong, E. F., Franks, D. G., Yayanos, A. A., 1997. Evolutionary relationships of cultivated psychrophilic and barophilic deep-sea Bacteria. Applied and environmental microbiology 63 (5), 2105–2108. (cite page 133)
- DeLong, E. F., Preston, C. M., Mincer, T., Rich, V., Hallam, S. J., Frigaard, N.-U., Martinez, A., Sullivan, M. B., Edwards, R., Brito, B. R., et al., 2006. Community genomics among stratified microbial assemblages in the ocean's interior. Science 311 (5760), 496–503. (cite page 170)
- DeLong, E. F., Yayanos, A., 1985. Adaptation of the membrane lipids of a deep-sea bacterium to changes in hydrostatic pressure. Science 228 (4703), 1101–1103. (cite page 133)
- Desa, R., Hastings, J. W., 1968. The characterization of scintillons bioluminescent particles from the marine dinoflagellate, *Gonyaulax polyedra*. The Journal of general physiology 51 (1), 105–122. (cite page 20)
- Dorn, J. G., Frye, R. J., Maier, R. M., 2003. Effect of temperature, pH, and initial cell number on *luxCDABE* and *nah* gene expression during naphthalene and salicylate catabolism in the bioreporter organism *Pseudomonas putida* RB1353. Applied and environmental microbiology 69 (4), 2209–2216. (cite page 17)
- Dowd, S., Callaway, T., Wolcott, R., Sun, Y., McKeehan, T., Hagevoort, R., Edrington, T., 2008a. Evaluation of the bacterial diversity in the feces of cattle using 16s rDNA bacterial tag-encoded FLX amplicon pyrosequencing (bTEFAP). BMC microbiology 8 (1), 125. (cite page 164)

- Dowd, S., Hanson, J. D., Rees, E., Wolcott, R., Zischau, A., Sun, Y., White, J., Smith, D., Kennedy, J., Jones, C., 2011. Research survey of fungi and yeast in polymicrobial infections in chronic wounds. *Journal of wound care* 20 (1), 40–47. (cite page 164)
- Dowd, S., Sun, Y., Secor, P., Rhoads, D., Wolcott, B., James, G., Wolcott, R., 2008b. Survey of bacterial diversity in chronic wounds using pyrosequencing, DGGE, and full ribosome shotgun sequencing. *BMC microbiology* 8 (1), 43. (cite page 164)
- Ducklow, H. W., Steinberg, D. K., Buesseler, K. O., 2001. Upper ocean carbon export and the biological pump. *Oceanography* 14 (4), 50–58. (cite page 180)
- Dunlap, P., 1984. Physiological and morphological state of the symbiotic Bacteria from light organs of ponyfish. *The Biological Bulletin* 167 (2), 410–425. (cite page 12, 19)
- Dunlap, P., Kojima, Y., Nakamura, S., Nakamura, M., 2009. Inception of formation and early morphogenesis of the bacterial light organ of the sea urchin cardinalfish, *Siphamia versicolor*. *Marine biology* 156 (10), 2011–2020. (cite page 21, 22)
- Dunlap, P. V., Kita-Tsukamoto, K., 2006. Luminous Bacteria. In : The Prokaryotes. Springer, pp. 863–892. (cite page 7, 12, 20, 120)
- Durrieu de Madron, X., Houpet, L., Puig, P., Sanchez-Vidal, A., Testor, P., Bosse, A., Estournel, C., Somot, S., Bourrin, F., Bouin, M., et al., 2013. Interaction of dense shelf water cascading and open-sea convection in the northwestern Mediterranean during winter 2012. *Geophysical Research Letters*. (cite page 56, 62)
- Eberhard, A., Hastings, J., 1972. A postulated mechanism for the bioluminescent oxidation of reduced flavin mononucleotide. *Biochemical and biophysical research communications* 47 (2), 348–353. (cite page 13, 158)
- Edgar, R. C., 2010. Search and clustering orders of magnitude faster than BLAST. *Bioinformatics* 26 (19), 2460–2461. (cite page 164)
- Edwards, M., Beaugrand, G., Hays, G. C., Koslow, J. A., Richardson, A. J., 2010. Multi-decadal oceanic ecological datasets and their application in marine policy and management. *Trends in ecology & evolution* 25 (10), 602–610. (cite page 31, 32, 219)
- Einen, J., Thorseth, I. H., Øvreås, L., 2008. Enumeration of Archaea and Bacteria in seafloor basalt using real-time quantitative PCR and fluorescence microscopy. *FEMS microbiology letters* 282 (2), 182–187. (cite page 162)
- Eley, M., 1972. Optimal environmental conditions and nutrient concentrations for the synthesis of bacterial luciferase in *Photobacterium phosphoreum*. *Journal of general microbiology* 72 (2), 415–417. (cite page 17)
- Eloe, E. A., Malfatti, F., Gutierrez, J., Hardy, K., Schmidt, W. E., Pogliano, K., Pogliano, J., Azam, F., Bartlett, D. H., 2011. Isolation and characterization of a psychropiezophilic alphaproteobacterium. *Applied and environmental microbiology* 77 (22), 8145–8153. (cite page 129)
- Eren, A. M., Zozaya, M., Taylor, C. M., Dowd, S. E., Martin, D. H., Ferris, M. J., 2011. Exploring the diversity of *Gardnerella vaginalis* in the genitourinary tract microbiota of monogamous couples through subtle nucleotide variation. *PloS ONE* 6 (10), e26732. (cite page 164)

- Fang, J., Zhang, L., Bazylinski, D. A., 2010. Deep-sea piezosphere and piezophiles : geo-microbiology and biogeochemistry. *Trends in microbiology* 18 (9), 413–422. (cite page 131)
- Favali, P., Beranzoli, L., 2006. Seafloor observatory science : a review. *Annals of Geophysics* 49 (2-3). (cite page 81)
- Flandrin, P., Rilling, G., Goncalves, P., 2004. Empirical mode decomposition as a filter bank. *Signal Processing Letters, IEEE* 11 (2), 112–114. (cite page 95, 96)
- Fleisher, K., Case, J., 1995. Cephalopod predation facilitated by dinoflagellate luminescence. *The Biological Bulletin* 189 (3), 263–271. (cite page 21)
- Fofonoff, N. P., Millard, R. C., 1983. Algorithms for computation of fundamental properties of seawater. (cite page 37)
- Fogel, M., Hastings, J., 1972. Bioluminescence : mechanism and mode of control of scintillon activity. *PNAS* 69 (3), 690–693. (cite page 20)
- Frazier, M., 1999. An introduction to wavelets through linear algebra. Springer-Verlag, New York. (cite page 82)
- Fritz, L., Morse, D., Hastings, J., 1990. The circadian bioluminescence rhythm of *Gonyaulax* is related to daily variations in the number of light-emitting organelles. *Journal of Cell Science* 95 (2), 321–328. (cite page 10, 102)
- Fucile, P., 1996. A low cost bioluminescence bathyphotometer. *Gulf of Maine Ecosystem Dynamics Symposium*, September 11-16, St Andrew's, New Brunswick, USA. (cite page 11)
- Gaarder, T., Gran, H. H., 1927. Investigations of the production of plankton in the Oslo Fjord. *Conseil permanent international pour l'exploration de la mer*. (cite page 160)
- Geesey, G., Alexander, G. V., Bray, R. N., Miller, A. C., 1984. Fish fecal pellets are a source of minerals for inshore reef communities. *Marine ecology progress series* 15 (1), 19–25. (cite page 23)
- Geistdoerfer, P., Cussatlegras, A.-S., 2001. Variations nycthémérales de la bioluminescence marine en Méditerranée et dans l'Atlantique nord-est. *Comptes Rendus de l'Académie des Sciences-Series III-Sciences de la Vie* 324 (11), 1037–1044. (cite page 12)
- Geistdoerfer, P., Vincendeau, M.-A., 1999. A new bathyphotometer for bioluminescence measurements on the Armorican continental shelf (northeastern Atlantic). *Oceanologica acta* 22 (2), 137–151. (cite page 11, 54)
- Gentile, G., De Luca, M., Denaro, R., La Cono, V., Smedile, F., Scarfi, S., De Domenico, E., De Domenico, M., Yakimov, M. M., 2009. PCR-based detection of bioluminescent microbial populations in Tyrrhenian Sea. *Deep Sea Research II* 56 (11), 763–767. (cite page 12, 13, 25, 64, 114, 120, 158, 175)
- Gerasimova, M., Kudryasheva, N., 2002. Effects of potassium halides on bacterial bioluminescence. *Journal of Photochemistry and Photobiology B : Biology* 66 (3), 218–222. (cite page 17)

- Ghorbani, M., 2013. Testing the weak stationarity of a spatio-temporal point process. *Stochastic Environmental Research and Risk Assessment* 27 (2), 517–524. (cite page 82)
- Gillibrand, E., Jamieson, A., Bagley, P., Zuur, A., Priede, I., 2007. Seasonal development of a deep pelagic bioluminescent layer in the temperate NE Atlantic Ocean. *Marine Ecology Progress Series* 341, 37–44. (cite page 10, 21)
- Goregues, C., Michotey, V., Bonin, P., 2005. Molecular, biochemical, and physiological approaches for understanding the ecology of denitrification. *Microbial ecology* 49 (2), 198–208. (cite page 163)
- Greenblatt, P., Feng, D., Zirino, A., Losee, J., 1984. Observations of planktonic bioluminescence in the euphotic zone of the California Current. *Marine Biology* 84 (1), 75–82. (cite page 11)
- Grinsted, A., Moore, J. C., Jevrejeva, S., 2004. Application of the cross wavelet transform and wavelet coherence to geophysical time series. *Nonlinear processes in geophysics* 11 (5/6), 561–566. (cite page 100)
- Grogan, D. W., 1984. Interaction of respiration and luminescence in a common marine bacterium. *Archives of microbiology* 137 (2), 159–162. (cite page 19, 134)
- Grossi, V., Yakimov, M. M., Al Ali, B., Tapilatu, Y., Cuny, P., Goutx, M., La Cono, V., Giuliano, L., Tamburini, C., 2010. Hydrostatic pressure affects membrane and storage lipid compositions of the piezotolerant hydrocarbon-degrading *Marinobacter hydrocarbonoclasticus* strain # 5. *Environmental microbiology* 12 (7), 2020–2033. (cite page 120)
- Haddock, S., Case, J., 1999. Bioluminescence spectra of shallow and deep-sea gelatinous zooplankton : ctenophores, medusae and siphonophores. *Marine Biology* 133 (3), 571–582. (cite page 5)
- Haddock, S. H., Moline, M. A., Case, J. F., 2010. Bioluminescence in the sea. *Marine Science* 2. (cite page 3, 4, 6, 21, 22, 54, 55, 135, 157, 174, 219)
- Hall, A., Staples, R., 1978. Bathyphotometer measurements of vertical bioluminescence in the NE Atlantic during May 1977. Vol. 3005. (cite page 11)
- Han, J., Li, G., Liu, H., Hu, H., Zhang, X., 2012. Stimulation of bioluminescence in *Noctiluca* sp. using controlled temperature changes. *Luminescence*. (cite page 16)
- Hansell, D. A., Carlson, C. A., 2001. Biogeochemistry of total organic carbon and nitrogen in the Sargasso Sea : control by convective overturn. *Deep Sea Research Part II* 48 (8), 1649–1667. (cite page 165)
- Hansell, D. A., Carlson, C. A., Repeta, D. J., Schlitzer, R., 2009. Dissolved organic matter in the ocean : A controversy stimulates new insights. (cite page 165)
- Hartline, D., Buskey, E., Lenz, P., 1999. Rapid jumps and bioluminescence elicited by controlled hydrodynamic stimuli in a mesopelagic copepod, *Pleuromamma xiphias*. *The Biological Bulletin* 197 (2), 132–143. (cite page 15)
- Harvey, E. N., 1952. Bioluminescence. Academic Press. (cite page 16)

- Hastings, J., 1983. Chemistry and control of luminescence in marine organisms. *Bulletin of marine science* 33 (4), 818–828. (cite page 120, 158)
- Hastings, J., Balny, C., 1975. The oxygenated bacterial luciferase-flavin intermediate. reaction products via the light and dark pathways. *Journal of Biological Chemistry* 250 (18), 7288–7293. (cite page 19)
- Hastings, J., Nealson, K., 1977. Bacterial bioluminescence. *Annual Reviews in Microbiology* 31 (1), 549–595. (cite page 12, 23, 138)
- Hastings, J., Potrikusv, C., Gupta, S., Kurfürst, M., Makemson, J., 1985. Biochemistry and physiology of bioluminescent Bacteria. *Advances in microbial physiology* 26, 235–291. (cite page 23)
- Hastings, J. W., 1986. Bioluminescence in Bacteria and Dinoflagellates. *Light Emission by Plants and Bacteria*, 363. (cite page 8)
- Hastings, J. W., Morin, J. G., 1991. in *Neural and Integrative Animal Physiology*. Wiley Interscience, New York. (cite page 195)
- Herndl, G. J., Reinthalter, T., Teira, E., van Aken, H., Veth, C., Pernthaler, A., Pernthaler, J., 2005. Contribution of Archaea to total prokaryotic production in the deep Atlantic Ocean. *Applied and Environmental Microbiology* 71 (5), 2303–2309. (cite page 167)
- Herren, C. M., Haddock, S. H., Johnson, C., Orrico, C. M., Moline, M. A., Case, J. F., 2005. A multi-platform bathyphotometer for fine-scale, coastal bioluminescence research. *Limnology and Oceanography : Methods* 3, 247. (cite page 11, 225)
- Herring, P., 1976. Bioluminescence in decapod Crustacea. *J. mar. biol. Ass. UK* 56, 1029–1047. (cite page 4)
- Herring, P., 1982. Aspects of the bioluminescence of fishes. *Oceanogr Marine Biol* 20, 415–470. (cite page 13)
- Herring, P., 2002. Marine microlights : the luminous marine Bacteria. *Microbiology Today* 29, 174–176. (cite page 157)
- Herring, P. J., 1985. Bioluminescence in the crustacea. *Journal of crustacean biology* 5 (4), 557–573. (cite page 2)
- Herring, P. J., 1987. Systematic distribution of bioluminescence in living organisms. *Journal of bioluminescence and chemiluminescence* 1 (3), 147–163. (cite page 2, 4, 54, 120)
- Herrmann, M., Estournel, C., Déqué, M., Marsaleix, P., Sevault, F., Somot, S., 2008. Dense water formation in the Gulf of Lions shelf : Impact of atmospheric interannual variability and climate change. *Continental Shelf Research* 28 (15), 2092–2112. (cite page 64)
- Hewitt, J., Thrush, S., Dayton, P., Bonsdorff, E., 2007. The effect of spatial and temporal heterogeneity on the design and analysis of empirical studies of scale-dependent systems. *The American Naturalist* 169 (3), 398–408. (cite page 26, 81)
- Hmelo, L. R., Mincer, T., Van Mooy, B. A., 2011. Possible influence of bacterial quorum sensing on the hydrolysis of sinking particulate organic carbon in marine environments. *Environmental microbiology reports* 3 (6), 682–688. (cite page 14, 15, 135, 219)

- Huang, N. E., Shen, Z., Long, S. R., Wu, M. C., Shih, H. H., Zheng, Q., Yen, N.-C., Tung, C. C., Liu, H. H., 1998. The empirical mode decomposition and the hilbert spectrum for nonlinear and non-stationary time series analysis. Proceedings of the Royal Society of London. Series A 454 (1971), 903–995. (cite page 86, 90, 110, 194, 221)
- Huang, N. E., Wu, Z., 2008. A review on Hilbert-Huang transform : method and its applications to geophysical studies. Review of Geophysics 46 (2007), 1–23. (cite page 90, 96)
- Huang, N. E., Wu, Z., Long, S. R., Arnold, K. C., Chen, X., Blank, K., 2009a. On instantaneous frequency. Advances in Adaptive Data Analysis 1 (2), 177–229. (cite page 90, 95, 96)
- Huang, Y., Schmitt, F. G., Lu, Z., Liu, Y., 2009b. Analysis of daily river flow fluctuations using empirical mode decomposition and arbitrary order hilbert spectral analysis. Journal of Hydrology 373 (1), 103–111. (cite page 95)
- Huthnance, J. M., 1995. Circulation, exchange and water masses at the ocean margin : the role of physical processes at the shelf edge. Progress in Oceanography 35 (4), 353–431. (cite page 88, 102)
- Kamimura, K., Fuse, H., Takimura, O., Yamaoka, Y., 1993. Effects of growth pressure and temperature on fatty acid composition of a barotolerant deep-sea bacterium. Applied and environmental microbiology 59 (3), 924–926. (cite page 133)
- Karl, D., Nealson, K., 1980. Regulation of cellular metabolism during synthesis and expression of the luminous system in *Beneckea* and *Photobacterium*. Journal of General Microbiology 117 (2), 357–368. (cite page 19, 138)
- Karner, M. B., DeLong, E. F., Karl, D. M., 2001. Archaeal dominance in the mesopelagic zone of the Pacific Ocean. Nature 409 (6819), 507–510. (cite page 167)
- Kato, C., 2008. Protein adaptation to high-pressure environments. Review of High Pressure Science and Technology 18 (2). (cite page 120)
- Kato, C., Sato, T., Smorawinska, M., Horikoshi, K., 1994. High pressure conditions stimulate expression of chloramphenicol acetyltransferase regulated by the *lac* promoter in *Escherichia coli*. FEMS microbiology letters 122 (1), 91–96. (cite page 121)
- Kato, C., Suzuki, S., Hata, S., Ito, T., Horikoshi, K., 1995. The properties of a protease activated by high pressure from *Sporosarcina sp.* strain DSK25 isolated from deep-sea sediment. JAMSTEC J. Deep Sea Res 32, 7–13. (cite page 121)
- Kirillova, T. N., Kudryasheva, N. S., 2007. Effect of heavy atoms in bioluminescent reactions. Analytical and bioanalytical chemistry 387 (6), 2009–2016. (cite page 17)
- Kita-Tsukamoto, K., Yao, K., Kamiya, A., Yoshizawa, S., Uchiyama, N., Kogure, K., Wada, M., 2006. Rapid identification of marine bioluminescent Bacteria by amplified 16S ribosomal RNA gene restriction analysis. FEMS microbiology letters 256 (2), 298–303. (cite page 120, 158)
- Kwiatkowski, D., Phillips, P. C., Schmidt, P., Shin, Y., 1992. Testing the null hypothesis of stationarity against the alternative of a unit root. Journal of Econometrics 54 (1-3), 159–178. (cite page 85)

- Lapota, D., Galt, C., Losee, J. R., Huddell, H. D., Orzech, J. K., Nealson, K. H., 1988. Observations and measurements of planktonic bioluminescence in and around a milky sea. *Journal of experimental marine biology and ecology* 119 (1), 55–81. (cite page 152)
- Lapota, D., Geiger, M., Stiffey, A., Rosenberger, D., Young, D., 1989. Correlation of planktonic bioluminescence with other oceanographic parameters from a Norwegian fjord. *Marine Ecology Progress Series* 55 (2-3), 217–228. (cite page 20, 157)
- Latz, M. I., Case, J. F., Gran, R. L., 1994. Excitation of bioluminescence by laminar fluid shear associated with simple couette flow. *Limnology and oceanography* 39 (6), 1424–1439. (cite page 15)
- Lauro, F. M., Tran, K., Vezzi, A., Vitulo, N., Valle, G., Bartlett, D. H., 2008. Large-scale transposon mutagenesis of *Photobacterium profundum* SS9 reveals new genetic loci important for growth at low temperature and high pressure. *Journal of bacteriology* 190 (5), 1699–1709. (cite page 120, 131)
- Lee, B.-S., Lee, J.-G., Shin, D.-H., Kim, E.-K., 2001. Statistical optimization of bioluminescence of *Photobacterium phosphoreum* KCTC2852. *Journal of bioscience and bioengineering* 92 (1), 72–76. (cite page 17)
- Legendre, P., Thrush, S., Cummings, V., Dayton, P., Grant, J., Hewitt, J., Hines, A. H., McArdle, B., Pridmore, R., Schneider, D., et al., 1997. Spatial structure of bivalves in a sandflat : Scale and generating processes. *Journal of Experimental Marine Biology and Ecology* 216 (1-2), 99–128. (cite page 26)
- Lloyd, D., James, C. J., Hastings, J. W., 1985. Oxygen affinities of the bioluminescence systems of various species of luminous bacteria. *Journal of general microbiology* 131 (9), 2137–2140. (cite page 19)
- Long, R. A., Azam, F., 2001. Microscale patchiness of bacterioplankton assemblage richness in seawater. *Aquatic Microbial Ecology* 26, 103. (cite page 187)
- Losee, J., Lapota, D., Lieberman, S. H., 1985. Bioluminescence : a new tool for oceanography. Mapping strategies in chemical oceanography. *Advances in chemistry series* 209, 211–234. (cite page 16)
- Makemson, J., 1986. Luciferase-dependent oxygen consumption by bioluminescent *Vibrios*. *Journal of bacteriology* 165 (2), 461–466. (cite page 12, 19, 146)
- Malave-Orengo, J., Rubio-Marrero, E. N., Rios-Velazquez, C., 2010. Isolation and characterization of bioluminescent Bacteria from marine environments of Puerto Rico. (cite page 25, 158)
- Malkassian, A., Nerini, D., van Dijk, M. A., Thyssen, M., Mante, C., Gregori, G., 2011. Functional analysis and classification of phytoplankton based on data from an automated flow cytometer. *Cytometry part A* 79 (4), 263–275. (cite page 196)
- Mardia, K., Kent, J., Goodall, C., Little, J., 1996. Kriging and splines with derivative information. *Biometrika* 83 (1), 207–221. (cite page 97)
- Marshall, J., Schott, F., 1999. Open-ocean convection : Observations, theory, and models. *Reviews of Geophysics* 37 (1), 1–64. (cite page 55, 56, 64, 82)

- Martín, J., Miquel, J.-C., Khripounoff, A., 2010. Impact of open sea deep convection on sediment remobilization in the western Mediterranean. *Geophysical Research Letters* 37 (13). (cite page 62)
- Martin-Cuadrado, A.-B., Lopez-Garcia, P., Alba, J.-C., Moreira, D., Monticelli, L., Strittmatter, A., Gottschalk, G., Rodriguez-Valera, F., 2007. Metagenomics of the deep Mediterranean, a warm bathypelagic habitat. *PLoS ONE* 2 (9), e914. (cite page 120)
- Martini, S., Al Ali, B., Garel, M., Nerini, D., Grossi, V., Pacton, M., Casalot, L., Cuny, P., Tamburini, C., 2013a. Effects of Hydrostatic Pressure on Growth and Luminescence of a Moderately-Piezophilic Luminous Bacteria *Photobacterium phosphoreum* ANT-2200. *PLoS ONE* 8 (6), e66580. (cite page 64, 115, 142, 144, 146, 147, 159, 177, 185, 192)
- Martini, S., Nerini, D., Tamburini, C., 2013b. Relation between deep bioluminescence and oceanographic variables : a statistical analysis using time-frequency decompositions. (submitted). (cite page 178, 194)
- Massei, N., Fournier, M., 2012. Assessing the expression of large-scale climatic fluctuations in the hydrological variability of daily Seine river flow (France) between 1950 and 2008 using Hilbert-Huang Transform. *Journal of Hydrology* 448-449, 119–128. (cite page 96)
- McDuffey, A., Bird, J. L., 2002. The underway survey system at the naval oceanographic office. In : OCEANS'02 MTS/IEEE. Vol. 3. IEEE, pp. 1722–1725. (cite page 11)
- Meighen, E., 1988. Enzymes and genes from the *lux* operons of bioluminescent Bacteria. *Annual Reviews in Microbiology* 42 (1), 151–176. (cite page 7, 8)
- Meighen, E., 1991. Molecular biology of bacterial bioluminescence. *Microbiological reviews* 55 (1), 123–142. (cite page 7)
- Meighen, E., 1993. Bacterial bioluminescence : organization, regulation, and application of the *lux* genes. *The FASEB journal* 7 (11), 1016–1022. (cite page 7, 23, 162)
- Mertens, C., Schott, F., 1998. Interannual variability of deep-water formation in the Northwestern Mediterranean. *Journal of physical oceanography* 28 (7), 1410–1424. (cite page 55, 56)
- Mesinger, A., Case, J., 1992. Dinoflagellate luminescence increases susceptibility of zooplankton to teleost predation. *Marine Biology* 112 (2), 207–210. (cite page 21)
- Michotey, V., Guasco, S., Boeuf, D., Morezzi, N., Durieux, B., Charpy, L., Bonin, P., 2012. Spatio-temporal diversity of free-living and particle-attached prokaryotes in the tropical lagoon of the atoll (Tuamotu Archipelago) and its surrounding oceanic waters. *Marine Pollution Bulletin* 65 (10), 525–537. (cite page 162, 163)
- Miller, M., Bassler, B., 2001. Quorum sensing in Bacteria. *Annual Reviews in Microbiology* 55 (1), 165–199. (cite page 7)
- Miller, S., Haddock, S., Elvidge, C., Lee, T., 2006. Twenty thousand leagues over the seas : the first satellite perspective on bioluminescent milky seas. *International Journal of Remote Sensing* 27 (23), 5131–5143. (cite page 158)

- Miller, S. D., Haddock, S. H., Elvidge, C. D., Lee, T. F., 2005. Detection of a bioluminescent milky sea from space. *PNAS* 102 (40), 14181–14184. (cite page 54, 61, 152, 158)
- Millot, C., 1999. Circulation in the western Mediterranean Sea. *Journal of Marine Systems* 20 (1), 423–442. (cite page 73)
- Millot, C., Taupier-Letage, I., 2005. The handbook of environmental chemistry, vol. 1, chap. circulation in the Mediterranean Sea, 29–66. (cite page 73)
- Moline, M. A., Blackwell, S. M., Case, J. F., Haddock, S. H., Herren, C. M., Orrico, C. M., Terrill, E., 2009. Bioluminescence to reveal structure and interaction of coastal planktonic communities. *Deep Sea Research II* 56 (3), 232–245. (cite page 157)
- Moutin, T., Raimbault, P., 2002. Primary production, carbon export and nutrients availability in western and eastern Mediterranean Sea in early summer 1996 (MINOS cruise). *Journal of Marine Systems* 33, 273–288. (cite page 166)
- Nagata, T., Tamburini, C., Arístegui, J., Baltar, F., Bochdansky, A. B., Fonda-Umani, S., Fukuda, H., Gogou, A., Hansell, D. A., Hansman, R. L., et al., 2010. Emerging concepts on microbial processes in the bathypelagic ocean, ecology, biogeochemistry, and genomics. *Deep Sea Research Part II* 57 (16), 1519–1536. (cite page 158, 165, 170)
- Nealson, D., 1985. Bio-optical measurement platforms and sensors. STD-R-1160. Johns Hopkins University, Applied Physics Laboratory. (cite page 11)
- Nealson, K., Arneson, A., Huber, M., 1986. Identification of marine organisms using kinetic and spectral properties of their bioluminescence. *Marine Biology* 91 (1), 77–83. (cite page 195)
- Nealson, K., Hastings, J. W., 1979. Bacterial bioluminescence : its control and ecological significance. *Microbiological reviews* 43 (4), 496. (cite page 13, 19, 54, 61)
- Nealson, K., Platt, T., Hastings, J. W., 1970. Cellular control of the synthesis and activity of the bacterial luminescent system. *Journal of bacteriology* 104 (1), 313–322. (cite page 13, 134, 158)
- Nealson, K. H., 1978. Isolation, identification, and manipulation of luminous Bacteria. *Methods in enzymology* 57, 153–166. (cite page 121)
- Nealson, K. H., Hastings, J. W., 1977. Low oxygen is optimal for luciferase synthesis in some Bacteria. *Archives of microbiology* 112 (1), 9–16. (cite page 134)
- Nealson, K. H., Hastings, J. W., 2006. Quorum sensing on a global scale : massive numbers of bioluminescent Bacteria make milky seas. *Applied and environmental microbiology* 72 (4), 2295–2297. (cite page 152)
- Neilson, D. J., Latz, M. I., Case, J. F., 1995. Temporal variability in the vertical structure of bioluminescence in the North Atlantic Ocean. *Journal of Geophysical Research : Oceans (1978–2012)* 100 (C4), 6591–6603. (cite page 11)
- Nerini, D., Durbec, J., Manté, C., 2000. Analysis of oxygen rate time series in a strongly polluted lagoon using a regression tree method. *Ecological modelling* 133 (1), 95–105. (cite page 196)

- Nunes-Halldorson, V., Duran, N. L., 2003. Bioluminescent Bacteria : *lux* genes as environmental biosensors. *Brazilian Journal of Microbiology* 34 (2), 91–96. (cite page 17)
- Olga, M., 2012. Influence of the temperature at the Black Sea ctenophores-aliens bioluminescence characteristics. *Advances in Bioscience and Biotechnology* 3 (3), 269–273. (cite page 16)
- Orndorff, S., Colwell, R., 1980. Distribution and identification of luminous Bacteria from the Sargasso Sea. *Applied and environmental microbiology* 39 (5), 983–987. (cite page 158)
- Paget, D., Elliott, D., 1972. An algorithm for the numerical evaluation of certain Cauchy principal value integrals. *Numerische Mathematik* 19 (5), 373–385. (cite page 93)
- Palanques, A., Puig, P., Durrieu de Madron, X., Sanchez-Vidal, A., Pasqual, C., Martín, J., Calafat, A., Heussner, S., Canals, M., 2012. Sediment transport to the deep canyons and open-slope of the western Gulf of Lions during the 2006 intense cascading and open-sea convection period. *Progress in Oceanography* 106, 1–15. (cite page 55)
- Piontkovski, S., Landry, M., Finenko, Z. Z., Kovalev, A. V., Williams, R., Gallienne, C., Mishonov, A., Skryabin, V., Tokarev, Y., Nikolsky, V., 2003. Plankton communities of the South Atlantic anticyclonic gyre. *Oceanologica Acta* 26 (3), 255–268. (cite page 157)
- Ploug, H., Grossart, H.-P., 2000. Bacterial growth and grazing on diatom aggregates : Respiratory carbon turnover as a function of aggregate size and sinking velocity. *Limnology and Oceanography* 45 (7), 1467–1475. (cite page 136)
- Pooley, D. T., 2011. Bacterial bioluminescence, bioelectromagnetics and function. *Photochemistry and Photobiology* 87 (2), 324–328. (cite page 135)
- Pooley, D. T., Larsson, J., Jones, G., Rayner-Brandes, M. H., Lloyd, D., Gibson, C., Stewart, W. R., 2004. Continuous culture of *Photobacterium*. *Biosensors and Bioelectronics* 19 (11), 1457–1463. (cite page 138)
- Porter, K. G., 1980. The use of DAPI for identifying and counting aquatic microflora. *Limnology and Oceanography* 25, 943–948. (cite page 122)
- Poupin, J., Cussatlegras, A.-S., Geistdoerfer, P., 1999. Plancton marin bioluminescent. Inventaire documenté des espèces et bilan des formes les plus communes de la mer d'Iroise. In, *Laboratoire d'Océanographie de l'École Navale, LOEN Lanvéoc-Poulmic, France*, 1–83. (cite page 2, 4)
- Prasher, D. C., Eckenrode, V. K., Ward, W. W., Prendergast, F. G., Cormier, M. J., 1992. Primary structure of the *Aequorea victoria* green-fluorescent protein. *Gene* 111 (2), 229–233. (cite page 9)
- Priede, I., Bagley, P., Way, S., Herring, P., Partridge, J., 2006. Bioluminescence in the deep sea : free-fall lander observations in the Atlantic Ocean off Cape Verde. *Deep Sea Research Part I* 53 (7), 1272–1283. (cite page 10, 12, 21, 54)

- Priede, I. G., Jamieson, A., Heger, A., Craig, J., Zuur, A. F., 2008. The potential influence of bioluminescence from marine animals on a deep-sea underwater neutrino telescope array in the Mediterranean Sea. Deep Sea Research Part I 55 (11), 1474–1483. (cite page 57)
- Puig, P., Durrieu de Madron, X., Salat, J., Schroeder, K., Martín, J., Karageorgis, A. P., Palanques, A., Roullier, F., Lopez-Jurado, J. L., Emelianov, M., et al., 2012. Thick bottom nepheloid layers in the western Mediterranean generated by deep dense shelf water cascading. Progress in Oceanography. (cite page 57)
- Pusceddu, A., Mea, M., Canals, M., Heussner, S., Durrieu de Madron, X., Sanchez-Vidal, A., Bianchelli, S., Corinaldesi, C., Dell'Anno, A., Thomsen, L., et al., 2013. Major consequences of an intense dense shelf water cascading event on deep-sea benthic trophic conditions and meiofaunal biodiversity. Biogeosciences 10 (4), 2659–2670. (cite page 57, 65)
- Rader, B. A., Nyholm, S. V., 2012. Host/microbe interactions revealed through omics in the symbiosis between the hawaiian bobtail squid *Euprymna scolopes* and the bioluminescent bacterium *Vibrio fischeri*. The Biological Bulletin 223 (1), 103–111. (cite page 21)
- Rao, A. R., Hsu, E.-C., 2008. Hilbert-Huang transform analysis of hydrological and environmental time series. Vol. 60. Springer. (cite page 82)
- Redfield, A. C., 1963. The influence of organisms on the composition of sea water. The sea, 26–77. (cite page 165)
- Rivers, T. J., Morin, J. G., 2012. The relative cost of using luminescence for sex and defense : light budgets in cypridinid ostracods. The Journal of Experimental Biology 215 (16), 2860–2868. (cite page 21)
- Robison, B., Ruby, E., Morin, J., 1977. Luminous bacteria associated with the gut contents of midwater fishes. West Soc Nat 58, 55. (cite page 23)
- Robison, B. H., 2004. Deep pelagic biology. Journal of Experimental Marine Biology and Ecology 300 (1), 253–272. (cite page 54)
- Roether, W., Manca, B. B., Klein, B., Bregant, D., Georgopoulos, D., Beitzel, V., Kočačević, V., Luchetta, A., 1996. Recent changes in eastern Mediterranean deep waters. Science 271 (5247), 333–335. (cite page 65)
- Rohr, J., Latz, M., Fallon, S., Nauen, J., Hendricks, E., 1998. Experimental approaches towards interpreting dolphin-stimulated bioluminescence. The Journal of Experimental Biology 201 (9), 1447–1460. (cite page 15)
- Roithmayr, C., 1970. Airborne low-light sensor detects luminescing fish schools at night. Commer. fish. rev 32, 42–51. (cite page 21)
- Ruby, E., Greenberg, E., Hastings, J., 1980. Planktonic marine luminous Bacteria : species distribution in the water column. Applied and environmental microbiology 39 (2), 302–306. (cite page 13, 120)

- Ruby, E., Morin, J., 1979. Luminous enteric Bacteria of marine fishes : a study of their distribution, densities, and dispersion. *Applied and Environmental Microbiology* 38 (3), 406–411. (cite page 23, 136)
- Ruby, E., Nealson, K., 1976. Symbiotic association of *Photobacterium fischeri* with the marine luminous fish *Monocentris japonica* : a model of symbiosis based on bacterial studies. *The Biological bulletin* 151 (3), 574–586. (cite page 7, 21, 22)
- Ruby, E., Nealson, K., 1978. Seasonal changes in the species composition of luminous Bacteria in nearshore seawater. *Limnology and Oceanography*, 530–533. (cite page 158)
- Rudyakov, Y., Tseytlin, V., 1989. Mesoplankton biomass and bioluminescence in the bathypelagic zone of the ocean. *Oceanology* 29, 619–622. (cite page 12)
- Santinelli, C., Nannicini, L., Seritti, A., 2010. DOC dynamics in the meso and bathypelagic layers of the Mediterranean Sea. *Deep Sea Research Part II* 57 (16), 1446–1459. (cite page 62, 64, 165, 166)
- Schröder, K., Gasparini, G., Tangherlini, M., Astraldi, M., 2006. Deep and intermediate water in the western Mediterranean under the influence of the Eastern Mediterranean Transient. *Geophysical Research Letters* 33 (21), L21607. (cite page 56, 62)
- Schweitzer, B., Huber, I., Amann, R., Ludwig, W., Simon, M., 2001. alpha-and beta-proteobacteria control the consumption and release of amino acids on lake snow aggregates. *Applied and environmental microbiology* 67 (2), 632–645. (cite page 136)
- Seliger, H., Carpenter, J., Loftus, M., McElroy, W., 1970. Mechanisms for the accumulation of high concentrations of dinoflagellates in a bioluminescent bay. *Limnology and Oceanography*, 234–245. (cite page 11)
- Send, U., Lankhorst, M., 2011. The global component of the US Ocean Observatories Initiative and the global OceanSITES project. In : OCEANS 2011. IEEE, pp. 1–3. (cite page 81)
- Shimomura, O., 2012. Bioluminescence : chemical principles and methods. World Scientific Publishing Company. (cite page 6, 9, 225)
- Shimomura, O., Johnson, F. H., 1969. Properties of the bioluminescent protein aequorin. *Biochemistry* 8 (10), 3991–3997. (cite page 9)
- Shimomura, O., Johnson, F. H., Saiga, Y., 1962. Extraction, purification and properties of aequorin, a bioluminescent protein from the luminous hydromedusan, *Aequorea*. *Journal of cellular and comparative physiology* 59 (3), 223–239. (cite page 8)
- Shively, J. M., Cannon, G. C., Heinhorst, S., Bryant, D. A., DasSarma, S., Bazylinski, D., Preiss, J., Steinbuchel, A., Docampo, R., Dahl, C., 2011. Bacterial and archaeal inclusions. eLS. (cite page 131)
- Shulman, I., Kindle, J., McGillicuddy Jr, D., Moline, M. A., Haddock, S. H., Nechaev, D., Phelps, M., 2005. Bioluminescence intensity modeling and sampling strategy optimization. *Journal of Atmospheric and Oceanic Technology* 22 (8), 1267–1281. (cite page 54)

- Sohrin, R., Sempéré, R., 2005. Seasonal variation in total organic carbon in the northeast Atlantic in 2000–2001. *Journal of Geophysical Research : Oceans (1978–2012)* 110 (C10). (cite page 72, 160)
- Soli, G., 1966. Bioluminescent cycle of photosynthetic dinoflagellates. *Limnology and Oceanography*, 355–363. (cite page 11)
- Soly, R., Mancini, J., Ferri, S., Boylan, M., Meighen, E., 1988. A new *lux* gene in bioluminescent Bacteria codes for a protein homologous to the bacterial luciferase subunits. *Biochemical and biophysical research communications* 155 (1), 351–358. (cite page 7)
- Somot, S., Sevault, F., Déqué, M., 2006. Transient climate change scenario simulation of the Mediterranean Sea for the twenty-first century using a high-resolution ocean circulation model. *Climate Dynamics* 27 (7-8), 851–879. (cite page 64)
- Stabb, E. V., 2005. Shedding light on the bioluminescence" paradox". *ASM News-American Society for Microbiology* 71 (5), 223–229. (cite page 7, 8, 14, 21, 219)
- Stabholz, M., Durrieu de Madron, X., Canals, M., Khripounoff, A., Taupier-Letage, I., Testor, P., Heussner, S., Kerhervé, P., Delsaut, N., Houpert, L., et al., 2013. Impact of open-ocean convection on particle fluxes and sediment dynamics in the deep margin of the Gulf of Lions. *Biogeosciences* 10 (2), 1097–1116. (cite page 55, 57, 62, 82)
- Stemmann, L., Hosia, A., Youngbluth, M., Søiland, H., Picheral, M., Gorsky, G., 2008. Vertical distribution (0–1000m) of macrozooplankton, estimated using the Underwater Video Profiler, in different hydrographic regimes along the northern portion of the Mid-Atlantic Ridge. *Deep Sea Research Part II* 55 (1), 94–105. (cite page 46, 186)
- Sterner, R. W., Andersen, T., Elser, J. J., Hessen, D. O., Hood, J. M., McCauley, E., Urabe, J., 2008. Scale-dependent carbon : nitrogen : phosphorus seston stoichiometry in marine and freshwaters. *Limnology and Oceanography* 53 (3), 1169. (cite page 165)
- Strehler, B. L., Johnson, F. H., 1954. The temperature-pressure-inhibitor relations of bacterial luminescence *in vitro*. *PNAS* 40 (7), 606. (cite page 17, 18, 219)
- Sung, N.-D., Lee, C. Y., 2004. Coregulation of *lux* genes and riboflavin genes in bioluminescent Bacteria of *Photobacterium phosphoreum*. *Journal of microbiology-Seoul* 42 (3), 194–199. (cite page 7)
- Swan, B., Martinez-Garcia, M., Preston, C., Sczyrba, A., Woyke, T., Lamy, D., Reinthal, T., Poulton, N. J., Masland, E. D., Gomez, M. L., et al., 2011. Potential for chemolithoautotrophy among ubiquitous Bacteria lineages in the dark ocean. *Science* 333 (6047), 1296–1300. (cite page 170)
- Swanson, K. S., Dowd, S. E., Suchodolski, J. S., Middelbos, I. S., Vester, B. M., Barry, K. A., Nelson, K. E., Torralba, M., Henrissat, B., Coutinho, P. M., et al., 2010. Phylogenetic and gene-centric metagenomics of the canine intestinal microbiome reveals similarities with humans and mice. *The ISME journal* 5 (4), 639–649. (cite page 164)
- Swift, E., Lessard, E. J., Biggley, W. H., 1985. Organisms associated with stimulated epipelagic bioluminescence in the sargasso sea and the gulf stream. *Journal of plankton research* 7 (6), 831–848. (cite page 11, 54)

- Takai, K., Horikoshi, K., 2000. Rapid detection and quantification of members of the archaeal community by quantitative PCR using fluorogenic probes. *Applied and Environmental Microbiology* 66 (11), 5066–5072. (cite page 162)
- Tamburini, C., Canals, M., Durrieu de Madron, X., Houpert, L., Lefevre, D., Martini, S., D'Ortenzio, F., Robert, A., Testor, P., Aguilar, J., et al., 2013. Deep-sea bioluminescence blooms after dense water formation at the ocean surface. *PLoS ONE* 8 (7), e67523. (cite page 45, 74, 81, 82, 102, 103, 154, 157, 159, 173, 177, 178, 182, 187, 220)
- Tamburini, C., Garcin, J., Bianchi, A., 2003. Role of deep-sea Bacteria in organic matter mineralization and adaptation to hydrostatic pressure conditions in the NW Mediterranean Sea. *Aquatic Microbial Ecology* 32 (3), 209–218. (cite page 140)
- Tamburini, C., Goutx, M., Guigue, C., Garel, M., Lefere, D., Charriere, B., Sempere, R., Pepa, S., Peterson, M. L., Wakeham, S., et al., 2009. Effects of hydrostatic pressure on microbial alteration of sinking fecal pellets. *Deep Sea Research Part II* 56 (18), 1533–1546. (cite page 126, 167)
- Team, R. C., 2012. R : A language and environment for statistical computing. R Foundation for Statistical Computing, Vienna, Austria, ISBN 3-900051-07-0. URL <http://www.R-project.org>. (cite page 123)
- Teira, E., Lebaron, P., Van Aken, H., Herndl, G. J., et al., 2006. Distribution and activity of Bacteria and Archaea in the deep water masses of the North Atlantic. *Limnology and oceanography* 51 (5), 2131–2144. (cite page 167)
- Testor, P., Gascard, J.-C., 2006. Post-convection spreading phase in the Northwestern Mediterranean Sea. *Deep Sea Research Part I* 53 (5), 869–893. (cite page 56, 61, 62, 73)
- Timmins, G. S., Jackson, S. K., Swartz, H. M., 2001. The evolution of bioluminescent oxygen consumption as an ancient oxygen detoxification mechanism. *Journal of molecular evolution* 52 (4), 321–332. (cite page 23, 147)
- Tokarev, Y. N., Williams, R., Piontkovski, S., 1999. Identification of small-scale structure of plankton communities of the Black and Ionian Seas by their bioluminescence characteristics. *Hydrobiologia* 393, 163–167. (cite page 157)
- Torrence, C., Compo, G., 1998. A Practical Guide to Wavelet Analysis. *Bulletin of the American Meteorological Society* 79 (1), 61–78. (cite page 86, 87, 100, 194)
- Torrence, C., Webster, P. J., 1999. Interdecadal changes in the ENSO-monsoon system. *Journal of Climate* 12 (8), 2679–2690. (cite page 100)
- Treguer, P., Le Corre, P., 1975. Analyse des sels nutritifs sur Autoanalyzer II : nitrates+ nitrites. Manuel d'Analyse des sels nutritifs dans l'eau de mer, University Bretagne Occidentale, France. (cite page 161)
- Turley, C., 2002. The importance of marine snow. *Microbiol. Today* 29, 177–179. (cite page 187)
- Turley, C., Mackie, P., 1995. Bacterial and cyanobacterial flux to the deep NE Atlantic on sedimenting particles. *Deep Sea Research Part I* 42 (8), 1453–1474. (cite page 187)

- Turner, J., White, E., Collins, M. A., Partridge, J., Douglas, R., 2009. Vision in lanternfish (*Myctophidae*) : adaptations for viewing bioluminescence in the deep-sea. Deep Sea Research Part I : Oceanographic Research Papers 56 (6), 1003–1017. (cite page 21)
- Ueda, I., Shinoda, F., Kamaya, H., 1994. Temperature-dependent effects of high pressure on the bioluminescence of firefly luciferase. Biophysical journal 66 (6), 2107–2110. (cite page 18, 219)
- Vacquié-Garcia, J., Royer, F., Dragon, A.-C., Vivant, M., Bailleul, F., Guinet, C., 2012. Foraging in the darkness of the southern ocean : Influence of bioluminescence on a deep diving predator. PloS one 7 (8), e43565. (cite page 10, 21)
- Van Haren, H., 2011. Meso- and small-scale vertical motions in the deep western mediterranean. Nuclear Instruments and Methods in Physics A 626-627, S84–S86. (cite page 62, 88, 102)
- Varela, M. M., Van Aken, H. M., Herndl, G. J., 2008. Abundance and activity of chloroflexi-type SAR202 bacterioplankton in the meso-and bathypelagic waters of the (sub) tropical Atlantic. Environmental microbiology 10 (7), 1903–1911. (cite page 171)
- Verhulst, P.-F., 1838. Notice sur la loi que la population suit dans son accroissement. Quetelet 10, 113–121. (cite page 122, 142, 144, 192)
- Vezzi, A., Campanaro, S., D'Angelo, M., Simonato, F., Vitulo, N., Lauro, F., Cestaro, A., Malacrida, G., Simionati, B., Cannata, N., et al., 2005. Life at depth : *Photobacterium profundum* genome sequence and expression analysis. Science 307 (5714), 1459–1461. (cite page 120)
- Vitukhnovskaya, L., Ismailov, A., 2001. Effect of Na<sup>+</sup> and K<sup>+</sup> ions on the luminescence of intact *Vibrio harveyi* cells at different pH values. Microbiology 70 (4), 456–461. (cite page 17)
- Warrant, E., Locket, N., 2004. Vision in the deep sea. Biological Reviews 79 (3), 671–712. (cite page 21)
- Watanabe, H., Mimura, N., Takimoto, A., Nakamura, T., 1975. Luminescence and respiratory activities of *Photobacterium phosphoreum* competition for cellular reducing power. Journal of biochemistry 77 (6), 1147–1155. (cite page 19)
- Watanabe, Y., Tanaka, Y., 2011. Bioluminescence-based imaging technique for pressure measurement in water. Experiments in fluids 51 (1), 225–236. (cite page 18)
- Weikert, H., Koppelman, R., Wiegratz, S., 2001. Evidence of episodic changes in deep-sea mesozooplankton abundance and composition in the Levantine Sea (Eastern Mediterranean). Journal of marine Systems 30 (3), 221–239. (cite page 65)
- Whitman, W. B., Coleman, D. C., Wiebe, W. J., 1998. Prokaryotes : the unseen majority. Proceedings of the National Academy of Sciences 95 (12), 6578–6583. (cite page 158)
- Widder, E., 2002. Bioluminescence and the pelagic visual environment. Marine and Freshwater Behaviour and Physiology 35 (1-2), 1–26. (cite page 10, 157)

- Widder, E., Bernstein, S., Bracher, D., Case, J., Reisenbichler, K., Torres, J., Robison, B., 1989. Bioluminescence in the Monterey Submarine Canyon : image analysis of video recordings from a midwater submersible. *Marine Biology* 100 (4), 541–551. (cite page 10, 54, 195)
- Widder, E., Case, J., Bernstein, S., MacIntyre, S., Lowenstine, M., Bowlby, M., Cook, D., 1993. A new large volume bioluminescence bathyphotometer with defined turbulence excitation. *Deep Sea Research Part I* 40 (3), 607–627. (cite page 11, 16)
- Widder, E., Johnsen, S., Bernstein, S., Case, J., Neilson, D., 1999. Thin layers of bioluminescent copepods found at density discontinuities in the water column. *Marine Biology* 134 (3), 429–437. (cite page 54)
- Widder, E. A., 2010. Bioluminescence in the ocean : origins of biological, chemical, and ecological diversity. *Science* 328 (5979), 704–708. (cite page 2, 5, 21, 54, 65, 135, 157)
- Widder, E. A., Latz, M. I., Case, J. F., 1983. Marine bioluminescence spectra measured with an optical multichannel detection system. *The Biological Bulletin* 165 (3), 791–810. (cite page 5)
- Wiles, S., Ferguson, K., Stefanidou, M., Young, D. B., Robertson, B. D., 2005. Alternative luciferase for monitoring bacterial cells under adverse conditions. *Applied and environmental microbiology* 71 (7), 3427–3432. (cite page 6)
- Williams, P., 1981. Microbial contribution to overall marine plankton metabolism-direct measurements of respiration. *Oceanologica Acta* 4 (3), 359–364. (cite page 160)
- Wood, S. N., 2003. Thin plate regression splines. *Journal of the Royal Statistical Society : Series B* 65 (1), 95–114. (cite page 97)
- Yamada, M., Nakasone, K., Tamegai, H., Kato, C., Usami, R., Horikoshi, K., 2000. Pressure regulation of soluble cytochromes c in a deep-sea piezophilic bacterium, *Shewanella violacea*. *Journal of bacteriology* 182 (10), 2945–2952. (cite page 120)
- Yanagibayashi, M., Nogi, Y., Li, L., Kato, C., 1999. Changes in the microbial community in Japan Trench sediment from a depth of 6,292 m during cultivation without decompression. *FEMS microbiology letters* 170 (1), 271–279. (cite page 121)
- Yano, Y., Nakayama, A., Ishihara, K., Saito, H., 1998. Adaptive changes in membrane lipids of barophilic Bacteria in response to changes in growth pressure. *Applied and environmental microbiology* 64 (2), 479–485. (cite page 133)
- Yayanos, A. A., 1986. Evolutional and ecological implications of the properties of deep-sea barophilic Bacteria. *PNAS* 83 (24), 9542–9546. (cite page 131)
- Yayanos, A. A., 1995. Microbiology to 10,500 meters in the deep sea. *Annual Reviews in Microbiology* 49 (1), 777–805. (cite page 120, 129, 131)
- Yetinson, T., Shilo, M., 1979. Seasonal and geographic distribution of luminous Bacteria in the eastern Mediterranean Sea and the Gulf of Elat. *Applied and environmental microbiology* 37 (6), 1230–1238. (cite page 12, 25, 158)

- Zarubin, M., Belkin, S., Ionescu, M., Genin, A., 2012. Bacterial bioluminescence as a lure for marine zooplankton and fish. PNAS 109 (3), 853–857. (cite page 23, 24, 136, 149, 158)
- ZoBell, C., Johnson, F., 1949. The influence of hydrostatic pressure on the growth and viability of terrestrial and marine bacteria. Journal of bacteriology 57 (2), 179. (cite page 120)

---

## Table des figures

---

1.1	Phylogenetic representation of the diversity of bioluminescent organisms, from Haddock et al. (2010) . . . . .	3
1.2	Classification of the number of bioluminescent species depending on their wavelength emission for marine organisms. . . . .	5
1.3	Schematic reaction inducing bioluminescence. . . . .	6
1.4	<i>Lux</i> -gene organization for the bioluminescent <i>Photobacterium phosphoreum</i> bacterial strain. . . . .	7
1.5	Biochemistry and physiology of reaction inducing <i>Vibrio fischeri</i> bioluminescence and <i>lux</i> genes involved into reactions are also . . . . .	8
1.6	Genetics and quorum sensing, from Stabb (2005). . . . .	14
1.7	Quorum sensing representation modified from Hmelo et al. (2011). . . . .	15
1.8	Effects of temperature and pressure conjointly on A) <i>Achromobacter fischeri</i> extract and <i>Photobacterium phosphoreum</i> living cells, from Strehler and Johnson (1954) and B) firefly luciferase, modified from Ueda et al. (1994). . . . .	18
1.9	Ecological roles of bioluminescence activity, from Haddock et al. (2010) . . . . .	22
1.10	A) Fecal pellets produced after feeding on small colony fragments of the bioluminescent bacterium. B) Glow of zooplankton ( <i>Artemia salina</i> ) after contacting and ingesting small particles broken off colonies of the bioluminescent bacterium <i>Photobacterium leiognathi</i> . . . . .	24
2.1	Representation of some of the international open-ocean biological records and time-series since 1900. From Edwards et al. (2010) . . . . .	32
2.2	A) Artistic representation of the ANTARES neutrino telescope in the deep Mediterranean Sea. B) Schematic representation of the IL07 instrumented line immersed close to the ANTARES telescope. . . . .	34
2.3	Optical module from the ANTARES neutrino telescope. . . . .	35
2.4	A) The AXIS 221 camera used on the instrumented line IL07. B) Floor 5 on the instrumented line IL07 of the ANTARES neutrino telescope. . . . .	36
2.5	Time series dataset sampled at the ANTARES station from December 2007 to July 2010. . . . .	39

2.6	Current speed horizontal intensity, incoming direction and frequency representations for 2008, 2009 and 2010. . . . .	41
2.7	Current speed horizontal intensity, direction and frequency representations focused on March 2009 and 2010. . . . .	41
2.8	Bioluminescence representation over the years 2008, 2009 and 2010 depending on direction of current speed, intensity and frequency. . . . .	42
2.9	Bioluminescence representation in March 2009 and 2010 depending on direction of current speed, intensity and frequency . . . . .	43
2.10	Regression trees for A) bioluminescence, B) salinity, C) temperature and D) current speed. Time series with the class mean values (black lines) defined by the leaves of regression trees. . . . .	44
2.11	Regression tree for the prediction of bioluminescence activity using oceanographic variables (salinity, temperature and current speed) from December 2007 to July 2010. Modified from Tamburini et al. (2013), supplementary data. . . . .	45
2.12	Example of images recorded by video-camera at the ANTARES site. . . . .	47
2.13	Bioluminescence emission and video records. A) The bioluminescence emission recorded from the ANTARES-IL07 photomultipliers. B) Bioluminescence events recorded from the two video-cameras using automatic detection on the ANTARES-IL07. . . . .	48
2.14	Representation of the video-event distribution between floor 1 and floor 5. . . . .	49
2.15	Correlation between the bioluminescence emission monthly integrated and the number of events recorded by video cameras at the same time scale. . . . .	50
2.16	Map of the NW Mediterranean Sea showing the location of the ANTARES, LION and Lacaze-Duthiers Canyon (LDC) sites (a) as well as the extension of open-sea convection area in the Gulf of Lion and beyond from 2008 to 2010 (b-d). . . . .	56
2.17	Time series measured at the ANTARES IL07 mooring line. . . . .	58
2.18	Links between bioluminescence, current speed and the modification of the properties of the Western Mediterranean Deep Water (WMDW). . . . .	60
2.19	Time series of oceanographic parameters measured at the Lacaze-Duthiers Canyon (LDC) and the open-sea convection region in the Gulf of Lion (LION) from January 2008 to June 2010. . . . .	63
2.20	Configuration of the mooring lines from which the data presented in this study were obtained. . . . .	68
2.21	(a) Raw counting rates from one photomultiplier (PMT) on the IL07 line (ANTARES site). (b) Median rates from the IL07 PMT (red) and mean of all median rates of the 885 ANTARES PMTs (blue) from January to April 2009. . . . .	69
2.22	Potential temperature versus salinity diagram of near-bottom CTD time-series at the ANTARES site from the IL07 line (red dots) and CTD profiles (lines) collected close to the ANTARES site. . . . .	70
2.23	Illustrative ocean colour satellite images used to outline the limits of winter open-sea convection areas in the Gulf of Lion. . . . .	71
2.24	Dissolved organic carbon and oxygen concentrations at the ANTARES site in 2010. . . . .	72
2.25	Artistic representation of newly-formed water masses in the Gulf of Lion and their impact on biological activity (bioluminescence) at the ANTARES station. . . . .	74

3.1	Map of the North-Western Mediterranean Sea and the ANTARES site (black dot) where the underwater neutrino telescope is immersed at 2,475 m depth. . . . .	83
3.2	Time series recorded in the Mediterranean Sea, at the ANTARES station, between January 2009 and July 2010, for bioluminescence, current speed ( $cm\ s^{-1}$ ), salinity, and temperature ( $^{\circ}C$ ). . . . .	84
3.3	Two examples of signal decomposition. On the left, the signal represented over time, on the right, the periodogram over frequencies A) non-stationary and B) stationary signal. . . . .	87
3.4	Time-frequency representation using the wavelet decomposition for A) bioluminescence B) current speed and C) salinity time series. . . . .	89
3.5	Schematic representation of the signal decomposition using the Hilbert-Huang method. . . . .	91
3.6	Example of significance for the IMFs decomposition from a partial set of data. . . . .	92
3.7	Hilbert-Huang decomposition for the bioluminescence signal into 10 intrinsic mode functions, from C1 to C10. . . . .	94
3.8	Representation of the empirical dyadic decomposition of the HHG method. . . . .	96
3.9	Spectral representation using HHG decomposition and thin-plate spline smoothing for A) bioluminescence, B) current speed and C) salinity from January 2009 to July 2010. . . . .	99
3.10	Cross spectrogram between bioluminescence and A) current speed and B) salinity, using the wavelet decomposition and coherence measurement. . . . .	104
3.11	Cross spectrogram between bioluminescence and oceanographic variables. . . . .	105
3.12	Representation of the most correlated intrinsic mode function for A) bioluminescence and current speed, B) bioluminescence and salinity. . . . .	106
3.13	Fourier decomposition of the sea level dataset during a tsunami event. . . . .	109
3.14	Time series decomposition within pass-band filter using the Hilbert-Huang decomposition method (see (Huang et al., 1998) and 3.1.2). . . . .	110
3.15	Time-frequency spectra using the Hilbert-Huang decomposition method (see (Huang et al., 1998) and 3.1.2). . . . .	111
3.16	A) Tsunami arrival time series and B) time-frequency spectra (frequency is $\frac{1}{Period}$ ). . . . .	111
4.1	<i>Photobacterium phosphoreum</i> ANT-2200 strain emitting bioluminescence in liquid growth medium and solid medium. . . . .	116
4.2	Neighbor-joining tree showing the phylogenetic position of <i>Photobacterium phosphoreum</i> ANT-2200 strain. . . . .	116
4.3	High-pressure bioluminescence system. . . . .	126
4.4	Example of logistic model fitting empirical growth data of <i>P. phosphoreum</i> ANT-2200. . . . .	127
4.5	Representation of growth curves for temperatures of 4, 13, 20, 30 and 37°C and for pressure of 0.1, 10, 22, 30, and 40 MPa. . . . .	128
4.6	Extrapolated-contour diagram of the temperature-pressure dependence of <i>P. phosphoreum</i> ANT-2200. . . . .	129
4.7	Cross diagram of the temperature-pressure dependence of <i>P. phosphoreum</i> ANT-2200. . . . .	130
4.8	Micro-photographs of <i>P. phosphoreum</i> ANT-2200 cells by electron microscopy. . . . .	132
4.9	Relative total fatty-acid composition (%) of <i>P. phosphoreum</i> ANT-2200. . . . .	133
4.10	Bioluminescence and growth of <i>P. phosphoreum</i> ANT-2200. . . . .	135

4.11 A) and B) Representation of the end cap for High Pressure Bottles (HPBs) with top end cap improved for oxygen and temperature sensors. A) Photograph of the external part, from above B) Photograph of the external part, from below. C) Photograph of the internal part. Schematic representation of the end cap for High Pressure Bottles (HPBs) with oxygen and temperature fibers and connections. . . . .	140
4.12 Test for oxygen measurement before inoculation and conditioning for high pressure experiment. . . . .	142
4.13 <i>Photobacterium phosphoreum</i> ANT-2200 is cultivated in ONR7a growth medium. . . . .	143
4.14 Bacterial metabolic and anabolic pathways within and without the cell. . . . .	148
5.1 Milky sea detection from satellite observation in the Indian Ocean. . . . .	153
5.2 Vertical profiles for temperature, salinity, DOC, $\text{NO}_3^-$ , $\text{PO}_4^{3-}$ , and $\text{Si}(\text{OH})_4$ using water sampling. Dots are samples values from the 6 sampling times, continuous lines are the profile using a local polynomial regression (loess method Cleveland and Grosse 1991) and dotted lines are the standard error for each profile. . . . .	165
5.3 Potential temperature versus salinity diagram of CTD time series at the ANTARES site in January, March, May, June, September, and October 2011. Data shown are above 1,200 m. Colored dots represent data point sampled at 2,000 m depth. Changes in water masses occur at depth below 2,000 m with a come back to the stable state in May 2011. . . . .	167
5.4 Quantitative estimation of A) 16S archaeal DNA (black bars) and RNA (grey bars) B) 16S bacterial DNA (black bars) and RNA (grey bars) among the year 2011, at the ANTARES station. . . . .	168
5.5 A) Denaturing Gradient Gel Electrophoresis (DGGE) analysis estimation of 16S archaeal rDNA among the year 2011, at the ANTARES station. B) Phylogenetic tree of the archaeal 16S rDNA gene sequence from the clones DGGE bands. . . . .	170
5.6 Denaturing Gradient Gel Electrophoresis (DGGE) analysis of A) 16S bacterial rDNA and B) 16S bacterial rRNA during the year 2011, at the ANTARES station. . . . .	171
5.7 Phylogenetic tree of the bacterial 16S rDNA gene sequence from the clones DGGE bands. . . . .	171
5.8 A) Venn diagram representation of total number of OTUs in October and May. B) Number of sequences per OTU for May and October samples showing a higher diversity for October than May. . . . .	172
5.9 Diversity percentages representation among major phyla for October and May samples. . . . .	173
5.10 A) Current speed time series B) Bioluminescence time series recorded by photomultiplier tubes at the ANTARES station over the year 2011. . . . .	174
5.11 Quantitative estimation of <i>luxF</i> genes for bacterial DNA (black bars) and RNA (grey bars) among the year 2011, at the ANTARES station. . . . .	175
5.12 Phylogenetic tree of the <i>lux</i> genes sequence from the clones DGGE bands. . . . .	176
5.13 Box-and-whisker plot of bioluminescence 7 days around water sampling periods and <i>lux</i> mRNA/bacterial rRNA ratio. . . . .	176
5.14 Chlorophyll- <i>a</i> time series recorded at the ANTARES station from satellite data, data acquisition. . . . .	179

6.1	The bioreactor platform with pH, O <sub>2</sub> , temperature and CO <sub>2</sub> data acquisition and control in real time and high frequency sub-sampling. . . . .	190
6.2	Data acquisition from the bioreactor. <i>Photobacterium phosphoreum</i> ANT-2200 strain has been cultivated in an ONR7a growth medium under controlled conditions. . . . .	192
6.3	Example of bioluminescence emission patterns. A) From the ANTARES observatory, B) In the literature. . . . .	195



---

## Liste des tableaux

---

1.1	Progress in research on bioluminescence, modified from Shimomura (2012)	9
1.2	Bathyphotometers developed for <i>in situ</i> bioluminescence measurements using mechanical stimulation. Modified from Herren et al. (2005). D : diameter, V : volume. NA : Non Available value.	11
3.1	KPSS-test for testing stationarity of each time series.	85
4.1	Composition of the rich Sea Water Complete medium (SWC) and impoverished SWC medium. SWC is described as rich due to its high carbon content (yeast extract, bio-polypeptone and glycerol concentrations). pH is set at 7.5.	138
4.2	Composition of the ONR7a medium with low carbon concentration. Before mixing, solutions 1 and 2 are autoclaved separately to avoid precipitation and solution 3 is filtered on 0.2 $\mu\text{m}$ . pH is set at 7.5	139
4.3	Summary of results measured in High Pressure Bottles. SWC : Sea Water Complete medium.	146
5.1	Average and standard deviation for the main environmental variables over the year 2011, sampled at 2,000 m depth. T = potential temperature. S = salinity. DOC = Dissolved Organic Carbon.	166
5.2	Values of molecular analysis survey in 2011 at the ANTARES station for both Archaea and Bacteria. ND : Not Determined.	169



## Résumé

La bioluminescence est l'émission de lumière par des organismes vivants. En milieu bathypélagique, où l'absence de lumière est une caractéristique majeure, ce phénomène semble avoir un rôle écologique primordial dans les interactions biologiques ainsi que dans le cycle du carbone. Ce travail cherche à déterminer si la bioluminescence peut être définie comme un proxy de l'activité biologique en milieu profond. Deux axes sont étudiés : *(i)* en milieu profond, la bioluminescence est décrite et expliquée au cours du temps *(ii)* la part de bioluminescence bactérienne est estimée dans l'émission de luminescence enregistrée *in situ*. Cette étude multidisciplinaire développe à la fois une approche *in situ* et en laboratoire.

Le télescope ANTARES, immergé en Méditerranée, à 2475 m de profondeur, a joué le rôle d'un observatoire océanographique enregistrant la bioluminescence ainsi que les variables environnementales à haute fréquence. L'analyse de ces séries temporelles, non-linéaires et non-stationnaires a permis de mettre en évidence deux périodes de forte activité de bioluminescence en 2009 et 2010. Ces évènements ont été expliqués par des phénomènes de convection dans le Golfe du Lion, impactant indirectement la bioluminescence enregistrée sur ANTARES. En laboratoire, la bioluminescence bactérienne a été décrite sur une souche modèle piezophile, isolée au cours d'un évènement de forte bioluminescence. La pression hydrostatique liée à la profondeur *in situ* (22 MPa) induit une plus forte bioluminescence qu'à pression atmosphérique (0.1 MPa). Enfin, le suivi des communautés procaryotiques profondes a été réalisé, sur le site ANTARES, au cours de l'année 2011. Ce suivi a montré la présence de 0.1 à 1% de bactéries bioluminescentes dans une période enregistrant une faible activité de bioluminescence. Ces cellules ont été définies comme majoritairement actives.

**Mots clés :** Bioluminescence, Milieu bathypélagique, Mer Méditerranée, Analyse de séries temporelles, Pression hydrostatique, Bactéries, Observatoire *in situ*

## Abstract

Bioluminescence is the emission of light by living organisms. In the bathypelagic waters, where darkness is one of the main characteristic, this phenomenon seems to play a major role for biological interactions and in the carbon cycle. This work aims to determine if bioluminescence can be considered as a proxy of biological activity in the deep sea. Two axes have been studied: (*i*) in the deep sea, we attempt to describe and explain the bioluminescence variability over time (*ii*) the part of bacterial bioluminescence is investigated in the light signal *in situ*. This multidisciplinary study develops both *in situ* and laboratory approaches.

The ANTARES telescope immersed in the Mediterranean Sea at 2,475 m depth has been used as an oceanographic observatory recording bioluminescence as well as environmental variables at high frequency. This time series analysis, defined as non linear and non stationary, highlighted two periods of high bioluminescence intensity in 2009 and 2010. These events have been explained by convection phenomena in the Gulf of Lion, indirectly impacting the bioluminescence sampled at this station. In the laboratory, bacterial bioluminescence has been described using a piezophilic bacterial model isolated during a high-bioluminescence-intensity event. Hydrostatic pressure linked to the *in situ* depth (22 MPa) induces a higher bioluminescence activity than under atmospheric pressure (0.1 MPa). Then, the survey of the deep prokaryotic communities has been done at the ANTARES station, over the year 2011. This survey shows the presence of about 0.1 to 1% of bioluminescent bacteria even during a low-bioluminescence-activity period. These cells were mainly actives.

**Key words :** Bioluminescence, Bathypelagic environment, Mediterranean Sea, Time series analysis, Hydrostatic pressure, Bacteria, *In situ* observatories